A quantitative framework for studying bacterial colonisation of the rhizoplane

Dáire Carroll

Presented for the degree of Doctor of Philosophy in the School of Life Sciences, University of Warwick

August 2021

Table of Contents

List of figures

List of tables

Acknowledgments

I would like to thank the three supervisors who began this PhD with me. Professor Lionel Dupuy, Professor Nicola Holden, and Professor Miriam Gifford have all provided an enormous amount of guidance not just to this project but to my development as a scientist. I would like to thank Dr Ashleigh Holmes, for stepping in as supervisor in the final months of my PhD and keeping me on track. Her guidance in the lab also helped make this thesis possible. My advisors at the University of Warwick, Dr Vardis Ntoukakis and Professor Orkun Soyer, as well as at the James Hutton Institute, Dr Steve Whisson, all worked with me to help make the most out of my time.

Thank you to Professor Gail Preston for providing fluorescent marker plasmids which made the work of this thesis significantly more productive. Thank you to Dr Beatriz Lagunas for providing equal measures of guidance on lab matters and chips when needed. To Dr Jacqueline Marshall for helping me deal with every problem that arose in the lab. To Dr Kathryne Wright, Dr Alison Roberts, and Ian Hands-Portman for their teaching and overall enthusiasm for imaging. A massive thank you to Yangminghao Liu who took time out of his own work to construct my chemotaxis chambers. Thank you also to Dr Daniel Patko, Dr Ilonka Engelhardt, and Dr Matthias Mimault for their advice on transparent soil and experimental design.

Thank you to all the staff at both the University of Warwick and the James Hutton Institute, in particular Nicola Glover and Laura Logie, who made working between the two institutes as smooth as possible and organized some of the most memorable events of my PhD. A thank you to both institutes for funding my PhD and letting me spend nearly four years of my life working with plants and bacteria.

There are so many other PhD students and friends who have helped me in many ways, but my biggest thanks to the lunch crew who stayed in touch when lunch was no longer an option, and the DnD crew who made Friday nights something to look forward too again when the world seemed to be falling apart.

Finally, thank you to my brother, sister, and parents for supporting everything I do. Above all, to my wife Jess, who has read every piece of nonsense I have written and given feedback on my ideas long before they are ready to see the light, I can never thank you enough for everything you do. Sharing this Scottish adventure with you has been the best years of my life.

Declaration

This thesis is submitted to the University of Warwick in support of my application for the degree of Doctor of Philosophy. It has been composed by myself and has not been submitted in any previous application for any degree.

The work presented (including data generated and data analysis) was carried out by the author except in the cases outlined below:

Construction of transparent soil mesocosm chambers in Chapter 4 and chemotaxis chambers in Chapter 5, was carried out by Yangminghao Liu, a PhD student at the James Hutton Institute.

Parts of this thesis have been published by the author:

A significant portion of the work presented in Chapter 3 has previously been published in Carroll et al. (2020), DOI: https://doi.org/10.3389/fmicb.2020.585443.

Abstract

Colonisation of the root surface, or rhizoplane, is one of the first steps for microorganisms within soil to become established in the plant microbiome. However, the timing and relative contributions of processes, such as microbial movement, attachment, and proliferation to colonisation are not well characterized. This limits our ability to comprehend the complex dynamics of microbial communities in soil. The aim of this thesis was to develop a set of experimental and theoretical frameworks that can be used to isolate and quantify key microbial processes involved in rhizoplane colonisation. A model plant and bacterial system, consisting of *Pseudomonas fluorescens* isolate SBW25, transformed with a fluorescent marker plasmid, and Lettuce (*Lactuca sativa*) was selected for characterisation. A liquid microcosm system was developed which enabled inoculation of plants with bacterial suspensions and manipulation of the plant following treatment. Using this system, a framework for the independent quantification of bacterial attachment and proliferation on the root surface was developed. This allowed previously indistinguishable components of the colonisation process to be independently quantified. The timing and spatial distribution of colonisation in a granular environment was further analysed through the live imaging of plants grown in transparent soil. A chemotaxis assay was developed for the measurement of bacterial movement in transparent soil in response to plant root exudate. Data from chemotaxis assays was used to construct a model of bacterial diffusion and convection in soil. These novel characterisations of bacterial movement, attachment to the root surface, and proliferation offers new insight into the timing of rhizoplane colonisation by *Pseudomonas fluorescens* SBW25. The techniques and analyses developed in this thesis could be applied to many different combinations of plants and microorganisms. Potential applications include the selection of microbial traits which improve maintenance of targeted isolates in agricultural systems, and the development of biological fertilizers.

Table of abbreviations

Abbreviation	Explanation
AIC	Akaike's information criterion
ANOVA	Analysis of variance
CFU	Colony forming unit
DAMP	Damage associated molecular patterns
ddH_2O	Double distilled water
dH_2O	Sterile deionised water
F	F-statistic
FDA	Fluorescein diacetate
GFP	Green fluorescent protein
HPLC	High performance liquid chromatography
LapA	Large adhesion protein
LB	Lysogeny broth
MAMP	Microbe associated molecular patterns
MOMP	Major outer membrane protein
MS	Murashige and Skoog
NLS	Non-linear least squares
P	P-value
PAMP	Pathogen associated molecular patterns
PBA	Phosphate buffered saline
PCR	Polymerase chain reaction
PDA	Partial differential equation
PDMS	Polydimethylsiloxane
PGP	Plant growth promoting
PRR	Pattern Recognition Receptor
Psf	Pseudomonas fluorescence
RD-MOPS	Rich defined (3-(N-morpholino)propanesulfonic acid)
SD	Standard deviation
Sp.	Species (singular)
Spp.	Species (pleural)
SRB	Sulforrhodamine-B
TBE	Tris Borate EDTA

Table of variables and parameters

Notation	Parameter	Unit
C_E	Approximate concentration of exudate at initiation	g ml^{-1}
A_c	Area classified as bacterial colonies	mm^2
k	Bacterial carrying capacity	CFU ml^{-1}
K	Bacterial carrying capacity	g mm^{-2}
U_B	Bacterial decay	g mm^{-2} s^{-1}
D_B	Bacterial diffusion parameter	mm^2 s^{-1}
ω	Bacterial fluorescence	mm^{-3}
M	Bootstrap replicates	NA
k	Carrying capacity	g^{-1}/ mm^{-3}/ Log_{10}CFU
CFU^0	CFU of inoculant	ml^{-1}
α	CFU to g of carbon conversion factor	gC
Q	Chemotactic parameter	g mm^{-2} s^{-1}
y_p	Colonisation density in the absence of attachment	g^{-1}
y	Colonisation density on root surface	g^{-1}
y_0^c	Colonisation density on root surfaces at hour 0 for total colonisation	g^{-1}
y_0^p	Colonisation density on root surfaces at hour 0 in the absence of attachment	g^{-1}
y^0	Colonisation density or bacterial density at hour 0 (g^{-1} or Log_{10}CFU)	g^{-1}/ Log_{10}CFU
$p(t)$	Contribution of attachment at t to total colonisation of the rhizoplane at hour 96	NA
h_B	Conversion factor, pixel intensity to bacterial density in g of carbon	g
h_E	Conversion factor, pixel intensity to exudate density in g of carbon	g
B	Estimated bacterial density	g mm^{-2}
E	Estimated exudate concentration	g mm^{-2}
Y_e	Experimental value at time t and position i	g mm^{-2}

Notation	Parameter	Unit
U_E	Exudate decay	g mm^{-2} s^{-1}
D_E	Exudate diffusion parameter	mm^2 s^{-1}
y^0	Initial bacterial density	CFU ml^{-1}
Y^0	Initial bacterial density	g mm^{-1}
h^0	Length of the lag phase	hour
$\hat{I}_{max}$	Maximum x_I value	NA
G	Maximum bacterial growth rate	g mm^{-2} s^{-1}
μ	Maximum bacterial growth rate	hour^{-1}
μ_c	Maximum growth rate for total colonisation (g^{-1} hour^{-1})	g^{-1} hour^{-1}
μ_p	Maximum growth rate in the absence of attachment	g^{-1} hour^{-1}
$\bar{y}$	Mean bacterial density in chambers at initiation	CFU ml^{-1}
$\bar{I}$	Mean pixel intensity	NA
$\bar{I}^0$	Mean pixel intensity of uninoculated chambers	NA
I^0	Mean value of I for images taken prior to inoculation	NA
V_{tot}	Mean volume of medium in chemotaxis chambers	ml
S	Microbial growth rate	g mm^{-2} s^{-1}
T	Microbial mortality rate	g mm^{-2} s^{-1}
Y_m	Model predicted value at time t and position i	g mm^{-2}
J	Monod affinity parameter	g mm^{-2}
$\hat{I}$	Normalised pixel intensity	NA
px	Number of pixels in an image	NA
$\hat{I}_\propto$	Proportion of maximum pixel intensity	NA
$A_\propto$	Proportion of root area classified as bacterial colonies	NA
R_a	Rate of attachment	g^{-1} hour^{-1}
R_p	Rate of proliferation on the root surface	g^{-1} hour^{-1}
R_p^y	Rate of proliferation on the root surface in the absence of attachment	g^{-1} hour^{-1}
R_c	Rate of total colonisation	g^{-1} hour^{-1}
A	Root area	mm^2
R_r	Root growth rate	mm hour^{-1}
l^1	Root length at t	mm

Notation	Parameter	Unit
l^0	Root length at $t-1$	mm
k_c	Root surface carrying capacity	g^{-1}
Wt	Root wright	(g)
N	Sample size	NA
I	Sum of pixel intensities along the width of the channel	NA
y_b^i	The i^{th} prediction of bootstrap sample b	g^{-1}/ mm^{-3}/ $Log_{10}CFU\ ml^{-1}$
y_b^i	The i^{th} prediction of bootstrap sample b	g^{-1}/ mm^{-3}/ $Log_{10}CFU\ ml^{-1}$
y_m	The mean predicted bootstrap value at b	g^{-1}/ mm^{-3}/ $Log_{10}CFU\ ml^{-1}$
t	Time	s/ hour
y_c	Total colonisation density	g^{-1}
V_{field}	Volume of image	mm^3/ml

Chapter1. Introduction

Within soil, a complex web of biotic and abiotic interactions determines the extent to which different organisms grow and colonise plant roots. The ability of soil-borne bacteria and other microorganisms to detect, seek out, and colonise roots is a key factor in determining crop health and productivity, and through this determining food security. Quantifying, modelling, and understanding bacterial interactions with roots has been the topic of extensive research. The level of complexity involved in these interactions, along with the hidden nature of the soil environment means that there are numerous questions left to be answered. This chapter lays out an overview of root colonisation by microorganisms and the factors which influence it. It highlights the key gaps in our understanding of the factors which determine the timing and patterns of colonisation which the work presented in this thesis seeks to fill.

Soil as a microbial habitat

Soil is a mixture of solids, liquids, and gases which combine to form a dynamic and heterogenous environment. The solid phase comprises of organic and inorganic particles of a range of sizes and shapes, giving soil its structure. The gaps between particles form pores, which can contain air, or hold liquids through capillary forces (Peng, Horn and Hallett, 2015; Young *et al.*, 2008). Soil particles, and the gaps between them, range in scale by several orders of magnitude, from extremes of 1e-7 m for clays to more than 0.01 m for gravels (Peng, Horn and Hallett, 2015). The diversity of factors interacting to give a soil its properties leads to large numbers of soil types. While certain soil compositions and structures are well characterised, many are poorly documented (Rabot *et al.*, 2018). Soil properties can impact plant growth and microbial activity (Xue *et al.*, 2018; Baveye *et al.*, 2018; Quan and Liang, 2017). Assessments of the three-dimensional structure of soils can be made through electrical resistance tomography (Zhou, Shimada and Sato, 2001), laser scanning (Aguilar, Aguilar and Negreiros, 2009), or X-ray tomography (Pires *et al.*, 2019). Well established protocols are in place for assessing aspects of soil chemistry such as pH and nutrient availability (Carter and Gregorich, 2007). Modelling of soil structure, and how this influences factors such as water flow and gas exchange, have been carried out (Feyen *et al.*, 1998; Malamoud *et al.*, 2009). However, the influence of these factors on the distribution of microbial populations is poorly understood.

Soil is one of the most diverse microbial habitats on earth. It is estimated that one gram of bulk soil, which is outside the influence of plant roots, hosts 10^6 bacterial cells and thousands of taxa (Roesch *et al.*, 2007; Watt *et al.*, 2006; Raynaud and Nunan, 2014). Other microorganisms

are also well represented in soil, such as fungi which can constitute 10-30 % of soil mass (Sylvia *et al.*, 2005).

Closer to the root, in the region influenced by plant activity known as the rhizosphere, the abundance of microbial cells increases, with estimates of between 10^7 and 10^{12} bacterial cells per gram (Young *et al.*, 2008; Hu *et al.*, 2020). It has been shown that only a small proportion of the total soil volume (< 1 %) is suitable for microbial growth, due to a lack of space or nutrients (Kuzyakov and Blagodatskaya, 2015). The position of regions with conditions favourable for microbial growth varies with time as nutrients are introduced and consumed. As a result, microhabitats are created, which are hotspots of microbial activity relative to the bulk soil. Such hotspots are highly variable across space and time (Bach *et al.*, 2018; Kuzyakov and Blagodatskaya, 2015) (Figure 1.1). Hotspots range in size from 10 µm up to 10 mm, with the minimum size being determined by the volume necessary to sustain microbial colonies and the maximum size being determined by pore space and connectivity (Grundmann *et al.*, 2001; Dechesne *et al.*, 2003). Pausch and Kuzyakov (2011) showed that potential microbial hotspots in soil surrounding *Lolium perenne* varied from 2e-3 mm up to 10 mm in size though imaging of radioactive ^{14}C released into soil in the form of plant exudates. Other studies have achieved similar estimates of hotspot size through visualisation of microbial processes such as oxygen consumption (Blossfeld *et al.*, 2011). The duration of hotspots is similarly variable. Seasonal vegetation cycles, for example, lead to an increase in available nutrients which can last for months (Philippot *et al.*, 2009). The increased nutrient input from a passing root tip, however, will be determined by the rate of root growth, and utilisation of nutrients by microorganisms. Labelling studies have indicated that organic molecules necessary for microbial growth may persist in soil for 10-20 hours after input (Jones *et al.*, 2005). Pausch and Kuzyakov (2011) calculated the lifetime of hotspots created by the passing of a *L. perenne* root tip to be 1-3 days.

Soil microorganisms can be growing and actively foraging for food, but a significant fraction also remain dormant, due to unsuitable growth conditions. This leads to the formation of banks of microbial diversity within soil which can regenerate following changes to their environment, such as the introduction of nutrients as the result of root growth (Lennon and Jones, 2011). In hotspots, there may be two to 20 times more active bacteria than in bulk soil (Kuzyakov and Blagodatskaya, 2015).

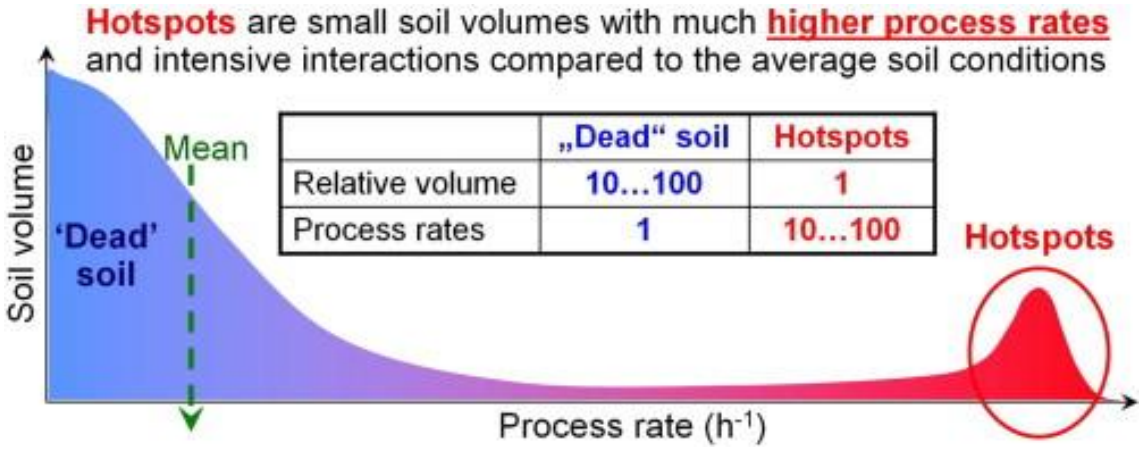

Figure 1.1. Hotspots represent a comparatively small volume of soil but are the location of a disproportionally large proportion of microbial processes. Microbial process rate here represent activities such as substrate utilisation and product formation. The green line represents the weighted average process rate in soil. For a hotspot to be present it is necessary to have the appropriate mix of both space and available nutrients, which is not present in the bulk 'dead' soil. Modified from Kuzyakov and Blagodatskaya (2015).

Traditional methods of studying microbial distributions in soil employ cross sectioning followed by culturing of viable microbes (Alexander and Jackson, 1954; Nunan *et al.*, 2003). Despite extensive efforts to develop cultivation techniques, as many as 99 % of microorganisms within soil cannot be reliably cultured (Bakken, 1997; Chaudhary, Khulan and Kim, 2019). As a result, modern assessments of microbial diversity in soil are reliant on molecular profiling of communities. Methods include sequencing of microbial marker genes, such as 16s rRNA for bacteria or the nuclear ribosomal internal transcribed spacer (ITS) region for fungi (Claesson *et al.*, 2010; Schoch *et al.*, 2012), or less selective shotgun metagenomic sequencing (Bulgarelli *et al.*, 2015; Sharpton, 2014). The heterogenous nature of the soil microbial community is often overlooked in assessments based on sequencing, resulting in an incomplete understanding of the soil ecosystem.

Bacterial interactions with plant roots

Plants interact with a complex microbiome of bacteria, fungi, archaea, and organisms from many other branches of the tree of life (de Faria *et al.*, 2021). Microorganisms can interact with plants in commensal, negative, or positive ways (Figure 1.2). Clear categorisation of these interactions is difficult, and highly variable based on a range of biotic and abiotic factors

(Schirawski and Perlin, 2018). Most interactions could be considered commensal with the microorganism benefitting, but no clear impact on plant health. Even in these cases, there may be undetected effects on plant health as commensal microorganisms compete with potential pathogens, plant growth promotors (PGPs), or pathogen supressing strains for resources (Berendsen, Pieterse and Bakker, 2012). For example de Boer *et al.* (2007) showed that a commensal community composed of *Pseudomonas* sp. and *Pedobacter* sp. supressed the growth of fungal pathogens *Fusarium culmorum* and *Rhizoctonia solani in vitro*.

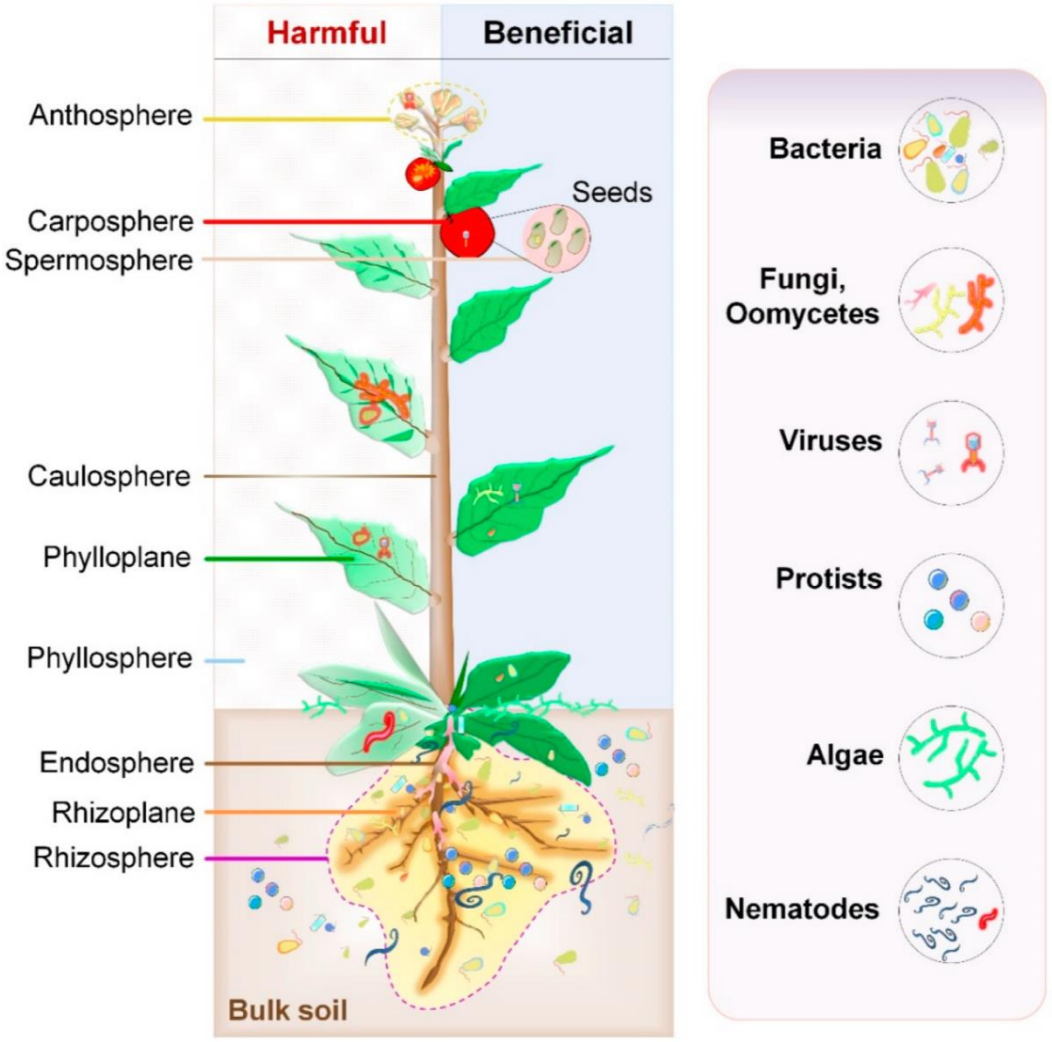

Figure 1.2. Schematic illustrating different plant associated habitats and the diversity of microorganisms which colonise these habitats and influence plant health. Modified from Shelake, Pramanik and Kim (2019).

A wide range of microbial plant pathogens exist across different taxa (Nazarov *et al.*, 2020; Savary *et al.*, 2019). They are responsible for the loss of up to 30 % of food grown globally (Savary *et al.*, 2019). Prior to 2010, kiwifruit (*Actinidia chinensis*) represented 68.5 % of New Zealand's fresh fruit exports, expected to be valued at approximately 1 billion USD by 2014. In 2010, a disease characterised by dieback in kiwi vines and loss of productivity, now known to be caused by the bacterial plant pathogen, *Pseudomonas syringae* pv. *actinidifoliorum*, was first reported in New Zealand. The same pathogen had caused an estimated 2 million EUR of damage in a single year in Italy following an outbreak in 2008. By 2014, the disease is

estimated to have caused more than 600,000 USD of damage to the New Zealand kiwi industry (Vanneste, Leach and Lindow, 2017). The root is an important region for infection by soil-borne plant pathogens, such as *Pseudomonas aeruginosa* and *Pseudomonas syringae (Walker et al., 2004b; Bais, Fall and Vivanco, 2004)*. *P. syringae* causes necrosis in the leaves and fruit of important crop plants, such as tomato (*Solanum lycopersicum*) (Arnold and Preston, 2019). Interactions between plants and pathogens are often highly specific (Sanguankiattichai *et al.*, 2019). The distinction between commensal and pathogenic microbial strains is often unclear, and highly dependent on environmental factors and plant health (Arnold and Preston, 2019; Wheeler, Dung and Johnson, 2019; Passera *et al.*, 2019).

Plant growth promoting (PGP) microorganisms can improve plant traits such as growth rate and stress tolerance (Berendsen, Pieterse and Bakker, 2012). The highly varied mechanisms through which they achieve these effects are the subject of numerous studies (Olanrewaju, Glick and Babalola, 2017). Some PGPs, such as bacteria in the genera *Rhizobium* are involved in the fixation of atmospheric nitrogen (Gage, 2004). PGPs, including members of *Pseudomonas* and *Bacillus*, can increase a plants ability to uptake nutrients (Egamberdiyeva, 2007). PGPs can also cause the upregulation of certain plant stress tolerance pathways (Vurukonda *et al.*, 2016). For example, Suarez *et al.* (2008) showed that the production of trehalose-6-phosphate by *Rhizobium etli* caused an upregulation of drought tolerance associated genes in common bean (*Phaseolus vulgaris*) resulting in an increase in yield of 50% under drought conditions. Pathogen supressing microorganisms, often referred to as microbial biocontrol agents, are antagonistic towards pathogens. They can act directly, for example by competing for resources or through the secretion of compounds. *Pseudomonas* spp., for example, produce a wide array of antimicrobial compounds (Haas and Keel, 2003). They can also act indirectly, for example by instigating a plant immune response (Audenaert *et al.*, 2002; Porcel *et al.*, 2014).

Plant root structure and function

Roots facilitate water and nutrient uptake by plants, as well as anchoring them in the ground. To achieve these functions, vascular plants have evolved a wide variety of root structures and mechanism of adaptation, enabling them to survive in diverse environments (Ryan *et al.*, 2016; Gašparíková, Mistrík and Čiamporová, 2002). Root architecture is varied and develops in response to the environment as well as interactions with microorganisms (Gamalero *et al.*, 2004b; Jovanovic *et al.*, 2007; Wojciechowski *et al.*, 2009). The root tip is one of the most

active areas of the root, and responsible for a disproportionate amount of water and nutrient uptake (Silk and Bogeat-Triboulot, 2014). Root tips can be divided into three key regions, with the region of division at the distal end of the root. This is a meristem in which cellular division is partially responsible for root growth. As the root grows, this region is the first area to encounter new environments. The region of division is crowned by the root cap, a loosely connected protective barrier of cells and gelatinous mucilage, composed primarily of complex polysaccharides (Knee *et al.*, 2001; Gašparíková, Mistrík and Čiamporová, 2002). The root cap is in an equilibrium between cell division and the loss of cells through sloughing (Kumpf and Nowack, 2015). Beyond the region of division, cell division and differentiation lead to the formation of vascular tissue, as well as protective layers known as the cortex and epidermis, in the region of elongation. Here, cell division progressively stops. Cell growth and elongation in this region is responsible for a large proportion of root growth. Beyond the region of elongation is the region of maturation (Figure 1.3). Here, root hairs develop, increasing the roots surface area and enabling water and nutrient uptake as well as a diverse range of other functions (Gašparíková, Mistrík and Čiamporová, 2002). The root surface, or rhizoplane, has a complex topology resulting from different root structures, such as epidermal cell junctions and root hairs (Schmidt *et al.*, 2018).

a)

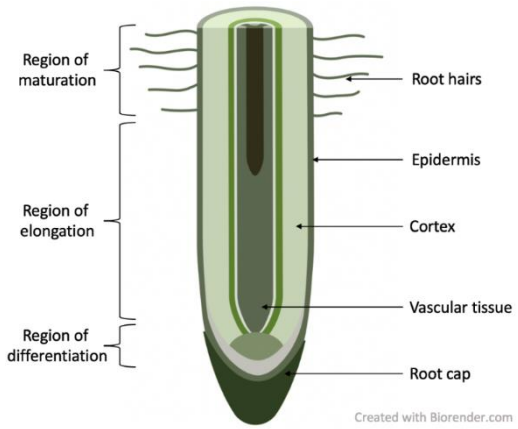

b)

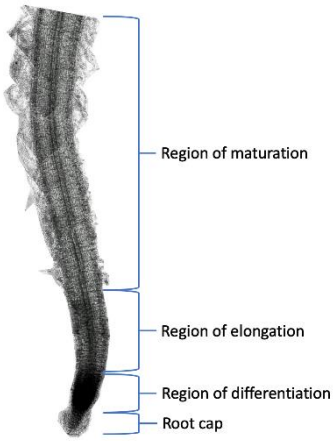

c)

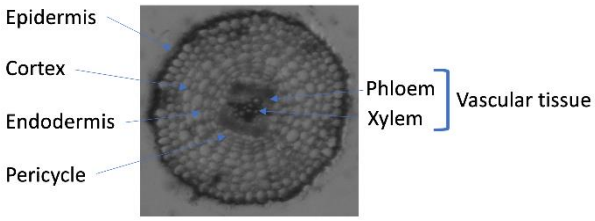

Figure 1.3. Diagram and images of the root tip. a) Diagram of a root tip, displaying root regions. b) Image of a lettuce root displaying root regions. c) Cross section of a lettuce root in the region of maturation.

Recent decades have seen the development of root phenotyping techniques and enabled the study of the development of root architectures (Wasson *et al.*, 2020). Root architectures can be observed at a single point in time by uprooting plants and washing away soil (Addo-Danso, Prescott and Smith, 2016; Box and Ramseur, 1993). Given the dynamic nature of root development, significant effort has been put into developing methods for observing the growth of living roots. X-ray and MRI can be used to observe live roots within natural soils, although contrast and resolution of these systems limit analysis of biological processes and are not sufficient to observe microbial activity (Pfeifer *et al.*, 2015; Atkinson *et al.*, 2019; Pflugfelder *et al.*, 2017). Greater insights, including the observation of microbial processes, can be obtained when imaging through artificial systems, such transparent gels (Jiang *et al.*, 2019), using a technique known as rhizotrons, which uses windows in soil to allow access to roots (Mao *et al.*, 2013), or using transparent soils (Downie *et al.*, 2015) (Figure 1.4). Gels offer a homogenous growing environment. This means that plant growth and bacterial processes can be more easily determined with lower levels of variance than is seen in heterogenous systems such as transparent soils (Massalha *et al.*, 2017; Downie *et al.*, 2015). However, the growing

environment of a plant heavily influences root architecture (Bengough *et al.*, 2011; Bingham and Bengough, 2003) and microbial colonisation patterns (Wieland, Neumann and Backhaus, 2001; Schreiter *et al.*, 2014), Artificial systems therefore inevitably trade high resolution imaging of roots for a decrease in biological relevance. The presence of particles, in particular, influences root architecture, slowing and altering the rate and direction of growth. In transparent soil, roots were found to thicken in response to force exerted by particles in opposition to the growing of a root. Deflection of the root also occurred in response to the 5% the most extreme opposing forces, with the overall result that the root developed a helical structure as it grew, which does not occur in gel (Martins *et al.*, 2019). Due to the influence of heterogeneity on root development, observations of plant and bacterial interactions in gel systems are limited to preforming comparative studies and models of processes developed or tested in these systems are unlikely to be useful for describing real world below-ground activities.

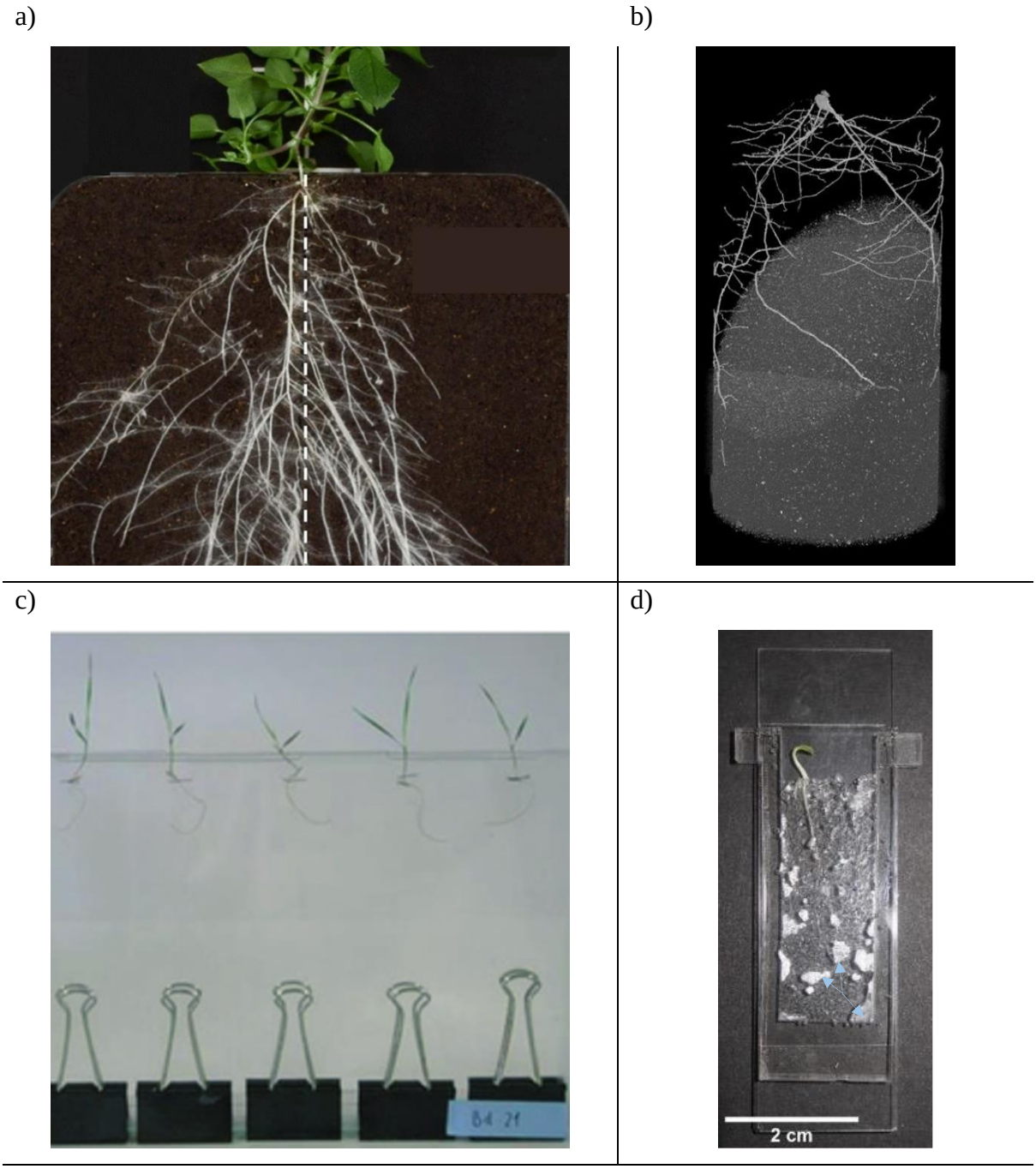

Figure 1.4. Methods for observing living roots. a) Rhizotrons are artificial windows in soil which allow access to the root. Modified from Tognacchini *et al.* (2020). b) X-ray-CT allows imaging of root architecture in natural soils; however, contrast and resolution of these systems limit analysis of biological processes. Modified from Atkinson *et al.* (2019). c) Gel media can be used to observe living roots growing in a homogenous environment. Modified from Gonazlez *et al.* (2016). d) Transparent soil allows visualisation of plant roots growing in a heterogenous environment.

The increasing availability of root architecture data has led to the development of models of root growth at varying degrees of complexity (Dupuy, Gregory and Bengough, 2010). These range from root depth models, which predict root depth and density within particular conditions (Gerwitz and Page, 1974; Mulia and Dupraz, 2006), to spatial models of root architecture, which predict the development of a root or root systems in two or three dimensions over time (Kalogiros *et al.*, 2016; Jiang *et al.*, 2019; Zhao *et al.*, 2017). Accounting for the influence of soil heterogeneity has been a challenge for models of root growth (Fakih *et al.*, 2019; Martins *et al.*, 2019). Only with recent developments in live imaging of roots has it become possible to couple such models with quantitative experimental data about microbial dynamics (Dupuy and Silk, 2016; Darrah, 1991c; Portell *et al.*, 2018). Models are useful tools for predicting plant growth traits but have yet to be fully integrated into modelling of bacterial processes in soil, beyond theoretical approaches.

Rhizodeposition and the formation of the rhizosphere

As plants grow through soil they release fluids, called exudates, lose cells, for example though root cap sloughing, and release mucilage. Generally, this release of material into the soil is referred to as rhizodeposition (Nguyen, 2003). The presence of roots changes the properties of a thin layer of soil. Rhizodeposition and nutrient exchange alter the chemical composition of the soil, leading to changes in both the microbiome and physical structure (Nuruzzaman *et al.*, 2006; Cooper *et al.*, 2018; Naveed *et al.*, 2017). Pressure from root growth can also lead to changes in structure and the increase in soil density around the root (Gobran, Clegg and Courchesne, 1998; Bodner, Leitner and Kaul, 2014). The resulting region under the influence of the root, termed the rhizosphere, is structurally, chemically, and functionally distinct from the bulk soil (Cooper *et al.*, 2018; Kuzyakov and Razavi, 2019) (Figure 1.5). Measurements of the rhizosphere vary across plant species and environmental conditions. Kuzyakov and Razavi (2019) state that it generally measures between 0.4 and 2 mm from the rhizoplane. As highlighted in Hinsinger *et al.* (2009), however, estimates of rhizosphere size vary depending on the definitions used and the soil process being examined. For example, early work establishing the definition of the rhizosphere studied the depletion of phosphorous around the root finding a zone of influence extended approximately 1 mm from the surface (Lewis and Quirk, 1967). The zone of potassium depletion, however, may be an order of magnitude greater (Jungk, 2002). Depending on the topic of a particular study, functional estimates of rhizosphere size can therefore vary greatly from the µm to mm scale (Figure 1.5) (Kuzyakov and Razavi, 2019).

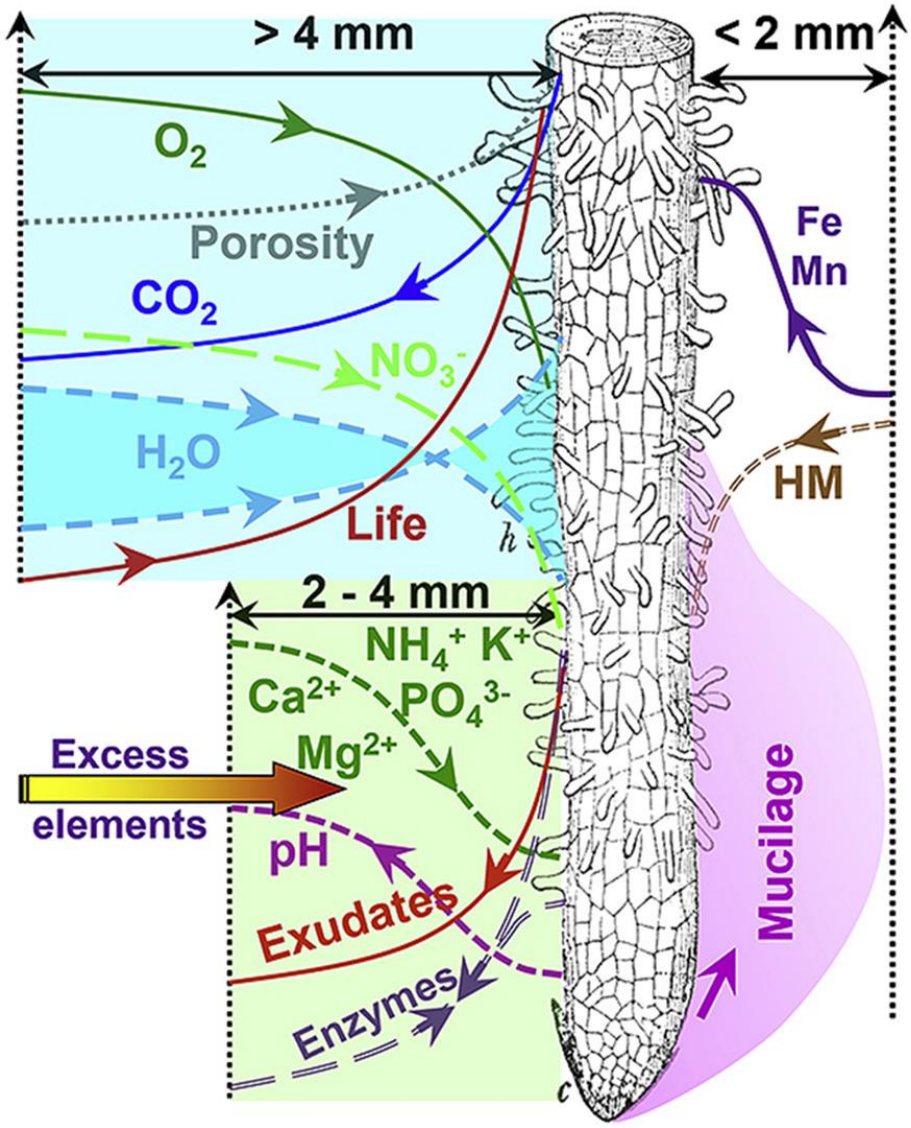

Figure 1.5. The root influences a thin layer of soil known as the rhizosphere. Root processes such as rhizodeposition, nutrient exchange, and growth all influence soil structure and composition. Modified from Kuzyakov and Razavi (2019).

Plant physiology, physical structure, and exudation patterns vary significantly across root regions (Kuzyakov and Blagodatskaya, 2015). As roots grow, the rhizosphere expands, certain areas mature, and new areas are created. Certain factors, such as exudate composition and volume, also vary based on plant circadian rhythms or change in response to stress (Hubbard *et al.*, 2018). As a result, the rhizosphere is a dynamic environment, in which successful maintenance of root colonisation by microorganisms necessitates the ability to detect and respond to changes in plant physiology.

Exudate composition and function

Between 20 and 40 % of the carbon which is assimilated by higher plants through photosynthesis is released as exudates (Badri and Vivanco, 2009). As a result, exudates, along with other forms of rhizodeposition, are a major source of available carbon and other nutrients for microorganisms within soil (Zhu *et al.*, 2014; Dennis, Miller and Hirsch, 2010). The majority of exudation is localised to the root tip (Sasse, Martinoia and Northen, 2018; Doan *et al.*, 2017). Exudates are a complex mix of sugars, polysaccharides, amino acids, peptides, and proteins (Hayat, Faraz and Faizan, 2017). They are composed mainly of primary metabolites, which are directly involved in normal plant growth and development, as well as a smaller proportion of secondary metabolites, which are not (Sasse, Martinoia and Northen, 2018; Jones, Nguyen and Finlay, 2009). Exudate composition varies between plant species and within species depending on growth stage and conditions (Williams *et al.*, 2021; Gargallo-Garriga *et al.*, 2018). For example, Neumann *et al*. (2014) analysed the relative abundance of 33 compounds in lettuce (*Lactuca sativa*) root exudates for plants grown in different soil types and found that each soil type led to distinct pattern of exudates. Tharayil and Triebwasser (2010) profiled exudation by knapweed (*Centaurea stoebe*) over 24 hours, and reported a consistent peak in the release of the secondary metabolite, catechin, six hours after exposure to sunlight.

The most basic function of exudates may be to dispose of excess carbon assimilated by the plant through photosynthesis. Exudates have a variety of other functions within the rhizosphere (Figure 1.6). They can either stabilise or weaken soil structure by gelling particles together or causing them to disperse (Naveed *et al.*, 2017). They can facilitate nutrient transport by increasing nutrient solubility (Dakora and Phillips, 2002). For example Brozostek *et al.* (2013) showed that extracellular enzymes released by roots in forest soils increased nitrogen-cycling. Exudates influence the fluid dynamics of soil, helping soil to retain moisture (Cooper *et al.*, 2018). They can also act as deterrents for pests, for example inducing a state of quiescence in plant-parasitic nematodes (Hiltpold, Jaffuel and Turlings, 2015).

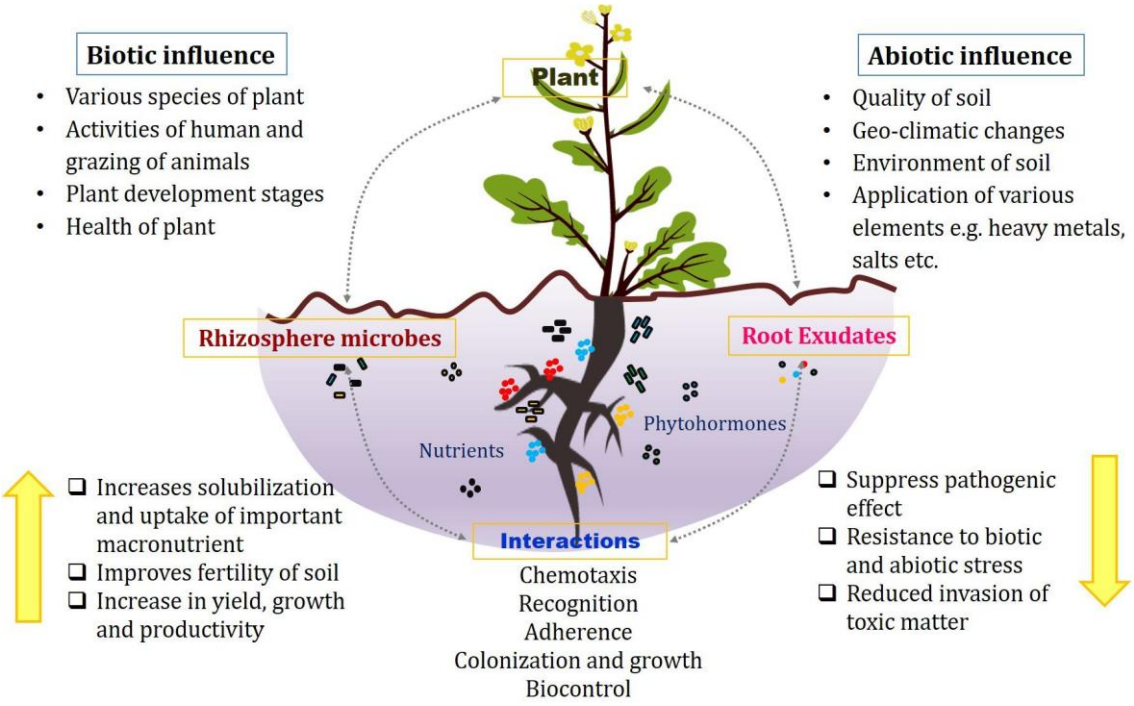

Figure 1.6. Schematic displaying the diverse range of functions plant root exudates have within soil. Modified from Vishwakarma *et al.* (2020).

Exudates contain specific signalling molecules which deter or recruit certain microorganisms to the rhizosphere, rhizoplane, or internal plant microbiome (Feng *et al.*, 2019; Feng *et al.*, 2018; Haichar *et al.*, 2014). For example, Feng *et al.* (2018) tested 98 components of root exudate and found that 39 of them acted as an attractant and five as a repellent for the plant growth promoting strain *Bacillus amyloliquefaciens* SQR9. Badri *et al.* (2013) suggested that sugars and amino acids were attractants for broad range microorganisms, increasing overall bacterial richness, while phenolic compounds recruit more specific taxa. Exudate composition changes in response to stress, leading to changes in the microbial community (Naylor and Coleman-Derr, 2018; Preece and Penuelas, 2016). Changes in the amount of exudate produced have been reported after a single day of drought stress and the effects can remain for months after the stress is removed (Gargallo-Garriga *et al.*, 2018; Preece *et al.*, 2018), however, the exact dynamics of these changes are not yet quantified due to the challenge of accurately assessing exudate production (Brunner *et al.*, 2015). Similarly, time courses quantifying the change in microbial composition in response to shifts in exudate composition are not available.

It can be confirmed that there are significant changes in the mass and composition of the rhizosphere community within a week of exposure to drought (Fuchslueger *et al.*, 2014).

Due to differences in molecular size and solubility, components of exudates are transported away from roots at different rates, with soil structure playing a large role in determining this. Proctor and He (2021) modelled the transport of organic compounds away from the root and predicted a difference of close to two orders of magnitude between glycine (0.31 nmol cm^{-1} $hour^{-1}$) and tartrate (7.98 nmol cm^{-1} $hour^{-1}$). The rate at which exudates are released, along with their diffusion into the soil, can be analysed through radioactive C^{14} imaging or soil sectioning (Sauer, Kuzyakov and Stahr, 2006; Darrah, 1991a). Collection and analysis of exudates can be achieved through a variety of methods, all of which risk influencing exudate composition (Vranova *et al.*, 2013b; Oburger and Jones, 2018). Plants can be grown in hydroponic systems and then transferred to liquid media and soaked for a set period, with the resulting solution containing exudates being collected (Giles *et al.*, 2017; George *et al.*, 2004; Kawasaki *et al.*, 2018). Using rhizotrons or soil cores, the exudates from specific sections of the root can also be sampled (Phillips, Finzi and Bernhardt, 2011; Shi *et al.*, 2011). Once collected, exudate composition can be analysed through high-performance liquid chromatography (HPLC) (Giles *et al.*, 2017) or other forms of chromatography (Monchgesang *et al.*, 2016).

The ability of exudate compounds to diffuse though soil, known as their diffusivity, have been measured (Kuzyakov, Raskatov and Kaupenjohann, 2003; Darrah, 1991a). This has been incorporated into models of exudation (Cooper *et al.*, 2018; Toal *et al.*, 2000; Proctor and He, 2021) and bacterial colonisation of roots (Dupuy and Silk, 2016). However, no comprehensive review or model of exudate diffusion in different soil systems is available.

The rhizosphere microbial community

The rhizosphere microbial community is taxonomically and functionally diverse. It is distinct from the bulk soil, usually containing higher cell numbers, less diversity, and higher levels of specialisation (Berg and Smalla, 2009). The movement of roots through soil creates hotspots of microbial activity as they release nutrients, with the area of highest activity being at the root tip. As discussed above under *soil as a microbial habitat*, these last for 1-3 days and follow the movement of the root (Pausch and Kuzyakov, 2011). The complex movement of water and solute through the granular structure of soils induced by root growth creates a heterogeneous and highly compartmentalised habitat (Kuzyakov and Blagodatskaya, 2015).

Within the rhizosphere, certain microbial strains form closer associations with roots, colonising the rhizoplane and becoming epiphytes. Others will enter the root, establishing themselves in the space between cells, the apoplast, and becoming endophytes. For soil-borne microorganisms, successful establishment in the rhizosphere, colonisation of the rhizoplane, and potentially internalisation and translocation within plant tissue, are the first steps towards becoming established in the plant microbiome (Walker *et al.*, 2004a; Berggren *et al.*, 2005). Many PGPs and microbial biocontrol agents colonise the root surface. From here they impact plant physiology or interact with potential pathogens (Shinde *et al.*, 2019; Köhl, Kolnaar and Ravensberg, 2019). By colonising the rhizosphere, soil-borne pathogens of humans and other animals can enter the food chain (Wright *et al.*, 2017; Holden, Pritchard and Toth, 2009). Inoculation of crops with PGPs has been a suggested method for improving plant growth and resilience without the need for increased chemical treatments (Berendsen, Pieterse and Bakker, 2012; Busby *et al.*, 2017). Unfortunately, integration of these approaches into agricultural systems has been slow, partially due to issues with maintaining target strains in association with roots (Bashan *et al.*, 2014; Vejan *et al.*, 2016).

The rhizoplane community is taxonomically distinct from the rest of the rhizosphere (Wieland, Neumann and Backhaus, 2001). At or near the rhizoplane, competition is intensified as microbes seek space in which to establish themselves. In this region, plant-derived substrates are immediately available to microbial-colonisers, providing a nutrient rich environment (Schmidt *et al.*, 2018). Microbes on the rhizoplane likely experience unique stresses resulting from physical forces as roots move through soil, although this is not well researched (Dupuy and Silk, 2016). Microbes secrete a diverse array of metabolites which can influence plant physiology (Olanrewaju, Glick and Babalola, 2017). Metabolites secreted from microbes on the rhizoplane are immediately available to plants. Despite clear benefits to rhizoplane colonisation, only a small proportion (0.4 – 3.5 %) of bacterial populations usually form attachments with roots, although this can be significantly higher (Rodriguez-Navarro, Dardanelli and Ruiz-Sainz, 2007).

The rhizoplane colonisation processes

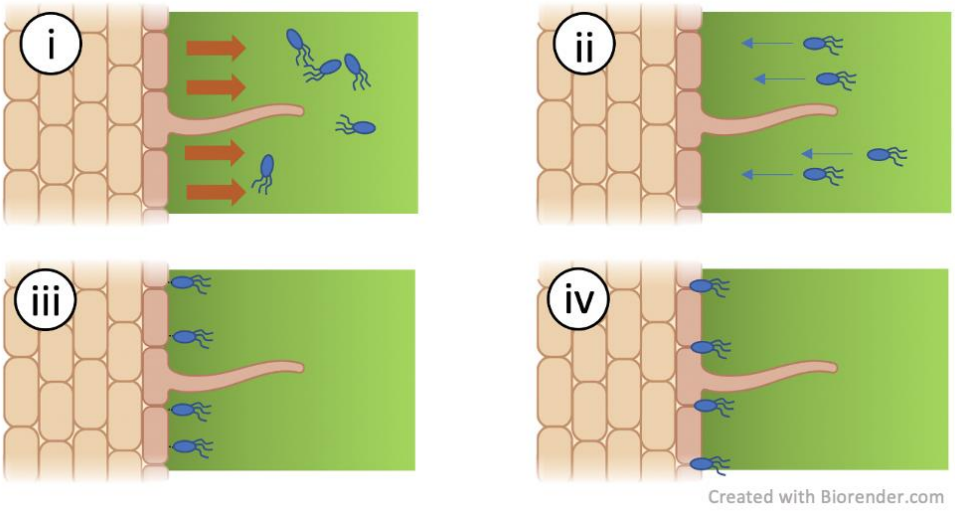

Figure 1.7. The stages of rhizoplane colonisation. i) Chemoattractants are release into the soil by the root in the form of exudates, mucilage, and sloughing root cap cells, establishing a concentration gradient. ii) Microorganisms detect these chemoattractants and respond through chemotaxis, the directional movement in response to a concentration gradient. iii) Microorganisms establish weak primary attachment to the rhizoplane. iv) Microorganisms establish strong secondary attachment to the rhizoplane. This may be followed by biofilm formation, or translocation into the root interior.

The first stage in rhizoplane colonisation is the detection of plant signalling molecules by soil-borne microorganisms (Figure 1.7) (Knights *et al.*, 2021; Rodriguez-Navarro, Dardanelli and Ruiz-Sainz, 2007). The ability of different taxa to detect and respond to a wide array of plant metabolites has been well documented (Feng *et al.*, 2018; de Weert *et al.*, 2002). Microorganisms then respond to these signalling molecules through chemotaxis, the directional movement in response to a concentration gradient (Hubbard *et al.*, 2018). The release of chemoattractants is variable with time, often following plant circadian rhythm. In maize (*Zea mays*) for example exudation during the day was found to be 1.5 times higher than at night (Kuzyakov, Raskatov and Kaupenjohann, 2003).

Numerous studies have shown that the inactivation of pathways responsible for chemotaxis or motility in bacteria results in reduced rhizoplane colonisation (de Weert *et al.*, 2002; Allard-Massicotte *et al.*, 2016; Knights *et al.*, 2021). The role that microbial movement on the root surface plays in establishing or maintaining colonisation levels has yet to be fully explored.

For *P. fluorescens*, 17 methyl accepting chemotaxis proteins responsible for the detection of components of rhizodepositions, such as malate and succinate were determined by Oku *et al.* (2014). They showed that mutants with higher levels of expression of the Pfl01_0728 and Pfl01_3768 genes, involved in the production of these chemotaxis proteins, were more competitive when colonising tomato roots. Oku *et al.* (2012) showed that *Pseudomonas fluorescens* mutants, which had low expression of *ctaA*, *ctaB*, and *ctaC* genes involved in the detection of amino acids, were less competitive when colonising tomato roots than the wild type. de Weert *et al.* (2002) showed that motility in *P. fluorescens* during colonisation of roots is based on a chemotactic response to exudate components by comparing the colonisation efficiency of cheA mutants, which maintained their motility but did not exhibit flagella-driven chemotaxis. They found that mutants were rapidly outcompeted by wild type bacteria.

The two most commonly observed mechanisms for bacterial motility involve swimming or swarming across surfaces using flagella (Alexandre, 2015; Kearns, 2013) and 'twitching motility' caused by the successive attachment and shortening of pili, allowing for movement across surfaces (Semmler, Whitchurch and Mattick, 1999). The energetic cost of these forms of motility increases in more viscous environments and may be replaced with the movement of smaller protein structures on the cell surface (Miyata *et al.*, 2020; Nan *et al.*, 2014). There are certain other taxa specific bacterial motility mechanisms, such as the movement of the cyanobacterium *Synechococcus* which forms waves in a viscous layer surrounding the cell, putting pressure on the surrounding media and propelling the cell forward at rates of up to 25 μm s^{-1} (Ehlers and Oster, 2012). Ping, Birkenbeil and Monajembashi (2013) described the mechanism for the flagella mediated movement of *P. fluorescens* SBW25 based on the observation of individually bacterial cells moving through a chemotactic medium. They note that *P. fluorescens* SBW25 generally has a single flagellum, although there is some variation in this. *P. fluorescens* is the one of the fastest swimmers in the *Pseudomonas* genus, moving at a maximum speed of 102.0 μm s^{-1} and capable of complex patterns of movement such as backing up and rapid changes in direction (Ping, Birkenbeil and Monajembashi, 2013).

Both bacterial cells and the root are generally negatively charged, meaning cells must overcome electrostatic repulsion before reaching the root surface (Figure 1.7) (Kendall and Roberts, 2015; Berne *et al.*, 2015). On arriving at the rhizoplane, the second stage in colonisation is primary attachment, resulting in the formation of weak bonds between microbes and roots (Rodriguez-Navarro, Dardanelli and Ruiz-Sainz, 2007; Knights *et al.*, 2021). Binding

through plant-lectins, bacterial binding proteins, and bacterial surface polysaccharides are involved in this step (Rodriguez-Navarro, Dardanelli and Ruiz-Sainz, 2007). Factors such as the major outer membrane protein (MOMP) have been implicated in the primary attachment of *P. fluorescens* to the rhizoplane (De Mot and Vanderleyden, 1991). *P. fluorescens* mutants which do not express the OprF gene, responsible for MOMPs, show reduced attachment to cucumber roots (Crespo and Valverde, 2009). Beyond overcoming electrostatic repulsion, bacterial organelles generally involved in movement, such as flagella and pili, play an important role in primary attachment, allowing bacteria to bind to surfaces and seek out favourable attachment sites (Rossez *et al.*, 2015; Rossez *et al.*, 2014).

The third stage in colonisation is strong, secondary attachment, (Figure 1.7) (Rodriguez-Navarro, Dardanelli and Ruiz-Sainz, 2007; Knights *et al.*, 2021). For bacteria, this involves the production of cellulose fibrils, alongside extracellular proteins, and polysaccharides (Martinez-Gil, Yousef-Coronado and Espinosa-Urgel, 2010; Matthysse, 1983). Microbial replication can then lead to the formation of microcolonies. For certain microbial strains, this will be followed by the development of biofilms, in which cells are embedded in an external matrix of polymeric compounds (Tomlinson and Fuqua, 2009; Noirot-Gros *et al.*, 2018). In gram-negative bacteria like *P. fluorescence* SBW25, biofilm formation is largely controlled by the GacA/S regulatory system (Gooderham and Hancock, 2009; Noirot-Gros *et al.*, 2019). GacS is a membrane bound sensor protein which is paired with a response regulator, GacA (Gooderham and Hancock, 2009). The GacA/S system can trigger the production of small regulatory RNAs; RsmZ and RsmY leading to changes in gene regulation and a signalling cascade which leads to biofilm formation (Tahrioui, Quesada and Llamas, 2013; Valverde *et al.*, 2003). Inactivation of either of the components of the GacA/S system reduces the production of extracellular polymers involved in biofilm formation, such as alginate and cellulose (Hassan *et al.*, 2010; Heeb and Haas, 2001; Noirot-Gros *et al.*, 2019). The wrinkly spreader genotype of *P. fluorescence* SBW25 overproduces a cellulosic like polymer (CLP), leading to a unique thick wrinkled appearance of colonies at the air-liquid interface compared to the usually smooth appearance of *P. fluorescence* SBW25 (Spiers *et al.*, 2003; Spiers, 2007; Bantinaki *et al.*, 2007). Spiers *et al.* (2002) showed that *P. fluorescence* SBW25 mutants which underproduced CLP lacked the ability to colonise the air-liquid interface. Spiers *et al.* (2003) showed that the level of acetylation of this cellulose also determines the expression of the wrinkly spreader phenotype and ability to colonise the air-liquid interface. The temporal dynamics of *P. fluorescence* SBW25 biofilm formation on plant roots were directly investigated by (Noirot-Gros *et al.*

(2018) through imaging and shown to pass through several distinct morphological stages as colonisation progressed, beginning with isolated microcolonies, and ranging up to dense and highly structured biofilms.

For certain strains, internalisation into the root endosphere will follow. Haptotaxis, directional growth in response to a concentration gradient, may also cause shifts in colonisation patterns (Roy *et al.*, 2017). The transition from primary to secondary attachment is often marked by distinct changes in microbial protein expression (Knights *et al.*, 2021). For example, the production of large adhesion proteins (LapA and LapD) marks the change from primary to secondary attachment for *P. fluorescens* and mutation of the large adhesion protein; LapD, causes a reduction in biofilm formation during static biofilm assays (Hinsa *et al.*, 2003; Hinsa and O'Toole, 2006).

Following successful colonisation of the rhizoplane, detachment and dispersal of microbial cells or colonies from the root surfaces likely plays a key role in determining rhizosphere community composition, as it allows for the shift in bacterial density on the root (Shimshick and Hebert, 1979; Richter-Heitmann *et al.*, 2016). The level to which disassociation of attached bacteria from the root influences colonisation levels or patterns is currently unknown. Although many aspects of rhizoplane colonisation have been studied in isolation, quantitative methods for recording or predicting the timing of the different stages outlined above have not been developed.

Factors influencing colonisation

Environmental control over colonisation

Numerous in-depth studies of plant signalling molecules, microbial chemotactic pathways, and adherence factors have been carried out (Knights *et al.*, 2021; Rodriguez-Navarro, Dardanelli and Ruiz-Sainz, 2007). Agriculturally important rhizosphere strains, such as the plant growth promotor *P. fluorescens*, have been a key focus for these studies (Humphris *et al.*, 2005; Turnbull *et al.*, 2001). Even in cases where the molecular components of colonisation are well understood, the success, timing, and spatial distribution of microbial colonisation of the rhizoplane remains unpredictable. Observations of trends in colonisation along the length of the root, as well as at smaller scales in relation to individual root epidermal cells or hairs are common (Schmidt *et al.*, 2018; Noirot-Gros *et al.*, 2018; Gamalero *et al.*, 2004a). The conditions which determine the favourability of attachment sites on the root are largely unknown.

Soil plays a large role in determining colonisation rates and patterns. Particle size influences the ability of chemoattractants to diffuse, and bacteria to more towards the root (Wieland, Neumann and Backhaus, 2001; Sood, 2003; Schreiter *et al.*, 2014). The influence of these factors on colonisation have not been fully described experimentally. Soil pH, water availability, and chemical composition also influence colonisation, particularly during primary attachment which is closely linked with electrostatic and hydrophobic interactions between microbial cells and the rhizoplane (Demoling, Figueroa and Baath, 2007; Kendall and Roberts, 2015; Knights *et al.*, 2021). The physical structure of the root also plays a key role. For soil-borne microorganisms, the rhizoplane is the first point of physical contact with the plant. The association between root cell structures, such as epidermal cell junctions and hairs, and high levels of colonisation has been noted for numerous taxa across different plant species and growing conditions (Schmidt *et al.*, 2018; Noirot-Gros *et al.*, 2018; Gamalero *et al.*, 2004a). Noirot-Gross *et al.* (2018) reported heavy colonisation of epidermal cell junctions on aspen (*Populus tremuloides*) roots by *P. fluorescens* isolate SBW25. Schmidt *et al.* (2018) showed an association between bacterial colonisation and cell junctions for *Kasakonia sacchari* on rice (*Oryza sativa*) roots. While these patterns may be the result of differences in nutrient availability, they could also be due to physical shielding of microbial colonies from the stresses associated with the rhizoplane. The result may be that, of the surface area of the root, only a small proportion is available for colonisation. This is not something which has been widely investigated. To isolate the impact of physical structures from the chemical component of colonisation, abiotic surfaces that mimic root structure can be created (Kumari, Sayas and Kleiman, 2020). However, given the close relationship between root surface chemistry and microbial adhesion, such approaches have limited value. The exact role of the root cap in determining rhizoplane colonisation is not known. Humphris *et al.* (2005) demonstrated that the removal of the root cap led to increased colonisation of wheat (*Triticum aestivum*) root tips by *P. fluorescens*. However, it is difficult to separate the impact of the loss of the physical structure from the potential increase in chemoattractants in the vicinity of damaged plant tissue, or slowing of root growth rate, both of which can increase colonisation (Watt, McCully and Kirkegaard, 2003; Wheatley and Poole, 2018).

Plant control over colonisation

Plants exhibit a great degree of control over the rhizosphere microbial community. Root growth rate can affect colonisation dynamics and patterns (Watt, McCully and Kirkegaard, 2003; Watt, Silk and Passioura, 2006). Certain rhizodepositions lead to specific attraction of microbial

strains (Schlaeppi *et al.*, 2014; Yin *et al.*, 2021). Plants also reward certain microbial strains or sanction others through modulation of nutrient availability or antimicrobial production (Besset-Manzoni *et al.*, 2018; Wendlandt *et al.*, 2019; Westhoek *et al.*, 2021). In legumes, the nutrients allocated to rhizobia in nodules has been directly related to the success of those nodules in nitrogen fixation (Kiers *et al.*, 2003).

Plants immune responses determine colonisation. Plants and microorganisms are in a constant state of molecular dialogue. Plants must discriminate between harmful and beneficial microorganisms (Romano, Ventorino and Pepe, 2020). The success of all microbes on the rhizoplane, including PGPs and pathogens, is reliant on avoiding triggering a plant immune response. Induced immune responses are associated with the presence of an elicitor, which is a stimulus that leads to a response from the plant. Plant cells have pattern recognition receptors (PRRs) on their surfaces which enable them to detect a wide variety of molecular patterns associated with microbes, such as bacterial flagella. Many of these microbe-associated molecular patterns (MAMPs) are tightly conserved across species. A subset of MAMPs are pathogen associated molecular patterns (PAMPs), which are associated with the detection of pathogens. In response to a pathogen, or an abiotic stress, damage associated molecular patterns (DAMPs) may be produced, which can be detected by PRRs in other areas of the plant (Henry, Thonart and Ongena, 2012; Boller and Felix, 2009).

Plant immune responses in the root are distinct from those observed above ground (Chuberre *et al.*, 2018). Despite roots being a point of infection for many economically important plant pathogens, the immune response in roots is poorly understood relative to that in aboveground structures. Immune responses include the release of phytohormones and DAMPs, production of antimicrobial reactive oxygen species, callose deposition, or modifications to the cell wall, among others (Chuberre *et al.*, 2018). As with other aspects of root biology, immune responses are highly dynamic, changing with root region, tissue, and time of day (Li *et al.*, 2020; Chuberre *et al.*, 2018). This reflects the variable morphology of the root. The region of division, for example, has strong mechanical defences against infection in the form of the root cap and mucilage. The region of elongation lacks this, and other mechanical defences present in more mature sections of root. During trial infections of pea (*Pisum sativum*) with the fungal pathogen *Nectria haematococca*, the region of division remained free of infection while the region of elongation displayed high levels (Gunawardena and Hawes, 2002). Elevated levels of PRRs have been reported in the region of elongation, likely compensating for the mechanical

vulnerability of the region (Beck *et al.*, 2014). The production of jasmonic acid, which is required for the induction of many plant immune responses, has been shown to follow a cyclical production pattern with reduced production at night (Karapetyan and Dong, 2018). This may be related to the reduction in exudation at night (Kuzyakov, Raskatov and Kaupenjohann, 2003) leading to fewer interactions between plants and soil borne microorganisms.

Rhizoplane colonising microbes can modulate the plant immune responses. Pathogens inject effectors directly into plant cells through a variety of secretion systems, which allow them to interfere with the immune responses triggered by PRRs (Trivedi and Wang, 2014; Castaneda-Ojeda *et al.*, 2017). The potential for complex interactions between pathogen effectors and plant immune responses leads to an evolutionary arms race concept named the 'zigzag model' by Jones and Dangel (2006). Immune responses can also be supressed by alterations to the root environment, such as a lowering of pH (Yu *et al.*, 2019). Certain beneficial microbial strains, such as beneficial *Pseudomonas* spp., trigger plant immune responses through secretions, interfering with other root colonising organisms and reducing competition (Bakker, Pieterse and van Loon, 2007).

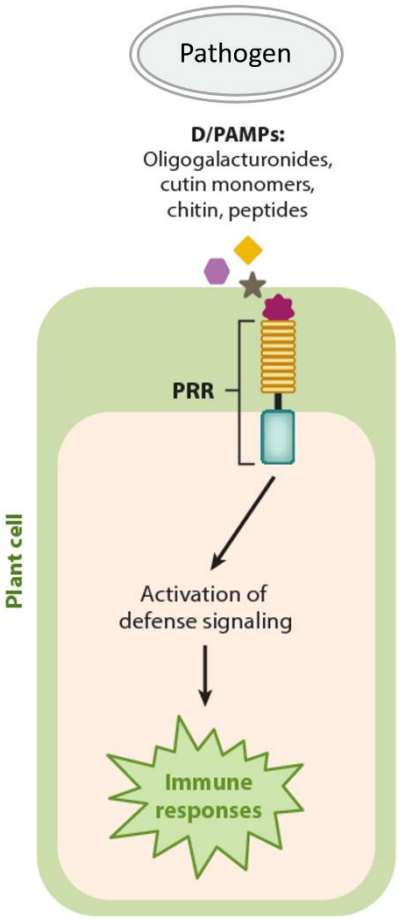

Figure 1.8. Schematic displaying the triggering of a plant immune response by molecular patterns. Pathogen associated molecular patterns (PAMPs) and damage associated molecular patterns (DAMPs) are detected by pattern recognition receptors (PRRs), leading to a plant immune response which can include the release of phytohormones and DAMPs, production of antimicrobial reactive oxygen species, callose deposition, or modifications to the cell wall**.** Modified from Mengiste *et al.* (2012).

Microbial competition and cooperation

For certain microbial strains, colonisation of the rhizoplane may be a strategy by which resources can be monopolised. As a result, levels of competition and antagonism between microbes on the rhizoplane are high. Observed colonisation patterns, such as dense biofilm formation, may be a mechanism for excluding other strains (Velmourougane, Prasanna and Saxena, 2017). Secretion of antimicrobial compounds also plays a role in competitive colonisation (Lugtenberg and Kamilova, 2009). Certain *Pseudomonas* spp., for example, secrete the antibiotic and biofilm instigator phenazine, among others (Haas and Keel, 2003;

Dietrich *et al.*, 2013). Such secretion is highly dependent on a wide array of environmental conditions, with examples including temperature, the metabolic conditions of microbial cells, and irrigation status (Haas and Keel, 2003; Raaijmakers, Vlami and de Souza, 2002; Mavrodi *et al.*, 2012). Massalha *et al.* (2017), for example showed that an increase in the density of a population of *Bacillus subtilis* near the root led to a proportional decrease in the density of a population of *Escherichia coli* (Figure 1.9).

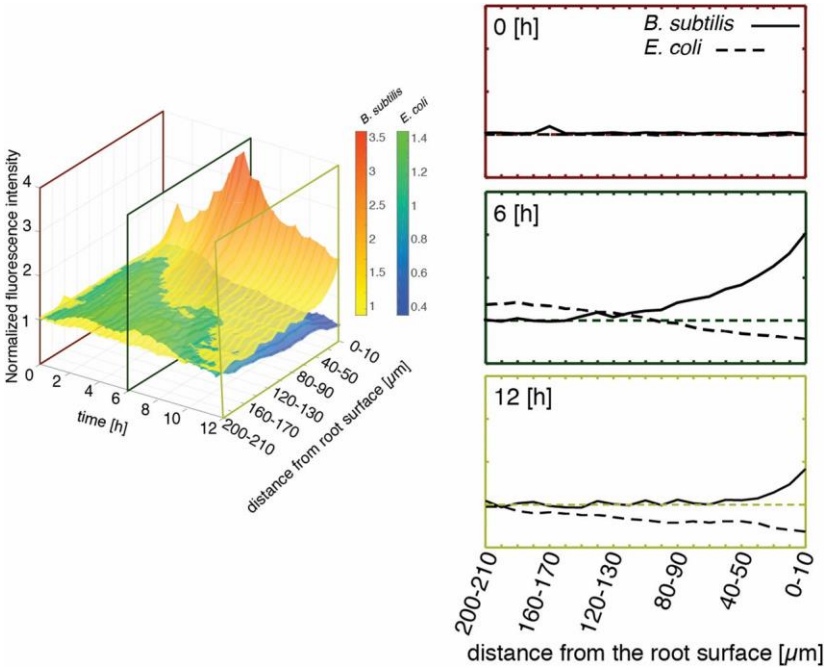

Figure 1.9. The increase in fluorescent signal as the result of a population of *Bacillus subtilis* near the root was associated with a decrease in the fluorescent signal as the result of a population of *Escherichia coli*. Modified from Massalha *et al.* (2017).

Other microbe-microbe interactions may involve cooperation (Besset-Manzoni *et al.*, 2018). Rhizoplane biofilms regularly contain multiple species and strains with no observed antagonism between them. Bogino *et al.* (2013), for example, reported approximately 95 bacterial strains present in biofilms on the surface of Alfalfa (*Medicago sativa*) roots. Within a microbial community, such diversity can lead to specialised functions and 'division of labour' between strains (Costa, Perez and Kreft, 2006; Besset-Manzoni *et al.*, 2018). Such organisation is a common occurrence for nitrogen fixing bacteria. During nitrification, ammonia is oxidised to nitrate. This is a two-step process beginning with the oxidation of ammonia to nitrite

followed by the oxidation of nitrite to nitrate. The two steps of this process are carried out by members of distinct bacterial clades within Proteobacteria (Costa, Perez and Kreft, 2006). It may also be beneficial to the plant to recruit multiple cooperating plant PGP strains as they can perform different functions. Vacheron *et al.* (2016) noted that, of the diverse range of plant beneficial functions performed by *Pseudomonas* spp. associated with maize (*Zea mays*) roots, only a small number were performed by each individual strain.

Quantifying rhizoplane colonisation

Given the inaccessibility of the soil environment, studying rhizoplane colonisation inevitably means interfering with it in some way. Traditional methods focus on quantifying the success of selected strain on the rhizoplane at set time points through cell counts (Mills and Bauer, 1985; Albareda *et al.*, 2006; Gamalero *et al.*, 2003). Such methods are destructive and, while effective for studying individual plant-microbial interactions, risk losing some of the nuance of the colonisation process which results from microbe-microbe interactions. The ability to profile microbial communities through sequencing means that a greater breadth of the diversity present on the rhizoplane can now be quantified (Gamalero *et al.*, 2003). These methods can still miss the spatiotemporal dynamics which result in complex patterns of colonisation observed on the rhizoplane. Increasingly, emphasis is being placed on the importance of understanding the rhizosphere as a dynamic system in order to predict the dynamics of microbial growth and the impact this might have on plant health (Kuzyakov and Blagodatskaya, 2015). Over recent years, advances in live imaging of roots have presented the opportunity to study the colonisation process in living roots as it develops (Downie *et al.*, 2015; Massalha *et al.*, 2017). Such methods retain some of the issues of earlier quantification methods relating to reduced complexity. As they are artificial, they lack the complex community of microorganisms which interact in soil. Tight control over experimental conditions is necessary to generate statistically relevant data. This means that fluctuations in abiotic conditions, such as temperature, light, and water flow, which determine colonisation patterns in natural soils do not occur.

Modelling bacterial processes

Microbial activities are inherently complex processes. Developing mathematical models contributes towards enabling these processes to be described, predicted, and better understood (de Jong *et al.*, 2017). Accurate models of rhizoplane colonisation could help to explain the formation of observed patterns. They can help predict the risk of rhizoplane colonisation by

plant or animal pathogens under certain environmental conditions. This information can be integrated into risk management strategies, for example by determining the appropriate level of chemical treatments for a disease given weather conditions (De Wolf and Isard, 2007; Pertot *et al.*, 2017). For PGPs and microbial biocontrol agents, modelling the colonisation process could help to select strains which will be successful under field conditions (Strigul and Kravchenko, 2006). The diverse range of interacting factors involved means that a systems approach to understanding and modelling microbial colonisation of rhizoplanes is needed. A common theme noted alongside the publication of models of any soil or rhizosphere process is that such models need to be parameterised and tested based on solid experimental data, which has been lacking in the past (Toal *et al.*, 2000; Dupuy and Silk, 2016).

Models of microbial growth have been utilised across many disciplines of microbiology for decades. At their most basic, they describe the growth of a microbial population based on core parameters such as division rate, mortality rate, and carrying capacity (Tsoularis and Wallace, 2002). More complex growth models can account for the influence of environmental conditions such as heat, pH or nutrient availability on the physiological state of a microbial population (Monod, 1966; Richards, 1959). Such models have been applied to the growth kinetics of bacteria in the rhizosphere and on the rhizoplane (Strigul and Kravchenko, 2006; Baranyi and Roberts, 1994).

The purpose of growth modelling is to predict the rate of change of a population under specific environmental conditions. Bacterial growth, along with many other biological processes, often follows a sigmoidal trajectory. The specific model which is best suited to predict this trajectory will depend on the data available, along with the aim of the study. Where there is no clear biological or technical reason for the selection of a specific model, multiple models are often fit to data and a measure of the relative error of each fit, such as Akaike Information Criterion (AIC) used to select the best (Pla *et al.*, 2015; de Jong *et al.*, 2017). In this thesis, four classic equations describing bacterial growth were used.

The logistic equation (Equation 1.1) (Tsoularis and Wallace, 2002), and Gompertz equation (Equation 1.2) (Gibson, Bratchell and Roberts, 1988) are the most simple of these, expressing the rate of change of bacterial density (y) with time (t) based on a carrying capacity (k), initial density (y^0), and maximum growth rate (μ) with the solutions in the form:

$$y = \frac{ky^0}{y^0 + (k - y^0)e^{-\mu t}}$$ Equation 1.1

$$y = ke^{\ln\left(\frac{y^0}{k}\right)e^{-\mu t}}$$ Equation 1.2

The relative simplicity of the logistic equation enables easy manipulation of formula and integration into calculations of other parameters, as is seen in Chapter 3 in which it is used to independently calculate bacterial attachment and proliferation rates on the rhizoplane. The logistic equation describes symmetrical growth, in which the change in growth rate at the beginning and end of the exponential phase are equal. The Gompertz equation describes asymmetric bacterial growth, with the decline in growth rate approaching k being more gradual than the increase seen at the beginning of the exponential phase. Selection between these two models will depend on the symmetry of observations during growth. Both lack a specific parameter defining the lag period prior to exponential growth and are relatively inflexible regarding environmental changes, which may alter parameters, such as the maximum bacterial population, defined by k.

The Baranyi equation (Equation 1.3) (Baranyi and Roberts, 1994) predicts the rate of change of bacterial density (y) with time (t) based on a carrying capacity (k), initial density (y^0), maximum growth rate (μ), and (h^0) which specifies the length of the lag phase with the solution in the form:

$$A = t + \frac{1}{\mu}\ln\left(e^{(-\mu t)-\mu t} + e^{-h^0} - e^{-\mu t - h^0}\right)$$ Equation 1.3

$$\ln(y) = \ln(y^0) + \mu A - \ln\left(1 + \frac{e^{\mu A} - 1}{e^{\ln(k)}} - \ln(y^0)\right)$$

The presence of a single parameter specifying the length of the lag phase gives the Baranyi equation an advantage over the previous two equation for cases in which there is delay between first measurement of population size and the beginning of exponential growth.

The final equation used in this thesis is the Monod equation (Equation 1.4) (Monod, 1966), which predicts the rate of change of bacterial density (y) with time (t) based on a affinity constant (J), maximum growth rate (μ), and substrate concentration (E).

$$\frac{dy}{dt} = \mu \frac{[E]}{[E] + J}$$ Equation 1.4

The Monod equation allows more flexibility in growth conditions than the previous three equations as it enables variability in the substrate, which ultimately determines the maximum population size. It is useful for understanding growth rates in an environment containing a known concentration of substrate. In cases where substrate concentration is constant and cannot be estimated, the previous three equations have an advantage and provide the system parameter k. None of these equations directly account for environmental variables such as temperature which may impact growth rates.

Models of microbial attachment on the rhizoplane have also been developed, such as the work of Shimshick and Hebert (1979), who described microbial attachment and detachment from the root surface. Such modelling is effective for describing the behaviour of a population of microbes; however, the lack of a spatial component means it is not suitable for describing or predicting colonisation patterns.

Spatial models are useful for describing dynamic processes, such as bacterial chemotaxis, and distributions within soil (Scott *et al.*, 1995; Muci *et al.*, 2012). When applied to the root, they can be used to predict colonisation dynamics and patterns based on a range of plant and microbial traits (Darrah, 1991b; Muci *et al.*, 2012; Darrah, 1991c). Past work has often neglected the dynamic nature of root traits such as exudation and growth rate. Dupuy and Silk (2016) present a model for bacterial colonisation of a moving root tip. This dynamic model incorporated many parameters of the dynamic rhizoplane neglected in the past, with a focus on the influence of exudation as well as root and bacterial movement. Past models of rhizoplane colonisation have been largely hampered by a lack of quantitative data. With the development of increasingly more biologically relevant live imaging systems, there is an opportunity to validate and populate past models or create new ones.

The scope of this thesis

The work presented in this thesis addresses gaps in our understanding of rhizoplane colonisation as a dynamic process. Based on the assumption that the early stages of microbial colonisation of the rhizoplane follows the key steps outlined in Figure 1.7, the aim was to develop a set of experimental and theoretical frameworks that can be used to isolate and quantify four microbial processes involved in root surface colonisation:

i) Bacterial growth in response to root derived nutrients.
ii) Bacterial attachment to the rhizoplane.
iii) Bacterial growth on the rhizoplane.
iv) Bacterial chemotaxis in a heterogenous soil like environment in response to the presence of plant exudates.

The principal behind this work was that by isolating and quantifying different rhizosphere processes, a better understanding of colonisation as a whole can be established.

Although the major focus of this thesis is bacterial colonisation of rhizoplanes, many of the frameworks developed could be applied to other microbial taxa and processes within soil. Using a biological model system of *Pseudomonas fluorescens* isolate SBW25 and lettuce (*Lactuca sativa*), a systems approach was taken to assessing colonisation. In Chapter 2, *P. fluorescens* SBW25 is transformed with a fluorescent marker plasmid, enabling live imaging of the colonisation process. Bacterial growth was also characterised in a range of conditions. Building on this foundation, in Chapter 3 a novel framework was developed which enables the contributions of bacterial attachment and proliferation on the rhizoplane to be determined, addressing aims (i), (ii), and (iii). In Chapter 4, a live imaging approach using transparent soil was taken to study the association of bacteria with living roots, and the spatial distribution of colonisation along the root, also contributing towards aims (i), (ii), and (iii). In Chapter 5 a novel framework was developed that allows the quantification and modelling of bacterial chemotaxis and movement in a granular environment, achieving aim (iv). Finally in Chapter 6, the implications of these newly developed frameworks, as well as suggested future avenues of research, were discussed.

Chapter 2. Model Selection and characterisation

Introduction

An overall aim of this thesis was to characterise the different stages of microbial colonisation of the rhizoplane. To achieve this, a model plant and bacterial system needed to be established and characterised. Lettuce (*Lactuca sativa* L. cultivar. All Year Round) has a short germination time, is easy to handle without damaging after germination, and is commonly grown in hydroponic systems. This made this plant an ideal model system for the study of rhizoplane colonisation in an important crop species (Li *et al.*, 2018).

Pseudomonas fluorescens (Psf) isolate SBW25 has been a relatively common model system for the study of root-bacteria interactions (Preston *et al.*, 2003), alongside other strains such as *Bacillus subtilis* (Earl, Losick and Kolter, 2008). It was chosen as a model isolate for the characterisation of rhizoplane colonisation, as it is a known promoter of plant growth in many species, including lettuce (Trippe *et al.*, 2013; Humphris *et al.*, 2005; Maroniche *et al.*, 2016), which readily forms association with root systems (Rainey, 1999). Psf SBW25 has been well studied since its isolation in 1986 (Rainey and Bailey, 1996), via physical and genetic characterisation (Rainey and Bailey, 1996; Silby *et al.*, 2009), molecular studies of its interactions with roots (Preston, Bertrand and Rainey, 2001) and root exudates (Mavrodi *et al.*, 2021), as well as direct observation of colonisation patterns (Unge and Jansson, 2001; Pavlova *et al.*, 2017).

The aim in this chapter was to transform Psf isolate SBW25 with two fluorescent marker plasmids; E1433 pGFP and E1434 pCherry, both of which are based on the pME6010 shuttle vector described by Heeb *et al.* (2000). This enabled visualisation of bacteria in Chapters Four and Five of this thesis, in which colonisation of plant roots, as well as the movement of bacteria in response to plant root exudates, are imaged in transparent soil (Downie *et al.*, 2015). Following transformation, a number of parameters needed to be quantified and adjusted to confirm that the process had not significantly impacted the ability of the strain to grow and colonise roots. This chapter also presents the characterisation of Psf SBW25 growth in different media and at different temperatures, along with the development of a plant growth system, which led to the establishment of protocols used to characterise rhizoplane colonisation in the remaining chapters of this thesis.

Methods

Preparation of bacterial isolates and plasmids

Overnight cultures of Psf isolate SBW25 (genome accession AM181176.4) (Rainey and Bailey, 1996) were prepared from an initial lysogeny broth (LB) (Sigma Aldrich, L9234, UK) agar plate. LB is a commonly used bacterial growth media, known to promote the growth of Psf isolate SBW25 (Preston, Bertrand and Rainey, 2001). It was chosen for the initial stages of many experiments in this thesis as it allows the rapid growth of bacteria, meaning visible colonies formed on plates and stocks of bacterial suspensions could be developed in a short space of time. A single colony forming unit (CFU) was isolated and inoculated into liquid LB (5 ml). This, along with a negative control of sterile LB (5ml), was incubated for 24 hours at 27 ^{o}C, shaking at 200 rpm. Aliquots of this liquid culture were then diluted to a ratio of 1: 4 glycerol: bacterial suspension and stored at -80 ^{o}C for subsequent use.

Psf SBW25 was transformed with two sperate fluorescent reporter plasmids, E1433 pGFP and E1434 pCherry (Heeb *et al.*, 2000). Both plasmids also conferred resistance to tetracycline (25 µg ml^{-1}), enabling selection for transformed bacteria during subsequent assays. Psf SBW25 was plated on LB containing tetracycline (25 µg ml^{-1}) and incubated at 27 ^{o}C for 24 hours to ensure that there was no growth of untransformed bacteria in the presence of antibiotic. Psf SBW25 containing the E1433 pGFP plasmid will be referred to as Psf E1433 pGFP. Psf SBW25 containing the E1434 pCherry plasmid will be referred to as Psf E1434 pCherry.

Plasmid DNA was extracted from *Pseudomonas* sp. using the QIAprep Spin Miniprep Kit (Qiagen) according to the manufacturer's instructions. The concentration of DNA in the resulting extraction was analysed using a NanoDrop^{TM} 2000 spectrophotometer (Themo Scientific, UK). DNA was further analysed through a restriction digestion assay. Extracted plasmid DNA (10 µl), buffer EcoRI (2 µl, Thermo Scientific, B12, UK), EcoRI restriction enzyme (1 µl, Thermo Scientific, ER0271, UK), and ddH_2O (7 µl, Sigma Aldrich, W4502, UK) were incubated at 37 ^{o}C for 1 hour. The products of these digestions were then run through an agarose gel in 1 x TBE buffer and compared to a 1000 kbp ladder (Invitrogen, 10787018, UK).

Transformation of bacterial isolates

In preparation for transformation, electrocompetent Psf SBW25, and a control of *Escherichia coli* isolate AAEC185a (Mobley *et al.*, 1990), were prepared. Overnight cultures (5 ml) of both

isolates were prepared. Growth conditions for Psf SBW25 were 27 ^{o}C with shaking at 200 rpm. Growth conditions for *E. coli* AAEC185a were 37 ^{o}C, also with shaking at 200 rpm. These cultures diluted to an optical density at 600 nm (OD_{600}) of 0.02, corresponding to approximately 3e7 CFU ml^{-1} in 100 ml of LB. OD_{600} was measured using an Ultraspec 2100pro spectrophotometer (Biochrom, UK). To record OD_{600}, the spectrophotometer was first blanked using a sterile aliquot (500 µl) of the same growth medium or buffer as the bacterial suspension. Cultures were incubated at the relevant temperature for four hours, beyond which OD_{600} was measured every 15 minutes. Once cultures had reached an OD_{600} of 0.3, flasks were chilled on ice for 30 minutes. Each culture was divided into four 50 ml conical falcon tubes (Sigma-Aldritch, CLS430828, UK) and pelleted by centrifugation at 4000 g for 15 minutes at 4 ^{o}C using a Megafuge 16R Centrifuge (ThermoFisher, USA). The supernatant was discarded, and the pellet was gently resuspended in ice-cold 1ml of 10 % w/v glycerol. For each isolate, the four resuspended pellets were pooled and made up to 50 ml with 10 % w/v glycerol. This was centrifuged for 15 minutes at 4000 g and 4 ^{o}C. Once more, the supernatant was discarded, and pellets gently resuspended in 1 ml of 10 % w/v glycerol. This centrifugation step was repeated using the same settings, the supernatant was discarded, and pellets was resuspended in 500 µl of 10 % w/v glycerol. 80 µl Aliquots of each electrocompetent isolate were then stored at -80 ^{o}C.

To perform transformations, aliquots of electrocompetent Psf SBW25 and *E. coli* AAEC185a were thawed on ice. 1 µl of either E1433 pGFP, E1434 pCherry plasmids, or a control plasmid pTOFetpD (Merlin, McAteer and Masters, 2002) were pipetted into aliquots of each isolate. Aliquots were then transferred to chilled electroporation cuvettes (Stratagene, 200321-42, USA). The outsides of cuvettes were dried, and they were electroporated at 1250 V using a Electroporator 2510 (Eppendorf, Germany). 500 µl of LB was then added to cuvettes and the contents were pooled for each isolate and plasmid in universal containers (Alpha Laboratories, CW3880, UK). These were incubated statically for four hours at 27 ^{o}C for Psf SBW25, or 37 ^{o}C for *E. coli* AAEC185a. LB agar plates containing tetracycline (25 µg ml^{-1}) were then streaked with 100 µl from each universal container. Plates were incubated at the relevant temperature for 24 hours. For plates on which bacterial growth was observed, CFU were counted and 3 CFU were pooled and restreaked on LB agar plates containing tetracycline (25 µg ml^{-1}). These were incubated at the relevant temperature for a further 24 hours. A single CFU was then selected and incubated in 5ml of liquid LB containing tetracycline (25 µg ml^{-1}) under the relevant growth conditions with shaking at 200 rpm. Aliquots of these liquid cultures were

then diluted to a ratio of 1: 4 glycerol: bacterial suspension and stored at -80 ^{o}C for subsequent use.

Measurements of fluorescence and imaging

The fluorescence of transformed Psf E1433, Psf E1434, and untransformed Psf SBW25 were compared. Overnight cultures were prepared, using tetracycline (25 µg ml^{-1}) for the transformed isolates. These were diluted to an OD_{600} of 0.02 using LB. 200 µl of each isolate was then pipetted into separate wells in a 96 well plate. This was transferred to a Varioskan Lux Plate Reader (Thermo Scientific, UK). Fluorescence was measured in relative fluorescence units (RFU) from the top of the plate, with a measurement time of 100 ms and a band width of 12 nm. Psf E1433 pGFP was analysed with an excitation wavelength of 488 nm and fluorescence recorded between 500 and 600 nm. Psf E1434 pCherry was analysed with an excitation wavelength of 587 nm and fluorescence recorded between 590 and 700 nm. The fluorescence of Psf SBW25, and a negative control of pure LB, was recorded for both excitation wavelengths.

Isolates were imaged on a Nikon A1R confocal laser scanning system mounted on a NiE upright microscope fitted with a NIR Apo 40 × 0.8 W water dipping lens with GaAsP detectors (Nikon, Japan). pGFP was excited at 488 nm with the emission being collected at 500–530 nm. pCherry was excited at 587nm and emission collected at 600-630nm.

Maintenance of the E1433 pGFP plasmid in bacteria

To determine the stability of the E1433 pGFP plasmid, overnight cultures Psf E1433 pGFP containing tetracycline (25 µg ml^{-1}) were prepared. 1 ml of the overnight culture was then inoculated into a conical flask containing 100 ml of LB with no antibiotic. A negative control, consisting of 5ml of sterile LB was also prepared. These was incubated at 27 ^{o}C with shaking at 200 rpm. Subculturing and preparation of a negative control was repeated every 24 hours for 144 hours. During subculturing, a 1ml sample was taken from the conical flask and diluted to an OD_{600} of 0.02 using LB. The fluorescence of this sample, measured in RFU, was then recorded with an excitation wavelength of 488 nm and emission wavelength of 512 using a Varioskan^{TM} Lux Plate Reader (Thermo Scientific, Singapore).

Measurement of bacterial growth

The growth of untransformed and transformed Psf isolates were compared through a manual analysis of the increase of OD_{600}. Overnight cultures of each isolate were prepared containing

the relevant antibiotic. 1 ml of each culture was inoculated into a conical flask containing 100 ml of LB, and the relevant antibiotics. A negative control of sterile LB was also prepared. These were incubated at either 27 ^{o}C or 18 ^{o}C with shaking at 200 rpm. Approximately every hour, a sample of each culture and control was taken and the OD_{600} measured using a Ultraspec 2100pro spectrophotometer (Biochrom, UK).

Rich defined 3-(*N*-morpholino)propanesulfonic acid (RD-MOPS) medium was prepared, containing: 100 mM 3-(*N*-morpholino)propanesulfonic acid (adjusted to a pH = 7.4 with KOH), 100 mM N-Tris(hydroxymethyl)methyl glycine (adjusted to a pH = 7.4 with KOH), 1 mM $FeSO_4$, 27.6 mM of K_2SO_4, 0.05 mM $CaCl_2$, 52.8 mM $MgCl_2$, 0.5 M NaCl, micronutrients consisting of: 0.3 μM $(NH_4)_6Mo_7O_{24}.H_2O$, 0.04 mM H_3BO_3, 0.003 mM $CoCl_2$, 0.001 mM $CuSO_4$, 0.008 mM $MnCl_2$, 0.001 mM $ZnSO_4$ (5 ml), 0.2 % v/v glycerol as a carbon source, 132 mM K_2HPO_4, 0.02 M thiamine HCl, 0.02 % v/v essential amino acid solution (Sigma Aldrich, M5550, USA), and 0.01 % v/v non-essential amino acids (Sigma Aldrich, M7145, USA) (Neidhardt, Bloch and Smith, 1974). While LB medium allowed for rapid bacterial growth, RD-MOPS was employed to prepare cultures for interaction with plants through a period of growth in a suboptimal nutrient environment (Wright *et al.*, 2017; Neidhardt, Bloch and Smith, 1974).

Automated cell density measurements of OD_{600} were taken using a Bioscreen microplate reader (Growthcurves Ltd., USA). Overnight cultures of each isolate were prepared containing the relevant antibiotic. 1 ml of these were pelleted by centrifugation at 4000 rpm for six minutes and resuspended in 5 ml of either LB or RD-MOPS medium. This was incubated for a further hour at 27 ^{o}C with shaking at 200 rpm before being diluted to an OD_{600} of 0.01 in the relevant medium. 200 μl of each culture was then pipetted into five wells of a 100 well honeycomb plate (Thermo Scientific, 9502550, UK). A further five wells were filled with sterile LB or RD-MOPS as negative controls. The plate was then placed in the microplate reader, which was run over 24 hours at either 27 or 18 ^{o}C taking measurements every half hour with intermittent shaking. Data was normalised by subtracting the mean value of OD_{600} for the relevant negative controls of the relevant medium for each experimental replicate.

Modelling of bacterial growth

Table 2.1. Model variables and parameters.

Notation	Parameter (unit)
Wt	Root mass (g)
CFU^0	CFU of inoculant (ml^{-1})
y	Colonisation density on root surface (g^{-1})
t	Time (hour)
k	Carrying capacity (OD_{600})
y^0	Colonisation density or bacterial density at hour 0 (OD_{600})
μ	Maximum growth rate ($hour^{-1}$)
h^0	Length of the lag phase (hour)
N	Sample number
M	Bootstrap replicates
y_b^i	The i^{th} prediction of bootstrap sample b (OD_{600})
y_m	The mean predicted bootstrap value at b (OD_{600})

Growth curves were fit to the data based on a non-linear least squares method (NLS). Initially, data was pooled and three classical bacterial growth models, the logistic equation (Equation 2.1) (Tsoularis and Wallace, 2002), the Gompertz equation (Equation 2.2) (Gibson, Bratchell and Roberts, 1988), and the Baranyi equation (Equation 2.3) (Baranyi and Roberts, 1994) were fit to each data set. The logistic equation predicts the rate of change of bacterial density (y) with time (t) based on a carrying capacity (k), initial density (y^0), and maximum growth rate (μ) with the solution in the form:

$$y = \frac{ky^0}{y^0 + (k - y^0)e^{-\mu t}} \qquad \text{Equation 2.1}$$

The Gompertz equation also predicts the rate of change of bacterial density (y) with time (t) based on a carrying capacity (k), initial density (y^0), and maximum growth rate (μ) with the solution in the form:

$$y = ke^{\ln\left(\frac{y^0}{k}\right)e^{-\mu t}} \qquad \text{Equation 2.2}$$

The Baranyi equation predicts the rate of change of bacterial density (y) with time (t) based on a carrying capacity (k), initial density (y^0), maximum growth rate (μ), and (h^0) which specifies the length of the lag phase with the solution in the form:

$$A = t + \frac{1}{\mu}\ln\left(e^{(-\mu t)-\mu t} + e^{-h} - e^{-\mu t - h^0}\right) \qquad \text{Equation 2.3}$$

$$\ln(y) = \ln(y^0) + \mu A - \ln\left(1 + \frac{e^{\mu A} - 1}{e^{\ln(k)}} - \ln(y^0)\right)$$

The best fit model was determined based on lowest Akaike Information Criterion (AIC) score. The Bootstrap method was used to estimate confidence intervals of the fit. Data was randomly sampled with replacement M times to produce a bootstrap sample. Models were then fit to this new data set based on a NLS method. The bootstrap estimate of the confidence interval for pooled data sets was then determined as:

$$CE = \frac{1}{M-1}\sqrt{\sum_{b=1}^{b=M}\frac{1}{N}\sum_{i=1}^{i=N}(y_b^i - y_m)^2} \qquad \text{Equation 2.4}$$

Where y_b^i is the ith predicted value on bootstrap sample b. y_m is the mean predicted bootstrap value at that time point M is the number of times the data is resample (here 1000, Table 2.1). Subsequently, the Baranyi model (Equation 2.3) was fit to each replicate in order to determine mean parameter values and standard deviation.

Correlation between measurements of bacterial density

The relationship between OD_{600} and CFU ml^{-1} was determined for Psf SBW25. Overnight cultures of Psf SBW25 were prepared. These were diluted to a variety of OD_{600} values using phosphate buffer saline (PBS). OD_{600} values were recorded, and samples were plated on Kings-B agar (Sigma Aldrich, 60786, UK) agar by 10-fold serial dilutions. Kings-B agar is selective for *Pseudomonas* and also has the advantage of instigating pigment production in fluorescent *Pseudomonas* which makes individual colonies easy to identify during colony counts (Johnsen and Nielsen, 1999). Throughout this thesis, Kings-B agar was used when counting Psf colonies was necessary. Negative controls of sterile LB and PBS were also plated. Plates were incubated for 24 hours at 27 ^{o}C before CFU were counted.

Abiotic biofilm formation assays

The ability of transformed and untransformed Psf SBW25 isolates to form biofilms on abiotic surfaces was investigated through a static biofilm assay (Merritt, Kadouri and O'Toole, 2006). Overnight cultures of Psf SBW25, Psf E1433 pGFP, and Psf E1434 pCherry were prepared. These were pelleted by centrifugation at 4000 rpm for six minutes and resuspended in either LB, RD-MOPS, or H_2O. Cultures were grown for a further hour at 27 ^{o}C with shaking at 200 rpm before being diluted to an OD_{600} of 0.02 in the relevant medium. 200 µl of each isolate in each medium was then pipetted into separate wells in a 96 well plate, and an equal number of control wells were filled with the same volume of sterile growth medium. The plate was covered and incubated at 27 ^{o}C for 24 hours. Liquid was then removed from the plate by brisk shaking. The plate was rinsed by submersion in PBS, then dried by vigorous shaking. 125 µl 0.1 % crystal violet solution was pipetted into each well and the plate was incubated at room temperature for ten minutes. The crystal violet solution was removed by shaking, and the plate washed by submerging twice in water. The plate was dried overnight at room temperature. 200 µl of a 1: 4 acetone: ethanol mixture was pipetted into each well to elute the dye. The contents of each well were then transferred to an optically clear 96 well plate and the OD_{600} was recorded. Data was normalised by subtracting the mean value of the negative controls for the relevant medium for each experimental replicate.

Plant growth conditions

Lettuce (*Lactuca sativa* L. cultivar. All Year Round) seeds (Sutton Seeds, United Kingdom) were surface sterilised by soaking in 20 ml of a solution of 2 % w/v calcium hypochlorite (Sigma Aldrich, 12116, UK) for 15 min. They were then washed six times in 20 ml of sterile

distilled water. Seeds were plated on 1.5 % water agar. Plates were sealed, covered with foil, and incubated at 21°C for 3 days.

The sterilisation protocol was assessed by making imprints of seeds which had and hadn't been surface sterilised. Imprints of seeds were made by placing them on non-selective LB agar for 30 seconds on two separate plates. Plates were sealed, covered with foil, and incubated at either 27 °C or 18 ºC for 24 hours before a visual inspection for contamination.

Test of microcosm systems

Following germination, plants were grown in a hydroponic system. This consisted of perlite (William Sinclair, UK) and 0.5 x concentration Murashige and Skoog medium (Sigma Aldrich, M5524, UK) with no sucrose (MS) in a 3: 2 ratio, in a 200 ml hydroponic pot (Greener bio-one, Austria). MS media is a plant growth media commonly employed for plant tissue culture and hydroponic growth. It was as the liquid component of colonisation assays throughout this thesis due to its similarity to soil like conditions in terms of available nutrients and pH (Murashige and Skoog, 1962; Downie *et al.*, 2012). Plants were grown for three days prior to further treatment.

A separate microcosm system was developed which allowed easier access to roots. Microcosms were constructed in 75 mm round bottom culture tubes (VWR, 211-0046, UK). 1.5 % water agar (1 ml) was melted and pipetted into culture tubes. These were set on their sides, allowing agar to form a slope and a well in which microbial suspensions could interact with the root. Once agar had set, a small section was removed to form a platform on which the germinated seed was placed. Each microcosm contained 1 ml of 0.5 × MS (Figure 2.1). Light was prevented from reaching roots by tape covering the lower half of the microcosmos. Plants were grown in growth chambers (SANYO, Japan). Growth conditions for both the hydroponic and microcosm systems were 21°C with 16 h of light at 60 µmol m^{-2} s^{-1} for three days prior to further treatment.

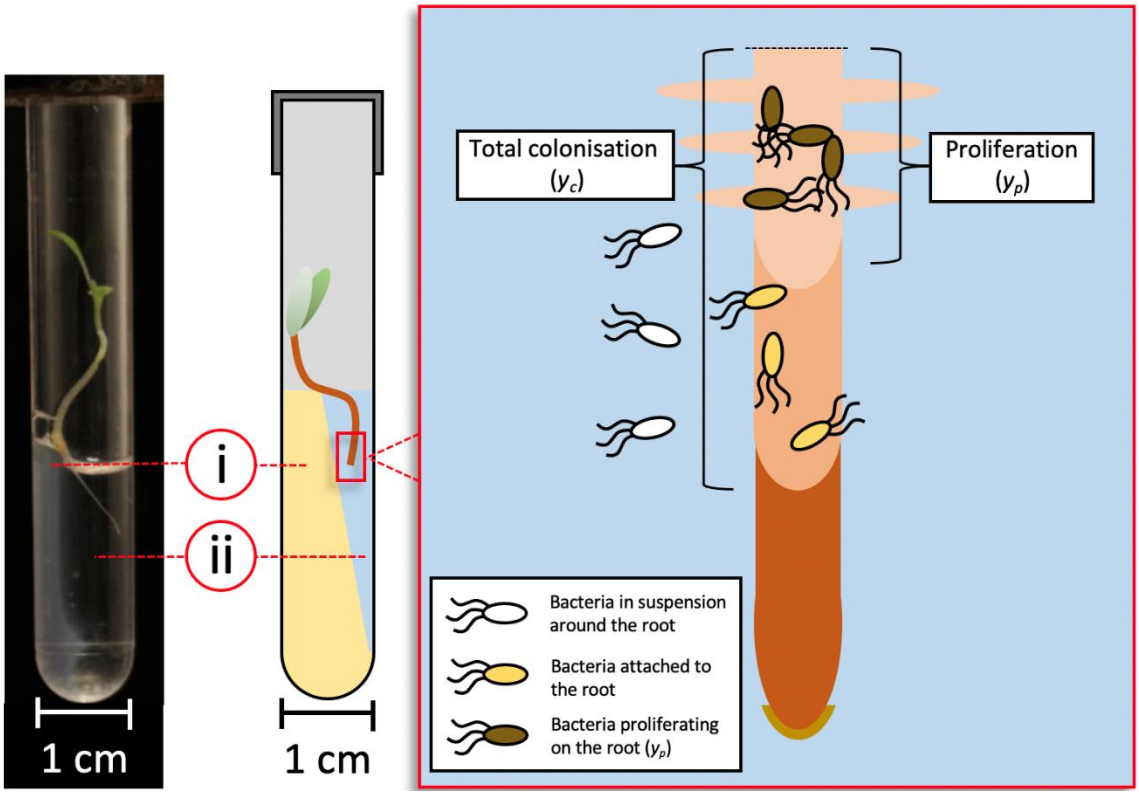

Figure 2.1. Microcosm system for the study of rhizoplane colonisation. (i) Plants were grown on a water agar platform. (ii) Liquid medium allowed bacterial inoculants to interact with the root. In Chapter 3, this system is used to separately quantify total colonisation (y_c), which is the result of recruitment from the surrounding medium (yellow) as well as proliferation from proliferation on the root surface in the absence of attachment (y_p, brown).

Measurement of root growth rates

A separate plant growth system was employed to acquire live measurements of root growth rate. Hydroponic pouches consisting of a filter paper envelope enclosed within a plastic sheath were wrapped in tinfoil and autoclaved. 10 ml of 0.5 × MS was pipetted into each plastic sheath. Sterile germinated lettuce seeds were placed at the top of each filter paper envelope, enabling the root to grow downwards into the pouch. Pouches were placed upright in a sterile transparent box which was then incubated at 21°C with 16 h of light at 60 μmol m^{-2} s^{-1}. Every 24 hours for five days images were acquired of the pouches along with a ruler in line with plant roots. Measurements of root growth rate were also taken destructively by removing plants from microcosm every 24 hours after the transfer of seedlings. Roots were placed on a microscope

slide and images acquired using a stereomicroscope with a graticule (Lecia, M167 FC. UK). All roots were measured along the longest axis of the primary root.

Root colonisation assay

To determine if bacterial transformations had had an impact on the ability of isolates to colonise root tissue, a root colonisation assay was performed. Bacterial suspensions in 0.5 x MS media were prepared. Overnight cultures of Psf SBW25, Psf E1433 pGFP, and Psf E1434 pCherry were prepared containing tetracycline (25 µg ml^{-1}) for transformed isolates. Bacteria were diluted with a 1: 50 ratios in 15 ml of RD-MOPS and incubated at 18 ^{o}C for a further 24 hours, then diluted to an OD_{600} of 0.02 using 0.5 x MS medium. An initial bacterial density (CFU^0) was determined based on 10-fold serial dilutions and plating on Kings-B agar containing the relevant antibiotic. Plants were grown in the hydroponic system for seven days prior to inoculation. Growth medium was removed using a Pasteur pipette and replaced with an equal volume of bacterial suspension or a negative control of 0.5 x MS medium. Plants were returned to growth conditions of 21°C with 16 h of light at 60 µmol m^{-2} s^{-1} for 24 hours. They were then gently removed from chambers and excess percol removed. Roots were dipped three times in PBS, separated from the phyllosphere (with the distinction between the two marked by the hypocotyl) using an ethanol-sterilized razor blade, and weighed in a sterile sample tube containing 500 µl of PBS (Eppendorf, 0030121023, UK). Roots were homogenized using a micro pestle. CFU counts were determined by 10-fold serial dilutions and plating on Kings-B agar containing tetracycline (25 µg ml^{-1}) for transformed isolates. Colonisation density (y, g^{-1}) was determined based on CFU counts, root mass (wt, g) and initial bacterial density according to the following equation:

$$y = \frac{CFU}{CFU^0 wt} \qquad \text{Equation 2.5}$$

Data analysis and use of software

All data analysis was carried out in R (R Core Team, 2018). Growth models were fit using the 'growthrates' package which employs a least squares method (Petzoldt, 2016). A one-way analysis of variance (ANOVA) was carried out to assess differences in mean biofilm formation between isolates and treatments, as well as differences in mean root colonisation between isolates. Following use of a confidence level of 95 %, subsequent *post hoc* testing using a Tukey range test was carried out. Linear regressions were performed with time as input variable

and root length as output variable to determine root growth rates based on live and destructive root length measurements. A linear regression was also run, with OD_{600} as input variable and CFU ml^{-1} of suspension as output variable to assess the relationship between different measurements of bacterial density. A linear regression with time as input variable and fluorescence as output variable was used to assess the stability of the E1433 pGFP plasmid over time. Images were acquired using NIS-elements AR software (Nikon, USA).

Results

Psf SBW25 was transformed with fluorescent marker plasmids

Psf SBW25 was transformed with fluorescent marker plasmids to enable visualisation of bacteria on root surfaces and in transparent soil. Initial plating of Psf SBW25 on LB containing tetracycline (25 µg ml^{-1}) prior to transformation confirmed that there was no growth in the presence of antibiotics when incubated at 27 ºC for 24 hours. This enabled the selection of transformed bacteria. 31.7 ng μl^{-1} of plasmid DNA was extracted from *Pseudomonas* sp. E1433 pGFP. 34.4 ng μl^{-1} of plasmid DNA was extracted from *Pseudomonas* sp. EcoRI restriction digestion assays of both extractions resulted in equal bands at approximately 10,000 base pairs, corresponding to the expected size of the plasmids (Heeb *et al.*, 2000). Five aliquots for each of the three plasmids of electrocompetent Psf SBW25 or *E. coli* AAEC185a underwent electroporation. Transformations of Psf SBW25 with the E1433 pGFP, E1434 pCherry, and pTOfetpD plasmids were successful, resulting in the growth of transformed isolates on LB containing tetracycline (25 µg ml^{-1}). Transformation of *E. coli* AAEC185a with the three plasmids was also successful, resulting in growth of transformed isolates on LB containing tetracycline (25 µg ml^{-1}). Fluorescence was measured twice for transformed and untransformed isolates with eight wells of a 96 well plate filled with each isolate. With an excitation wavelength of 488 nm, Psf E1433 pGFP had a peak fluorescence at 512 nm (Figure 2.2a), while Psf E1434 pCherry had a peak fluorescence at 612 nm (Figure 2.2b). Both isolates were visible under the microscope using the relevant excitation and emission settings (Figure 2.3). The transformed isolates of Psf SBW25 were suitable for the live imaging used to quantify bacterial processes in later chapters.

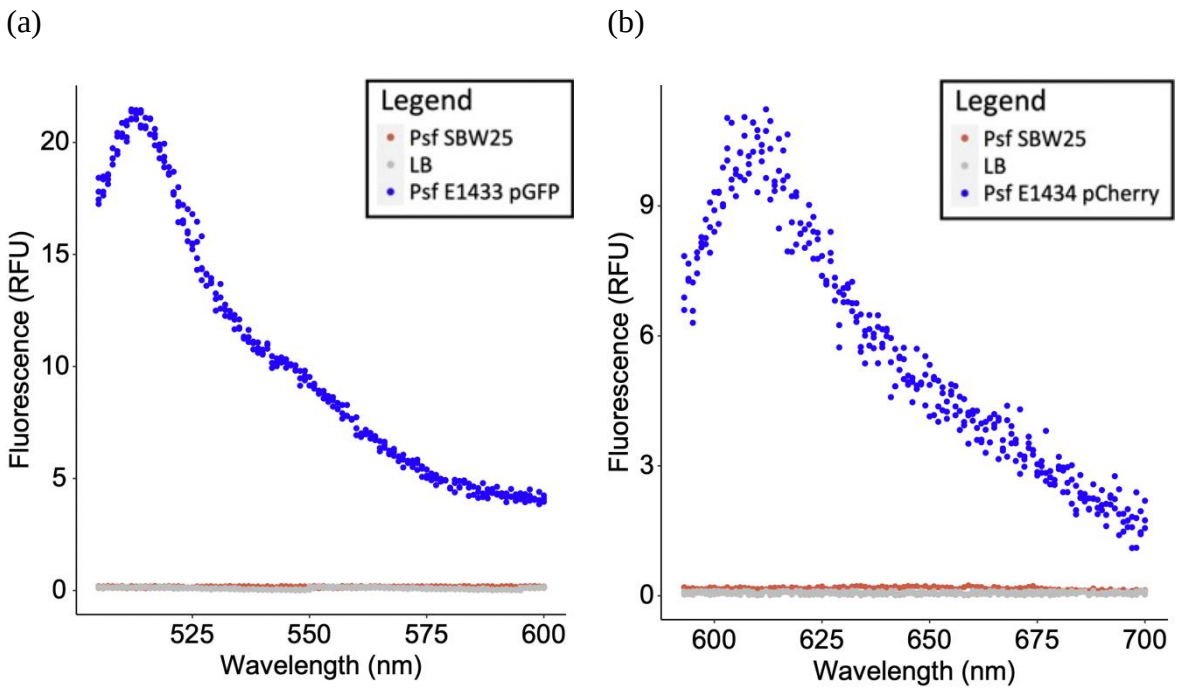

Figure 2.2. The fluorescence of each isolate was recorded to determine the correct settings for confocal imaging. The fluorescence of transformed bacterial strains were recorded at a) an excitation wavelength of 488nm, with a peak in fluorescence at 512 nm for Psf E1433 pGFP and b) an excitation wavelength of 575 nm with a peak in fluorescence at 612 nm for Psf E1433 pCherry. The fluorescence of four samples of each isolate at an OD_{600} of 0.02 are shown.

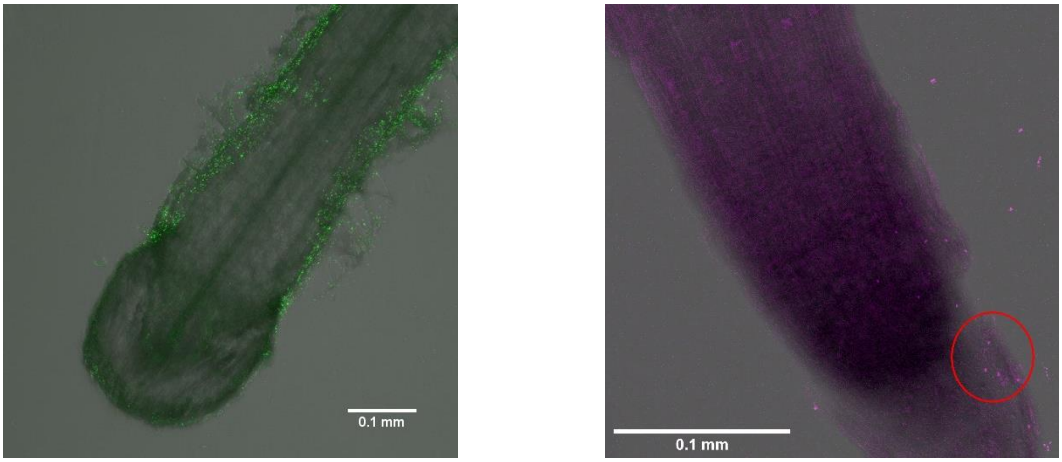

Figure 2.3. Confocal images of transformed bacteria overlaid on transmission images of roots. A) Psf E1433 pGFP on the surface of a lateral root in cross section. B) Image of Psf E1434 pCherry (circled in red) on the surface of a root tip. Digital gain of image has been increased to make bacteria more evident in low density.

Experiments in later chapters involved growing bacteria for several days without renewing antibiotics. For this reason, the fluorescence of a suspension with a set concentration of Psf SBW25 E1433 pGFP at and excitation wavelength of 488 and an emission wavelength of 512 nm was assessed when growing in bacterial growth media (LB) in the absence of a plant with and without antibiotics over the course of 144 hours with daily sampling and subculturing. This protocol was carried out three times. Based on a linear regression, there was no significant correlation between time and fluorescence over 144 hours when Psf E1433 was grown in the absence of antibiotics ($R^2 = 0.229$, $F(1,5)$, $P = 0.692$, $N = 7$) (Figure 2.4). It was concluded that the E1433 plasmid was maintained in Psf SBW25 for at least seven days/168 hours (Figure 2.4).

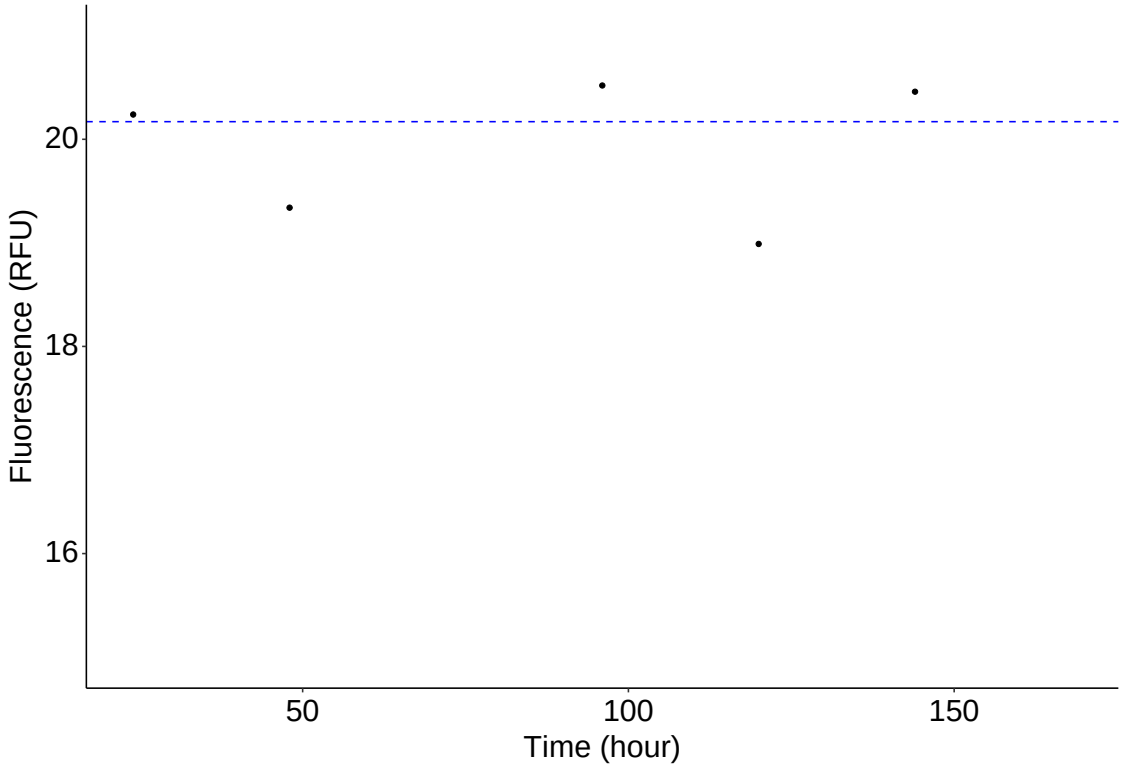

Figure 2.4. The pGFP plasmid was stable in Psf SBW25 in the absence of antibiotics. The stability of the E1433 pGFP plasmid in Psf SBW25 the absence of antibiotics was investigated by observing the fluoresce of a consistent bacterial density of Psf E1433 pGFP at an excitation wavelength of 488 nm and emission wavelength of 512 nm over 168 hours. No significant change in fluorescence with time was found based on a linear regression (R^2 = 0.229, F(1,5), P = 0.692, N = 7).

Growth rates of transformed and untransformed isolates were modelled

The growth of transformed and untransformed Psf SBW25 was quantified in order to determine the impact of transformations on bacterial activity, as well as to provide information on growth stages which would be used to establish consistent inoculation protocols in later chapters. Initial measurements of the growth of Psf SBW25, Psf E1433 pGFP and Psf E1434 pCherry through manual sampling and measurement of OD_{600} were carried out three times for each growth condition. These were carried out to determine if the overall trend in growth observed in manual and automatic measurements matched (Figure 2.5).

(a) 27 ºC (b) 18 ºC

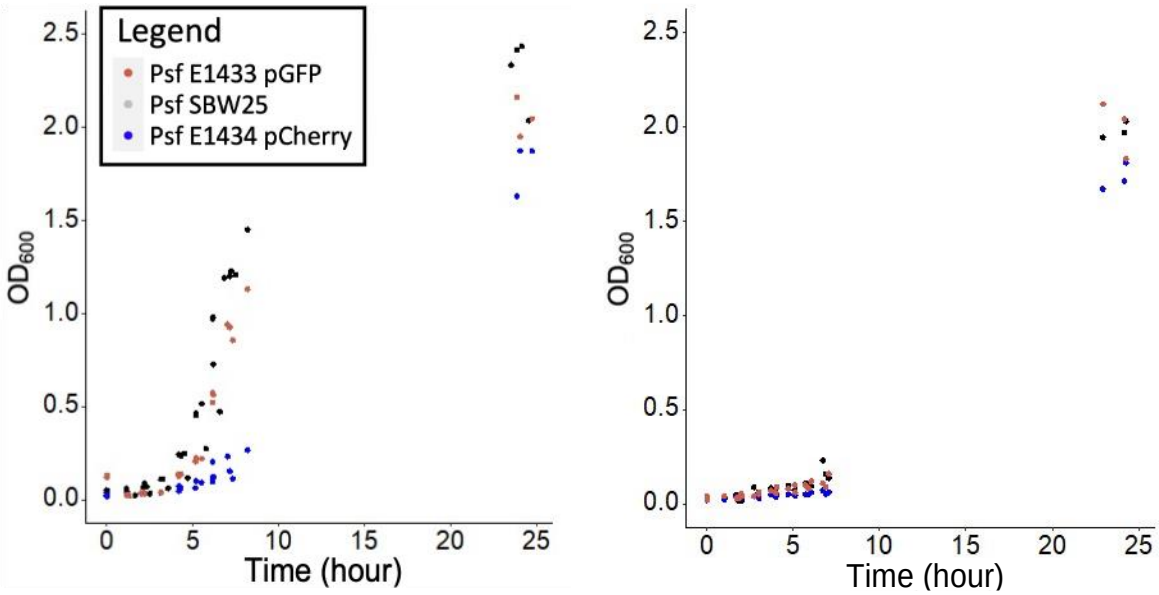

Figure 2.5. Bacterial growth was quantified through manual sampling. Growth of untransformed type Psf SBW25 (black) and transformed Psf E1433 pGFP (orange) and Psf E1434 pCherry (blue) bacterial strains obtained manually. A) Growth observed using LB medium at 27 ºC and b) Growth observed using LB medium at 18 ºC. The experiment was repeated three times for each isolate.

Subsequent automated measurements of growth using the spectrophotometer plate reader enabled continuous measurement of OD_{600}, meaning data could be modelled. For each temperature and growth medium, growth in five wells inoculated with each of the three isolates was measured across two replicates. Initially, data for each condition was pooled. Growth generally followed classical bacterial growth patterns, with slower growth seen at 18 ºC for all isolates in both LB and RD-MOPs and density plateauing at lower OD_{600} values in RD-MOPs compared to LB (Figure 2.6). In all growth conditions, Psf E1434 pCherry showed slower growth rates and a lower mean OD_{600} at 24 hours compared to the other two isolates (Table 2.2). Patterns of bacterial growth were consistent between manual and automated measurements. The Baranyi model (Equation 2.3) was the best fit for all isolates in at both 18 and 27º C. (Figure 2.6, Table 2.3). Bootstrap confidence intervals (CI), were calculated for each growth curve for pooled data (Table 2.3). Subsequently, the Baranyi model (Equation 2.3) was the best fit to each replicate within each data set and mean parameter values, along with

their standard deviation, was calculated. The differences in maximum growth rates evident between the untransformed isolate and Psf E1434 pCherry indicated that transformation had impacted bacterial growth, while Psf E1434 pGFP showed a similar pattern of growth to the untransformed isolate.

Table 2.2. Mean OD_{600} measurements for transformed and untransformed Psf SBW25 grown in different conditions after 24-hours of growth ± SD. For each condition, growth in five wells inoculated with each of the three isolates was measured across two replicates.

Isolate	18° LB	18° RD-MOPS	27° LB	27° RD-MOPS
Psf SBW25	0.7 ± 0.024	0.57 ± 0.029	0.065 ± 0.003	0.52 ± 0.011
Psf E1434 pCherry	0.57 ± 0.15	0.42 ± 0.033	0.56 ± 0.037	0.46 ± 0.013
Psf E1433 pGFP	0.63 ± 0.025	0.63 ± 0.018	0.66 ± 0.017	0.6 ± 0.06

(a) 27 ºC LB medium

(b) 18 ºC LB medium

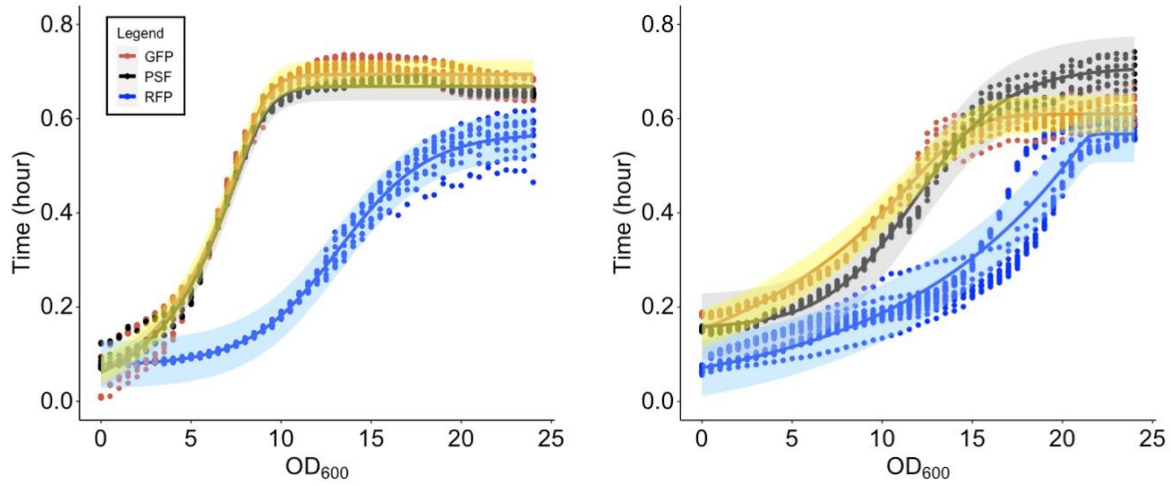

(c) 27 ºC RD-MOPS medium

(d) 18 ºC RD-MOPS medium

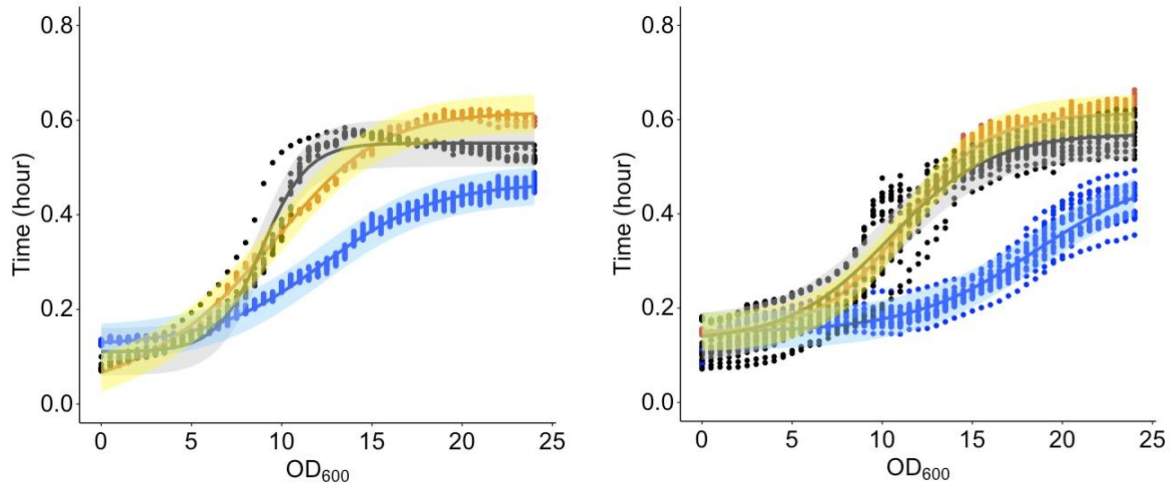

Figure 2.6. Bacterial growth was quantified through automatic sampling. Growth of untransformed Psf SBW25 (black), transformed Psf E1433 pGFP (orange), and Psf E1434 pCherry (blue) were obtained using an automated plate reader. The Baranyi equation (Equation 2.3) was fit to pooled data using a least squares method to estimate parameter values. Solid lines represent the calculated values of OD_{600} for the relevant time point based the Baranyi equation with parameter estimates for the relevant isolate (Table 2.3). Shaded regions represent the bootstrap confidence intervals calculated for each model. a) LB medium at 27 ºC. b) LB medium at 18 ºC. c) RD-MOPS medium at 27 ºC. d) RD-MOPS medium at 18 ºC. For each condition, growth in five wells inoculated with each of the three isolates was measured across two replicates.

Table 2.3. Parameter values and bootstrap confidence intervals for bacterial growth models.

Isolate	Conditions	AIC	Bootstrap CI (OD_{600})	Parameter (unit)	Fit pooled data	Fit individual replicate ± standard deviation
Psf SBW25	LB 27 ºC	-2667.51	0.03	$y^0\ (OD_{600})$	0.08	$0.08 = \mp 0.02$
				$k\ (OD_{600})$	0.68	$0.68 = \mp 0.004$
				$\mu\ (hour^{-1})$	0.6	$0.6 = \mp < 0.001$
				$h^0\ (hour)$	1.68	$1.64 = \mp 0.3$
	LB 18 ºC	-2012.32	0.07	$y^0\ (OD_{600})$	0.16	$0.16 = \mp 0.005$
				$k\ (OD_{600})$	0.71	$0.7 = \mp 0.015$
				$\mu\ (hour^{-1})$	0.39	$0.39 = \mp 0.016$
				$h^0\ (hour)$	3.17	$3.19 = \mp 0.17$
	RD-MOPS 27 ºC	-2132.09	0.04	$y^0\ (OD_{600})$	0.11	$0.1 = \mp 0.004$
				$k\ (OD_{600})$	0.55	$0.56 = \mp 0.047$
				$\mu\ (hour^{-1})$	0.79	$0.6 = \mp < 0.001$
				$h^0\ (hour)$	5.47	$3.45 = \mp 0.288$
	RD-MOPS 18 ºC	-2862.91	0.05	$y^0\ (OD_{600})$	0.14	$0.14 = \mp 0.035$
				$k\ (OD_{600})$	0.57	$0.57 = \mp 0.023$
				$\mu\ (hour^{-1})$	0.36	$0.38 = \mp 0.1$
				$h^0\ (hour)$	2.36	$2.57 = \mp 0.976$
Psf E1433 pGFP	LB 27 ºC	-3110.46	0.03	$y^0\ (OD_{600})$	0.08	$0.09 = \mp 0.004$
				$k\ (OD_{600})$	0.7	$0.70 = \mp 0.016$
				$\mu\ (hour^{-1})$	0.6	$0.06 = \mp < 0.001$
				$h^0\ (hour)$	1.65	$1.69 = \mp 0.51$
	LB 18 ºC	-2175.1	0.04	$y^0\ (OD_{600})$	0.19	$0.19 = \mp 0.006$
				$k\ (OD_{600})$	0.62	$0.62 = \mp 0.025$
				$\mu\ (hour^{-1})$	0.43	$0.43 = \mp 0.003$
				$h^0\ (hour)$	3.12	$3.14 = \mp 0.366$
	RD-MOPS 27 ºC	-1178.16	0.07	$y^0\ (OD_{600})$	0.08	$0.08 = \mp < 0.001$
				$k\ (OD_{600})$	0.62	$5 = \mp < 0.001$
				$\mu\ (hour^{-1})$	0.32	$0.31 = \mp 1.59$
				$h^0\ (hour)$	1	$1.59 = \mp 0.108$
	RD-MOPS 18 ºC	-2711.79	0.04	$y^0\ (OD_{600})$	0.15	$0.15 = \mp 0.005$
				$k\ (OD_{600})$	6.14	$6.14 = \mp 0.018$
				$\mu\ (hour^{-1})$	0.43	$0.43 = \mp < 0.001$

Psf E1434 pCherry	LB 27 ºC	-2089.35	0.05	$h^0\ (hour)$	3.4	$3.4 = \mp 0.007$
				$y^0\ (OD_{600})$	0.09	$0.08 = \mp 0.004$
				$k\ (OD_{600})$	0.57	$0.57 = \mp 0.037$
				$\mu\ (hour^{-1})$	0.4	$0.4 = \mp 0.029$
	LB 18 ºC	-3314.34	0.06	$h^0\ (hour)$	3.34	$3.35 = \mp 0.35$
				$y^0\ (OD_{600})$	0.11	$0.12 = \mp 0.016$
				$k\ (OD_{600})$	0.68	$0.72 = \mp 0.12$
				$\mu\ (hour^{-1})$	0.3	$0.34 = \mp 0.09$
	RD-MOPS 27 ºC	-2959.37	0.05	$h^0\ (hour)$	3.43	$4.21 = \mp 1.12$
				$y^0\ (OD_{600})$	0.12	$0.12 = \mp 0.003$
				$k\ (OD_{600})$	0.47	$0.5 = \mp < 0.001$
				$\mu\ (hour^{-1})$	0.31	$0.25 = \mp 0.028$
	RD-MOPS 18 ºC	-4297.35	0.04	$h^0\ (hour)$	2.63	$1.73 = \mp 0.377$
				$y^0\ (OD_{600})$	0.15	$0.15 = \mp 0.018$
				$k\ (OD_{600})$	0.5	$0.6 = \mp 0.179$
				$\mu\ (hour^{-1})$	0.28	$0.25 = \mp 0.06$
				$h^0\ (hour)$	4.08	$3.59 = \mp 0.9$

Calibration of OD_{600} measurement for estimation of bacterial density

In later chapters, optical density at 600nm (OD_{600}), measured using a Varioskan Lux Plate Reader, was used to estimate the bacterial density of inoculants in CFU ml^{-1}. For this reason, the relationship between OD_{600}, measured using this equipment, and CFU ml^{-1} for a suspension of Psf SBW25. Based on a linear regression, OD_{600} had a significant positive correlation with CFU ml^{-1} (R^2 = 0.958, F(1,19) = 435.2, P < 1e-4, N = 16) for Psf SBW25, with a slope of 1e9 CFU ml^{-1} per absorbance unit and an intercept of approximately -1e7 CFU ml^{-1} (Figure 2.7). This enabled estimates of bacterial densities in CFU ml^{-1} to be made based on OD_{600}.

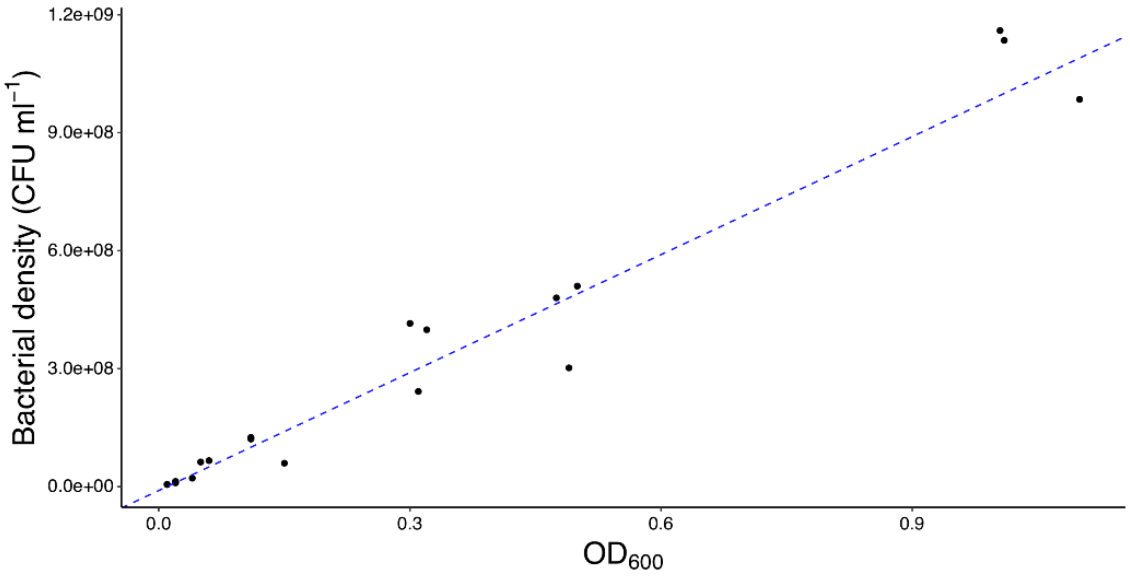

Figure 2.7. The relationship between bacterial density at 600 nm (OD_{600}) and bacterial density (CFU ml^{-1}) was determined. Based on a linear regression, a significant positive corelation (R^2 = 0.958, F(1,19) = 435.2, P < 1e-4, N = 16) between the two was found with a slope of approximately 1e9 CFU ml^{-1} per absorbance unit and an intercept of approximately -1e7 CFU ml^{-1} CFU ml^{-1}. This relationship is represented by the blue dashed line.

Biofilm formation in different growth mediums was quantified

Biofilm formation on an abiotic surface was compared between bacterial isolates in different growth media. In principle, this assay involves the staining of negatively charged components of both cells and the extracellular biofilm matrix adhering to an abiotic surface (here the liquid-solid interface between solid plastic and a growth media) with crystal violet. Through washing of the surface, unattached components of the bacterial population are removed along with excess dye. The remaining dye is then eluted, and a measure of its concentration is determined based on optical density. While this form of assay is standard practice in microbiology (Spiers *et al.*, 2003; Kragh *et al.*, 2019), it should be noted that crystal violet will bind to proteins not involved in biofilm formation. Nonetheless as a method for comparing the ability of bacterial isolates to adhere to a surface and the level of protein deposition it is widely accepted to be a good indicator of biofilm formation (Kragh *et al.*, 2019). For the purposes of this chapter an increase in OD_{600} resulting from the staining of components on the surface was taken as an indicator of biofilm formation, however further investigation could be carried out into this

through imaging or comparison to a mutant strain which does not form biofilms (Kampf *et al.*, 2018; Kragh *et al.*, 2019; Barahona *et al.*, 2010). The biofilm assay protocol was repeated twice with eight wells of a 96 well plate filled with each isolate in each growth medium. While there was a significant difference in mean biofilm formation, measured based on optical density at 600 nm (OD_{600}) measured using an Ultraspec 2100pro spectrophotometer (Biochrom, UK), for the different growth conditions ($F(5,123.8) =$, $P < 1e\text{-}4$, based on a one-way ANOVA), within the same medium, there was no significant difference in biofilm formation between isolates, based on *post hoc* testing (Figure 2.8, Table 2.4). This indicates that, under these conditions, transformation did not impact on isolates ability to colonise abiotic surfaces.

Table 2.4. Mean OD_{600} for recorded in biofilm assays for transformed and untransformed isolates of Psf SBW25 in different growth media.

Isolate	Medium	Mean OD_{600} ±SD
Psf SBW25	Water	0.32 ± 0.04
	LB	0.13 ± 0.03
	RD-MOPS	0.31 ± 0.03
Psf E1433 pGFP	Water	0.3 ± 0.04
	LB	0.12 ± 0.03
	RD-MOPS	0.33 ± 0.03
E1433 pCherry	Water	0.31 ± 0.1
	LB	0.1 ± 0.02
	RD-MOPS	0.28 ± 0.05

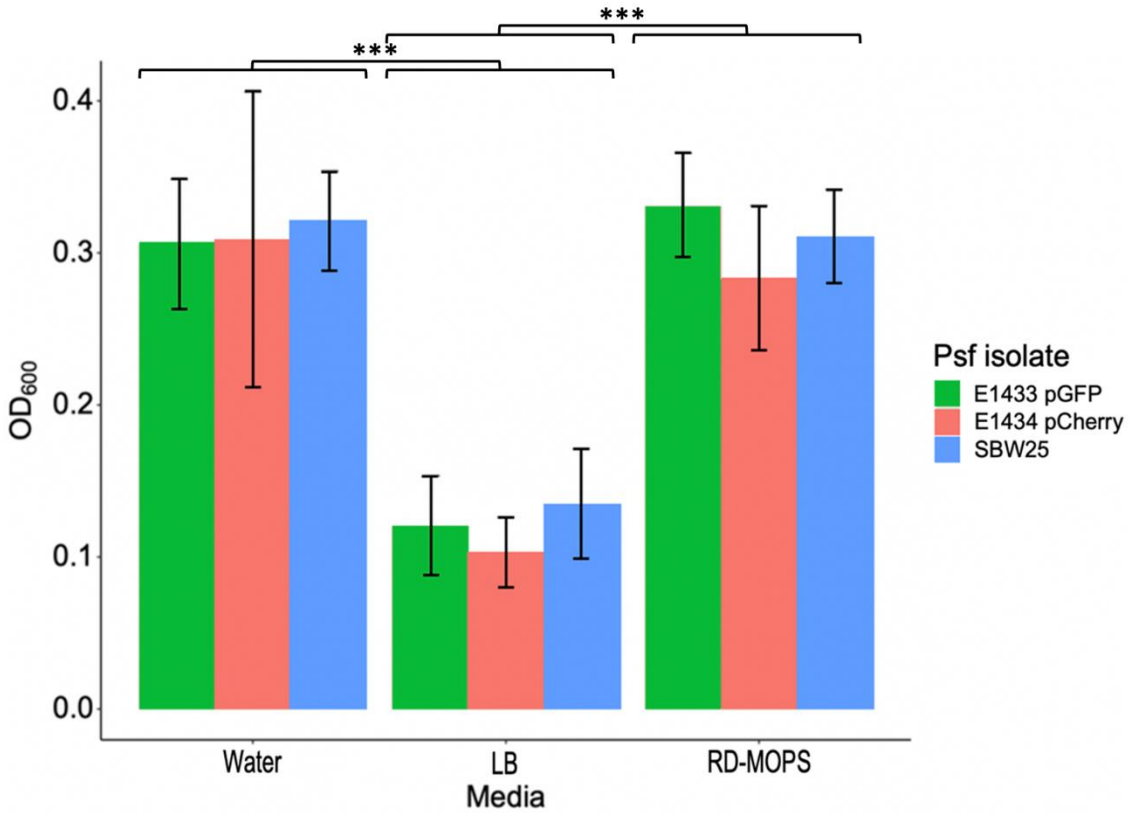

Figure 2.8. Static biofilm assays were used to compare biofilm formation of transformed and untransformed Psf SBW25. Based on a one way ANOVA, a significant difference in variance was seen across groups (F(5,123.8) =, P < 1e-4,), however subsequent *post hoc* testing indicated that there was no significant difference between Psf SBW25, Psf E1433 pGFP, and Psf E1434 pCherry for any of the three-growth media. Error bars represent standard error of the mean. *** indicates a significant difference (P < 0.001). Each bar represents the mean OD_{600} value for eight wells of the same condition across two replicates of the biofilm assay protocol.

Root growth rate was determined in a microcosm system suitable for the quantification of rhizoplane colonisation

The theoretical model of bacterial colonisation of a growing root tip developed by Dupy et al. (2016) indicated that root growth rate should be an important factor in determining bacterial colonisation density and patterns as the result of dilution of bacterial colonies on an expanding surface. In Chapter 5, root growth rate is incorporated into a model of bacterial chemotaxis. Different plant growth systems were tested for measuring plant growth rate.

Seeds were surface sterilised to remove epiphytic microorganisms which could interfere with later colonisation assays. The surface sterilisation assay was tested by making imprints of 30 surface sterilised seeds on non-selective LB agar. Imprints of 15 unsterilised seeds were also made. Within 24 hours of incubation at 27 and 18 ^{o} C unsterilised imprints were covered with a number of indistinguishable colonies of unidentified bacteria and fungi. Imprints of sterilised seeds showed no signs of bacterial growth after 24 hours of incubation at either 27 or 18 ^{o}C. Across replicates, seeds had a germination rate of 89 % (SD = 11%), which was taken as an indication that plants were not negatively impacted by sterilisation.

Within both plant growth systems, a single measurement was determined for each plant at the relevant time point by measuring root length along the longest axis of the primary root. Of two trials of eight plants each in hydroponic pouches, only four plants grew without contamination for the full five days. Although visibly contaminated roots were discarded, it is likely that growth rate was impacted by the fact that the system was not sterile. A linear regression showed a significant positive correlation between time and length measured for live roots (R^2 = 0.45, F(1,28) = 24.47, P < 1e-4, N = 30), however due to the low sample number and issues of contamination, this method was not investigated further and no attempt to determine the accuracy of the live measurement system was made. Roots grown in the microcosm systems did not show the same levels of contamination. Over three replicates, five roots grown in microcosms were destructively sampled every 24 hours for five days. A linear regression also showed a significant correlation between root length and time based on destructive measurement of plants grown in microcosm systems (R^2 = 0.56, F(1,73) = 94.14, P < 1e-4, N = 75) with a mean root growth rate of 0.01 cm hour^{-1} (Figure 2.9). Root growth rates measured destructively were later replaced in models with live measurements of roots grown in transparent soil.

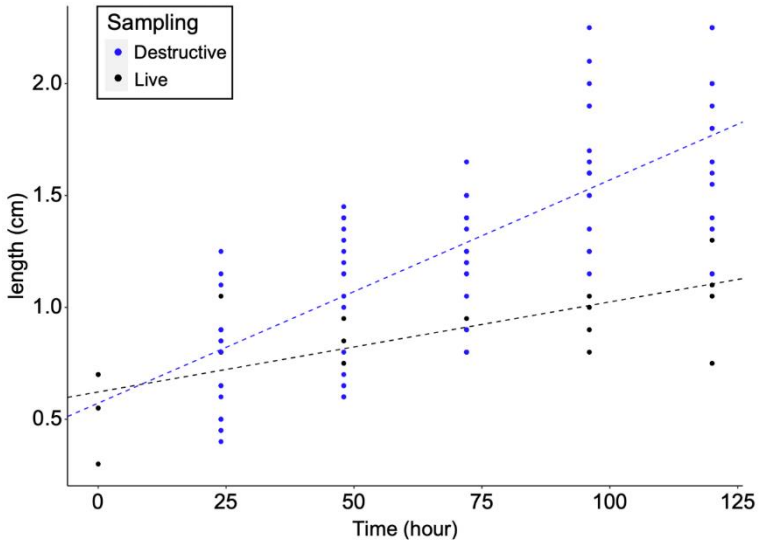

Figure 2.9. Root growth rate was investigated through live and destructive measurement techniques. Hour 0 here represents the initial measurement of root growth immediately following transfer of a germinated seed to the relevant growth system (three days after the sterilisation and soaking of seeds). Based on a linear regression, growth rate observed in hydroponic pouch experiments was 0.004 cm hour^{-1} (black line) (R^2 = 0.45, F(1,28) = 24.47, P < 1e-4, N = 30). However, this method resulted in high levels of contamination. Based on a linear regression, growth rate measured non-destructively in agar (blue line) resulted in a growth rate of 0.01 cm hour^{-1} (R^2 = 0.56, F(1,73) = 94.14, P < 1e-4, N = 75).

Measurement of root colonisation

To ensure that the transformation of bacteria had not impacted the ability of isolates to colonise plant roots, root colonisation was assessed in a hydroponic growth system. To ensure that the system contained no culturable bacteria other than intentional inoculants, fifteen uninoculated plants were homogenised and plated on non-selective LB agar. No bacterial growth was found on these negative control plates. This, along with the fact that colony counts were carried out on selective Kings-B agar containing tetracycline, was taken to indicate that colony counts represented Psf which had colonised the root during the assay. During the assay, fifteen plants for each isolate were sampled 24 hours post inoculation. A significant difference in mean colonisation density (y) of lettuce roots was found between the three isolates using a one-way ANOVA (F(2,42) = 6.712, P = 0.007, figure 2.10). Subsequent *post hoc* testing indicated that mean colonisation density of Psf SBW25 (mean = 0.145 g^{-1}, SD = 0.15 g^{-1}, N = 15) was significantly different from Psf E1434 pCherry (mean = 0.05 g^{-1}, SD = 0.02 g^{1}, N = 15) (P =

0.02). No significant difference in mean was found between Psf SBW25 and Psf E1433 pGFP (mean = 0.12, SD = 0.086, N = 15) (P = 0.77) or Psf E1434 pCherry and Psf E1433 pGFP (P = 0.09, N = 15). Due to its similar performance to the untransformed isolate in growth and colonisation assays, Psf E1433 pGFP was used as the model isolate for studying bacterial activity though imaging in later chapters.

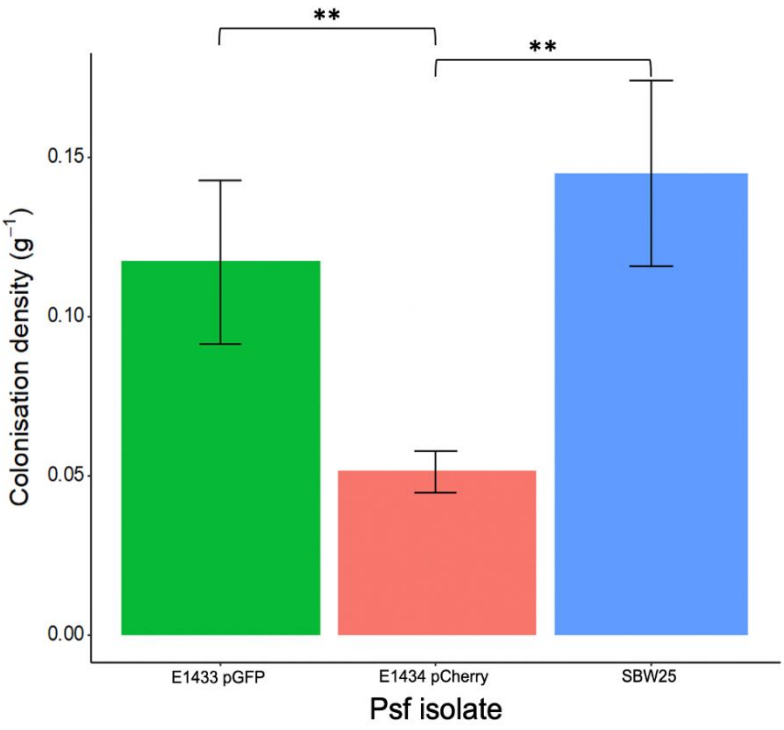

Figure 2.10. The ability of untransformed Psf SBW25 (blue), transformed Psf E1433 pGFP (green), and Psf E1434 pCherry (peach) to colonise lettuce roots was investigated in a hydroponic system. Mean colonisation density of Psf E1434 pCherry was found to be significantly different from the other two groups based on a one-way ANOVA ($F(2,42) = 6.712$, $P = 0.007$) and subsequent post-hoc testing. Error bars represent standard error of the mean. ** indicates a significant difference ($P < 0.01$). Each bar represents the mean colonisation density on the roots of fifteen plants for each isolate.

Discussion

The work in this chapter aimed to establish a model plant and bacterial system which could be used to visualise bacterial colonisation of plant roots. To ensure that transformed isolates were suitable for use in subsequent experiments, their performance was compared to untransformed bacteria when growing in different conditions, forming biofilms on abiotic surfaces, and colonising roots over short time periods. The transformation of Psf SBW25 with the E1433 pGFP and E1434 pCherry plasmids provided two isolates which could be used to image bacterial processes, such as chemotaxis and root colonisation, in transparent media. The antibiotic resistance of transformed isolates also enabled selection during destructive colonisation assays.

Biofilm formation is a key factor in the ability of many bacterial strains to colonise the rhizoplane (Tomlinson and Fuqua, 2009; Noirot-Gros *et al.*, 2018). Biofilm formation on an abiotic surface was investigated in this chapter as a simple method for comparing transformed and untransformed isolates. All three isolates performed similarly in biofilm assays, however there were differences between the untransformed isolate and Psf E1434 pCherry in terms of growth rate and colonisation of lettuce roots after 24 hours. Given the need for a model system which could be used to characterise a biologically relevant root colonisation process, Psf E1434 pCherry was not used in further experiments. Observed differences could be the result of toxicity from the pCherry protein or the metabolic cost of maintaining the plasmid at high copy numbers (Shaner, Steinbach and Tsien, 2005). Changes to bacterial growth rates or morphology are common following transformation with fluorescent marker plasmids (Barbier and Damron, 2016).

Having two easily distinguished isolates could be beneficial to future adaptations of the live imaging frameworks described in Chapters Four and Five. For example, the relative proportion of colonisation by different isolates could be examined following inoculation at different time points. In future, should a second fluorescently marked isolate be required, other fluorescent proteins, such as mRuby2 could be incorporated into the pME6010 shuttle vector (Wilton *et al.*, 2018). Alternatively, the relevant antibiotic resistance and fluorescent protein genes could be integrated into the Psf SBW25 chromosome (Unge *et al.*, 1999). Given the success of Psf E1433 pGFP as a model system, this isolate was sufficient to pursue the questions in this work, and a further isolate was not developed.

In terms of growth, biofilm formation, and root colonisation, Psf E1433 pGFP performed similarly to untransformed Psf SBW25. Plasmids based on the pME6010 shuttle vector have been used as fluorescent markers in Psf SBW25 in previous studies, and are stable for at least two weeks in the rhizosphere in the absence of an antibiotic (Wilton *et al.*, 2018). This was one reason why it was chosen as backbone for marker plasmids used in this chapter. The work presented above has shown that the E1433 pGFP is stable in Psf SBW25 in a nutrient rich medium for at least one week in the absence of antibiotics. Given its stability, physiological similarities to the untransformed isolate, and advantages for selection and imaging, Psf E1433 pGFP was chosen as the model bacterial system for further experiments in this thesis.

The growth of Psf isolates was also characterised extensively. This was partially to ensure that transformation had not impacted the physiology of the isolates to the point that the dynamics of colonisation were no longer biologically relevant. It was also to establish the growth dynamics of isolates in a range of growth conditions which was useful for predicting the growth stage of inoculants used in later chapters, and for comparing to the growth of isolates in other media, such as plant root exudates in Chapter 3. The parameters of bacterial growth models are impacted by bacterial isolate and growth conditions (such as temperature), making it difficult to directly compare the results of this chapter to the literature. Nonetheless, the overall pattern of growth observed for all three isolates falls in line with previous observations of Psf in different growth conditions, with growth of Psf E1434 pCherry being notable slow (Wilton *et al.*, 2018; Ardre, Dufour and Rainey, 2019).

Published studies of colonisation rarely involve quantified it over the short time periods reported in this chapter (24 hours). As a simple method of comparing the overall colonisation levels of the three isolates, this protocol was sufficient for the work presented in this chapter, alongside measures of bacterial growth and biofilm formation. Moving forward, capturing this stage of colonisation remained necessary, however assessments of colonisation in Chapters Three and Four also incorporated later time points to achieve the aim of characterising rhizoplane colonisation as a dynamic process.

Observations of colonisation by Psf SBW25 and Psf E1433 pGFP in the hydroponic system (a mean of 6.48 and 6.36 $Log_{10}CFU\ g^{-1}$ respectively) were lower than those reported by Noirot-Gros *et al.* (2018) for Psf SBW25 on aspen (*Populus tremula*) roots six days post inoculation (7.7 $Log_{10}CFU\ g^{-1}$) or Unge and Jansson (2001) on wheat (*Triticum aestivum*) roots six days

post inoculation (8.06 to 8.63 $Log_{10}CFU\ g^{-1}$). The methods used to quantify colonisation in this chapter fall in line with well-established protocols for assessing colonisation based on destructive sampling and CFU counts (Mills and Bauer, 1985; Kisluk *et al.*, 2012). Destructive sampling places limitations on the detail in which the colonisation proves can be observed and means the progress of colonisation for an individual root cannot be tracked. It also makes it difficult to assess spatial patterns of colonisation, although this can be achieved through destructive imaging (Schmidt *et al.*, 2018). Other techniques, such as live imaging in transparent media, as described in Chapter 4, overcome these disadvantages, however they require more expensive equipment and more time consuming protocols, generally leading to lower sample numbers being processed (Downie *et al.*, 2015). For this reason, destructive sampling and CFU counts remain an important component for the quantification of colonisation. They are paired with live imaging in this thesis to provide verification of systems and densely sampled time courses.

The development of root adherence assays may have benefited from the inclusion of a negative control mutant strain which did not colonise plant roots. However, such a strain would be difficult to develop with any guarantee that colonisation would be eliminated. Barahone *et al.* (2010) reported on the development of a Psf f113 mutant strain with low expression of genes involved in biofilm initiation (gacS (G), sadB (S) and wspR (W)). Compared to the wild type, the resulting strain showed low levels of biofilm formation, however colonisation of plant roots was not impacted. They theorised that colonisation was maintained by adherence of bacteria to mucigel on the plants surface. The complex interaction of bacteria with roots means developing a strain with any assurance that it would be a reliable measurement of a non-colonisation scenario would be a complex project falling outside the scope of this thesis. Further, such a strain would have limited value for the generation of the type of the quantitative data necessary to achieve the aim of developing a set of experimental and theoretical frameworks that can be used to isolate and quantify microbial processes involved in root surface colonisation. The lack of surface colonisation in the absence of an inoculant was assured in later experiments through the rigorous examination of sterilised root imprints on gels and imaging of uninoculated roots.

Going forward, the hydroponic plant growth system was abandoned in favour of the novel microcosm system. Microcosms had several key advantages. The first was that roots could be extracted with far less risk of damage, allowing the characterisation of bacterial attachment made in Chapter 3. The second was the ease with which large numbers of plants could be set

up and processed in a short space of time. Both of the plant growth systems contained liquid media, which likely impacted root growth rate (Ascough and Fennell, 2004), as well as bacterial colonisation rates (Wieland, Neumann and Backhaus, 2001). The gel and liquid microcosm system also lacked the structural component offered by percol, which is likely to have impacted colonisation (Juyal *et al.*, 2021). These issues were addressed in later experiments by observing the colonisation process in transparent soil.

The growth rate for lettuce roots recorded in microcosm systems (0.01 cm $hour^{-1}$) was relatively slow compared to those presented in Watt *et al.* (2006) for *Arabidopsis thaliana* (0.036 cm $hour^{-1}$) on agar or maize (*Zea mays*) (0.31 cm $hour^{-1}$) in a hydroponic system. Differences may be the result of stress to the plant, physiological changes resulting from different growth conditions, or the different measurement techniques employed. Root growth rate is an important factor for rhizoplane colonisation (Beauchamp, 1993; Watt, Silk and Passioura, 2006) and live measurements of roots are preferable to destructive sampling as it enables the development of an individual plant to be tracked (Downie *et al.*, 2015). Given the issues which arose around contamination of hydroponic pouches however, the rates calculated based on destructive sampling in microcosm chambers are likely more accurate. Environmental conditions affect root growth rate, meaning measurements from systems with no soil structure are likely different from that which would be observed in soil or other agricultural growth systems (Martins *et al.*, 2020; Li *et al.*, 2018). To address this, in later chapters, measurements of root growth rate in transparent soil were made by live imaging, which enabled continual assessment of individual plants over short time periods as well as in more agriculturally relevant conditions. In conclusion, the growth rates measured in this chapter are likely to be the result of artificial growing conditions and were disregarded in later chapters in favour of rates measured in transparent soil.

Conclusion

The work described in this chapter produced a model system which was used during subsequent experiments to quantify key components of the rhizoplane colonisation process. Observations of bacterial growth rates and colonisation during attachment assays enabled design of experiments used to separately estimate the contribution of bacterial growth and attachment to colonisation.

Chapter 3. Characterisation of colonisation and attachment rates

This chapter is based on data published in Carroll et al. (2020),

DOI: https://doi.org/10.3389/fmicb.2020.585443.

Introduction

There are two ways for microbial numbers to increase on the rhizoplane; (i) recruitment from the surrounding environment, resulting in attachment and/or (ii) proliferation of established microbes on the root. Precise data on the specific contribution of recruitment and proliferation to colonisation allows for more accurate modelling of the colonisation process (Shimshick and Hebert, 1979; Dupuy and Silk, 2016). In turn, this will allow spatial and temporal patterns of colonisation to be predicted and understood with a higher degree of accuracy. Total rhizoplane colonisation can be examined by determining bacterial density, either through imaging or counts of viable bacteria (Schmidt *et al.*, 2018; Hsu and Micallef, 2017). These methods cannot distinguish between sources of change in colonisation density (Richter-Heitmann *et al.*, 2016). This is a limitation of both traditional microbial assays and modern live imaging techniques. This lack of data has applied limitations on previously developed models of bacterial colonisation which attempt to account for the relative contribution of recruitment and attachment.

To address this knowledge gap, the aim of this chapter was to develop an experimental and mathematical framework that can be used to dissect key bacterial processes contributing to recruitment and maintenance on the rhizoplane. The model plant and bacterial system, described in Chapter 2 composed of lettuce (*Lactuca sativa*) and *Pseudomonas fluorescens* isolate SBW25 transformed with a fluorescent marker plasmid (Psf E1433 pGFP), was used in a series experiments designed to characterise colonisation. A theoretical framework that can be used to independently calculate rates of attachment and proliferation on the rhizoplane was then developed. This framework can be used to link the relative contribution of attachment and proliferation to the overall colonisation rate of the root.

Methods

Plant growth conditions

Lettuce (*Lactuca sativa* L. cultivar. All Year Round) seeds (Sutton Seeds, United Kingdom) were surface sterilised by soaking them in 20 ml of a solution of 2 % w/v calcium hypochlorite (Sigma Aldrich, 12116) for 15 min. They were then washed six times in 20 ml of sterile distilled water. Plates were sealed, covered with foil, and incubated at 21° C for 3 days.

A hydroponic microcosm system was used to quantify the colonisation of lettuce roots (Chapter 2, Figure 2.1). Microcosms were constructed in 75 mm round bottom culture tubes (VWR, 211-0046, UK). 1 ml of 1.5 % water agar was melted and pipetted into culture tubes. These were set on their sides, allowing agar to form a slope and a well in which microbial suspensions could interact with the root. Once agar had set, a small section was removed to form a platform on which the germinated seed was placed. Each microcosm contained 1 ml of 0.5 × Murashige and Skoog medium with no sucrose (MS) (Sigma Aldrich, M5524, UK). Light was prevented from reaching roots by tape covering the lower half of the microcosm. Unless being inoculated or sampled, microcosms were incubated in growth chambers (SANYO Electric Biomedical, Japan) at 21 °C with 16 h of light at 60 µmol m^{-2} s^{-1}. Following the three-day germination period, plants were transferred to microcosms.

Bacterial growth conditions

To prepare bacterial inoculants used in this chapter, Psf SBW25 or Psf E1433 pGFP were removed from storage in 20 % glycerol at -80 ºC and streaked onto Kings-B (Sigma Aldrich 60786, UK) agar. To ensure the maintenance of the E1433 pGFP plasmid, all growth media used to prepare Psf E1433 pGFP contained tetracycline (25 ng μl^{-1}). Plates were incubated for 24 hours at 27 ºC. Individual colonies were selected and inoculated into 5ml of liquid LB, which was incubated at 27 ºC with shaking (200 rpm) for 24 hours. A 1:100 dilution of this suspension in a rich defined MOPS (RD-MOPS) medium was then made. RD-MOPS medium contained; 100 mM 3-(*N*-morpholino)propanesulfonic acid (adjusted to a pH = 7.4 with KOH), 100 mM N-Tris(hydroxymethyl)methyl glycine (adjusted to a pH = 7.4 with KOH), 1 mM $FeSO_4$, 27.6 mM of K_2SO_4, 0.05 mM $CaCl_2$, 52.8 mM $MgCl_2$, 0.5 M NaCl, micronutrients consisting of; 0.3 µM $(NH_4)_6Mo_7O_{24}.H_2O$, 0.04 mM H_3BO_3, 0.003 mM $CoCl_2$, 0.001 mM $CuSO_4$, 0.008 mM $MnCl_2$, 0.001 mM $ZnSO_4$ (5 ml), 0.2 % v/v glycerol as a carbon source, 132 mM K_2HPO_4, 0.02 M thiamine HCl, 0.02 % v/v essential amino acid solution (Sigma Aldrich, M5550, USA), and 0.01 % v/v non-essential amino acids (Sigma Aldrich, M7145,

USA) (Neidhardt, Bloch and Smith, 1974). Bacterial suspensions were incubated for 24 hours at 18 ^{o}C with shaking (200 rpm). Suspensions in 0.5 x MS plant growth media for inoculating roots were made by diluting this to an optical density at 600 nm (OD_{600}) of 0.02 in 0.5 x MS medium, corresponding to an approximate bacterial density of 3e7 colony forming units (CFU) ml^{-1} (Figure 2.7).

Optical densities were measured using an Ultraspec 2100pro spectrophotometer (Biochrom, UK) blanked with a 500 µl sterile aliquot of the relevant medium. Plants were grown in microcosms for three days prior to inoculation. To inoculate microcosms, plant growth medium was replaced with an equal volume of bacterial suspension. Prior to each inoculation, 10-fold serial dilutions of a 100 µl sample of the inoculant were plated on Kings-B agar containing tetracycline (25 µg ml^{-1}). Plates were incubated at 27 ^{o}C for 24 hours before a CFU count was established, giving a value for bacterial density in the inoculant (CFU^{0}).

Root exudate collection

Plants were grown in sterile microcosms for eight days. Plants were then removed and the liquid growth medium from each microcosm was retrieved. Two methods were used to ensure the sterility of exudates. First, 100 µl filtered exudate solution from each microcosm was plated on non-selective LB agar. These plates were incubated at 27 ^{o}C for 24 hours before being visually inspected for contamination. If there was no visible contamination, a 16S PCR was used to test for the presence of bacterial rDNA (Marchesi *et al.*, 1998). Separate PCR reactions (25 µl) were set up for the exudate collected from each microcosm. A positive control consisting of a suspension of Psf E1433 pGFP in 0.5 x MS medium at an OD_{600} of 0.02, prepared as described above under *Bacterial growth conditions*., and a negative control of ddH_2O (Sigma Aldrich, W4502, UK) were also included. Each reaction contained GoTaq polymerase (0.125 µl, Promega, Holland), GoTaq buffer (0.125 µl, Promega, Holland), 0.2 mM dNTPs (2.5 µl), forward primer; 0.5 µM 16s_63F (0.25 µl, 5'-CAGGCCTAACACATGCAAGTC-3'), reverse primer; 16s_1387R (0.25 µl, 5'-GGGCGGTGTGTACAAGGC-3'), template (1 µl) and ddH_2O. A thermocycler (Biometra, Germany) was set with the following cycle: denaturing at 95 ^{o}C for 2 minutes, 30 cycles of 94 ^{o}C for 30 seconds, 58 ^{o}C for 30 seconds, and 72 ^{o}C for 90 seconds, followed by a final extension at 72 ^{o}C for 7 minutes. PCR products were then run through a 1 % agarose gel alongside a 100 bp ladder (Promega, G2101, Holland) in 1 x TBE buffer. Sterile exudates were pooled.

Benedict's reagent ($CuSO_4$, Sigma Aldrich, 11954, USA) was used to estimate the total amount of reducing sugar in exudates. 25 µl of exudate and 50 µl of Benedict's reagent were pipetted into a sample tube. This was heated to 99 ^oC for five minutes in a thermocycler (Biometra, Germany). Reducing sugar content was then estimated based on comparison to a range of glucose solutions of known concentration. Aliquots of exudate were stored at -80 ^oC between experiments.

Biofilm formation in exudate

The impact of the presence of exudate on biofilm formation was assessed through a static biofilm assay (Merritt, Kadouri and O'Toole, 2006). Overnight cultures of Psf SBW25 and Psf E1433 pGFP were prepared as described above under *Bacterial growth conditions*. These were pelleted by centrifugation at 4000 rpm for six minutes using a Megafuge 16R Centrifuge (ThermoFisher, USA). They were then resuspended in 5ml of either, exudate, 0.5 x MS, or a 2.5e-3 g ml^{-1} glucose solution. Suspensions were incubated for a further hour at 27 ^oC with shaking at 200 rpm before being diluted to an OD_{600} of 0.02 in the relevant medium, corresponding to an approximate bacterial density of 3e7 CFU ml^{-1} (Figure 2.7). 200 µl of each isolate in each medium was then pipetted into five separate wells in a 96 well plate. Control wells, containing 200 µl of the relevant sterile medium, were also set up. Plates were covered and incubated at 27 ^oC for 24 hours. Liquid was then removed from the plate by brisk shaking. The plate was rinsed by submersion in sterile phosphate buffer saline (PBS), then dried by vigorous shaking. 125 µl of 0.1 % crystal violet solution was pipetted into each well and the plate was incubated at room temperature for ten minutes. The crystal violet solution was removed by shaking, and the plate washed by submerging twice in water. The plate was dried overnight at room temperature. 200 µl of a 1: 4 acetone: ethanol mixture was pipetted into each well to elute the dye. The contents of each well were then transferred to an optically clear 96 well plate and the OD_{600} was recorded. Data was normalised by subtracting the mean value of the negative controls for the relevant medium for each experimental replicate.

Characterisation of bacterial growth

The growth of Psf E1433 pGFP in microcosms containing no plant was investigated in the presence and absence of roots and root exudates. Liquid cultures of Psf E1433 pGFP in RD-MOPS medium were prepared as described above under *Bacterial growth conditions*, with cultures diluted to an OD_{600} of 0.02 in either sterile 0.5 x MS or exudate. Sterile microcosms containing no plant were inoculated with each suspension. Microcosms were incubated at 21°

C. At 2, 24, 48, 72, 144, and 168 hours post inoculation, a 100 µl sample of medium was taken from each chamber. 10-fold Serial dilutions of these samples were plated on Kings-B agar containing tetracycline (25 µg ml^{-1}). Plates were incubated at 27 ºC for 24 hours before CFU counts were determined.

The proliferation of Psf E1433 pGFP in the medium surrounding a root was investigated. Microcosms containing plants, and control chambers with no plants were inoculated with a bacterial suspension as described above under *Bacterial growth conditions*. Microcosms were incubated as described above under *Plant growth conditions*. A 100 µl sample of medium was taken from each chamber at 2, 24, 48, 72, and 96 hours post inoculation. 10-fold serial dilutions of these samples were plated on Kings-B agar containing tetracycline (25 µg ml^{-1}). Plates were incubated at 27 ºC for 24 hours before CFU counts were determined.

Internalisation assays and root cross sectioning

An internalisation assay and imaging were used to assess the fraction of rhizoplane bacteria that migrate within the tissue during the early stages of colonisation. Microcosms containing plants were inoculated as described above under *Bacterial growth conditions*. At 2, 24, 48, and 72 hours post inoculation samples were taken. Plants were removed from microcosms, dipped three times in sterile PBS and roots were separated from the phyllosphere (with the distinction between the two marked by the hypocotyl) using an ethanol-sterilized razor blade.

For the internalisation assay, roots were surface sterilised by placing them in a 10 ml 0.03 % w/v sodium hypochlorite solution and incubating at room temperature for three minutes with gentle shaking. To determine if surface sterilisation had been effective at removing external bacteria, imprints were made by placing the roots on Kings-B agar containing tetracycline (25 µg ml^{-1}) for 30 seconds, on each side. Plates were incubated at 27 ºC for 24 hours and then visually inspected for contamination. Following surface sterilisation, roots were placed in 1.5 ml sample tubes and weighted using a fine balance (Ohaus, USA). 100 µl of Sterile PBS was then added, and roots were homogenised using a micro pestle. 10-fold serial dilutions of these suspensions were plated on Kings-B agar containing tetracycline (25 µg ml^{-1}). Plates were incubated at 27 ºC for 24 hours before a CFU count was determined.

Cross sections were prepared based on a modification of the protocol described in Lagunas *et al.* (2018). Roots sections of 5 mm were prepared. 100 ml of 5 % w/v agar was heated to the point that the agar was fully dissolved. The agar was poured in a plate and allowed to cool to

50 ºC with constant stirring. Root sections were then submerged vertically in the agar. Plates were stored at 4 ºC for an hour. 1 cm^2 blocks, containing root sections, were then cut from the agar. These were glued to a vibratome specimen holder (Campden Instruments, UK) using superglue. 70 μm sections of root were then cut using a 7000 smz Tissue Sliver (Campden Instruments, UK) at an amplitude of 2 mm and a frequency of 80 Hz. Where possible, sections were obtained from the first, last and central millimetre of the root. Sections were placed on microscope slides and imaged using a Nikon A1R confocal laser scanning system mounted on a NiE upright microscope fitted with a NIR Apo 40 × 0.8 W water dipping lens with GaAsP detectors (Nikon, Japan). pGFP was excited at 488 nm with the emissions being collected at 500–530 nm.

Quantification of root surface colonisation

Bacterial density on the roots of plants grown in microcosms was quantified though colonisation assays based on CFU counts. Plants were inoculated with a bacterial suspension as described under *Bacterial growth conditions*. At the relevant time point, plants were removed from microcosms and dipped three times in sterile PBS. Roots were separated from the phyllosphere (with the distinction between the two marked by the hypocotyl) using an ethanol-sterilized razor blade. Roots were placed in 1.5 ml sample tubes and weighted using a fine balance. 100 μl of PBS was added to each sample, and roots were homogenised using a micro-pestle. 10-fold serial dilutions of the resulting suspension were plated on Kings-B agar containing tetracycline (25 μg ml^{-1}) and incubated at 27° C for 24 hours prior to obtaining a CFU count.

Total colonisation density (y_c) is the result of both attachment and proliferation on the rhizoplane (Figure 3.1). This was determined by quantifying bacterial density for the whole rhizosphere based on CFU counts at 2, 18, 24, 48, 54, 72, and 96 hours with further sampling every two hours between hours 18 and 54.

Proliferation on the root surface (y_p) was quantified independently (Figure 3.1). Plants were inoculated as described above under *Bacterial growth conditions*. Two hours post inoculation they were gently removed from their chambers, dipped in sterile PBS, and placed in new sterile microcosms. Sterile 0.5 x MS medium (1 ml) was added to each microcosm. An initial round of sampling was carried out to quantify colonisation density two hours post inoculation.

Microcosms were then sealed and returned to the growth chamber. Further sampling was carried out at 24, 48, 72, and 96 hours post inoculation.

Analysis of attachment and time of recruitment

To account for differences in root size and initial experimental conditions, colonisation density (y, g^{-1}) was determined based on counts (CFU), root mass (wt, g) and initial bacterial density (CFU^0) according to:

$$y = \frac{CFU}{CFU^0 wt} \qquad \text{Equation 3.1}$$

Three classical bacterial growth models, the logistic equation (Equation 3.2 & 3.3) (Tsoularis and Wallace, 2002), the Gompertz equation (Equation 3.4) (Gibson, Bratchell and Roberts, 1988), and the Baranyi equation (Equation 3.5) (Baranyi and Roberts, 1994) were fit to total colonisation (y_c), proliferation on the root surface (y_p), proliferation in the presence of a root, and proliferation in root exudate data sets (Table 3.1). The logistic equation predicts the rate of change of bacterial density (y) with time (t) based on a carrying capacity (k), initial density (y^0), and maximum growth rate (μ):

$$\frac{dy}{dt} = \mu y\left(\frac{K - y}{K}\right) \qquad \text{Equation 3.2}$$

Solution of the logistic equation are in the form:

$$y = \frac{ky^0}{y^0 + (k - y^0)e^{-\mu t}} \qquad \text{Equation 3.3}$$

The Gompertz equation can also be used to predict the rate of change of bacterial density (y) with time (t) based on a carrying capacity (k), initial density (y^0), and maximum growth rate (μ) with the solution in the form:

$$y = ke^{\ln\left(\frac{y^0}{k}\right)e^{-\mu t}} \qquad \text{Equation 3.4}$$

The Baranyi equation predicts the rate of change of bacterial density (y) with time (t) based on a carrying capacity (k), initial density (y^0), maximum growth rate (μ), and (h^0) which specifies the length of the lag phase with the solution in the form:

$$A = t + \frac{1}{\mu}\ln\left(e^{(-\mu t)-\mu t} + e^{-h} - e^{-\mu t - h^0}\right) \quad \text{Equation 3.5}$$

$$\ln(y) = \ln(y^0) + \mu A - \ln\left(1 + \frac{e^{\mu A} - 1}{e^{\ln(k)}} - \ln(y^0)\right)$$

A separate model, representing logistic decline, was developed for the change in bacterial density in the absence of a root or root exudate:

$$y = a + b\left(1 - e^{(-c/time)}\right) \quad \text{Equation 3.6}$$

The best fit model for each data set was determined based on lowest Akaike Information Criterion (AIC) score. The Bootstrap method was used to estimate confidence intervals of the fit. Data was randomly sampled with replacement M times to produce a bootstrap sample. Models were then fit to this new data set based on a nonlinear least squares (NLS) method. The bootstrap estimate of the confidence interval (CI) was then determined as:

$$CI(t) = \frac{1}{M-1}\sqrt{\sum_{b=1}^{b=M}\frac{1}{N}\sum_{i=1}^{i=N}(y_b^i - y_m)^2} \quad \text{Equation 3.7}$$

Where N is the size of the data set, y_b^i is the ith predicted value on bootstrap sample b, and y_m is the mean predicted bootstrap value at that time-point. M is the number of times the data is resample (here 1000).

Attachment rate (R_a, g^{-1} hour^{-1}) cannot be measured experimentally. A mathematical framework was developed to determine R_a based on models of total colonisation density (y_c) and proliferation on the root surface (y_p). R_a was derived based on the difference between the rate of total colonisation (R_c, g^{-1} hour^{-1}) and the rate of proliferation on the root surface

(R_p):$R_c = R_p + R_a$. Equation 3.2 represents the change in total colonisation with time. The rate of change in total colonisation (R_c) can therefore be obtained by differentiation of this Equation:

$$R_c = \frac{k_c \left(\frac{k_c}{y_c^0} - 1\right) e^{\mu_c}}{\left[1 + \left(\frac{k_c}{y_c^0} - 1\right) e^{\mu_c t}\right]^2}$$ Equation 3.8

R_c is the result of attachment and proliferation on the root surface. Proliferation is dependent on the density of bacteria already present on the root surface as described in Equation 3.3. At a given time point, in conditions in which both attachment and proliferation are occurring, the rate of proliferation will be dependent on total colonisation on the root (y_c) at that point. To account for this, the contribution of proliferation to colonisation rate was determined as a function of the bacterial density determined in Equation 3.3 fit to total colonisation data (y_c) at time t:

$$R_p = \mu_p y_c \left(\frac{k_c y_c}{k_c}\right)$$ Equation 3.9

Rate of attachment (R_a) can then be calculated based on the difference between the rate of total colonisation (R_c) and the rate of proliferation (R_p):

$$R_a = R_c - R_p = \frac{k_c \left(\frac{k_c}{y_0^c} - 1\right) e^{\mu_c}}{\left[1 + \left(\frac{k_c}{y_0^c} - 1\right) e^{\mu_c t}\right]^2} - \mu_p y_c \left(\frac{k_c y_c}{k_c}\right)$$ Equation 3.10

R_a can then be characterised as a function of total colonisation density using the proliferation coefficient μ_p.

Based on the above, the role of timing in the success of bacteria colonising the root surface was investigated. The relative contribution of attachment at any given time (t) to total colonisation

of the rhizoplane (y_c) was calculated as the proportion (p) of the final bacteria that originate from those attached at (t):

$$p(t) = \frac{R_a(t)}{k_c} \int_t^{96} \mu_p y_c \left(\frac{k_c - y_c}{k_c}\right) dt$$

Equation 3.11

Table 3.1. Model variables and parameters.

Notation	Parameter (unit)
Wt	Root wright (g)
CFU^0	CFU of inoculant (ml^{-1})
y	Colonisation density on root surface (g^{-1})
t	Time (hour)
k	Carrying capacity (g^{-1} or Log_{10}CFU)
y^0	Colonisation density or bacterial density on root surface at hour 0 (g^{-1} or Log_{10}CFU)
μ	Maximum growth rate ($hour^{-1}$)
h^0	Length of the lag phase (hour)
y_c	Total colonisation density (g^{-1})
k_c	Root surface carrying capacity (g^{-1})
y_0^c	Colonisation density on root surfaces at hour 0 for total colonisation (g^{-1})
μ_c	Maximum growth rate for total colonisation (g^{-1} $hour^{-1}$)
y_p	Colonisation density in the absence of attachment (g^{-1})
y_0^p	Colonisation density on root surfaces at hour 0 in the absence of attachment (g^{-1})
μ_p	Maximum growth rate in the absence of attachment (g^{-1} $hour^{-1}$)
R_c	Rate of total colonisation (g^{-1} $hour^{-1}$)
R_p	Rate of proliferation on the root surface (g^{-1} $hour^{-1}$)
R_p^y	Rate of proliferation on the root surface in the absence of attachment (g^{-1} $hour^{-1}$)
R_a	Rate of attachment (g^{-1} $hour^{-1}$)
$p(t)$	Contribution of attachment at t to total colonisation of the rhizoplane at hour 96
N	Sample number
M	Bootstrap replicates
y_b^i	The i^{th} prediction of bootstrap sample b (g^{-1} or Log_{10}CFU ml^{-1})
y_m	The mean predicted bootstrap value at b (g^{-1} or Log_{10}CFU ml^{-1})

Data analysis and use of software for growth rate modelling

All data analysis was carried out in R (Team, 2018). Growth models were fit using a non-linear least squares method (NLS) using the growthrates package (Petzoldt, 2016). Replicates of different treatments were pooled together prior to analysis. Time was measured in hours for all

data sets. Measurements of bacterial density in root exudate, in the media surrounding the root, and in microcosms in the absence of any plant or exudate were expressed as Log_{10}CFU ml^{-1}. Measurements of colonisation density for total colonisation and proliferation in the presence of exudate were normalised based on Equation 1. Confidence intervals (CI) were calculated for selected models by bootstrapping with 1000 replicates. Non-parametric cubic spline models were also fit on the dataset for total colonisation density (y_c) and proliferation (y_p). The same analysis, using standard growth models fit using a least squares method was applied and the results produced with the two different approaches were compared. Rate of change of total colonisation density (R_c) and proliferation on the root surface in the absence of attachment (R_p^y) were calculated based on the finite difference approximation of the derivative of the splines and growth models. The relationship between root mass and Log_{10}(CFU ml^{-1}) per root, for total colonisation density and proliferation data, was investigated by preforming two separate linear regressions with root mass (g) as input variable and Log_{10}(CFU ml^{-1}) as output variable. A one-way analysis of variances (ANOVA) was carried out to assess differences in mean biofilm formation between isolates and treatments, along with a subsequent Tukeys range test. Root images were acquired using NIS-elements AR software (Nikon, USA).

Results

The stimulation of bacterial growth and biofilm formation by plant root exudates was quantified

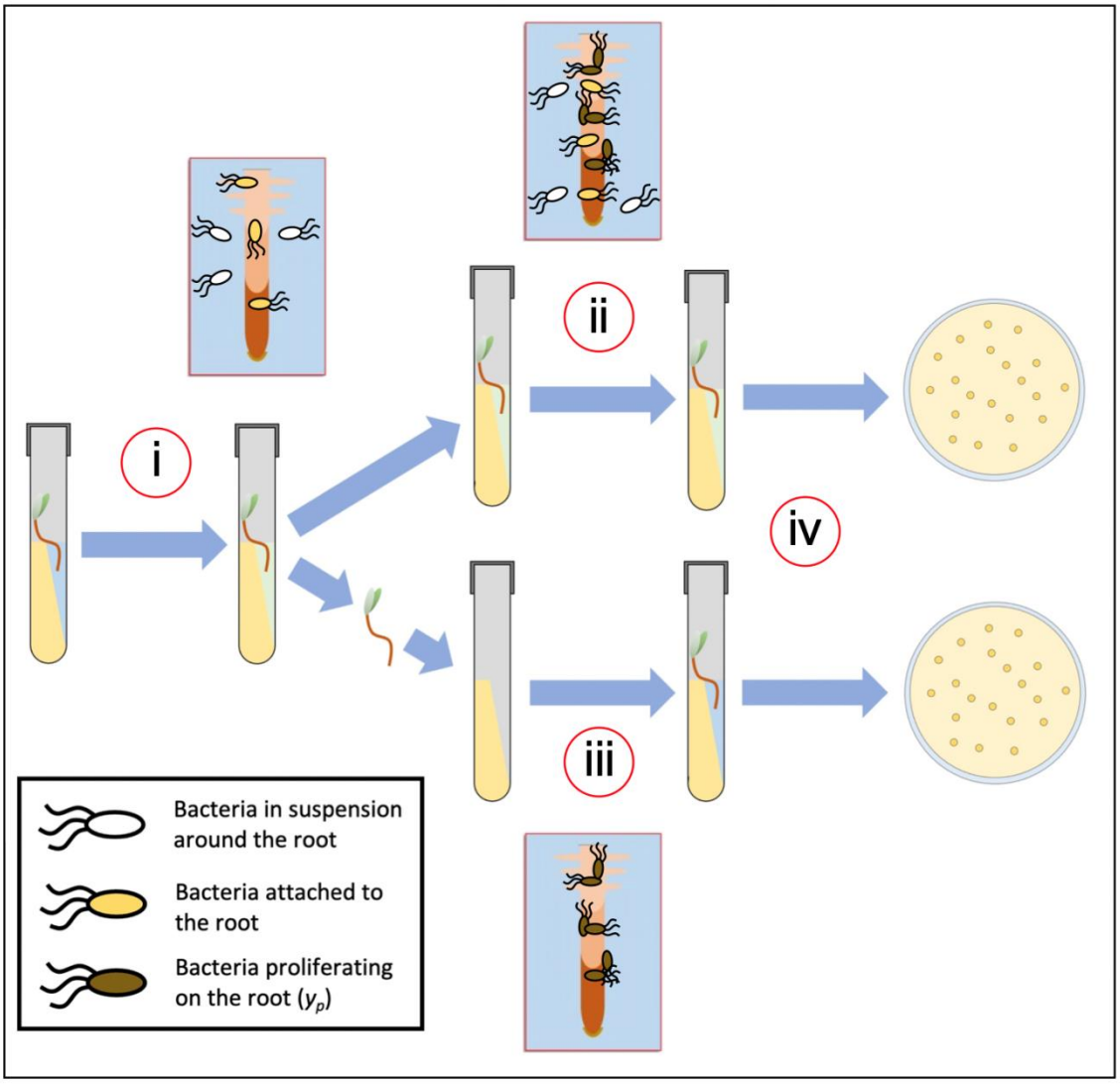

Figure 3.1. Components of root surface colonisation were independently quantified. (i) Plants were grown in microcosm chambers and inoculated with bacterial suspension. (ii) Total colonisation density (y_c) resulted from bacterial attachment as well as proliferation on the root. (iii) Proliferation on the root surface (y_p) was quantified by moving roots to sterile microcosms following inoculation, eliminating attachment from the surrounding media. (iv) Roots were destructively sampled at dense time intervals post inoculation.

To assess the ability of bacteria to grow in the presence of root exudates, plants were grown in hydroponic conditions in sterile microcosms. Exudates were collected from 30 microcosms.

To test for contamination, for each collection, a sample was plated on non-selective LB agar and used as a template for a 16s PCR. No bacterial growth on was observed on LB agar plates. PCR was used to amplify a positive control of Psf E1433 pGFP at an OD_{600} of 0.02 and the root exudates from a single plant. Contaminated exudates were discarded. Other exudates were considered sterile and pooled. Comparison to solutions of glucose at known concentrations when a Benedict's test indicated that pooled exudates had a reducing sugar concentration of approximately 2.5e-3 g ml^{-1}.

To determine if root exudates instigated biofilm formation by bacteria, static biofilm assays were used to compare biofilm formation on an abiotic surface in exudates, plant growth medium (0.5 x MS), and a glucose solution (2.5e-3 g ml^{-1}) (Figure 3.2). The static biofilm assay was repeated twice, and data pooled for analysis. For both Psf SBW25 and Psf E1433 pGFP, a significant difference in mean $OD_{600,}$ indicating biofilm formation, was found in the presence of exudates, 0.5 x MS containing no glucose, and glucose solution based on a one-way ANOVA (Table 3.2, $F(5,90) = 28.69, P < 1e\text{-}4$). Subsequent *post hoc* testing indicated that mean biofilm formation in exudate was higher, with statistical significance, than either 0.5 x MS ($P < 1e\text{-}4$ for Psf SBW25, $P = 3.8e\text{-}6$ for Psf E1433 pGFP) or glucose solution ($P < 1e\text{-}4$ for both Psf SBW25 and Psf E1433 pGFP). No significant difference was found in mean OD_{600} between isolates for any of the three media or between 0.5 x MS and glucose solution.

Table 3.2. Mean OD_{600} values obtained during static biofilm assays for different bacterial isolates and growth medium (± SD).

Medium	Psf SBW25	Psf E1433 pGFP
Exudate	0.436 ± 0.054	0.42 ± 0.062
0.5 x MS	0.31 ± 0.03	0.3 ± 0.04
2.5e-3 g ml^{-1} glucose solution	0.288 ± 0.047	0.284 ± 0.051

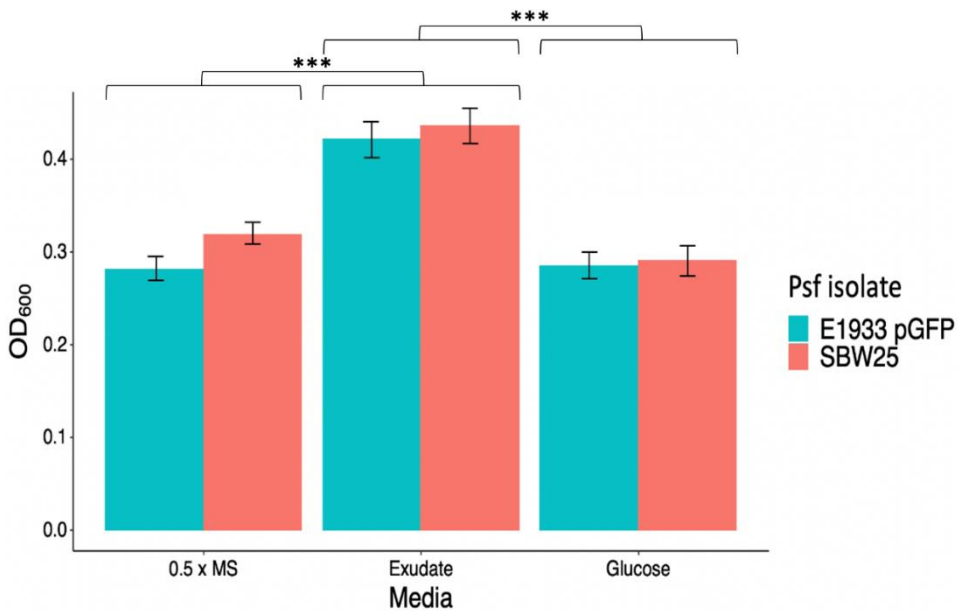

Figure 3.2. Mean biofilm formation, measured based on staining and analysis of fluorescence, was significantly different in root exudates from either glucose solution or 0.5 x MS. Based on a one-way ANOVA ($F(5,90) = 28.69, P < 1e\text{-}4$) and subsequent post-hoc testing**,** The mean biofilm formation of Psf E1433 pGFP (teal) and Psf SBW25 (orange) in exudate was higher than in either 0.5 x MS containing no glucose or 0.25 % w/v glucose solution. There was no significant difference between the two isolates within treatments. Bars represent standard error of the mean. *** indicates a significant difference ($P < 0.001$). Each bars represent the mean value for a group containing the pooled data from two replicates of the static biofilm assay.

To investigate the role of rhizodeposition in providing a nutrient source to bacteria in microcosms, the ability of bacteria to grow in exudates and in the presence of a root were quantified. Eight microcosms were inoculated with bacteria for each treatment, along with an equal number of negative controls. In microcosms without a root or root exudates, bacterial count remained constant from the point of inoculation until hour 96. Beyond 96 hours, bacterial count began to decline (Figure 3.3a). In the presence of root exudates, bacterial density increased up until hour 72, beyond which it remained steady for the study period (Figure 3.3b). In the presence of a root, bacterial density increased up until hour 24 beyond which it remained steady (Table 3.3, Figure 3.3c).

Table 3.3. Mean values for bacterial density in the presence and absence of a root and root exudates in $Log_{10}CFU\ ml^{-1}$ (± SD).

	Mean at hour 2	Mean at final time point
Root present	7.12 ± 0.409	6.67 ± 0.16 (t = 192 hours)
Exudate Present	7.85 ± 0.041	8.09 ± 0.045 (t = 96 hours)
Root and exudate absent	5.22 ± 0.026	7.41 ± 0.332 (t = 96)

The logistic decline model (Equation 3.7) was found to offer the best fit for the change in bacterial density for microcosms in the absence of a plant root or exudates (AIC = -76.92, R^2 = 0.82, CE = 0.08 $Log_{10}CFU\ ml^{-1}$, N = 33, Figure 3.3a, Table 3.4). The logistic growth model (Equation 3.3) was found to offer the best fit for the change in bacterial density in the presence of root exudates (AIC = -16, R^2 = 0.87, CE = 0.68 $Log_{10}CFU\ ml^{-1}$, N = 46, Figure 3.3b, Table 2). The Gompertz model (Equation 3.4) was found to offer the best fit for the change in bacterial density in the presence of a plant root (AIC = 123, R^2 = 0.78, CE = 0.41 $Log_{10}CFU\ ml^{-1}$, N = 112, Figure 3.3c, Table 3.4). This showed that bacteria proliferate in the presence of the root as the result of plant derived nutrients. Models fit to these data sets provided parameter values which were later incorporated into models of bacterial movement in soil (Chapter 5).

a)

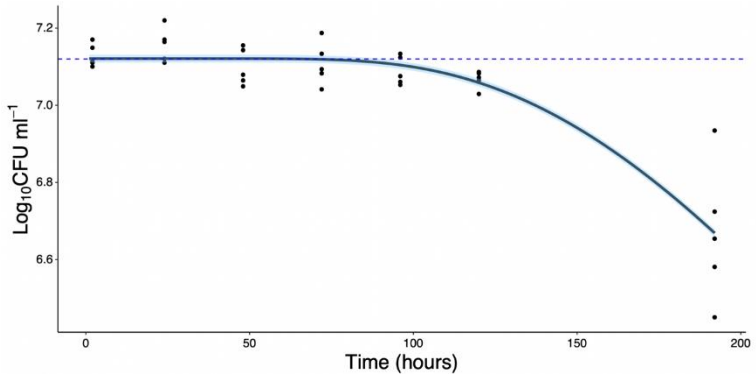

b)

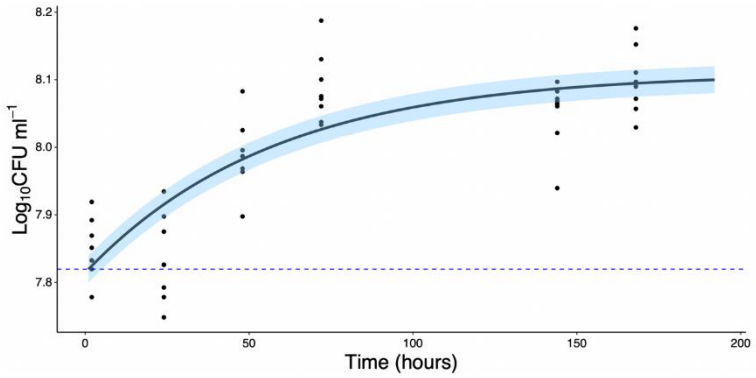

c)

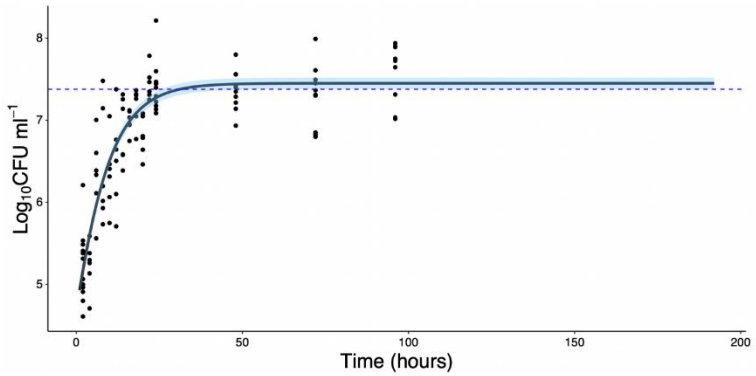

Figure 3.3. Bacterial proliferation was observed in the presence of a root or root exudates but not in 0.5 x MS. Each point represents a single measurement of CFU ml^{-1}. Models were fit to pooled data using a least squares method to estimate parameter values. Solid lines represent the estimated bacterial concentration in $Log_{10}CFU\ ml^{-1}$ for the relevant time point based the best fit model. Blue shaded regions represent bootstrap confidence intervals for the model (Table 3.4). Blue dashed lines represent the initial density of the

inoculant for each group. a) The change in bacterial density over time in microcosms containing no plant or root exudate (N = 35). b) The change in bacterial density over time in root exudate in the absence of a plant (N = 48). c) The change in bacterial density over time in the media in microcosms containing a plant root (N = 144).

Table 3.4. Models selected based on lowest AIC for each data set along with fit parameter values.

Data set	Selected model	Bootstrap confidence intervals (CI)	Parameters
Total colonisation (y_c)	Logistic (Equation 3.3)	0.54 g^{-1}	$y^0 = 0.007\ g^{-1}$ $k = 8.856\ g^{-1}$ $\mu = 0.1847\ hour^{-1}$
Proliferation on root surface (y_p)	Logistic (Equation 3.3)	0.82 g^{-1}	$y^0 = 0.025\ g^{-1}$ $k = 9.04\ g^{-1}$ $\mu = 0.099\ hour^{-1}$
Proliferation in root presence	Gompertz (Equation 3.4)	0.07 $Log_{10}CFU\ ml^{-1}$	$y^0 = 4.667\ Log_{10}CFU$ $k = 7.45\ Log_{10}CFU$ $\mu = 0.124\ hour^{-1}$
Proliferation in exudate	Logistic (Equation 3.3)	0.01 $Log_{10}CFU\ ml^{-1}$	$y^0 = 7.814\ Log_{10}CFU$ $k = 8.11\ Log_{10}CFU$ $\mu = 0.018\ hour^{-1}$
Proliferation in the absence of root or exudate	Logistic decline (Equation 3.7)	0.02 $Log_{10}CFU\ ml^{-1}$	$a = -5.151$ $b = 12.272$ $c = 633.798$

Bacterial attachment and growth on the rhizoplane both make contributions towards colonisation

The microcosm system was used to quantify colonisation under different conditions. To quantify total colonisation (y_c), resulting from the combination of both attachment and proliferation on the rhizoplane, each plant was grown in a single microcosm and colonisation density was quantified destructively at various time points. To quantify proliferation in the absence of attachment (y_p), plants were transferred to sterile microcosms two hours after inoculation (Figure 3.1). For both total colonisation and proliferation on the root surface in the absence of attachment, a minimum of five inoculated plants, along with an equal number of negative controls, were sampled at each time point and both experiments were carried out three times. Imprints of sterilised seeds on non-selective LB agar remained clean, as did plates with homogenised roots from negative control microcosms throughout the subsequent experiments. This indicates that the experimental set up remained free of culturable contamination.

The presence of bacteria within root interiors was quantified through an internalisation assay and further investigated through root cross sectioning and imaging. Cross sections from three plants, along with a single negative control, from each time point were examined using this method. Images revealed very low levels of fluorescent bacterial colonies within roots, even when high levels of colonisation were visible on root exteriors (Figure 3.4a & b). During the internalisation assay, five microcosms were sampled for each time point, along with an equal number of negative controls. Root surfaces were sterilised to remove bacteria from the root exterior. Imprints of sterilised roots were made to test the sterilisation protocol. Imprints were found to be free of bacterial growth, indicating that bacteria on the root surface had been removed by the surface sterilisation process. Internalisation was limited to < 0.2 % of mean total colonisation density (g^{-1}) in root tissue at hour 96 (Figure 3.6). No significant difference in internalisation was observed with time (R^2 = -0.038, F(1,17) = 0.0347, P = 0.564, N = 18). As a result, internalisation was considered insignificant and was not included in modelling and analysis.

a) b)

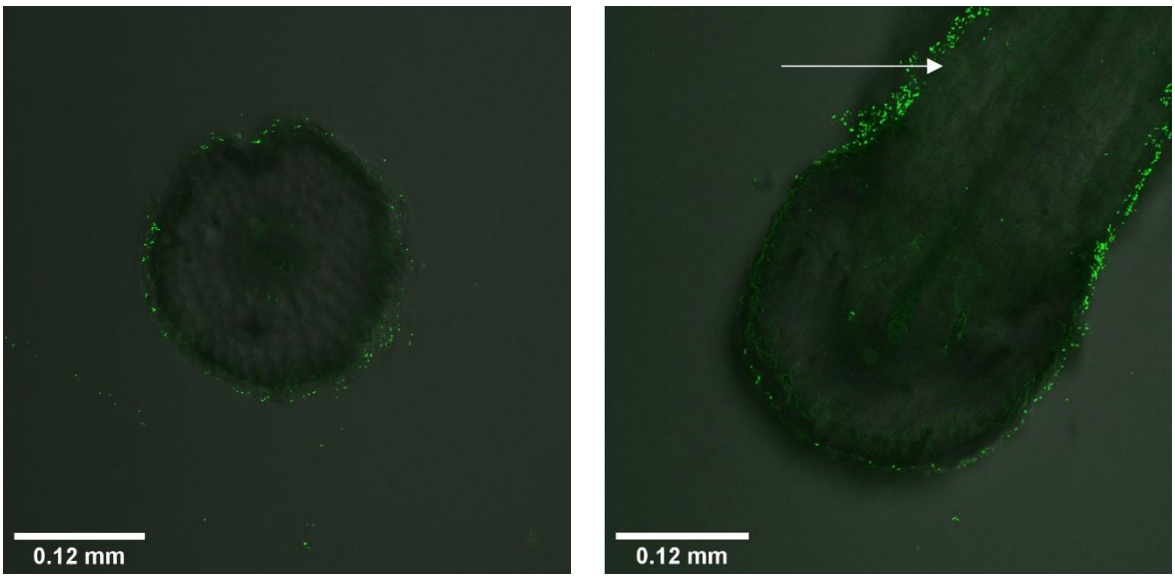

Figure 3.4. Bacterial colonies were not visible in root interiors, even when high levels of colonisation were visible on the root surface. Fluorescence (confocal laser scanning microscope) and transmission images of root cross sections displaying the colonisation of Psf E1433 pGFP on root exteriors (displayed in green with an excitation wavelength of 488 nm and emission of 500-530 nm) and low levels of bacterial fluorescence in root interiors. a) 48 hours post inoculation at 0.5 mm from the root tip b) 72 hours post inoculation with a lateral root visible emerging in the top right of the image (indicated by a white arrow) 0.5 mm from the root tip.

Despite growing under the same conditions, plants showed high levels of variability in root size (Figure 3.5). To account for this, measures of bacterial density were normalised for root mass. Root mass (g) had a significant positive correlation with bacterial density (Log_{10}CFU ml^{-1}) at hour 96 for total colonisation (slope = 214.5508 Log_{10}CFU ml^{-1} g^{-1}, intercept = 5.2912 Log_{10}CFU ml^{-1}, R^2 = 0.4856, F(1,19) = 19.88, P < 1e-4, N = 21). No significant correlation was found for root mass (g) and bacterial density (Log_{10}CFU ml^{-1}) for proliferation in the absence of attachment beyond hour two (R^2 = -0.02097, F(1,16) = 0.65, P = 0.432, N = 18, Figure 3.5). Root mass and initial total CFU counts (CFU_0) were used to determine normalised colonisation density (y, Equation 3.1) to control for differences in plant size.

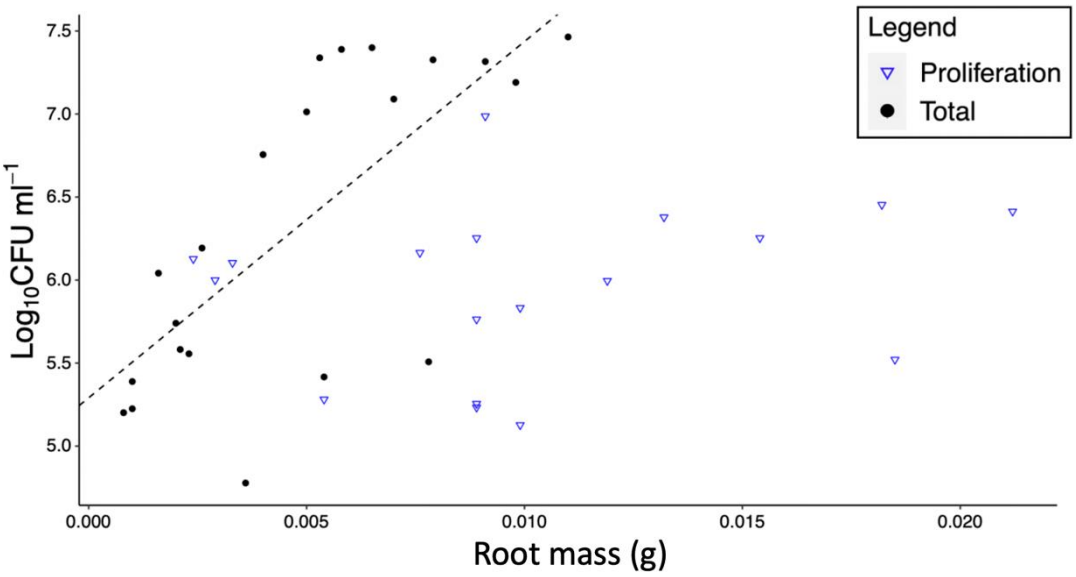

Figure 3.5. Bacterial numbers on the rhizoplane and root mass at 96 hours for roots in the total colonisation group were positively correlated. Points represent individual destructive measurements of root mass and bacterial density divided into total colonisation (black, N = 21) and proliferation on the root surface (blue, N = 18) groups. Black dashed line represents the linear model for total colonisation (slope = 214.5508 Log_{10}CFU ml^{-1} g^{-1}, intercept = 5.2912 Log_{10}CFU ml^{-1}, R^2 = 0.4856, F(1,19) = 19.88, P < 1e-4).

Quantification of total colonisation on the rhizoplane (y_c) showed an increase in colonisation density with time, rising from a mean of 0.4 g^{-1} at hour two, to a plateau with a mean of 9.97 g^{-1} at hour 72. A similar pattern was observed for the colonisation process in the absence of attachment beyond hour 2 (y_p), with colonisation density rising from a mean of 0.13 g^{-1} at hour two and beginning to plateau at hour 96 with a mean of 8.78 g^{-1}. Colonisation density remained variable between samples even after normalisation, therefore variability was likely the result of biological variability between plants and bacterial populations. Classical bacterial growth models were fit to experimental data. The logistic model (Equation 3.3) was found to be the best fit for both total colonisation (AIC = 1286, R^2 = 0.42, CE = 0.56 g^{-1}, N = 223) and proliferation in the absence of attachment (AIC = 498, R^2 = 0.48, CE = 3.32 g^{-1} N = 88, Table 3.2, Figure 3.6) data sets.

Non-parametric cubic spline models were also fit on the dataset for total colonisation density (y_c) and proliferation (y_p). The objective was to assess whether the use of parametric growth model, which are heavily constrained, introduces bias when computing rates of attachment and proliferation on the root. Cubic spline fits showed similar trends for total colonisation and proliferation in the absence of attachment (Figure 3.7a) and for rate of colonisation and proliferation (Figure 3.7b). This suggested that bias was not introduced by the choice of model.

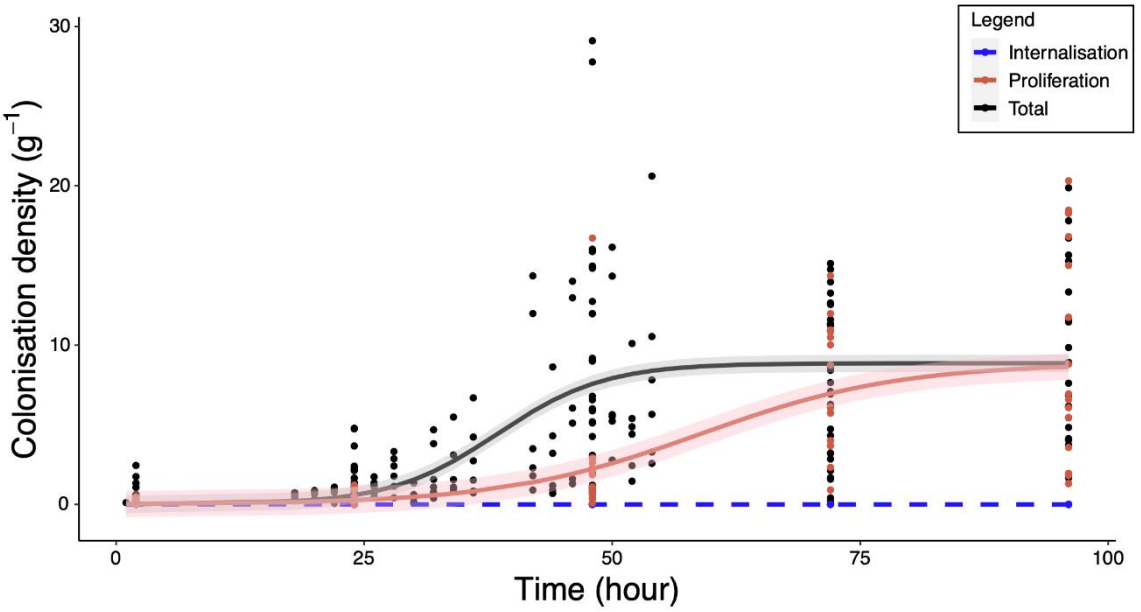

Figure 3.6. Colonisation density (g^{-1}) was quantified and modelled for total colonisation (y_c) and proliferation on the root surface in the absence of attachment (y_p). Models were fit to pooled data using a least squares method to estimate parameter values. The best fit model was selected based on the lowest AIC values for each data set. The logistic model was found to be the best fit for both the increase in total root colonisation density (black, N = 49) and the increase in colonisation density in the absence of attachment beyond hour 2 (pink, N = 36) (Table 3.4). Internalisation of bacteria (blue) remained at negligibly low levels over the experimental period with no significant increase with time. A linear regression found no significant corelation between these two variables (R^2 = -0.038, F(1,17) = 0.0347, P = 0.564, N = 18). Each point represents a destructive sampling of colonisation density, measured in CFU normalised for root mass and original inoculant (Equation 3.1), solid lines represent the best fit model for each data set, the dashed line represents the linear model fit to internalisation data (slope = 1e-5 g^{-1} hour^{-1}, intercept = 1e-4 g^{-1}) and shaded regions represent bootstrap confidence intervals.

Table 3.5. Mean values for colonisation density for total colonisation (N = 36) and bacterial proliferation (N = 18) on the root surface data sets (± SD).

Data set	Mean colonisation density at t = 2 hours	Mean colonisation density at t = 96 hours
Total colonisation (y_c)	0.4 ± 0.533 g^{-1}	9.97 ± 5.44 g^{-1}
Proliferation on the root surface (y_p)	0.13 ± 0.144 g^{-1}	8.78 ± 6.44 g^{-1}

a) b)

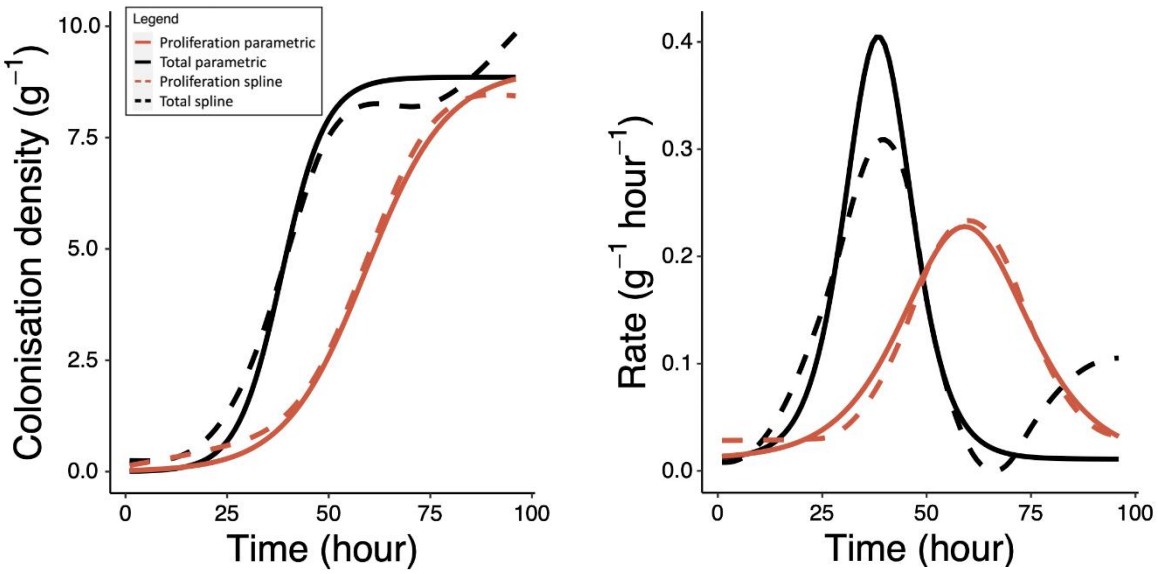

Figure 3.7. Parametric growth models and cubic splines offered a similar fit of the data and predictions for colonisation rate. a) Colonisation density data fit with parametric models (solid) (Table 3.4) and cubic splines (dashed) for total colonisation data (black, N = 49) and proliferation on the root surface in the absence of attachment data (red, N = 36). b) Colonisation rates were calculated based on the finite difference approximation of the derivative of the splines (dashed) and growth models (solid).

Mathematical modelling allows separate proliferation and attachment rates to be determined

A mathematical framework was developed to estimate attachment rate (R_a) from experimental growth curves fit to total colonisation (y_c) and proliferation in the absence of attachment (y_p) (Equation 3.10). y_c and y_p were used to determine experimental colonisation and proliferation rates (R_c and R_p^y respectively). Next, proliferation rate was expressed as a function of bacterial colonisation density. R_a was calculated based on the difference between total colonisation rate (R_c) and the proliferation rate during the total colonisation experiment (R_p) (Figure 3.8a). Bacteria present on the root surface due to attachment can be estimated by integrating the equation for attachment rate (Figure 3.8b). Attachment rate had a similar pattern to total colonisation, with a peak of 0.18 g^{-1} $hour^{-1}$ at hour 38. This indicates that the level of colonisation of the root affects further attachment or recruitment from the surrounding media.

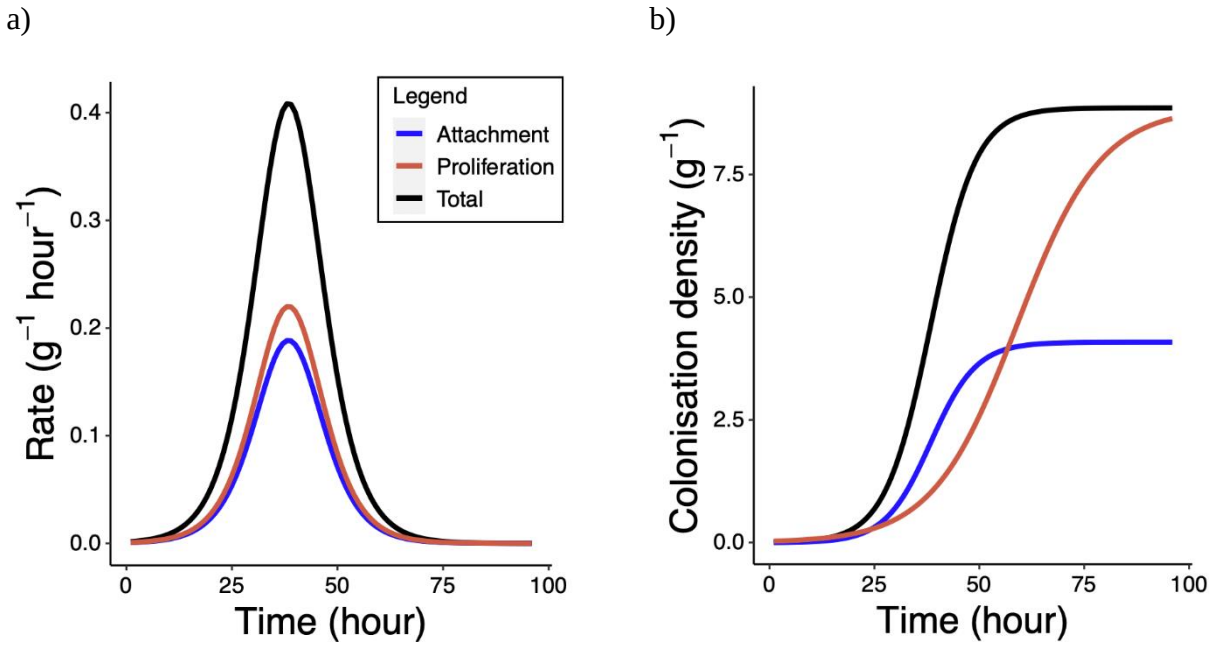

Figure 3.8. A newly developed mathematical framework allowed estimation of the contribution of different bacterial processes to colonisation. a) Equations 3.8, 3.9 & 3.10 were used to estimate colonisation rates for total colonisation (black), proliferation on the root surface (orange), and attachment (blue). b) integration of Equation 3.10 was used to estimate colonisation density due to attachment.

Factors affecting attachment and colonisation

The rate of attachment of Psf E1433 pGFP to lettuce roots was calculated based on equation 3.11. Attachment rate (R_a, g^{-1} hour^{-1}) varied across time, increasing from a starting value of 7.5e-4 g^{-1} hour^{-1} to reach a peak of 0.188 g^{-1} hour^{-1} at hour 38 and declining to a value of 1.82e-5 g^{-1} hour^{-1} at hour 96 (Figure 3.8a). The relationship between R_a and total colonisation density (y_c, g^{-1}) can be expressed as a quadratic function (Equation 3.12, Figure 3.9a). R_a peaked, with a value of 0.19 g^{-1} hour^{-1} when y_c had a value of 4.26 g^{-1}. These values corresponded to hour 38 post inoculation (Figures 3.9a & 3.8a).

$$R_a = -1.19e-11 + 8.52e-1y_c - 9.98e-3y_c^2 \quad \text{Equation 3.12}$$

The timing of attachment was found to influence the success of rhizoplane colonisation. The contribution of attached bacteria at any time (t) to the total density of bacteria at hour 96 was investigated based on the bacterial proliferation rate (R_p) using Equation 3.11 (Figure 3.9b).

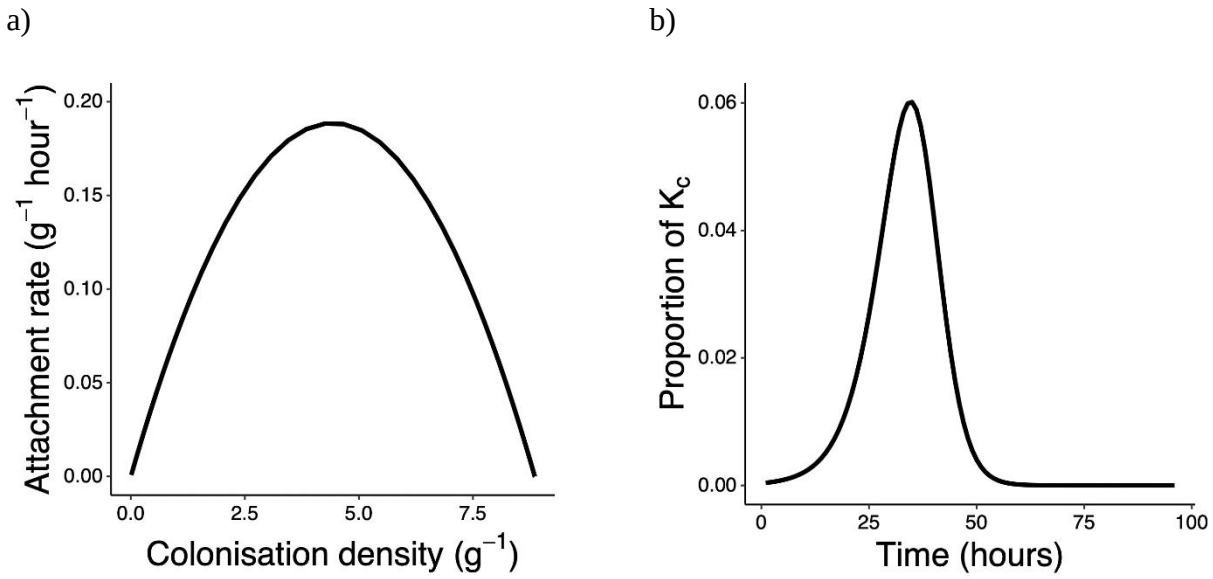

Figure 3.9. The relationship between attachment and colonisation density over time. a) Expressing rate of attachment as a function of total colonisation ($R_a = -1.19e-11 + 8.52e-1y_c - 9.98e-3y_c^2$). b) The proportion of K_c at hour 96 made up of bacteria which attach at any time ($p(t)$) (Equation 3.11).

Discussion

The aim of this chapter was to develop an experimental and mathematical framework that can be used dissect key bacterial processes contributing to recruitment and maintenance on the rhizoplane. The method for determining attachment rates developed in this chapter enables resolution of variations in attachment, proliferation, and colonisation rates not previously available. The protocols used to quantify bacterial density on root surfaces in this chapter are in line with past studies of colonisation over longer time periods (Schmidt *et al.*, 2018; Hansen *et al.*, 1997) and assessment of attachment over short time frames (Mills and Bauer, 1985; Albareda *et al.*, 2006). Quantification of bacterial density, carried out at widely spaced time intervals is common in the study of plant-bacterial interactions (Unge and Jansson, 2001; Schmidt *et al.*, 2018). For example, Unge and Jansson (2001) quantified Psf SBW25 density on wheat (*Triticum aestivum*) roots every seven days, from six to sixty-five days post inoculation. Generally, unattached bacteria are removed by washing and the numbers of remaining bacteria are determined through plating or imaging. Since destruction of the sample is necessary, these studies often lack the temporal resolution necessary to map out the dynamic rhizoplane colonisation process. The experimental system used in this chapter has similar limitations due to the destructive nature of sampling, but significant effort was put into overcoming these limitations through sampling at dense time intervals, allowing the precise kinetics of attachment to be quantified.

There was a large amount of variation in the colonisation density observed for individual roots in this chapter, which was not fully explained by normalising for root mass (Figure 3.5). This may be an indication that root mass alone is not the factor of root morphology which determines colonisation patterns. This is unsurprising given the known correlation between colonisation and root structures, such as cell junctions (Schmidt *et al.*, 2018). It may be the case that another measure of root size, such as volume or width to length ratio, would provide a better value for normalisation of colonisation. Acquiring such measurements, however, would result in a slower assay, with more handling of plant material and thus more risk of contamination. Live imaging, as is carried out in Chapter 4, is one potential way to overcome these issues.

Destructive quantification methods, such as those used in this chapter, are commonly used to assess colonisation by plant growth promoting (PGP) bacteria (Bach *et al.*, 2016; Hsu and Micallef, 2017). Colonisation efficiency is a key component of the success of PGP bacteria (Chin-A-Woeng *et al.*, 2000; Kamilova *et al.*, 2006). Despite this, quantification is often

overlooked when assessing PGP bacterial strains (Kour *et al.*, 2019; Cipriano *et al.*, 2016). Previous studies have reported colonisation levels similar to those we report. Unge & Jansson (2001) reported between 8.06 and 8.63 $Log_{10}CFU\ g^{-1}$ of root six days after inoculating wheat (*Triticum aestivum*) with *Psf* SBW25. We report lower values at 6.96 $Log_{10}CFU\ g^{-1}$ of root five days post inoculation. This lower colonisation density is unlikely to be the result of the shorter experimental period (5 vs. 6 days), given that the logistic model fit to total colonisation data predicts that the system will be approaching carrying capacity within approximately two days (Figure 3.6). Observed differences are more likely the result of differences in plant species, maturity, and growing conditions. This highlights a flaw which is common in studies of colonisation, including in the work presented in this chapter. Studies based on exposure of roots to bacterial inoculants over short periods, in tightly controlled conditions, are limited in scope due to the range of factors which impact colonisation (Schmidt *et al.*, 2018; Massalha *et al.*, 2017). Such flaws can be mitigated against by testing observations of colonisation made in controlled conditions in more variable natural systems.

Colonisation assays offer a simple method by which many samples can be assessed in a single experiment. Applying such methods to quantification of more specific components of colonisation, such as attachment, presents a challenge (Richter-Heitmann *et al.*, 2016). They cannot directly distinguish attachment and proliferation meaning individual rates cannot be obtained through experimentation. Attachment rate is difficult to obtain over any meaningful amount of time. While it is possible to track individual bacterial cells and visualise their attachment to a surface (Ipina *et al.*, 2019; Duvernoy *et al.*, 2018) this is impractical within the soil or rhizosphere environment or across an entire root system. Typically, attachment is quantified over short time periods following inoculation, over which proliferation is limited (Shimshick and Hebert, 1979; Albareda *et al.*, 2006; Rossez *et al.*, 2014). Mills and Bauer (1985) quantified the attachment of *Rhizobium trifolii* to white clover (*Trifolium repens*) through viable cell counts after 40 minutes of root exposure to a bacterial suspension. Variations of this approach have been tested on many combinations of different plant and bacterial systems (Albareda *et al.*, 2006).

The work presented in this chapter addresses the limitations of previous approaches to quantifying attachment, by combining sampling with high temporal resolution and a mathematical framework which links attachment and proliferation rates. Using these, system parameters which have not been obtainable through simple experimental protocols can be

calculated. The importance of quantifying attachment is highlighted by the fact that there was a noticeable lag time (approximately 24 hours) before strong attachment began to approach its maximum rate (Figure 3.8a). This fact would not have been detected by previous studies of attachment. Attachment rate changes with time, as the result of changes in bacterial density and gene expression that affects plant physiological features. In the early work of Shimshick and Hebert (1979), a dynamic model of root attachment is proposed based on adsorption-desorption theory. This model is limited by the fact that it does not consider bacterial proliferation on the root, which this chapter has shown is a large component of total colonisation, and likely impacts attachment (Figure 3.9). Therefore, future models should incorporate both aspects of bacterial activity when attempting to describe or predict the colonisation process.

Applications of attachment rate estimations

A mathematical framework was developed in this chapter which allows attachment and proliferation rates on the root surface to be individually estimated. The estimations of attachment presented in this chapter have wide ranging applicability. The colonisation assays that they rely on are common practice and do not require sophisticated experimental or analytical techniques. The key limitations of the system are a consequence of its simplicity. It lacks a physical structure in the substrate, as well as the complex interactions which occur between different microbes in the rhizosphere, which likely introduce a level of positive bias to estimates of attachment rate. Recovering and quantifying specific bacterial strains or isolates in field conditions through plating is difficult and limits research to culturable bacteria. Molecular methods can be used for more specific quantification (Mendis *et al.*, 2018). Colonisation data can be obtained from roots in natural systems through fluorescent *in-situ* hybridization (Gamez *et al.*, 2019), sequencing (Mitter, de Freitas and Germida, 2017), or qPCR (Mendis *et al.*, 2018). Non culturable *Pseudomonas* has been quantified through fluorogenic PCR assays, for example (Lloyd-Jones, Laurie and Tizzard, 2005). While these methods present opportunities to study the total colonisation process in more biologically relevant conditions, they present their own challenges, and still do not allow direct quantification of attachment rates.

Destructive colonisation assays, such as those presented in this chapter, are not suitable for determining spatial variations in attachment rate on the root. The use of hydroponics also neglects the role of transport to the root surface. Modern live imaging offers solutions to some

of these challenges. The structural component of soil can be simulated by transparent soil, while also enabling direct observation of colonisation patterns (Downie *et al.*, 2015). In advanced microscopy systems, large numbers of roots can be observed in three dimensions (Berthet and Maizel, 2016), along with bacterial densities in the presence of a root (Massalha *et al.*, 2017; Pavlova *et al.*, 2017). It is even possible that colonisation can be characterised automatically using machine learning techniques (Carbone *et al.*, 2017). Some of these approaches are further developed in the remaining chapters: in Chapter 4 of this thesis, spatial patterns of colonisation are more fully explored through live imaging of roots in transparent soil; in Chapter 5, the role of transport is more fully explored through quantification and modelling of chemotaxis in transparent soil. While both methods provided valuable and novel data, they are limited in the ability to access and manipulate the root post inoculation as was carried out in this chapter. As a result, mathematical frameworks, such as the ones developed in this chapter, and destructive sampling will remain an important component of establishing links between attachment rates, root growth, bacterial proliferation, and the complex patterns of colonisation observed on the rhizoplane.

Proposed stages of attachment during colonisation

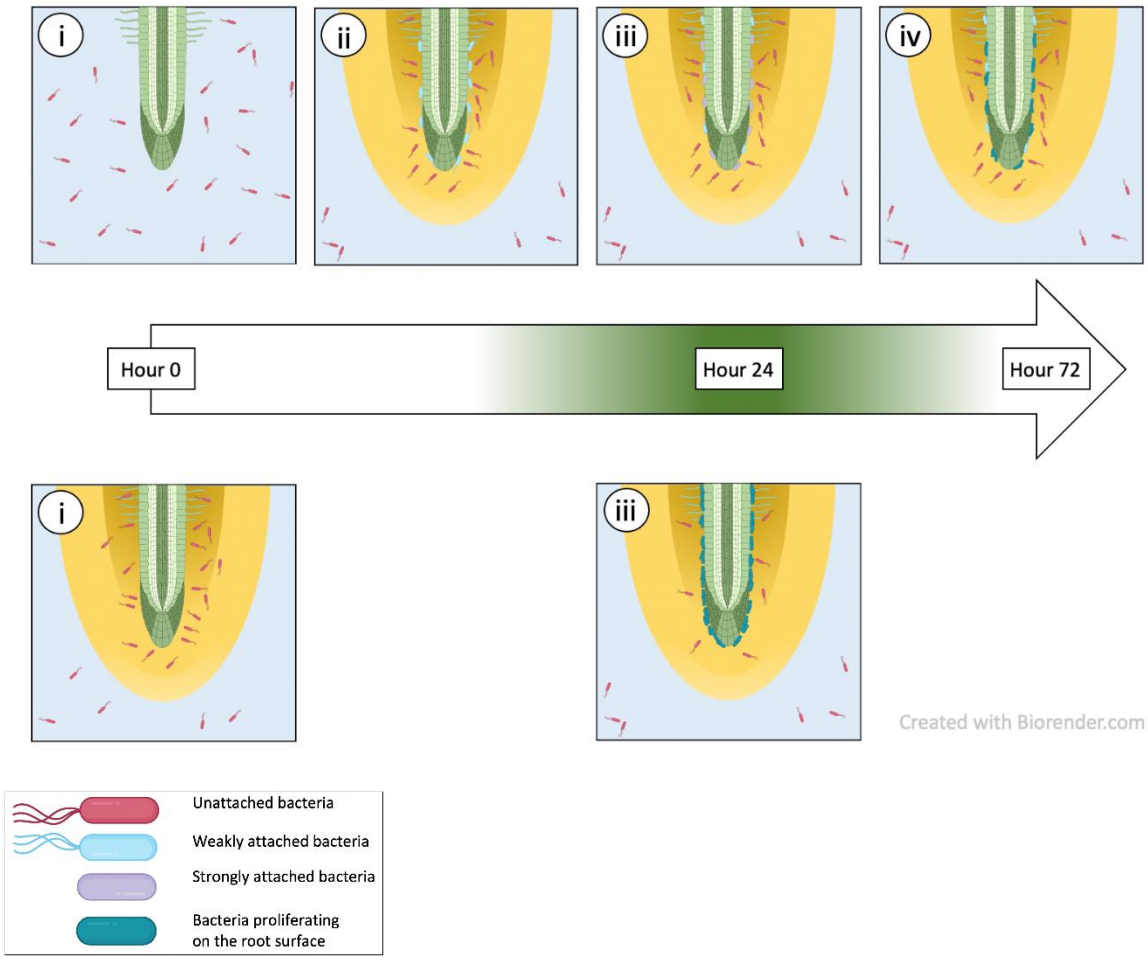

Figure 3.10. Proposed timing for the colonisation of lettuce roots by Psf E1433 in liquid media. Stage i) Bacteria encounter a concentration gradient of root exudates and other rhizodepositions (in yellow). Bacterial movement establishes a dense bacterial population near the root (shown in green). ii) Over the first 24 hours, weak attachments between bacteria and root likely form, however these are not detected by destructive sampling. iii) At approximately hour 24, the rate of strong attachment to the root, along with bacterial proliferation on the root surface begins to increase, peaking at hour 38. iv) Attachment and proliferation rate begins to decline, reaching carrying capacity at approximately hour 72 at which point recruitment to the root surface and proliferation are at equilibrium with death and disassociation.

Exploring the dynamics of root colonisation can indicate the nature of processes which may be occurring when bacteria first interact with a root. Based on the observations in this chapter, it

is possible to speculate on the timing of key stages of the colonisation process. In a first step, microbes encounter root exudates and other rhizodepositions. In the case of a hydroponic system, these will diffuse freely outwards, however in soil there may be more limitations on exudate transport. Bacteria respond to the presence of exudates by moving towards the root. Exudates will also stimulate bacterial proliferation in the media surrounding the root; this step is explored through chemotaxis assays in Chapter 5. Secondly, weak attachment is formed between bacteria and the root. This will establish a large proportion of bacterial density in close association with the root but not immediately lead to an increase in observed colonisation density. Evidence for these steps is seen in the low rates of colonisation predicted between hours 0 and 24 in this chapter, as well as the apparent decrease in bacterial density in the media of microcosms containing a root relative to the original inoculant (Figure 3.3c). In a third step, between hours 24 and 38, strong attachment to the root is established. Recorded colonisation and attachment rates begin to increase, and proliferation of attached bacteria further increases colonisation. In this chapter, bacteria colonising between hours 24 and 48 are predicted to make the largest contribution to the final colonisation density of the root once it reaches carrying capacity. This may be the result of priming activity occurring. From hour 38 onwards, proliferation and attachment rates begin to decrease, becoming negligible by hour 72. From this point, the rate of attachment and proliferation on the rhizoplane is matched by death and dissociation, leading to an equilibrium. Over longer time periods, it is likely that the carrying capacity of the root will change with shifts in root size and plant physiology (Guyonnet *et al.*, 2018). The insights offered into the timing of root colonisation by the work presented in this chapter will allow future models of the process to incorporate more realistic bacterial activity, such as lag times prior to the formation of strong attachment.

Conclusion

In this chapter, a novel method for separately quantifying and modelling bacterial attachment to and proliferation on the root surface was presented. It can be used to isolate different components of colonisation and determine their relative importance to the establishing bacterial density on the root. The work presented lays a solid groundwork for future studies which address the impact of more nuanced factors on attachment and colonisation. It highlighted the need for an analysis of spatial patterns of colonisation, as seen in Chapter 4, and the need to develop a method to quantify bacterial movement in a soil environment, as seen in Chapter 5.

Chapter 4. Live quantification of bacterial colonisation

Introduction

In this chapter, the colonisation of living lettuce roots is quantified through live imaging of fluorescent bacteria. The work presented in the previous chapter developed a framework for the study of bacterial attachment and proliferation rates on the root in a liquid media system. Such homogenous systems are widely used in the study of plant bacterial interactions due to the ease with which plants can be accessed and manipulated (Aufrecht *et al.*, 2018; Guichard *et al.*, 2020). The work carried out in Chapter 3 used rapid but destructive detection of bacterial density on the root to characterise the timing of strong attachment and proliferation on the rhizoplane. However, the behaviour of bacterial populations prior to attachment cannot easily be detected through traditional colonisation assays, as strong attachment with roots has not yet been formed. Further, the growth environment in liquid microcosms (Chapter 3, Figure 3.1) is very remote from natural soil conditions and it is unclear how soil structure may affect the colonisation process (Juyal *et al.*, 2021). Verifying the stages of colonisation outlined in Chapter 3 required the ability to quantify the presence of bacteria on and in close association with living roots. This can be achieved through live imaging.

Live imaging systems are increasingly popular in the study of plant bacterial interactions because of their ability to generate quantitative data based on continuous measurements of live roots (Noirot-Gros *et al.*, 2020; Massalha *et al.*, 2017 Guichard; *et al.*, 2020). At their most basic, live imaging experiments consist of homogenous transparent gel media (von Wangenheim *et al.*, 2017). Massalha e*t al.* (2017) studied the colonisation of *Arabidopsis thaliana* roots by fluorescent *Bacillus subtilis* using a microfluidics set up. This allowed the roots of plants growing within gel to be imaged. They quantified the movement of bacteria towards the root and subsequent colonisation. Similarly, Noirot-Gros *et al*. (2020) used a microfluidics setup to study the colonisation of aspen (*Populus tremuloides*) roots growing in gel medium by *Pseudomonas fluorescens*. They reported on the development of bacterial biofilms and the profile of bacterial colonisation along the root. Such microfluidics setups allow continuous imaging of colonisation and for the control of factors such as liquid flow around the root, however the lack of structure in gel media reduces their similarity to the soil environment. Low resolution imaging of live roots in natural soil is possible through X-ray and MRI; however, such imaging systems are limited in their ability to detect bacteria or microscopic root structures (Pfeifer *et al.*, 2015; Atkinson *et al.*, 2019). To achieve the high-resolution imaging of roots in a structured environment necessary to quantify bacterial

processes, transparent soil can be used (Downie *et al.*, 2015). Transparent soil allows continuous live imaging of root processes in conditions which are closer to natural soils than gel media, at resolutions which are not possible in using X-ray or MRI.

This aim of this chapter was to characterise and profile bacterial colonisation on live roots in a quantitative manner. Through live imaging of fluorescently transformed *Pseudomonas fluorescence* (Psf) SBW25 bacteria on lettuce (*Lactuca sativa*) roots growing in transparent soil, estimates of colonisation were extracted. This allowed the profile of bacterial establishment along the length of the root to be examined in a quantitative manner based on fluorescent signal. Estimates of colonisation were compared to destructive sampling techniques, based on homogenisation, and plating of roots followed by viable cell counts, similar to the techniques used in Chapter 3. A machine learning approach was used to develop pixel-based segmentations of root images allowing images to be automatically classified into root, particles, and bacterial colonies.

Methods

Plant growth conditions

Lettuce (*Lactuca sativa* L. cultivar. All Year Round) seeds (Sutton Seeds, United Kingdom) were surface sterilised by soaking them in 20 ml of a solution of 2 % w/v calcium hypochlorite (Sigma Aldrich, 12116, UK) for 15 min. They were then washed six times in 20 ml of sterile distilled water. Seeds were plated on 1.5 % water agar. Plates were sealed, covered with foil, and incubated at 21 °C for 3 days.

Transparent soil and mesocosm design

Transparent soil was generated by treatment of Nafion®. Nafion® is a material with a refractive index of 1.34, which is similar to that of water (1.33). Nafion® pellets (Ion Power Inc., USA) were fractured using a 6850-mill freezer (Spex CertPrep, UK). Sieves with varying mesh sizes were used to collect fractured particles between 0.25 and 0.125 mm in size. Particles were treated to ensure that that they had a surface chemistry suitable for plant growth (Downie *et al.*, 2012). Particles were soaked in a 15 % KOH solution and incubated at 80 ^{o}C for five hours. They were then rinsed with sterile deionised water (dH_2O) and incubated for 30 minutes at room temperature. Following another rinse with dH_2O, they were soaked in a 15 % nitric acid solution and incubated at room temperature for 18 hours. Particles were once more rinsed with dH_2O. They were then soaked in a 1 M sulfuric acid solution and incubated at 65 ^{o}C for one hour. Once particles and sulfuric acid solution had cooled to room temperature, particles were rinsed with dH_2O and incubated at 65 ^{o}C for one hour. Once the particles had cooled to room temperature, they were rinsed five times with dH_2O and then soaked in a 3 % hydrogen peroxide solution. This was incubated at 65 ^{o}C for one hour and cooled to room temperature. Particles were rinsed five times with dH_2O. The pH of the particles was adjusted to seven by titration with 0.5 x Murashige and Skoog medium with no sucrose (MS) (Sigma Aldrich, M5524, UK). Particles were soaked in 0.5 x MS at room temperature for 30 minutes. The solution was decanted, and the pH of the solution tested. This was repeated until the particles had reached pH 7. The resulting transparent soil was stored at room temperature in dH_2O between experiments. Particles were recycled between experiments by repeating the above steps to remove organic and inorganic contaminants and balance pH.

Soil was stained with sulforrhodamine-B (SRB, Sigma-Aldrich, S1402, UK). A 0.4 % w/v solution of SRB in 1 % acetic acid was prepared and particles were soaked in it for 24 hours before being rinsed three times with dH_2O.

To achieve live imaging of roots, plants were grown in transparent soil mesocosms which could be placed on a standard microscope stage (Figure 4.1a). Transparent soil mesocosm chambers were constructed by Yangminghao Liu at the James Hutton Institute as described in Liu *et al.* (2021). Each mesocosm chamber consisted of two microscope slides (VWR, UK) separated by a 0.3 x 0.3 cm wall of polydimethylsiloxane (PDMS, Sigma-Aldrich, UK). Mesocosms had a volume of 2.97 cm^3 (Figure 4.1b). To prepare mesocosms for plant growth, transparent soil was rinsed three times with 0.5 x MS. A 2: 1 mixture of transparent soil and 0.5 x MS was then used to fill mesocosm chambers. Approximately 2 cm^3 of soil was placed in the chambers. A sterile needle was used to create two shallow indentations in the soil at the top of each chamber. A single germinated lettuce plant was placed in each chamber with the radicle in one of these indentations. The second indentation would later be used during bacterial inoculation. Mesocosms were placed in clear sterile boxes and light was prevented from reaching roots by covering the lower half of mesocosms with foil. Unless being inoculated or sampled, they were incubated in growth chambers (SANYO Electric Biomedical, Japan) at 21 °C with 16 h of light at 60 μmol m^{-2} s^{-1}. Plants were grown for three days prior to further treatment.

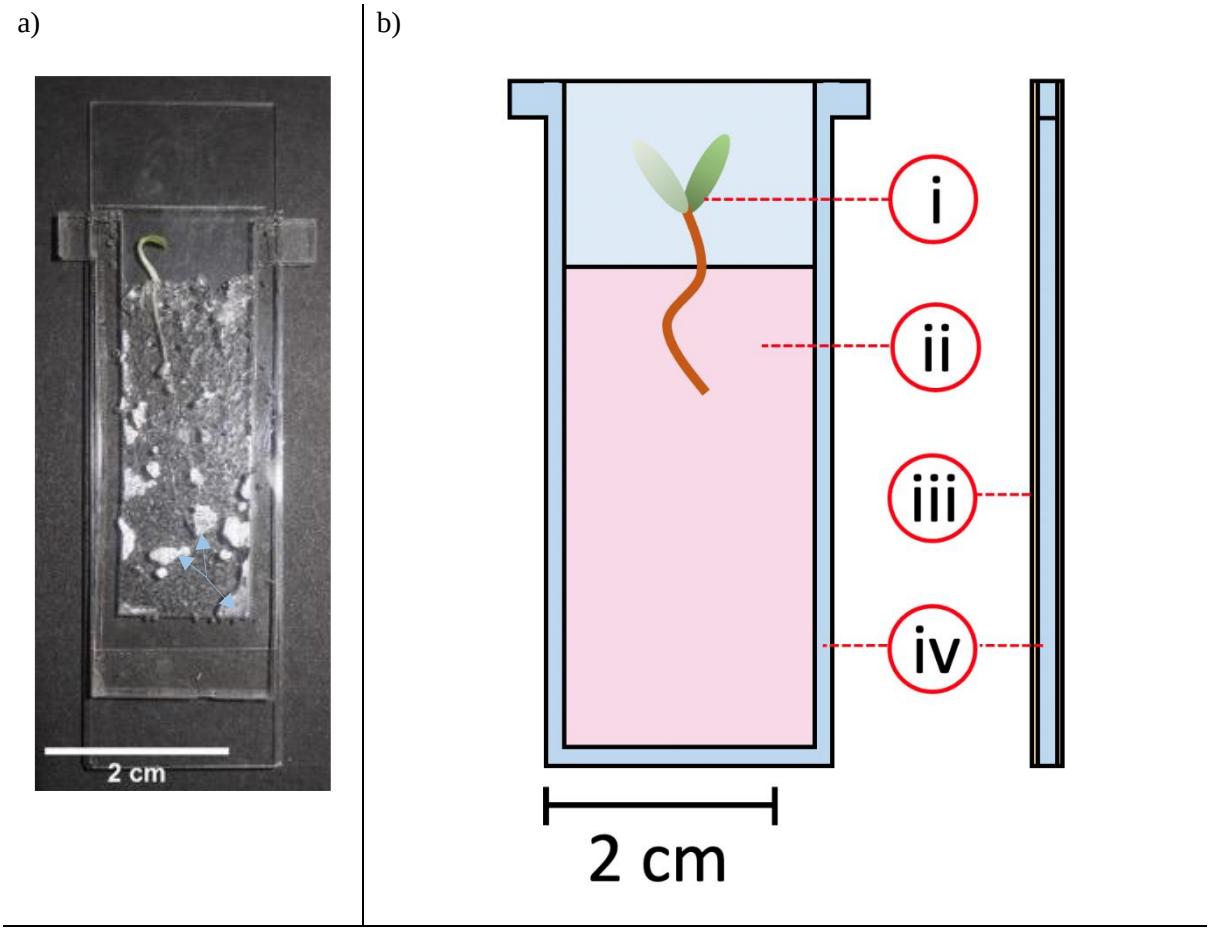

Figure 4.1. Plants were grown in transparent soil mesocosm chambers, enabling live imaging of roots. a) A mesocosm chamber containing a lettuce plant growing in transparent soil. Air bubbles are indicated by blue arrows. b) Schematic of the mesocosm chambers. (i) Germinated plants were transferred from gel medium to transparent soil. (ii) Chambers were 2.97 cm^3 in volume and contained approximately 2 cm^3 of a 1: 2 transparent soil: plant growth media mixture. Chambers were constructed of (iii) two microscope slides, (iv) separated by a 0.3 cm wall of PDMS.

Bacterial growth conditions

To prepare bacterial inoculants used in this chapter, *Pseudomonas fluorescens* (Psf) E1433 pGFP was removed from storage in 20 % glycerol at -80 ^oC and streaked onto Kings-B (Sigma Aldrich, 60786, UK) agar. To ensure the maintenance of the E1433 pGFP plasmid, all growth media used to prepare Psf E1433 pGFP contained tetracycline (25 ng μl^{-1}). Plates were incubated for 24 hours at 27 ^oC. Individual colonies were selected and inoculated into 5 ml of liquid LB, which was incubated at 27 ^oC with shaking (200 rpm) for 24 hours. To obtain more physiologically reproducible bacterial populations, this culture was inoculated at a 1: 100

dilution into rich defined 3-(*N*-morpholino)propanesulfonic acid (RD-MOPS) medium. RD-MOPS contained; 100 mM 3-(*N*-morpholino)propanesulfonic acid (adjusted to a pH = 7.4 with KOH), 100 mM N-Tris(hydroxymethyl)methyl glycine (adjusted to a pH = 7.4 with KOH), 1 mM $FeSO_4$, 27.6 mM of K_2SO_4, 0.05 mM $CaCl_2$, 52.8 mM $MgCl_2$, 0.5 M NaCl, micronutrients consisting of; 0.3 µM $(NH_4)_6Mo_7O_{24}.H_2O$, 0.04 mM H_3BO_3, 0.003 mM $CoCl_2$, 0.001 mM $CuSO_4$, 0.008 mM $MnCl_2$, 0.001 mM $ZnSO_4$ (5 ml), 0.2 % v/v glycerol as a carbon source, 132 mM K_2HPO_4, 0.02 M thiamine HCl, 0.02 % v/v essential amino acid solution (Sigma Aldrich, M5550, USA), and 0.01 % v/v non-essential amino acids (Sigma Aldrich, M7145, USA) (Neidhardt, Bloch and Smith, 1974). This suspension was incubated for 24 hours at 18 ^oC with shaking (200 rpm). Suspensions for inoculating roots were made by diluting the suspension to an optical density at 600 nm (OD_{600}) of 0.044 in 0.5 x MS medium. Optical densities were measured using an Ultraspec 2100pro spectrophotometer (Biochrom, UK) blanked with a 500 µl sterile aliquot of the relevant media. To inoculate mesocosms, a sterile 1 ml syringe (Henke-Sass Wolf, Germany) was used to draw 0.3 ml of plant growth media from the chamber, with the syringe tip placed in the soil indent formed as described above. Bacterial suspension (0.3 ml) was then injected into the same indent, resulting in a calculated mean OD_{600} of 0.02 for the entire chamber, corresponding to a bacterial density of approximately 3e7 colony forming units (CFU) ml^{-1}.

Imaging

Imaging was carried out using a Nikon A1R confocal laser scanning system mounted on a NiE upright microscope fitted with a NIR Apo 20 × 0.8 water dipping lens with GaAsP detectors (Nikon, Japan). pGFP was excited at 488 nm with the emission being collected at 500–530 nm. SRB was excited at 530 nm with the emission being collected at 570-600 nm. Transmission images were also captured. Settings and gain levels were established to avoid saturation of images based on imaging of a suspension of Psf E1433 pGFP at an OD_{600} of 0.02. All subsequent images were acquired with the same settings and saved in NIS format, containing metadata. Images of roots were acquired by turning mesocosms on their side and placing them on the stage. Images were taken to capture the entire length of the root, along with a significant area on either side. In cases where lateral roots were present, the primary root was the focus of imaging. To capture the root surface, 30 x 5 µm z-stacks of each section of root were acquired, beginning at the point the first root structure or bacterial colony came into focus and proceeding down through the root.

Each plant was imaged over a 24-hour period. Initial root images were taken prior to inoculation. They were then taken at 2, and 24 hours. A separate group of roots were inoculated and imaged at 24 and 48 hours post inoculation. A further group were inoculated, and images taken at 48 and 72 hours post inoculation.

Destructive quantification of root surface colonisation

Following the imaging period, colonisation density was estimated for each root based on destructive measurements of CFU. Following the final imaging of each root, plants were carefully removed from mesocosms and dipped three times in sterile phosphate buffer saline (PBS) to remove loosely adherent bacteria. Roots were separated from the phyllosphere (with the distinction between the two marked by the base of the hypocotyl) using an ethanol-sterilized razor blade. Roots were placed in 1.5 ml sample tubes and weighted using a fine balance (Ohaus, USA). 100 µl of sterile PBS was then added, and roots were homogenised using a micro pestle. Serial dilutions of these suspensions were plated on Kings-B agar containing tetracycline (25 µg ml^{-1}). Plates were incubated at 27 ^{o}C for 24 hours before CFU counts were determined.

Analysis of bacterial colonisation through destructive sampling

Table 4.1. Variables and parameters.

Notation	Definition	Unit
Wt	Root mass	(g)
CFU^0	CFU of inoculant	(ml^{-1})
y	Colonisation density on root surface	(g^{-1})
t	Time (hour)	(hour)
k	Carrying capacity	(g^{-1} or mm^{-3})
y^0	y on root surface at t = 0	(g^{-1} or mm^{-3})
μ	Maximum growth rate	($hour^{-1}$)
h^0	Length of the lag phase (hour)	(hour)
N	Sample number	NA
M	Bootstrap replicates	NA
y_b^i	The i^{th} prediction of bootstrap sample b	(g^{-1} or mm^{-3})
y_m	The mean predicted bootstrap value at b	(g^{-1} or mm^{-3})
$A_\propto$	Proportion of root area classified as bacterial colonies	NA
A_c	Area classified as bacterial colonies	(mm^2)
A	Root area	(mm^2)
ω	Bacterial fluorescence	(mm^{-3})
$\bar{I}$	Mean pixel intensity	NA
$\bar{I}^0$	Mean pixel intensity of uninoculated chambers	NA
px	Number of pixels in an image	NA
V	Volume of image	(mm^3)
R_r	Root growth rate	(mm $hour^{-1}$)
l^1	Root length at t	mm
l^0	Root length at $t-1$	mm

As in the Chapter 3, bacterial colonisation was modelled based on destructive measurements of CFU. To account for differences in root size and initial experimental conditions, colonisation density (y, g^{-1}) was determined based on CFU (CFU) counts, root mass (wt, g) and an initial bacterial density (CFU^0). CFU^0 was estimated, based on the relationship between CFU ml^{-1} and OD_{600} investigated in Chapter 2 (Chapter 2, Figure 2.6), to be 3e7 CFU ml^{-1}. y was calculated based on the equation:

$$y = \frac{CFU}{CFU^0 wt} \qquad \text{Equation 4.1}$$

Three classical bacterial growth models, the logistic equation (Equation 4.2) (Tsoularis and Wallace, 2002), the Gompertz equation (Equation 4.3) (Gibson, Bratchell and Roberts, 1988), and the Baranyi equation (Equation 4.4) (Baranyi and Roberts, 1994) were fit to the destructive measurement of y data (Table 4.1). The logistic equation predicts the rate of change of bacterial density (y) with time (t) based on a carrying capacity (k), initial density (y^0), and maximum growth rate (μ). Solutions of the logistic equation are in the form:

$$y = \frac{ky^0}{y^0 + (k - y^0)e^{-\mu t}} \qquad \text{Equation 4.2}$$

The Gompertz equation predicts the rate of change of bacterial density (y) with time (t) based on a carrying capacity (k), initial density (y^0), and maximum growth rate (μ) with the solution in the form:

$$y = ke^{ln\left(\frac{y^0}{k}\right)e^{-\mu t}} \qquad \text{Equation 4.3}$$

The Baranyi equation predicts the rate of change of bacterial density (y) with time (t) based on a carrying capacity (k), initial density (y^0), and maximum growth rate (μ) and (h^0) which specifies the length of the lag phase with the solution in the form:

$$A = t + \frac{1}{\mu} ln\left(e^{(-\mu t)-\mu t} + e^{-h} - e^{-\mu t - h^0}\right) \qquad \text{Equation 4.4}$$

$$ln\,(y) = ln\,(y^0) + \mu A - ln\left(1 + \frac{e^{\mu A} - 1}{e^{lnln\,(k)}} - ln\,(y^0)\right)$$

The Richards equation predicts the rate of change of bacterial density (y) with time (t) based on a carrying capacity (k), initial density (y^0), maximum growth rate (μ), and (β) which specifies the curvature of growth, with the solution in the form:

$$y = K\left(1 - e^{-\beta\mu t}\left(1 - \frac{y^0}{k}\right)^{-\beta}\right)^{-\frac{1}{\beta}} \quad \text{Equation 4.5}$$

The best fit model was determined based on lowest Akaike Information Criterion (AIC) score. The Bootstrap method was used to estimate confidence intervals of the fit. Data was randomly sampled with replacement M times to produce a bootstrap sample. Models were then fit to this new data set based on a nonlinear least squares (NLS) method. The bootstrap estimate of the confidence interval (CI) was then determined as:

$$CI(t) = \frac{1}{M-1}\sqrt{\sum_{b=1}^{b=M}\frac{1}{N}\sum_{i=1}^{i=N}(y_b^i - y_m)^2} \quad \text{Equation 4.6}$$

Here, N is the size of the data set, y_b^i is the ith predicted value on bootstrap sample b, and y_m is the mean predicted bootstrap value at that time point. M is the number of times the data is resampled (1000).

Image based quantification of bacterial proliferation along the root

When possible, images were tiled automatically with 10 % overlap. In cases where changes in root depth prevented automatic tiling, roots were manually tiled with approximately 10 % overlap.

To determine root dimensions and growth rates (R_r), root widths and lengths, as well as the length of the regions of division, elongation, and maturation, were measured. Root dimensions were measured using transmission images. Root width was measured at the widest point. Root length was measured from the root cap to the point at which the root entered the soil. The length of the region of division was measured from the root cap to the point at which vascular tissue became evident. The length of the region of elongation was measured from the point at which vascular tissue became evident to the first root hair. The length of the region of maturation was measured from the first root hair to the point at which the root entered the soil (Pacheco-

Escobedo *et al.*, 2016). Root growth rates (R_r) were calculated individually for each plant based on initial length (l^0), final length (l^1) and time (t):

$$R_r = \frac{l^1 - l^0}{t} \qquad \text{Equation 4.7}$$

The profile of bacterial fluorescence along roots was established. To extract profiles, 2-dimensional images of straightened roots were generated. Projections of confocal images were created from z-stacks based on the sum of slices of the pGFP channel. The central axis of each root was then traced with a line to measure root width and root length. A custom-made ImageJ plugin was used to perform a geometric transformation of the image to map the bacterial distribution in the root curvilinear coordinate system (Dupuy, 2016). The mean pixel intensity of the image was recorded, along with the profile of mean pixel intensity along the length of the root.

To determine the increase in bacterial fluorescence (ω, mm^{-3}) over time, the total fluorescence intensity recorded in an image was used. Bacterial fluorescence was estimated based on pixel number (px) and the mean pixel intensity of the root ($\bar{I}$), normalised based on the mean pixel intensity of uninoculated roots ($\bar{I}^0$) and volume of the image, calculated based on the depth of the image, which was constant at 0.168 mm, and area of the image which varied depending on the size of the root (V mm^3):

$$\omega = \frac{(\bar{I} - \bar{I}^0)px}{V} \qquad \text{Equation 4.8}$$

The logistic equation (Equation 4.2), the Gompertz equation (Equation 4.3), the Baranyi equation (Equation 4.4) and the Richards equation (Equation 4.5) were fit to the live measurement of bacterial fluorescence data (ω) substituting y for ω (Table 4.1). The best fit model was determined based on lowest Akaike Information Criterion (AIC) score. The Bootstrap method was used to estimate confidence intervals of the fit (Equation 4.6).

Images were manually divided into particles, identified based on the SRB channel, and void, in which no particle or root was present. The mean pixel intensities ($\bar{I}$) if the pGFP channel for these areas were recorded as described above.

Image based quantification of regions colonised by bacteria

A machine learning approach was used to segment images into five classes: root, root colony, particle, particle colony, and void. The Trainable Weka Segmentation plugin was used in ImageJ (Arganda-Carreras *et al.*, 2017; Schneider, Rasband and Eliceiri, 2012). Projections of confocal images were created in ImageJ from z-stacks based on the sum of slices of the pGFP and SRB channels. An initial training area (1.96 mm^2) was selected from an image of a root at 48 hours post inoculation. Three different training protocols were then used to manually classify this region (Table 4.2). The classifier was then trained (random forest classification, initialised with 200 trees). Gaussian blurs, Hessian, and Sobel filters were applied as training features. Three models for image segmentation were produced. To assess the models, five testing areas (0.88 mm^2), representing uninoculated roots and hours 2, 24, 48, and 72 post inoculation, were classified.

Each of the three models was then used to classify each image. As above, geometric transformation was applied on images to map results in the root curvilinear coordinate system. Root coverage for segmented images ($A_\propto$) was calculated based on the area classified as bacterial colonies on the root surface (A_c, mm^2) and total root area (A, mm^2):

$$A_\propto = \frac{A_c}{A} \qquad \text{Equation 4.9}$$

The logistic equation (Equation 4.2), the Gompertz equation (Equation 4.3), the Baranyi equation (Equation 4.4) and the Richards equation (Equation 4.5), along with a linear model, were fit to the resulting root coverage ($A_\propto$) data, substituting y for $A_\propto$ (Table 4.1). The best fit model for each data set was determined based on lowest Akaike Information Criterion (AIC) score. The Bootstrap method was used to estimate confidence intervals of the fits (Equation 4.6).

Table 4.2. Image features utilised for training of classifiers.

Class	Model 1	Model 2	Model 3
Root	Whole root outline	Visible sections of root	Whole root outline
Root colony	Small clusters of colonies	Small clusters of colonies	Large, clustered outlines
Particle	Whole particle	Whole particle	Whole particle
Particle colony	Clusters on particles	Clusters on particles	Clusters on particles
Void	Large sections of void	Large sections of void	Large sections of void

Data analysis and use of software for image processing and growth rate modelling

Initial image generation and automatic tiling was carried out using NIS-elements AR software (Nikon, USA). Further processing was carried out in ImageJ (Schneider, Rasband and Eliceiri, 2012), using the Trainable Weka Segmentation plugin for segmentation of images (Arganda-Carreras *et al.*, 2017). Model fitting, bootstrapping, and further analysis was carried out in R (R Core Team, 2018). Growth models were fit using an NLS method using the growthrates package (Petzoldt, 2016). Replicates of different treatments were pooled together prior to analysis. Time was measured in hours for all data sets. Confidence intervals were calculated for selected models by bootstrapping with 1000 replicates. To test for a difference in fluorescence between root regions, a linear mixed-effects model, with mean pixel intensity ($\bar{I}$) as dependent variable, root region as a fixed-effect, and time (t) as a random effect was fit to data using the 'nlme' package (Pinheiro *et al.*, 2006). The relationship between mean pixel intensity and time for particles and voids was investigated by preforming a linear regression with time as input variable and mean pixel intensity as output variable. The relationship between bacterial fluorescence and colonisation density was investigated by preforming a linear regression with colonisation density, based on destructive sampling and CFU counts (y, g^{-1}), as input variable and bacterial fluorescence (ω, mm^{-3}) below a value of 44 mm^{-3} as output variable. Based on this relationship, values of y were estimated from live images.

Results

Transparent soil allowed live quantification of root and bacterial processes

Plants were grown in transparent soil so that the colonisation of roots could be quantified through live imaging. A minimum of six plants were imaged per time point. To better understand the dynamic process of root growth in soil, root dimensions were established based on transmission images of live roots during the final imaging of each plant (Table, 4.3, Figure 4.2). Average root growth rate, calculated based the change in length of individual roots (R_r), was 0.065 mm hour^{-1} (SD of 0.012 mm hour^{-1}, N = 18). Measurements of different root regions were used to investigate spatial patterns in colonisation (Figure 4.7).

Table 4.3. Mean root dimensions during final imaging (± SD)

	Mean measurement (mm) (N = 18)
Width	1.19 ± 0.32
Length	8.86 ± 3.66
Region of division	0.87 ± 0.06
Region of elongation	4.09 ± 1.7
Region of maturation	3.9 ± 3.28

a)

b)

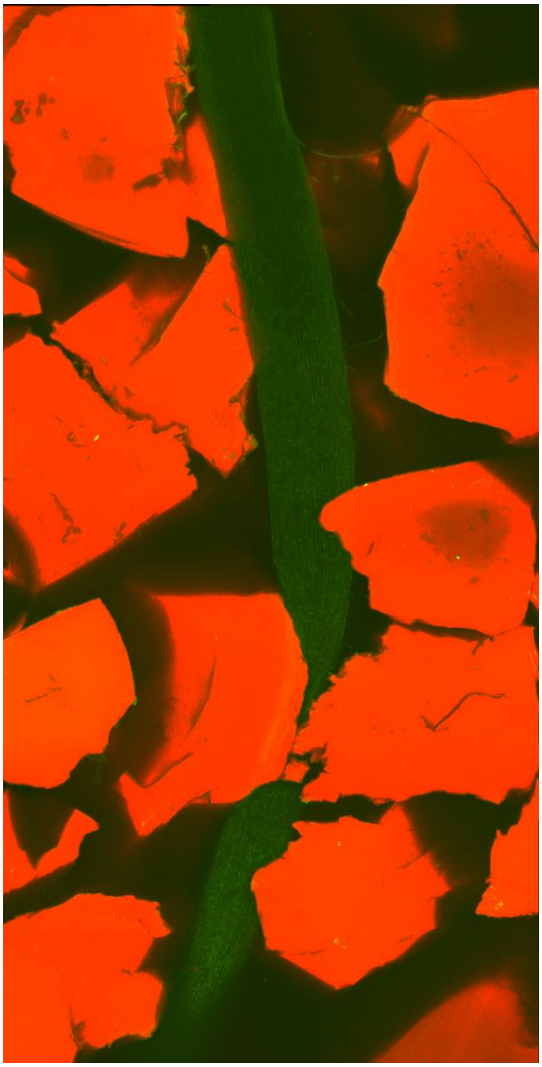

Figure 4.2. Roots were imaged growing in transparent soil. a) Transmission images were used to determine dimensions. b) Pixel values, extracted from confocal images were used to determine bacterial fluorescence (Equation 4.8), here the pGFP channel is shown in green and the SRB channel is shown in red.

The accumulation of bacterial density along the length of the root was quantified by imaging fluorescent bacteria interacting with plant roots in transparent soil. No fluorescent bacterial colonies were detected on roots prior to inoculation. After inoculation, bacterial colonies were visible on root surfaces as small points of fluorescence. At hour two, these were scattered across the root surface, beyond this point they were generally located at junctions between epidermal cells, with a visible increase evident across time (Figure 4.3a). Detail of individual colonies

was lost during the projection of z-stacks into two-dimensional images due to the wide spacing of slices. However, an increase in the fluorescence of roots over time could still be observed (Figure 4.3b).

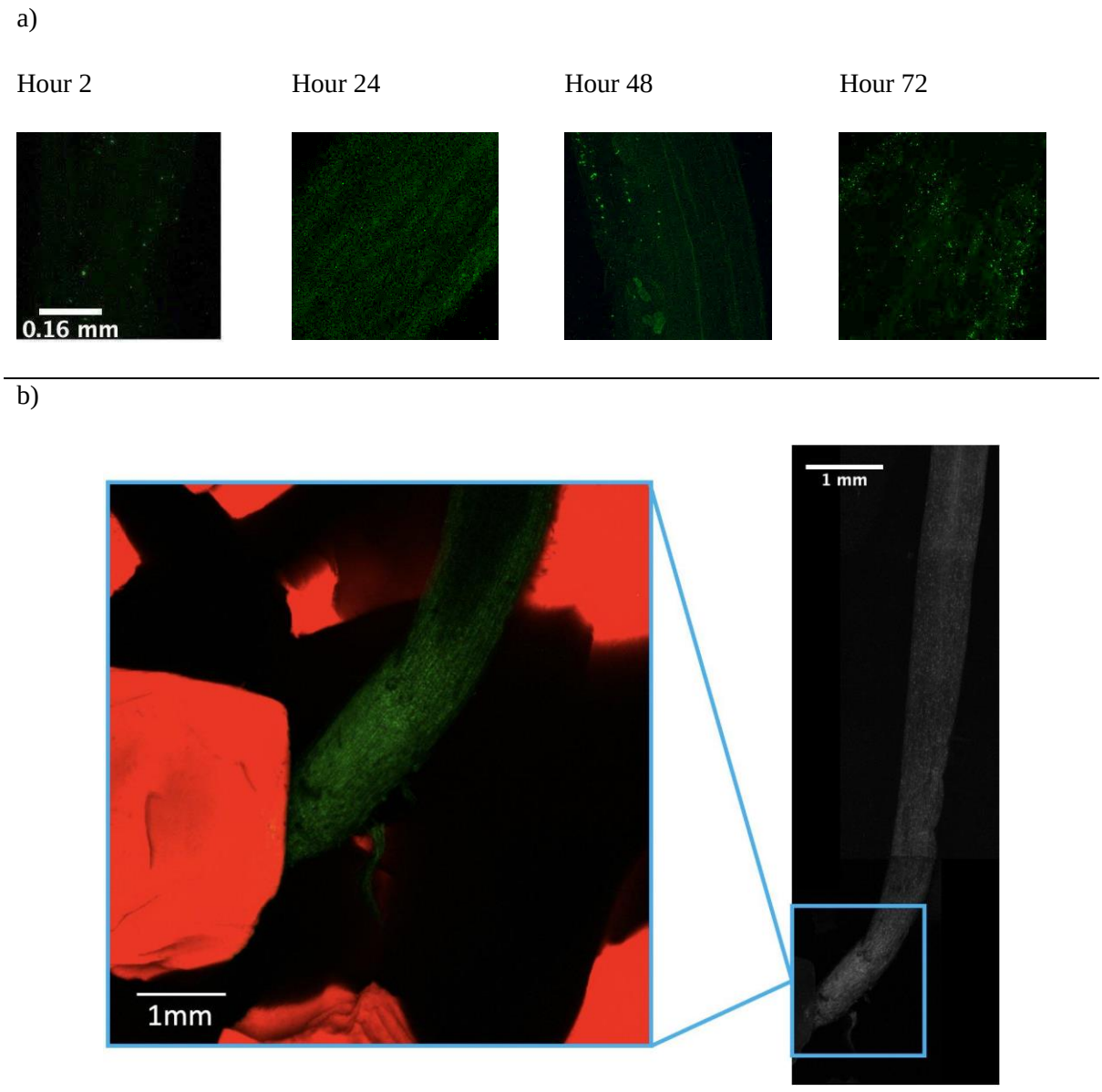

Figure 4.3. Bacterial colonies were visible on the roots surface. a) Bacterial colonisation (green) was visible on the root surface during live imaging. b) Confocal image of lettuce roots in transparent soil 48 hours post inoculation showing the pGFP channel in green and the SRB channel in red. Individual confocal images were tiled and projected by summing pixel values from each channel to make 2-dimensional images.

To account for root autofluorescence and normalised values of mean pixel intensity ($\bar{I}$) between images, bacterial fluorescence (ω, mm^{-3}) was calculated for each root image according to Equation 4.8 (Figure 4.4). An overall increase was seen from a mean of 9.86 mm^{-3}, (SD = 10.21 mm^{-3}) at hour 0, to a mean of 47.09 mm^{-3} (SD = 19.08 mm^{-3}) at hour 72. The Gompertz equation was the best fit model for this data (AIC = 207.56, R^2 = 0.35, CE = 4.29 mm^{-3}, N = 32, Figure 4.5, Table 4.4). This data described the growth of a bacterial population near the root, capturing strongly attached bacteria, as well as unattached and weakly attached bacteria which were not quantified in destructive measurements of colonisation density.

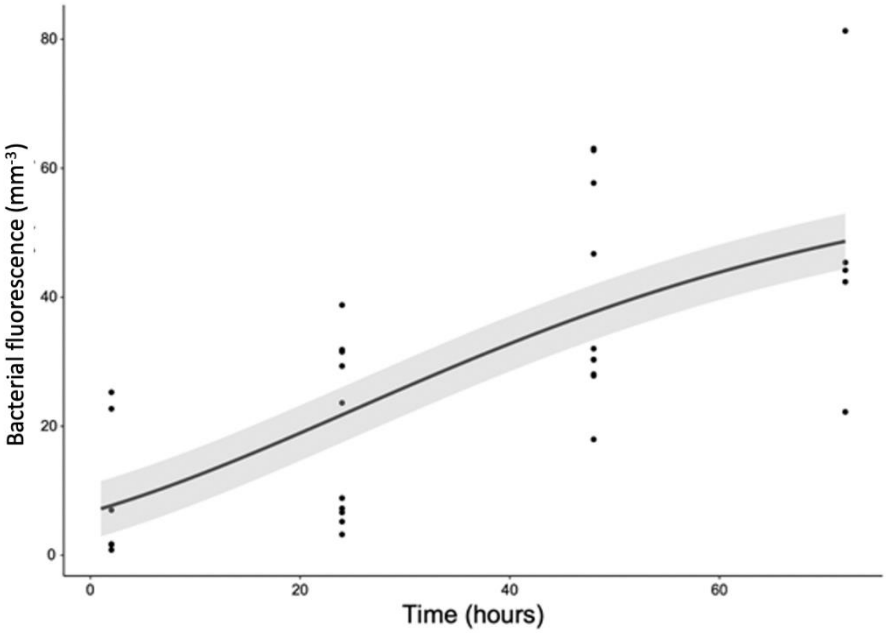

Figure 4.4. Bacterial fluorescence on the root surface was quantified and modelled. The Gompertz equation (Equation 4.3) was fit to the data for the increase in bacterial fluorescence (ω) on live roots based on a least squares method (AIC = 207.56, R^2 = 0.35, CE = 4.29 mm^{-3}, N = 32). Each point represents a single live measurement of ω. The solid line represents the best fit model, and shaded region represents the bootstrap confidence interval. Model parameter values can be seen in Table 4.4.

Table 4.4. Models selected based on lowest AIC for each data set along with fit parameter values.

Data set	Selected model	Bootstrap CI	Parameters
Bacterial fluorescence (ω)	Gompertz (Equation 4.3)	4.29 mm^{-3}	$y^0 = 6.72\ mm^{-3}$ $k = 60.9\ mm^{-3}$ $\mu = 0.032\ hour^{-1}$
Colonisation density based on destructive measurements (y)	Baranyi (Equation 4.4)	0.32 g^{-1}	$y^0 = 0.35\ g^{-1}$ $k = 5.69\ g^{-1}$ $\mu = 0.11\ hour^{-1}$ $h_0 = 2.67\ hours$
Proportion of root area classified as bacterial colonies ($A_\propto$): Model 1	Linear	7.83e-05	$Slope = 8.24e-6$ $Intercept = 2.73e-4$
Proportion of root area classified as bacterial colonies ($A_\propto$): Model 2	Logistic (Equation 4.2)	8.66e-05	$y^0 = 2.5e-4$ $k = 9.2e-4$ $\mu = 4.4e-2$
Proportion of root area classified as bacterial colonies ($A_\propto$): Model 3	Logistic (Equation 4.2)	9.08e-05	$y^0 = 2.5e-4$ $k = 9.2e-4$ $\mu = 4.4e-2$

To identify trends in bacterial growth and activity in the media surrounding the root, images were manually divided into 'particles', identified based on the SRB channel, and 'void', in which no particle or root was present. Bacterial colonies were evident on soil particles in the area around the root as small points of fluorescence, generally located within cracks or indentations on edges. Mean pixel intensity ($\bar{I}$) on particles increased from 6.35 (SD = 2.47), at hour 2, to 13.36 (SD = 3.77) at hour 72. Mean pixel intensity of particles was found to be positively correlated with time (slope = 0.198, intercept = 5.4, $R^2 = 0.28$, $F(1,30) = 13.1$, $P = 0.029$, $N = 32$, Figure 4.5). Individual bacteria were not visible in the medium/ voids containing

no particles or roots under the magnification and settings required to avoid saturation of root images. Across hours, mean pixel intensity in voids ($\bar{I}$) was 2.44 (SD = 1.16). No significant correlation between mean pixel intensity of voids was found with time (R^2 = < 1e4, F(1,30) = 0.02, P = 0.887, N = 32, Figure 4.5). The imaging protocol was successful at quantifying overall trends in bacterial populations on the root and particles, but not in medium surrounding the root.

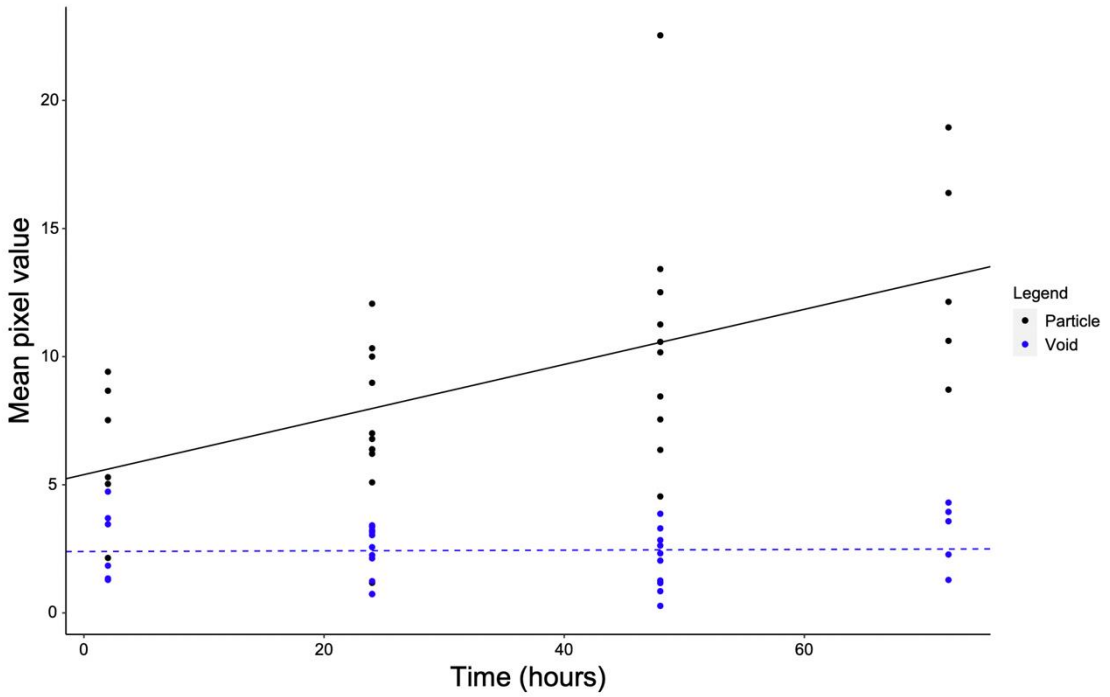

Figure 4.5. Bacterial fluorescence on soil particles increased with time, but no change in fluorescence in media was observed. Based on a linear regression, there was a significant positive correlation between mean pixel intensity ($\bar{I}$) for particles and time (black, R^2 = 0.28 F(1/30) = 13.31, P < 1e-4, N = 31). A linear regression found no significant correlation between $\underline{I}$ for voids (areas between particles and roots) and time (blue, R^2 = 0.0007, F(1,30) = 0.02, P = 0.887, N = 32). Each point represents a single measurement of $\bar{I}$ of either particles or void. The solid black line represents the significant relationship between $\bar{I}$ and time for particles (slope = 0.11, intercept = 5.4). The blue dashed line represents the non-significant relationship between $\bar{I}$ and time for voids between particles and roots (intercept = 2.39).

Differences in colonisation were observed in transparent soil compared to liquid media

Root colony formation by Psf E1433 pGFP was quantified by destructive sampling of root colonisation density (y, Equation 4.1). The fluorescence of individual bacteria was assumed to remain constant throughout the experimental period. This allowed the comparison of colonisation levels for roots grown in transparent soil mesocosms and liquid media microcosms. Destructive quantification of colonisation was carried out for fifteen plants. Colonisation density on roots in transparent soil rose from a mean value of 0.67 g^{-1} (SD = 0.6 g^{-1}) at hour 24 to a mean of 5.39 g^{-1} (SD = 0.277 g^{-1}) at hour 72. The Baranyi equation was the best fit model for this data (AIC = 71.25, R^2 = 0.5, CE = 0.32 g^{-1}, N = 18, Figure 4.6b, Table 4.4).

At lower levels of bacterial fluorescence (ω < 44 mm^{-3}), a significant correlation between bacterial fluorescence and measurements of colonisation density (y, g^{-1}) was found (slope = 10 mm^{-3} g, intercept = 10.39 mm^{-3}, R2 = < 0.37, F(1,8) = 5.7, P = 0.043, N = 9, Figure 4.6a). y can then be predicted from live measurements of ω based on the equation:

$$y = 10\omega + 10.39 \qquad \text{Equation 4.10}$$

However, values of y above 3.39 g^{-1} cannot be reliably estimated based on imaging data (Figure 4.6b). This is likely due to increasingly dense bacterial colonies blocking fluorescent signal, with variation introduced by root topography and colony structure. Estimates of y were made for live images of roots based on Equation 4.10. A mean y value of 0.05 g^{-1} (SD = 1.02 g^{-1}) was estimated at hour two then values began to rise above 3.39 g^{-1} at hour 48, meaning reliable y values could not be calculated (Figure 4.6b). Due to the unreliability of high estimates of y, a model was not fit to these predicted colonisation densities, however the overall trend in increase of colonisation density over time was similar to that observed during destructive measurements, with a lag period over the first 24 hours, rapid increase between hours 24 and 48, and a plateau being reached by hour 72 (Figure 4.6b).

(a)

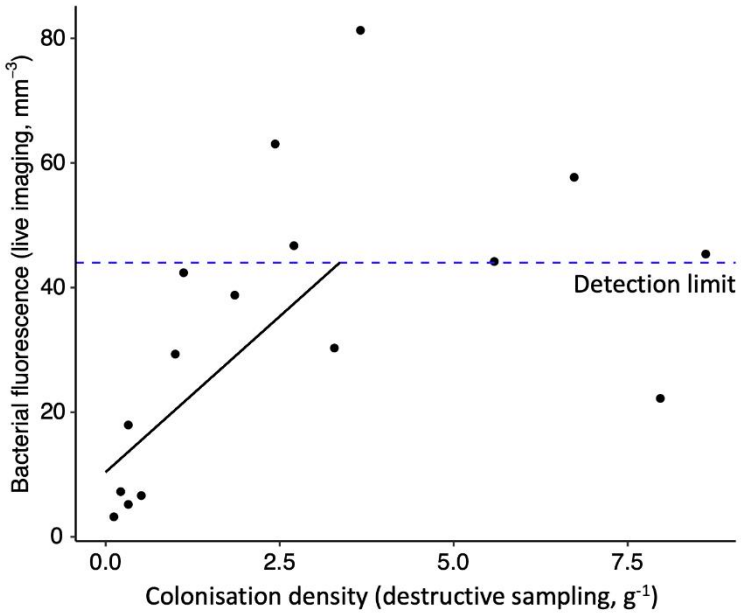

(b)

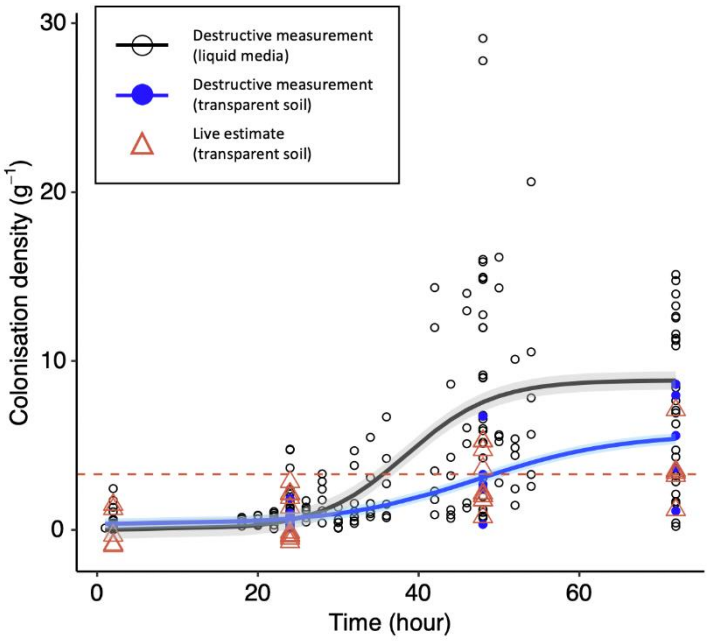

Figure 4.6. Destructive measurements of colonisation density were carried out to facilitate a comparison between imaging and measures of colonisation and attachment made in Chapter 3. The fluorescence of individual bacteria was assumed to remain constant throughout the experimental period. a) A linear regression found that bacterial fluorescence (ω, mm^{-3}) on live roots below a value of 44 mm^{-3} had a significant positive correlation with colonisation density (y) measured based on destructive sampling (slope = 10 mm^{-3} g,

intercept = 10.39 mm^{-3}, R2 = < 0.37, F(1,8) = 5.7, P = 0.043, N = 9). This allowed values of colonisation density up to 3.36 g^{-1} to be predicted, above which estimates were inaccurate, likely due to colonisation not captured by imaging. Solid black line represents the linear model for predicting ω based on y. b) The Baranyi equation (Equation 4.4) fit to the data for destructive quantification of colonisation density (y) on the surface of roots grown in transparent soil using a least squares method (blue, AIC = 71.25, R^2 = 0.5, CE = 0.32 g^{-1}, N = 18). Overall, mean values of y were lower for roots grown in transparent soil mesocosms than for roots grown in liquid media microcosms at equivalent times post-inoculation (black, N = 49, see Chapter 3, Figure 3.6). Each point represents a destructive sampling of colonisation density, calculated based on Equation 4.1. Triangles represent predictions of y based on ω. Solid lines represent the best fit model for each data set, and shaded regions represent bootstrap confidence intervals. Red dashed line represents the cut-off for accurate prediction of y based on ω (3.36 g^{-1}).

Significant spatial variations in colonisation were not observed

To investigate spatial variation in bacterial colonisation of roots, mean pixel intensity ($\bar{I}$) was extracted from images of different root regions. A linear mixed-effects model indicated that the effect on mean pixel intensity of root region was weak, with overlapping confidence intervals (CI, Table 4.5, Figure 4.7, N = 6). Given that $\bar{I}$ represented the entire bacterial population, rather than just strongly attached bacteria, it is not clear if spatial variation in colonisation was present but undetected due to the presence of unattached bacteria in the media.

Table 4.5. Output from linear mixed-effects model investigating the relationship between mean pixel intensity and root region.

Region	Estimate	95% CI lower	95% CI upper	SE	t
Division	9.09	3.45	14.71	1.1	-1.87
Elongation	11.15	7.71	14.59	1.73	6.44
Maturation	8.50	2.87	14.13	1.1	-2.4

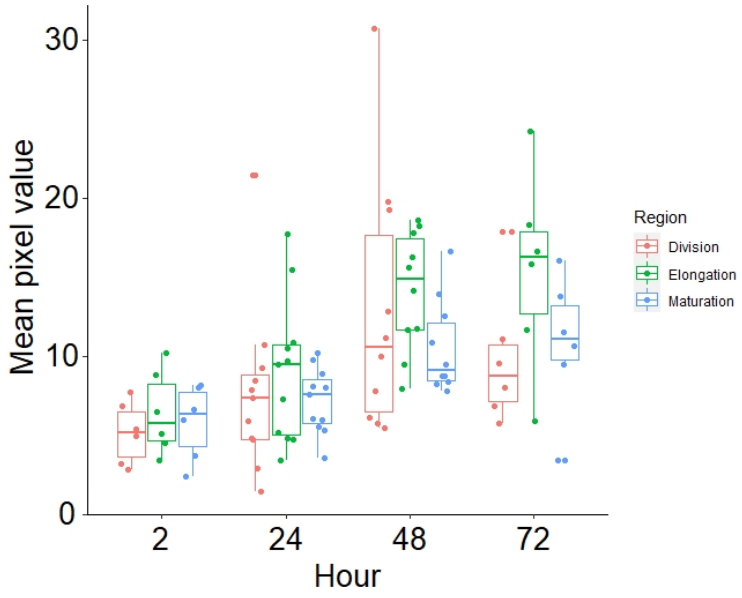

Figure 4.7. Although a general increase in mean pixel intensity ($\bar{I}$) was observed over time, the relationship between $\bar{I}$ and root region was weak. A linear mixed-effects model indicated that the effect on mean pixel intensity of root region was weak, with overlapping confidence intervals (Table 4.5, N = 6). The mean pixel intensity of root regions; division (orange), elongation (green), and maturation (blue) are shown. Each point represents a single measurement of fluorescence for a particular root region, normalised for the area. Horizontal lines represent the median for each group. Boxes represent the interquartile range. Vertical lines represent the range of data within 1.5 times the interquartile range,

To further explore the spatial variation of colonisation density on the root surface, a machine learning approach was used to classify images (Figure 4.8). The protocols used to train three models (Table 4.2) each produced visibly different classifications when applied to training areas (Figure 4.9).

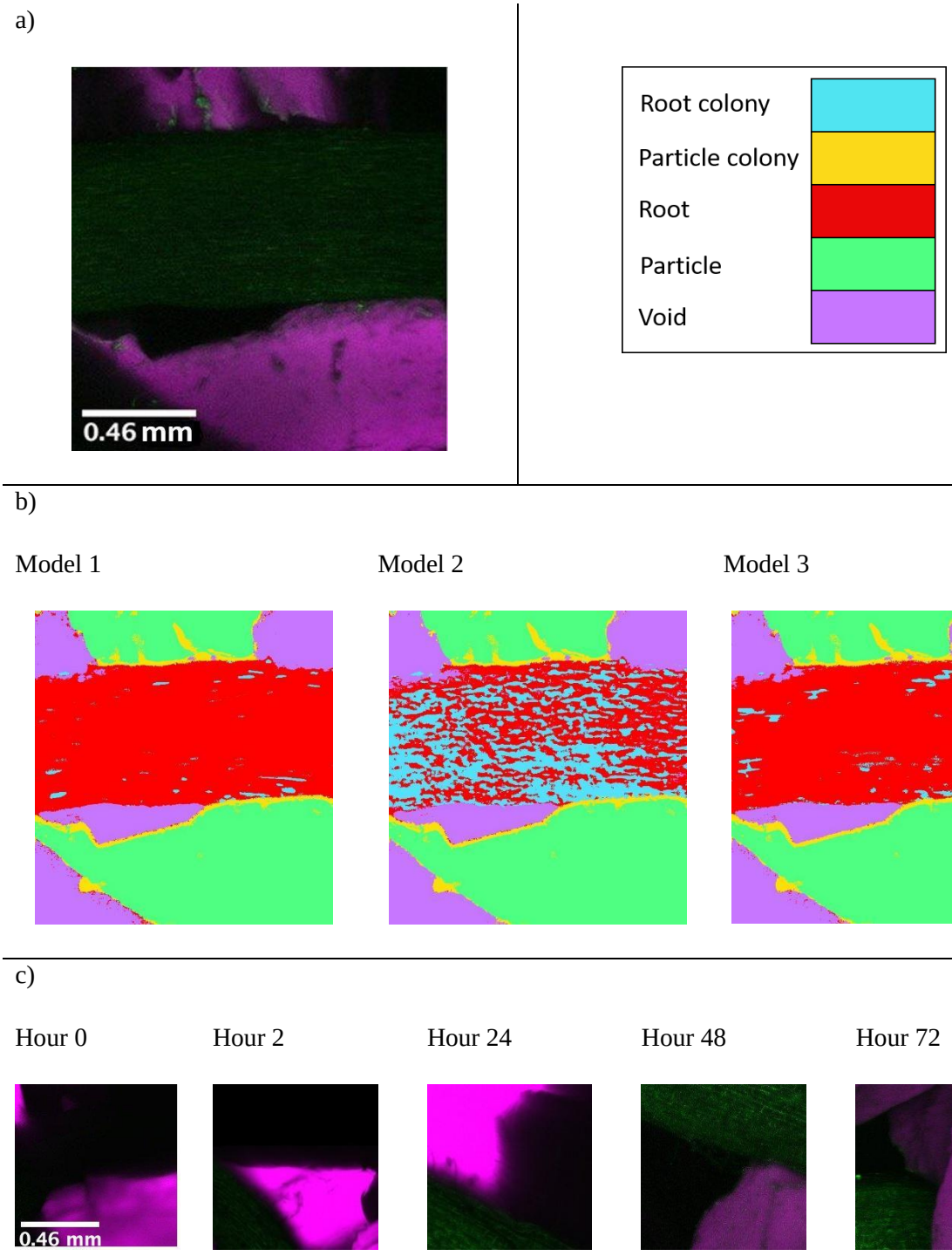

Figure 4.8. A machine learning approach was used to categorise spatial patterns in bacterial fluorescence on the root. a) Training of segmentation models was carried out based on manual classification of a training area into five classes. b) Three models were created based on different training protocols (Table 4.2). c) A single representative testing area was initially classified from each time point to assess each model.

Based on classification of training areas, use of Model 1 was the most successful at classifying the root, with models 2 and 3 classifying small sections of the root as particle; use of Model 1 did however classify some sections of particle as roots. Use of Models 1 & 3 classified smaller areas of the root as bacterial colonies than Model 2 which tended to classify large sections of root as bacterial colonies, approaching near complete coverage of the root at hours 48 and 72. At later timepoints, use of Models 1 and 3 both misidentified some bacterial colonies on the root as colonies on particles, likely due to similarities between the signals from both colony types. As expected, use of models to classify training areas did not identify root colonies in uninoculated chambers (Figure 4.9). Use of all three models failed to identify roots in the absence of bacteria, likely because the fluorescence of the entire root region is increased by both attached and unattached bacteria. All three models had limitations distinguishing bacterial colonies, both on the root and on particles, from the edges of particles. Imaging rarely captured the entire surface of particles, as z-stacks start and stop points were selected based on the root. This may have resulted in particle surfaces being captured only at the edge. As a result, bacterial colonisation may have only been visible on particle boundaries. The classification of these areas as bacterial colonies by all three models may be due to difficulties with providing accurate training data at the edge of particles, with or without bacteria. However, the increase in intensity observed through time on particles can only be attributed to colonisation. It is worth noting that false positives at this stage do not impact the observed trends in fluorescence reported on the root or particles (Figures 4.4 and 4.5) as calculation of bacterial fluorescence are based on the actual fluorescence intensity.

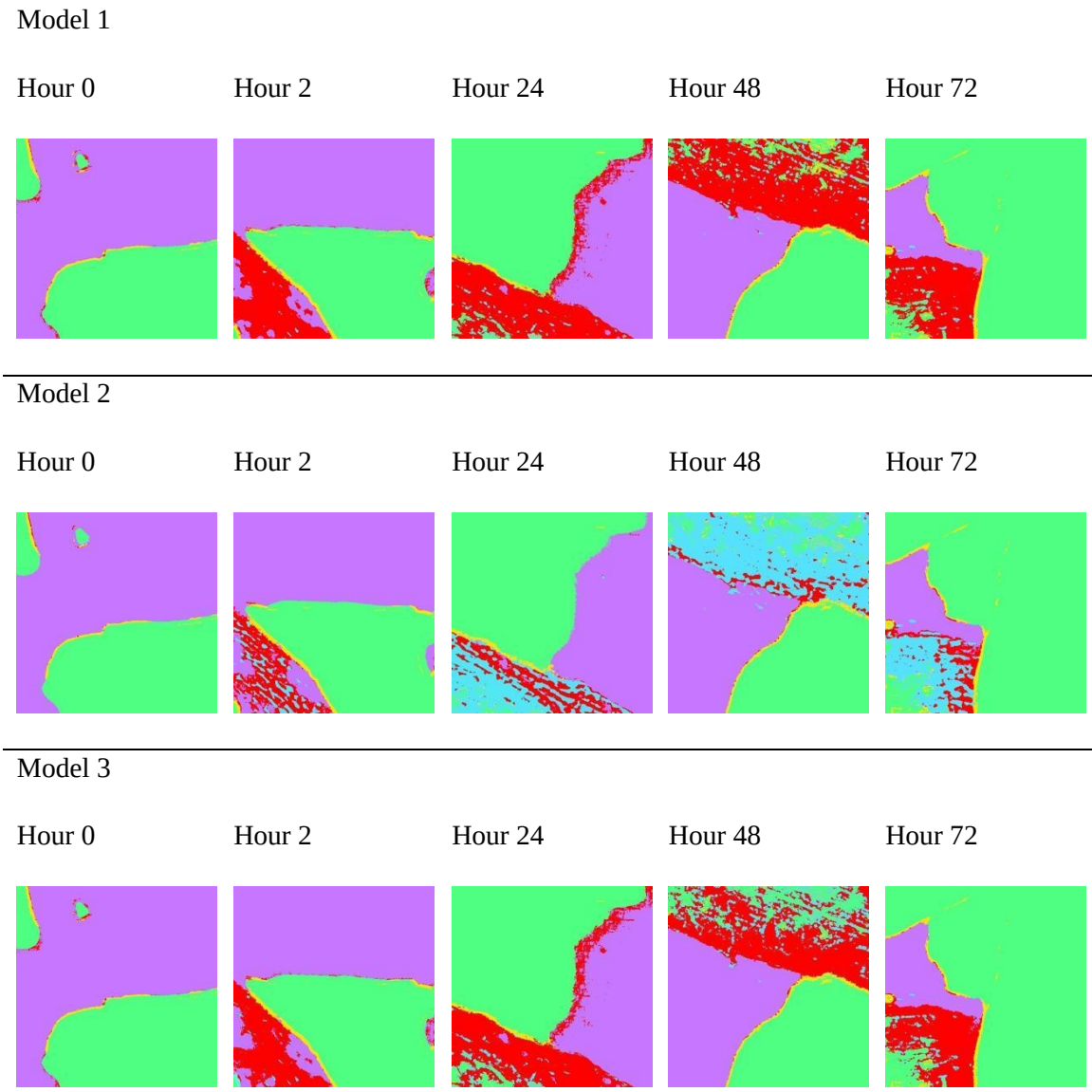

Figure 4.9. Root images were segmented into five classes (Table 4.1). Training areas were originally classified to assess the models for root image classification generated from each of the three training protocols.

For each model, the proportion of total root area classified as root colonies $A_{\propto}$ was calculated. As expected, based on analysis of fluorescence and colonisation density (Figures 4.4 and 4.6b), use of all three models showed an increase in $A_{\propto}$ from hour 2 to hour 72 (Table 4.6). Unexpectedly, none of the models showed evidence of the plateauing or levelling off which was observed consistently for other measures of colonisation (Figure 4.6b). A linear model was

found to be the best fit to data classified with Model 1 (AIC = -425.23, R^2 = 0.29, CE = 7.83e-5, N = 32, Figure 4.10a), while the logistic model was found to be the best fit for data classified with Models 2 (AIC = -423.5, R^2 = 0.21, CE = 8.66e-5, N = 32, Figure 4.10b) and 3 (AIC = -422.92, R^2 = 0.3, CE = 9.08e-5, N = 32, Figure 4.10c, Table 4.4). While all three models captured the increased levels of colonisation on the root surface with time, they lacked the level of accuracy which would be necessary to analyse small scale distributions of colonisation on the root surface. Alongside quantifications of bacterial density which were based on direct observations of bacterial fluorescence, semi-automated classification detected an overall trend in colonisation. While modifications to the imaging and training protocols may be needed to make full use of these approaches, results show the potential for combining live imaging with semi-automated classification.

Table 4.6. Mean and standard deviations for proportion of root area classified as bacterial colonises ($A_\propto$) in each of the three machine learning models (N = 6, ± SD).

	Hour 2	Hour 72
Model 1	2.72e-4 ± 1.3e-4	6.9e-4 ± 1.6e-4
Model 2	2.1e-3 ± 2.5e-3	8.3e-3 ± 1.5e-3
Model 3	2.4e-4 ± 1.2e-4	8.3e-4 ± 1.5e-4

a)

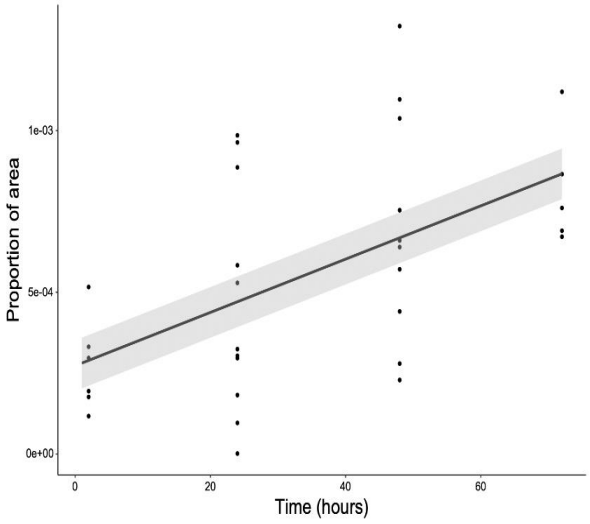
Proportion of area
1e-03
5e-04
0e+00
0
20
40
60
Time (hours)

b)

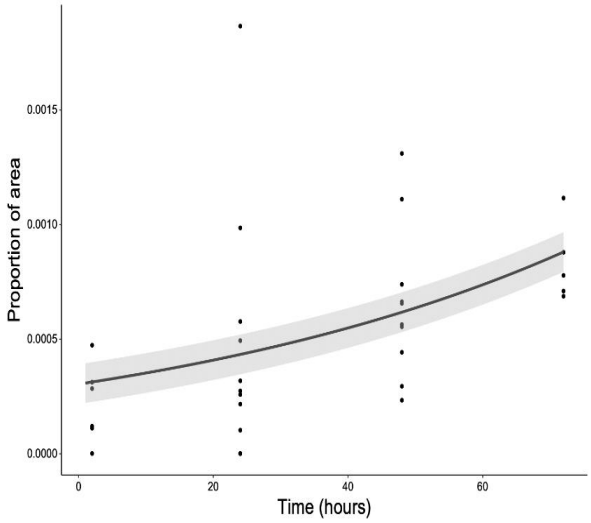
Proportion of area
0.0015
0.0010
0.0005
0.0000
0
20
40
60
Time (hours)

c)

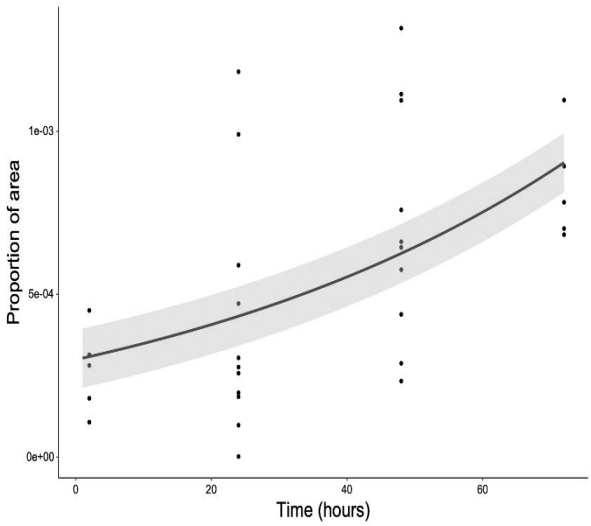
Proportion of area
1e-03
5e-04
0e+00
0
20
40
60
Time (hours)

Figure 4.10. A machine learning approach was used to generate three models for the automatic classification of root images and identification of bacterial colonies. Models were fit to data sets using a least squares method and the best fit model selected based on lowest AIC. a) A linear model was found to be the best fit to proportion of root area classified as bacterial colonies ($A_{\propto}$) for classifications based on Model 1. b) The logistic model (Equation 4.2) was found to be the best fit for classifications based on Model 2. c) The logistic model was also the best fit for classifications based on Model 3. Each point represents a calculation of $A_{\propto}$ based on the classification of a single root; the solid line represents the best fit model; the shaded region represents bootstrap confidence intervals; model parameter values can be seen in Table 4.4 (N = 32).

Discussion

The aim of this chapter was to characterise and profile bacterial colonisation of live roots. Trends in bacterial fluorescence on lettuce roots growing in transparent soil were determined as they interacted with *Pseudomonas fluorescens* SBW25. Analysis of root colonisation patterns through imaging has been common practice for decades with roots being removed from growth media and images taken at various resolutions through light or electron microscopy (Noirot-Gros *et al.*, 2018; Gamalero *et al.*, 2004). Detailed studies of the patterns established by communities of bacteria on the rhizoplane can also be carried out through molecular methods such as DNA sequencing (Baudoin, Benizri and Guckert, 2002; Garcia-Lemos *et al.*, 2019). Colonisation patterns can be described qualitatively (Gamalero *et al.*, 2004; Gamalero *et al.*, 2005) or quantitatively analysed and directly related to aspects of root architecture, such as distance from the tip or position relative to roots structures (Schmidt *et al.*, 2018). In recent years, live imaging using transparent media has increased in popularity (Aufrecht *et al.*, 2018; Noirot-Gros *et al.*, 2020), with transparent soil offering the possibility of studying plant and bacterial processes in a heterogenous environment (Downie *et al.*, 2015). Live imaging has the advantage over destructive techniques that the development of a single root can be observed. Currently, the main drawbacks of live imaging are that it is usually carried out in low replicate numbers, and that plants are grown in an artificial environment, potentially missing some of the complex interactions which occur between soil, plants, and bacteria in natural soil (Berthet and Maizel, 2016; Downie *et al.*, 2015). These limitations were present in the mesocosm set up used during this chapter and so to overcome these, a significant effort was made to ensure that growth conditions in transparent soil were as close as possible to those found in natural soils.

The work in this chapter follows directly from Chapter 3, in which colonisation and bacterial proliferation are quantified in a liquid medium set-up. Both systems have distinct advantages and disadvantages. The system developed in Chapter 3 allowed for large numbers of replicates and dense temporal sampling. By contrast, the live imaging system developed in this chapter allows fine spatial mapping of bacterial cell density, along the root and in the soil. Limitations were observed due to image analysis, not being able to capture the entire volume of the root, and imprecision induced by automatic segmentation of image data. The latter likely influences the results less since consistent errors by the segmentation algorithms were false positive for colonisation on the particles, and these do not affect total intensity counts which were based on the GFP channel only. Hence, by pairing the live and destructive quantification systems,

high-quality data can be assembled to establish a more robust foundation for quantitative analysis of the dynamics of bacterial establishment on the root. Colonisation was found to proceed through the same stages in transparent soil as in a liquid medium in Chapter 3, with similar timing (Chapter 3, Figure 3.10).

The development of live roots was quantified over short time periods in this chapter. While it is possible to observe the development of root architecture within natural soil through X-ray or MRI (Pfeifer *et al.*, 2015; Atkinson *et al.*, 2019), these systems do not yet have the resolution necessary to study bacterial colonisation patterns or detailed roots structures, such as hairs or tips. As a live imaging system, transparent soil is a step closer to the natural conditions in which plants and bacteria interact, compared to homogenous media (Downie *et al.*, 2015). Higher resolution images can be achieved within transparent soil by using an index matching fluid, such as a colloid suspension of silica particles or a concentrated sugar solution, which match the refractive index of the nutrient solution to that of the soil (Downie *et al.*, 2012). In this chapter, no index matching fluid was used, to avoid disrupting the colonisation process through the movement of media or introduction of variable nutrients. Within the mesocosm system, imaging of bacterial colonies was possible without an index matching fluid, however within a larger volume of soil, such as would be required to study colonisation for more mature plants, it may be necessary. The experimental framework developed during this chapter will therefore provide valuable insight for the development of the next generation of transparent soil mesocosms. These will incorporate aspects of a natural soil environment neglected from the work in this chapter, such as liquid flow within the soil, and variability in particle saturation. Further, light sheet microscopy is currently being used to study the colonisation process in three dimensions. To make the most of the systems developed in this chapter, further work is needed to confirm that bacterial fluorescence remains constant in the presence of the root. In Chapter 2, Psf E1933 pGFP was grown in the absence of an antibiotic or a plant over six days. The fluorescence of a set concentration of this culture was confirmed to be stable over this period (Figure 2.4). It is possible, however, that interaction with plant roots led to changes in bacterial fluorescence over time, which would have impacted the results and conclusion made in this chapter. The findings reported in this chapter could be supported by targeted quantification of fluorescence through imaging of individual bacteria over the course of the experimental period, in different states such as free swimming, attached to the root, or bacterial colonies.

Mesocosms also present an opportunity to study competition between different strains of fluorescent bacteria. In Chapter 3, it was predicted that bacteria colonisation between hours 24 and 48 would make the largest contribution to final colonisation density of the root at carrying capacity. By inoculating strains at different times, the observations of the role of timing in successfully colonisation made in Chapter 3 could be verified and built upon.

Root architecture and soil structure both heavily influence the colonisation process (Nunan *et al.*, 2003). At the same time soil influences root growth rate and patterns (Martins *et al.*, 2020). Average root growth rates observed in mesocosms (mean = 0.065 mm hour^{-1}) were higher than those reported in Chapter 2 (0.01 mm hour^{-1}), although the differences in growing conditions make comparison between the two unreliable. The rates reported in this chapter were in line with those reported in other systems (Watt, Silk and Passioura, 2006). Transparent soil mesocosms were a better system for measuring root growth rate than either of the liquid medium microcosms or hydroponic pouches used in Chapter 2 due to their similarity to a natural soil environment and the fact that individual roots can be tracked over time.

The framework presents opportunities for quantitative analysis of root colonisation patterns

The work in this chapter aimed to study the dynamics of the entire bacterial population on roots. Changes in colonisation density were successfully tracked on live roots based on imaging of fluorescent bacteria. Despite this success, much detail on the fine scale distribution of bacteria was lost as a result of the imaging settings and processing used. By taking higher resolution images of a smaller subsection of roots, local patterns in bacterial distribution could be quantified, potentially leading to a better understanding of the factors influencing root carrying capacity. For example, Schmidt *et al.* (2018) showed an association between bacterial colonisation and cell junctions for *Kasakonia sacchari* on rice (*Oryza sativa*) roots by taking a single high-resolution image of each region of the root.

Drastically different colonisation patterns are often observed between bacterial strains and isolates. The pattern of colonisation observed in this chapter, with colonies gathering along root cell junctions, is commonly reported. On aspen (*Populus tremuloides*) roots grown in agar, Noirot-Gross *et al.* (2018) reported heavy colonisation of root epidermal cell junctions by Psf isolate SBW25 two weeks after inoculation. After five weeks, they report dense biofilms of the isolate. This may indicate that longer term observation of colonisation could reveal new trends which were not detected during the work presented in this chapter. Gamalero *et al.* (2004)

studied the distribution of Psf isolate A6R1 on tomato roots, grown in a solid gel agar system, through destructive confocal and electron microscopy. At three days post inoculation, they reported an initial stage in which bacterial cells were randomly distributed on roots. After five days they reported pairs of bacterial cells at the junctions between epidermal cell walls. After seven days, they reported strings of bacterial cells at junctions. While it took considerably more time for the pattern to be established, this falls in line with the findings reported in this chapter. Differences in timing may be the result of different plant species, growth conditions, bacterial isolate, or initial inoculation. In contrast to the above findings, Gamalero *et al.* (2005) reported no trend in the distribution of Psf isolate 92rkG5 on tomato roots over similar time periods and using similar methods. The population level modelling of bacterial fluorescence carried out in this chapter did not assess spatial distributions of colonisation, therefore future work could address this by linking colonisation patterns to available colonisation sites on the root.

The distribution of bacteria can be highly variable between root regions. On aspen roots, Noirot-Gross *et al.* (2018) report heavier colonisation by Psf SBW25 on the first third of the root, although this changed to a more homogenous distribution over time. In contrast, Humphris *et al.* (2005) report colonisation levels on maize roots by Psf SBW25 being higher further away from the root tip, based on destructive imaging of attached bacteria. The lack of a significant trend in mean pixel intensity reported in this chapter may be the result of the early stage of colonisation being quantified relative to previous studies. Alternatively, patterns of colonisation may be masked by the presence of unattached bacteria on or near the root surface, which would contribute to the overall fluorescence of the root. The results presented in this chapter indicate that bacterial density is relatively homogenous along the length of the root during the early stages of colonisation. Patterns of attachment, however, may be more variable.

In this chapter, use of a semi-automated classification of root images was carried out to explore the distribution of bacteria on roots. Semi-automated image analysis of bacterial colonisation patterns through machine learning approaches is popular in other fields of microbiology (Zielinski *et al.*, 2017; Fredborg *et al.*, 2015) and these approaches can be applied to the study of plant-bacterial interactions, such as the automated approach used to identify root structures by Schmidt *et al.* (2018). In this chapter, classification of images indicated an increase in the proportion of the root area classified as bacterial colonies over time. The coupling of a machine learning framework with transparent soil showed promising results. It is likely that it would be more advantageous when applied to smaller scale, but higher resolution images, to identify root

structures and bacterial colonisation patterns. Each classification model developed had advantages and disadvantages. Model 1, which was most successful at identifying roots, could be used to automatically track root growth over time. Models 1 & 3 could be used to identify and map out the increase in dense bacterial colonies on the root surface, while model 2 may be more useful for tracking the increase in bacteria loosely associated with the root. In future work, the combination of different models, or models containing different classes and trained on more images, could help to separate the signal from attached bacteria on the root and unattached bacteria in suspension around the root.

In Chapter 3, four key stages in the colonisation of roots were outlined (Chapter 3, Figure 3.10); i) bacteria detect the presence of rhizodeposits, begin to proliferate and move towards the root, ii) weak attachments are formed between bacteria and the root surface, establishing a large proportion of the bacterial population in close association with the root, iii) strong attachments between bacteria and the root form, bacterial proliferation on the root surface begins, together this leads to an increase in colonisation rate, and iv) a carrying capacity is reached at which the rate of attachment and proliferation on the root surface are in equilibrium with death and disassociation of bacteria. The framework developed in Chapter 3 was successfully used to independently quantify strong attachment and the proliferation of bacteria on the root surface, however it was not suitable for studying the first two of these stages, as weakly associated bacteria were not quantified. The live imaging system developed in this chapter supports the view of the colonisation process presented in Chapter 3. Through imaging, bacteria in loose association with the root were captured, and are potentially responsible for the reduction in lag time visible when comparing colonisation quantified through imaging in Figures 4.5 and 4.7b with colonisation quantified through destructive sampling in Figure 3.5 (Chapter 3).

The imaging carried out in this chapter was calibrated to capture bacterial colonies on roots, while avoiding saturation from dense bacterial colonies or autofluorescence. This may account for the apparent lack of increase in bacterial fluorescence in the medium surrounding the root, as the signal from dispersed bacteria in suspension was too weak to be captured at these settings (Figure 4.6). Alternatively, bacteria in the proximity of the roots may be responding to their presence by moving towards them, leading to a zone of depletion. Similarly, while a significant increase in fluorescent signal on soil particles was observed, it was a minor change relative to what was observed on roots. Future work should aim to calibrate imaging protocols to better capture less dense colonisation patterns in the root surroundings.

Conclusion

The work presented in the chapter offers insight into the colonisation process which would not be possible without the use of a live imaging system. Automated classification of images has wide ranging applicability and the potential to increase the capacity for analysis of plant and bacterial activity within soil. Moving forward, the framework developed here should be used to study colonisation at finer scales with higher resolution images of root subsections and with a greater degree of replication. Most importantly, the growth and colonisation of individual roots should be tracked over longer time periods. Although there is more work to be done, the framework has provided valuable insight into the colonisation process and raised questions about microbial distributions in soil and how they are influenced by the presence of root exudates. Some of these questions are addressed in Chapter 5 of this thesis, in which the role of bacterial movement in colonisation is quantified and modelled.

Chapter 5. A dynamic model of bacterial movement and root colonisation

Introduction

In this chapter, the movement of a population of fluorescent bacteria in transparent soil is quantified through imaging and modelled. In Chapter 3, an outline of the colonisation process was proposed in which the first step was the detection of plant derived chemoattractants by microbes, and the establishment of a dense microbial population near the root (Chapter 3, Figure 3.10). This process was quantified in Chapter 4, in which low levels of fluorescence, indicating bacterial density, were observed in the medium surrounding the root, relative to on or very near the root surface. Observations of trends in bacterial density in both the bulk soil and the rhizosphere are common (Nunan *et al.*, 2003; Watt *et al.*, 2006; Ramos, Molbak and Molin, 2000). However, subsequent colonisation patterns of the root, and trends in bacterial density surrounding the root, are largely unpredictable. A plausible reason for such variability may be bacterial migration through soil during the colonisation process.

Chemotaxis is a directional movement of cells in response to a concentration gradient. It is known to play an important role in allowing soil-borne microorganisms to detect and move towards plant roots (Feng *et al.*, 2018; Knights *et al.*, 2021; Zhalnina *et al.*, 2018). Exudates and other forms of rhizodepositions contain a range of chemoattractants (Oku *et al.*, 2014). Past methods of quantifying chemotaxis have largely focused on assessing microbial movement in liquid or gel media (Reyes-Darias *et al.*, 2016; Law and Aitken, 2005). Chemotaxis in soil has been investigated by taking soil cores at discrete distances from a starting point and quantifying bacterial density within them, or through assays using soil columns, however these methods do not allow continuous measurement of bacterial movement (Brumley *et al.*, 2019; Bashan, 1986)

Soil structure and other factors such as moisture content effect the ability of potential chemoattractants to diffuse away from the root and establish a concentration gradient (Proctor and He, 2021; Nguyen, 2003). Microbial movement is also heavily impacted by soil (Sood, 2003). Assays in homogenous mediums are therefore of limited value for quantifying the movement of microbes in conditions biologically relevant to root colonisation (Bhattacharjee *et al.*, 2021). Very few experiments and models have studied the effect of soil structure on mobility and subsequent colonisation of the root surface.

The aim of this chapter was to develop an experimental and mathematical framework for quantifying and modelling microbial movement in response to chemoattractants in a granular environment and to integrate it into a root colonisation model. To this end, a chemotaxis assay in transparent soil was designed which allowed a concentration gradient of a nutrient source to be established and the directional movement of a population of fluorescent bacteria to be tracked over time. This assay was tested with exudates collected from lettuce (*Lactuca sativa* L. cultivar. All Year Round) roots, and the model bacterial isolate, *Pseudomonas fluorescens* SBW25 (Psf) E1433 pGFP, developed in Chapter 2. The movement of exudates was inferred through the imaging of fluorescent dyes. A model that predicts the movement of microbes in response to the concentration gradient of a nutrient source was then developed. To enable meaningful comparisons between chemotaxis assays and assessments of root colonisation made in previous chapters, bacterial proliferation in root exudates was incorporated into this model. To test the ability of the model to predict bacterial movement in the rhizosphere, simulations were run examining bacterial movement in response to a nutrient and chemoattractant released from a growing root under high, medium, and low diffusivity conditions. The frameworks developed in this chapter have the potential to be used to increase our understanding of numerous bacterial processes which occur within soil.

Methods

Bacterial growth conditions

To prepare bacterial inoculants used in this chapter, Psf E1433 pGFP was removed from storage in 20 % glycerol at -80 ºC and streaked onto Kings-B (Sigma Aldrich, 60786, UK) agar. All growth media used to prepare Psf E1433 pGFP contained tetracycline (25 ng μl^{-1}). Plates were incubated for 24 hours at 27 ºC. Individual colonies were selected and inoculated into 5ml of liquid LB, which was incubated at 27 ºC with shaking (200 rpm) for 24 hours. A 1: 100 dilution of this suspension in rich defined 3-(*N*-morpholino)propanesulfonic acid (RD-MOPS) medium was made. RD-MOPS contained; 100 mM 3-(*N*-morpholino)propanesulfonic acid (adjusted to a pH = 7.4 with KOH), 100 mM N-Tris(hydroxymethyl)methyl glycine (adjusted to a pH = 7.4 with KOH), 1 mM $FeSO_4$, 27.6 mM of K_2SO_4, 0.05 mM $CaCl_2$, 52.8 mM $MgCl_2$, 0.5 M NaCl, micronutrients consisting of; 0.3 µM $(NH_4)_6Mo_7O_{24}.H_2O$, 0.04 mM H_3BO_3, 0.003 mM $CoCl_2$, 0.001 mM $CuSO_4$, 0.008 mM $MnCl_2$, 0.001 mM $ZnSO_4$ (5 ml), 0.2 % v/v glycerol as a carbon source, 132 mM K_2HPO_4, 0.02 M thiamine HCl, 0.02 % v/v essential amino acid solution (Sigma Aldrich, M5550, USA), and 0.01 % v/v non-essential amino acids (Sigma Aldrich, M7145, USA) (Neidhardt, Bloch and Smith, 1974). Suspensions were incubated for 24 hours at 18 ºC with shaking (200 rpm). Bacterial suspensions used in motility and chemotaxis assays were made by diluting this to an appropriate optical density at 600 nm (OD_{600}) in 0.5 x concentration Murashige and Skoog medium (Sigma Aldrich, M5524, UK) with no sucrose (MS). Optical densities were measured using an Ultraspec 2100pro spectrophotometer (Biochrom, UK) blanked with a 500 µl sterile aliquot of the relevant media.

Plant growth conditions and exudate collection

Root exudates were collected to study their impact on bacterial movement. Lettuce (*Lactuca sativa* L. cultivar. All Year Round) seeds (Sutton Seeds, United Kingdom) were surface sterilised by soaking them in 20 ml of a solution of 2 % w/v calcium hypochlorite (Sigma Aldrich, 12116, UK) for 15 min. They were then washed six times in 20 ml of sterile distilled water. Plates were sealed, covered with foil, and incubated at 21 °C for 3 days.

Following a three-day germination period, plants were grown for eight days in a hydroponic microcosm system (Chapter 2, Figure 2.1). Microcosms were constructed in 75 mm round bottom culture tubes (VWR, 211-0046, UK). 1 ml of 1.5 % water agar was melted and pipetted into culture tubes. These were set on their sides, allowing agar to form a slope and a well. Once agar had set, a small section was removed to form a platform on which the germinated seed

was placed. Light was prevented from reaching roots by tape covering the lower half of the microcosm. Microcosm also contained 1 ml of 0.5 x MS. Microcosms were incubated in growth chambers (SANYO Electric Biomedical, Japan) at 21 °C with 16 h of light at 60 µmol m^{-2} s^{-1}. Following the 8 days growth period, plants were removed and the liquid from each microcosm was retrieved. The solution was sterilised using a 0.45 µm filter (Fisher Scientific, 10619672, USA). Aliquots of exudate were stored at -80 ºC between experiments.

Two methods were used to ensure the sterility of exudates. First, 100 µl of filtered exudate solution from each microcosm was plated on non-selective LB agar. These plates were incubated at 27 ºC for 24 hours before being visually inspected for contamination. If there was no visible contamination, a 16S PCR was used to test for the presence of bacterial rDNA (Marchesi *et al.*, 1998). Separate PCR reactions (25 µl) were set up for the exudate collected from each microcosm. A positive control consisting of a suspension of Psf E1433 pGFP in 0.5 x MS medium at an OD_{600} of 0.02, corresponding to an approximate bacterial density of 3e7 CFU ml^{-1}, and a negative control of ddH_2O (Sigma Aldrich, W4502, USA) were also included. Each reaction contained GoTaq polymerase (0.125 µl, Promega), GoTaq buffer (0.125 µl, Promega), 0.2 mM dNTPs (2.5 µl), forward primer; 0.5 µM 16s_63F (0.25 µl, 5'-CAGGCCTAACACATGCAAGTC-3'), reverse primer; 16s_1387R (0.25 µl, 5'-GGGCGGTGTGTACAAGGC-3'), template (1 µl) and ddH_2O (15.975 µl, Sigma Aldrich, W4502). A thermocycler (Biometra, Germany) was set with the following cycle: denaturing at 95 ºC for 2 minutes, 30 cycles of 94 ºC for 30 seconds, 58 ºC for 30 seconds, and 72 ºC for 90 seconds, followed by a final extension at 72 ºC for 7 minutes. PCR products were then run through a 1 % agarose gel alongside a 100 bp ladder (Promega, G2101, Holland). Sterile exudates were pooled.

Benedict's reagent ($CuSO_4$, Sigma Aldrich, 11954, USA) was used to estimate the total amount of reducing sugar in exudates. 25 µl of exudate and 50 µl of Benedict's reagent were pipetted into a sample tube. This was heated to 99 ºC for five minutes in a thermocycler (Biometra, Germany). Reducing sugar content was then estimated based on comparison to a range of glucose solutions of known concentration.

Motility assay in semisolid agar

A bacterial motility assay was carried out (Wolfe and Berg, 1989). 0.25 % w/v agar was prepared (Sigma Aldrich, 86686, UK). While liquid, approximately 15 ml of agar was poured

into sterile petri dishes. These were covered and allowed to cool for at least two hours. The resulting agar was partially solidified. Lettuce root exudate was collected. Filter paper disks (Sigma Aldrich, 74146, UK) were soaked to saturation in exudate (approximately 100 µl) or a negative control of 0.5 x MS medium. Disks were then placed on semisolid agar plates and pressed into the agar. Plates were left at room temperature for two hours, to allow exudate or control medium to diffuse into the agar. A suspension of Psf E1433 pGFP in 0.5 x MS, at an OD_{600} of 1, corresponding to an approximate bacterial density of 1e9 CFU ml^{-1} (Chapter 2, Figure 2.7), was prepared. At a marked point 2 cm from the filter paper disc, 1.5 µl of bacterial suspension was stabbed into the middle of the semi-solid agar. Plates were sealed and incubated at 27 ^{o}C for 24 hours. Under UV light, the distance that a visible bacterial front had moved from the point of inoculation towards the filter paper disc was then recorded.

Chemotaxis assay in semisolid agar

To measure the directional movement of bacteria in response to the presence of root exudate, a chemotaxis assay in semisolid agar was performed (Adler, 1973). Movement was confined to a single direction within capillary tubes, and a concentration gradient of exudate was established through diffusion. 0.25 % w/v agar was prepared (Sigma Aldrich, 86686, UK). Capillary tubes (5 µl, Sigma Aldrich, Z543241, USA) were filled with warm liquid agar. They were then placed on their side and allowed to cool for at least two hours. Lettuce root exudate was collected. A suspension of Psf E1433 pGFP in 0.5 x MS at an OD_{600} of 0.02, corresponding to an approximate bacterial density of 3e7 CFU ml^{-1} (Chapter 2, Figure 2.7), was prepared. 0.5 ml sample tubes were filled with either a bacterial suspension, plant root exudate, or 0.5 x MS and sealed with parafilm®, which was pierced with an ethanol sterilised needle. One end of each capillary tubes was then placed in either root exudate or 0.5 x MS as a negative control and the other was placed in bacterial suspension. Capillary tubes were placed on their side, covered to block out light and incubated at 21 ^{o}C. At two and 24 hours post inoculation, capillary tubes were examined for the presence of a bacterial front under a light microscope (Olympus BH2, Olympus, Japan) at 20 and 40 x magnification (Zeiss, Germany).

Chemotaxis assays in transparent soil

Chemotaxis chambers

Chemotaxis chambers were developed which could be placed on a standard microscope stage, enabling imaging of bacteria as they interacted with exudate. Chambers were constructed by Yangminghao Liu at the James Hutton Institute where each chamber consisted of a microscope

slide (VWR, UK) bonded to a 0.3 cm thick layer of polydimethylsiloxane (PDMS, Sigma-Aldrich, UK). Within the PDMS layer, were two circular wells, each with a radius of 5 mm and a volume of 235.62 mm^3. The first of these wells was intended to hold a bacterial inoculant, while the second held a chemoattractant. Wells were connected by a channel which was 35 mm in length, 3 mm in width, and had a volume of 315 mm^3. Following treatment, the chemoattractant diffuses down the channel, forming a concentration gradient (Figure 5.1). A second, removable, microscope slide was placed on top of chambers to seal them. The movement of bacteria or fluorescent dyes was then quantified through imaging.

a)

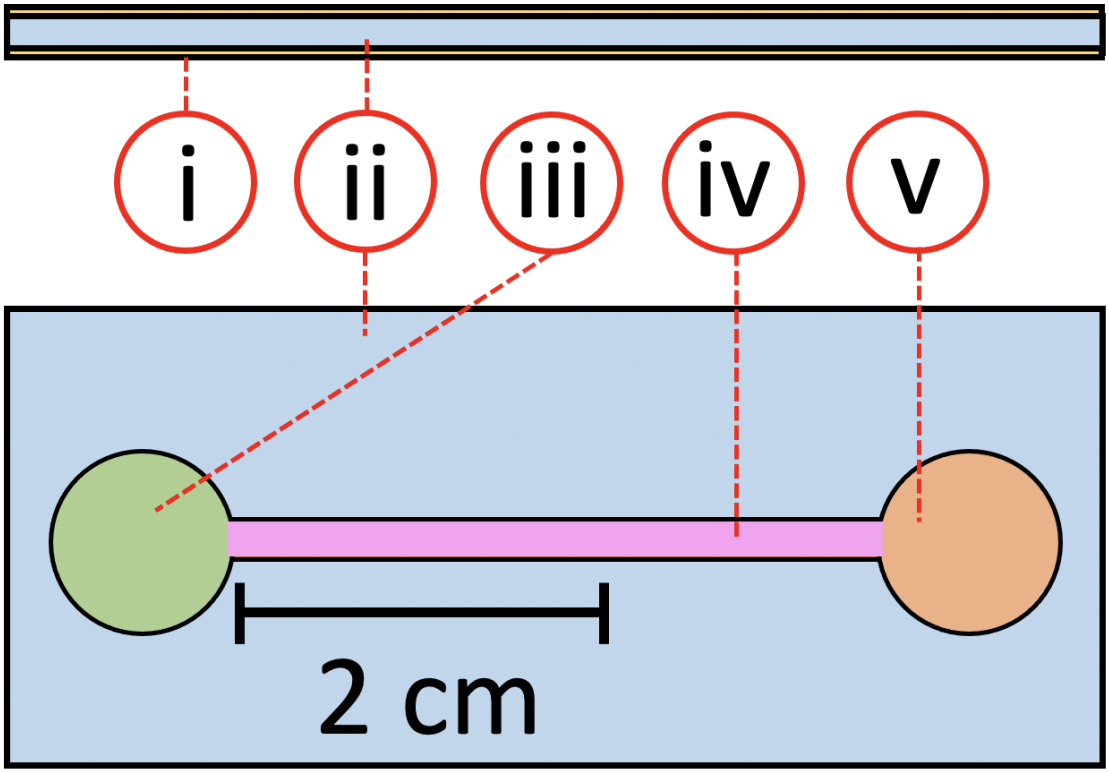

b)

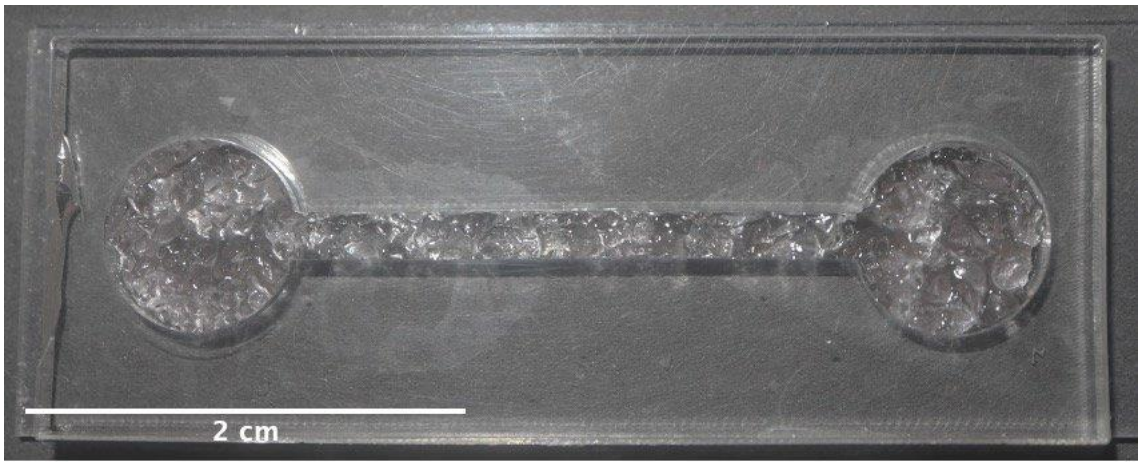

Figure 5.1. Chemotaxis chambers were used to quantify bacterial movement in a granular environment. a) Chambers consisted of i) a microscope slide ii) bonded to a 0.3 cm thick layer of polydimethylsiloxane (PDMS). iii) A well in the PDMS held bacterial inoculant. iv) fluorescent bacteria were imaged as they moved through a 3.5 cm long channel. v) A second well held a chemoattractant. b) Both wells and the channel were filled with transparent soil.

Transparent soil

Transparent soil was generated and prepared for plant growth following the protocol described in Chapter 4; Transparent soil and mesocosm design.

Experimental conditions

Experiments were carried out in a temperature-controlled room (approximately 21 ^{o}C). To prepare chemotaxis chambers, transparent soil was rinsed three times with 0.5 x MS. A 2:1 mixture of transparent soil: 0.5 x MS was then used to fill the wells and channel in each chamber. To determine the volume of liquid medium in chambers (V_{tot}), they were filled, weighed, then allowed to airdry for seven days before being weighed again. The density of 0.5 x MS medium was assumed to be 1 g ml^{-1}. V_{tot} was calculated based on the difference in mass between dry and wet chambers.

To fill one of the two wells, 50 µl of medium was drawn off from the edge of the well. 50 µl of bacterial inoculant, a chemoattractant, or a dye was then injected into the soil at the edge of the well. Food dye was placed in the chemoattractant well and its diffusion through the channel observed by eye over the course of six hours.

Two fluorescent dyes with extreme adsorption properties were used as an indicator of potential rates of exudate diffusion within the channel. A 0.04 g ml^{-1} solution of sulforrhodamine-B (SRB, Sigma-Aldrich, S1402, UK) in 1% acetic acid or a 20-µg ml^{-1} solution of fluorescein diacetate (FDA, Invitrogen, F1303, USA) were added to the chemotaxis well of a chamber and the movement of the dye was quantified through imaging.

To carry out chemotaxis assays, lettuce root exudate was collected as described above under Plant growth conditions and exudate collection. Exudate, or a negative control of 0.5 x MS was placed in the chemoattractant well. A suspension of Psf E1433 pGFP in 0.5 x MS at an OD_{600} of 0.02 was prepared and placed in the suspension well. The movement of fluorescent bacteria within the chamber was quantified through imaging.

Imaging

Imaging was carried out using a Nikon A1R confocal laser scanning system mounted on a NiE upright microscope fitted with a NIR Apo 20 × 0.8 water dipping lens with GaAsP detectors (Nikon, Japan). pGFP and fluorescein were excited at 488 nm with the emission being collected at 500–530 nm. SRB was excited at 530 nm with the emission being collected at 570-600 nm.

Settings and gain levels for pGFP were established to avoid saturation of images based on imaging of a suspension of Psf E1433 pGFP at an OD_{600} of 0.02. Subsequent images of bacteria were taken with the same settings. Settings and gain levels for fluorescent dyes were set to avoid saturation based on imaging of the appropriate dye at the concentration of the original treatment. Each chamber was imaged prior to treatment. Chambers were placed on the microscope stage immediately after treatment and the first image taken. Chambers remained in place for the duration of the assay, with subsequent images taken every hour for four hours. Images were focused approximately 0.5 mm below the surface of the soil. Images of the entire length of the channel in each chemotaxis chamber were captured at each time point. Images were saved in NIS format, containing metadata.

Image processing

Table 5.1. Variables and parameters

Notation	Definition	Unit
C_E	Approximate concentration of exudate at initiation	g ml^{-1}
k	Bacterial carrying capacity by CFU	ml^{-1}
K	Bacterial carrying capacity by mass	g mm^{-2}
U_B	Bacterial decay	g mm^{-2} s^{-1}
D_B	Bacterial diffusion parameter	mm^2 s^{-1}
α	CFU to g of carbon conversion factor	g
Q	Chemotactic parameter	g mm^{-2} s^{-1}
h_B	Conversion factor, pixel intensity to bacterial density in g of carbon	g
h_E	Conversion factor, pixel intensity to exudate density in g of carbon	g
B	Estimated bacterial density	g mm^{-2}
E	Estimated exudate concentration	g mm^{-2}
Y_e	Experimental value at time t and position i	g mm^{-2}
U_E	Exudate decay	g mm^{-2} s^{-1}
D_E	Exudate diffusion parameter	mm^2 s^{-1}
y^0	Initial bacterial density	CFU ml^{-1}
Y^0	Initial bacterial density in g of carbon	g mm^{-1}
$\hat{I}_{max}$	Maximum x_I value	NA
μ	Maximum bacterial growth rate	$hour^{-1}$
G	Maximum bacterial growth rate	g mm^{-2} s^{-1}
$\bar{y}$	Mean bacterial density in chambers at initiation	CFU ml^{-1}
I^0	Mean value of I for images taken prior to inoculation	NA
V_{tot}	Mean volume of medium in chemotaxis chambers	ml
S	Microbial growth rate	g mm^{-2} s^{-1}
M	Microbial mortality rate	g mm^{-2} s^{-1}
Y_m	Model predicted value at time t and position i	g mm^{-2}
J	Monod affinity parameter	g mm^{-2}
$\hat{I}$	Normalised pixel intensity	NA
$\hat{I}_\propto$	Proportion of maximum pixel intensity	NA
N	Sample size	NA
I	Sum of pixel intensities along the width of the channel	NA
t	Time	s
V_{field}	Volume of image	ml

Images were processed to extract a profile of fluorescence from either dyes or bacteria along the length of the chamber. Images of the channel were tiled automatically with 10 % overlap.

Total pixel intensity values at time t were extracted across the width of the chamber for each position i, $I(i,t)$. To reduce noise in the data, resulting from the heterogeneity of the transparent soil, a median filter was applied to each data set.

Estimating bacterial density in terms of carbon content

To account for differences in soil structure, values of $I(i,j,t)$ were transformed to correct for background fluorescence prior to inoculation (I^0) and to convert pixel intensity values into bacterial cell density (B) measured in g of carbon per mm^{-2} (g mm^{-2}, Table 5.1):

$$B = \frac{h_B}{dx^2}\hat{I} = \frac{h_B}{dx^2}(I - I^0) \qquad \text{Equation 5.1}$$

B is the bacterial density expressed in g mm^{-2}, while h_B (g) is a conversion factor which enables pixel intensity to be converted into bacterial cell density in g of carbon. The area of pixels for each position i (dx^2) is 0.19 mm^2. $\hat{I}$ is pixel intensity corrected for the background fluorescence. Each chamber contained 50 µl of bacterial suspension at an estimated bacterial density of 3e7 CFU ml^{-1} (Chapter 2, Figure 2.7). Chambers are therefore initiated containing approximately 1.56e6 CFU. Bacterial density in chambers, denoted $y(i,j,0)$ (CFU ml^{-1}), can be used to determine the pixel conversion factor k_B, using mean volume of liquid medium in chambers V_{tot} (ml). First, the mean bacterial density $\bar{y}$ is determined:

$$\bar{y} = \frac{1.5e6}{V_{tot}}. \qquad \text{Equation 5.2}$$

The sum of $\hat{I}$ across the entire chamber is related to the total number of cells within a volume defined by the depth of field of the microscope objective, V_{field}, and CFU to g of carbon conversion factor α, which was based on the value of g CFU^{-1} given by (Fukuda *et al.*, 1998) of 1e-14 g CFU^{-1}:

$$h_B \sum_{i,j} \hat{I} = \alpha V_{field} \bar{y} \qquad \text{Equation 5.3}$$

The conversion factor for images of fluorescent bacteria was therefore calculated as:

$$h_B = \frac{\alpha V_{field} \bar{y}}{\sum_{i,j} \hat{I}}$$ Equation 5.4

Estimating fluorescent dye density in terms of carbon content

A similar set of calculations with several distinctions was carried out in order to convert data obtained from fluorescent dye images into a comparable unit to allow a comparison between images acquired using different settings. Images of dyes were obtained using different microscope settings, meaning it was first necessary to express $\hat{I}$ as a proportion of maximum normalised pixel intensity for each profile ($\hat{I}_{max}$) based on:

$$\hat{I}_{\propto} = \frac{\hat{I}}{\hat{I}_{max}}$$ Equation 5.5

$\hat{I}_{\propto}$ is the proportion of maximum normalised pixel intensity. A similar process to above was applied to estimate the concentration of fluorescent dyes (E) expressed in g of carbon mm^{-2}:

$$E = \frac{h_E}{dx^2} \hat{I}_{\propto}$$ Equation 5.6

E is the bacterial density expressed in g mm^{-2}, while h_E (g) is a conversion factor which enables the proportion of maximum pixel intensity to be converted into exudate density in g of carbon. This is distinct from the h_B bacterial conversation factor. Once more, the area of pixels for each position i (dx^2) is 0.19 mm^2. The sum of $\hat{I}_{\propto}$ across the entire chamber is related to the total exudate concentration within a volume defined by V_{field}. The value of $\hat{I}_{\propto}$ immediately following treatment was taken to be equivalent to the total mass of exudate carbon in the volume imaged.

An approximate estimation of initial exudate concentration (C_E) g ml^{-1} within V_{field} was made based on reducing sugar content of exudates, estimated using benedict's reagent. Assuming a homogenous distribution of C_E, $\hat{I}_{\propto}$ can therefore be converted to g of carbon based on:

$$h_E \sum_{i,j} \hat{I}_{\propto} = V_{field} C_E$$ Equation 5.7

The conversion factor for images of fluorescent dyes was therefore calculated as:

$$h_E = \frac{V_{field} C_E}{\sum_{i,j} \hat{I}_{\propto}}$$ Equation 5.8

Modelling of diffusion and convection in transparent soil

The movement of bacterial density and exudate was modelled using partial differential equations. Models were developed which represented the change in density of exudate (E) and bacterial carbon (B) with time (t, s). Two partial differential equations were developed representing control conditions, in which there was no interaction between bacteria and exudate. These were on based separate diffusion parameters (D_E and D_B, mm^2 s^{-1}, for E and B respectively), representing diffusivity, and decay parameters (U_E and U_B, g mm^{-2} s^{-1}, for E and B respectivly) representing the loss of fluorescent signal over the course of experiments:

$$\frac{dE}{dt} = \nabla(D_E \nabla E) - U_E E$$ Equation 5.9

$$\frac{dB}{dt} = \nabla(D_B \nabla \mathrm{B}) - U_B B - \nabla Q \frac{dE}{dx} \nabla B$$ Equation 5.10

The directional movement of bacterial density in response to the gradient of exudate (chemotaxis), was represented based on the Keller Segal model (Keller and Segel, 1971). with parameter Q (g mm^{-2} s^{-1}), and the gradient of E. The two equations are linked with each other through the growth of bacterial population, modelled with the coefficient S (g mm^{-2} s^{-1}). S was not recorded during chemotaxis assays, but it was incorporated into models of chemotaxis from observations of bacterial proliferation in exudates, made in Chapter 3 (Chapter 3, Figure 3.3 b). Based on observations of the lack of bacterial growth in the absence of any plant input, and growth in the presence of either a root or root exudate made in Chapter 3 (Chapter 3, Figure 3.3), the assumption was made that growth was dependent on exudate concentration (E).

Bacterial growth was therefore incorporated into Equation 5.12 based on the Monod equation assuming mortality is accounted for by the overall intensity decline U_B (Monod, 1966):

$$S = G\frac{E}{E+J}. \qquad \text{Equation 5.11}$$

G (g mm^{-3} s^{-1}) is the maximum growth rate, J an affinity constant (g mm^{-3} s^{-1}). For the purposes of constructing a two-dimensional model, all bacterial growth within the imaged volume was assumed to be occurring on a two-dimensional plane and the parameters for the Monod equation were expressed in terms of g mm^{-2} s^{-1}. The decrease in E as a result of bacterial growth was assumed to be proportional to S and linked with a coupling parameter (Z), which represented both the inefficiency of bacteria at converting available carbon to biomass, and the unavailability of some exudate carbon for bacterial use. Within the experimental system, there was a set mass of exudate at the beginning of each time course which did not increase. Therefore, there was no need to incorporate any introduction of exudate into equations in order to accurately model the system. This worked well over the short experimental period in which it could be assumed that carbon would not be a limiting factor on bacterial growth (based on observations of bacterial growth in exudate made in Chapter 3) and exudate production by a plant would be negligible, based on the fact collected exudates represented eight days of plant growth in the absence of any bacteria. The resulting coupled equations predict bacterial diffusion, chemotaxis, and growth, alongside exudate diffusion, consumption, and the loss of fluorescent signal over the course of experiments:

$$\begin{cases} \dfrac{dE}{dt} = \nabla D_E \nabla E - U_E E - S \\ \dfrac{dB}{dt} = \nabla D_B \nabla \mathrm{B} - U_E B - \nabla Q \dfrac{dE}{dx} \nabla B + ZS \end{cases} \qquad \text{Equation 5.12}$$

Fitting of model parameters

Model parameters were fit to experimental data. To account for the differences in initial conditions of experimental data, resulting from the heterogeneity of transparent soil, experimental data at the first recorded point post treatment (t = 0 hours) was used as the starting point for models. As wells on either end of the chamber were not imaged, the value of either B

or E at either end of the imaged area (the channel) was taken to be the value within the well. A measure of total model error was calculated according to:

$$Cost\ Function = \sum_{b=1}^{b=t}\left(\sqrt{\frac{\sum_{i=1}^{i=N}(Y_e(i,t) - Y_m(i,t))^2}{N}}\right) \quad \text{Equation 5.13}$$

Where $Y_m(i,t)$ is the model predicted value of either E or B at time t and position i. $Y_m(i,t)$ is the experimental value of either E or B at time t and position i. N is the number of positions along the chamber.

Model parameters were fit to experimental data based on minimisation of the cost function using the Nelder-Mead method (Gao and Han, 2012). Model parameters D_E, D_B, U_E and U_B were fit to negative control and fluorescent dye data sets based on Equations 5.9 and 5.10, with the value of Q set to 0, respectively. The mean fit value of these parameters were then held as fixed, and model parameter Q was fit to data from chemotaxis assays based on Equation 5.12.

Bacterial proliferation was incorporated into models of chemotaxis (Equation 5.12). In Chapter 3, the proliferation of bacteria in the presence of root exudate was quantified and modelled using the logistic equation (Chapter 3, Figure 3.3b). The logistic equation predicts the rate of change of bacterial density (y) with time (t) based on a carrying capacity (k) and maximum growth rate (μ):

$$\frac{dy}{dt} = \mu y\left(\frac{k-y}{k}\right) \quad \text{Equation 5.14}$$

Parameter values fit to data based on the quantification of CFU ml^{-1} in Chapter 3 were converted to g ml^{-1} based on the CFU to g of carbon conversion factor α. For each growth parameter, the calculated value within the volume of the image (V_{field}) was taken to be equivalent to the value on a two-dimensional plane with an area equal to the area of the chemotaxis channel (g mm^{-2} (Table 5.2).

Table 5.2. Parameters for the logistic equation fit to proliferation in the presence of exudate data in Chapter 3 were converted from CFU ml^{-1} to g mm^{-2} based on the conversion factor α and the assumption that activity within the volume of the image (V_{field}) was occurring on a two-dimensional plane.

Logistic parameters (y, CFU ml^{-1})	Converted logistic parameters $\left(*\,{}^{\alpha}/_{V_{field}}\right)$ (B, g mm^{-2})
k = 1.28e8 CFU ml^{-1}	K = 1.43e-3 g mm^{-2}
μ = 1.04 CFU hour^{-1}	G = 3.25e-15 g s^{-1}
y^0 = 6.5e7 CFU ml^{-1}	Y^0 = 7.28e-4 g mm^{-2}

As both the logistic and Monod equation predict the rate of change of B with t, under the same growth conditions:

$$G\frac{E}{E+J} - M = GB\left(\frac{K-B}{K}\right) \qquad \text{Equation 5.15}$$

Initial growth conditions for the proliferation of bacteria in the presence of root exudate experiment, described in Chapter 3, were assumed (Table 3.4). M was assumed to be 0. The value of E was assumed to be equal to the reducing sugar content of root exudate within V_{field} (C_E, g ml^{-1}) under the assumption that activity within the volume was occurring on a two-dimensional plane (g mm^{-2}). The value of B was assumed to be equal to initial bacterial density in g mm^{-2} (Y_0). J was then calculated based on:

$$J = C_E V_{field}\left(\frac{K}{Y_0(K-Y_0)} - 1\right) \qquad \text{Equation 5.16}$$

Difference between the Monod and logistic predictions was taken to be the result of the inefficiency of bacteria at converting available carbon to biomass, and the unavailability of some exudate carbon for bacterial use. In Equation 5.12, this is represented by the coupling coefficient (Z). To determine Z, a homogenous distribution of bacterial density B and exudate concentration C_E with no decay ($U_E = 0, U_B = 0$) was assumed. Equation 5.12 was then solved

in two different scenarios. In the first scenario, Y_e values were calculated based on simulation of the growth of a bacterial population (S) using the logistic equation. In the second, Y_m values were calculated based on simulation of the growth of a bacterial population, where S was based on the Monod equation. Z was then fit based on the minimisation of the cost function (Equation 5.13) using the Nelder-Mead method (Gao and Han, 2012).

Testing of chemotaxis models

Equation 5.12 was solved in a one-dimensional simulation over the length of the chemotaxis chamber, including the two wells and the channel (5.5 cm). Initial conditions for E were given by the mean value of data at each point for fluorescent dyes. Mean fit values of model parameters were used. Experimental data was imported to give the starting conditions for B. Coupled partial differential equations were solved at a time step of 1 second and a resolution of 0.1 mm over three hours.

Equation 5.12 was then solved in a two-dimensional simulation for a 324 mm^2 area. Mean fit values of model parameters were used. An initial homogenous value for B was set based on the mean value of $\hat{I}$ across chambers at the beginning of chemotaxis assays, converted to g mm^{-1} according to Equation 5.1. The production of exudate by a root was incorporated in the model empirically. Values of E were set to 0 everywhere except a 0.28 cm x 0.2 cm root domain, which retained a value of E equal to the mean value of $\hat{I}_\propto$ across chambers at the beginning of chemotaxis assays, converted to g mm^{-1} according to Equation 5.6. Coupled partial differential equations were solved at a time step of 1 second and a resolution of 0.01 mm^2 over three hours.

A root growth rate (R_r) was incorporated into the simulation. Initial conditions for the two-dimensional simulation were set out as described above, with a starting length for the root domain of 1 mm. U_E and U_B were set to 0 for these longer-term simulations. Mean fit values of model parameters were used. At each t, the root domain increased in length based on R_r, which was established based on live quantifications of root growth rate made during Chapter 4. Coupled partial differential equations were solved at a time step of 1 second and a resolution of 0.01 mm^2 over 72 hours.

The above simulation, incorporating root growth rate, was solved for high and low values of D_E, which were determined based on the highest and lowest values of D_E fit to fluorescent dye

data sets. For other model parameters, mean fit values were used. Coupled partial differential equations were solved at a time step of 1 second and a resolution of 0.01 mm^2 over 72 hours.

Data analysis and use of software

For motility assays, a Student's T-test was used to test for a significant difference in mean distance travel by bacteria in the presence and absence of exudate in R (R Core Team, 2018). Initial image generation and automatic tiling was carried out using NIS-elements AR software (Nikon, USA). Further processing and extraction of fluorescence profiles were carried out in ImageJ (Schneider, Rasband and Eliceiri, 2012). For each time course of chemotaxis chambers, values of pixel intensity (I) were converted to g mm^{-2} based on the method described above, using I extracted from the first images taken post treatment. Models were solved using FiPy, an object oriented, partial differential equation (PDE) solver (Guyer, Wheeler and Warren, 2009). Zero-flux boundary conditions were applied. Chemotaxis modelled with the coefficient Q, was applied as a non-linear convection term. Diffusion, with the coefficient D_E or D_B, was applied through a constant diffusion term. Decay, with the coefficient U_E or U_B, was applied through a source term, as was bacterial proliferation based on Monod growth kinetics (Equation 5.12). Equations for E and B were implicitly coupled. Parameters were fit based on cost functions minimised using the Nelder-Mead method in the minimisation module of SciPy (Virtanen *et al.*, 2020).

Results

Bacterial movement increased in the presence of root exudate

To assess the impact of root exudates on bacterial movement, plants were grown in hydroponic conditions in sterile microcosms. Exudates were collected prior to carrying out motility and chemotaxis in semisolid agar assays, and prior to chemotaxis in transparent soil assays. Exudates were collected from 30 microcosms following eight days of growth. The lack of bacterial growth following plating of exudates on non-selective LB agar, along with the negative results of 16S PCR assays, indicated that exudates were sterile following filtration. Exudates were then pooled; comparison to solutions of glucose at known concentrations during the Benedict's test indicated that both collections of exudates had a reducing sugar concentration of approximately 2.5e-3 g ml^{-1}.

Motility assays in semisolid agar were carried out to determine if the presence of root exudate increased bacterial movement. Fifteen assays with exudate and an equal number of negative

controls were carried out; data was pooled for analysis. A Student's T-test found a significant difference in mean distance travelled by bacterial fronts from the point of inoculation in the presence of exudate (mean = 4.1 cm, SD = 0.04 cm) compared to negative controls (mean = 0.75 cm, SD = 0.06 cm, T(17.095) = -4.7, P < 1e-4, N = 30, Figure 5.2).

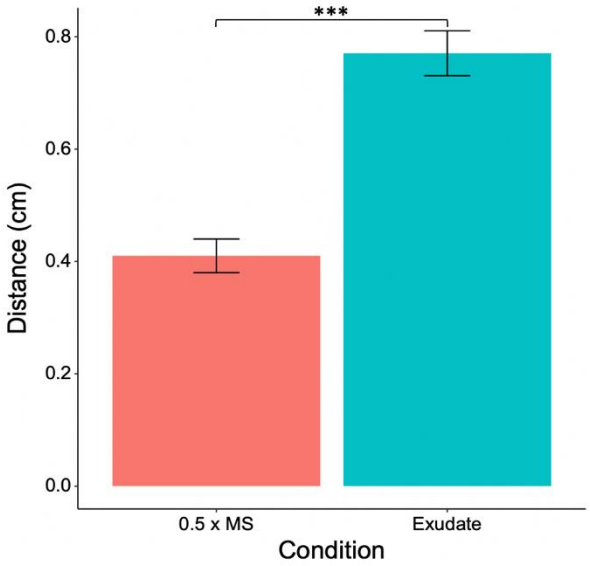

Figure 5.2. Bacterial motility in semisolid agar increased in the presence of root exudates. As significant difference in mean distance travelled by a visible bacterial front in semisolid agar was found for bacteria in the presence of root exudate compared to a negative control of 0.5 x MS medium based on a Student's T-test (T(17.095) = -4.7, P < 1e-4, N = 30). Error bars represent standard error of the mean. *** indicates a significant difference (P < 0.001).

These assays did not allow directional movement to be determined so bacterial movement in response to exudate was further investigated through chemotaxis assays. Chemotaxis assays in semisolid agar were carried out to quantify the movement of bacteria in response to a concentration gradient of root exudate. Over fifteen assays, a clear bacterial front could not be detected in capillary tubes. The inability to consistently image the entire length of capillary tubes made them unsuitable for tracking bacterial movement over time. This method was therefore abandoned.

Bacterial chemotaxis was quantified in a granular environment

A framework for quantifying chemotaxis in transparent soil was developed in order to assess bacterial movement in response to a concentration gradient in a heterogenous, soil-like environment. Chemotaxis chambers were developed which allowed a concentration gradient of a chemoattractant to be established and the movement of fluorescent bacteria in transparent soil to be quantified through imaging. Initial observations of food dye in chemotaxis chambers indicated that a moving gradient would be established along the length of the channel. Even after six hours, a homogenous distribution of dye was not established. Observation at the time of inoculation indicated that dye moved into the channel as the well was being filled, as the result of the inoculation method rather than diffusion (Figure 5.3).

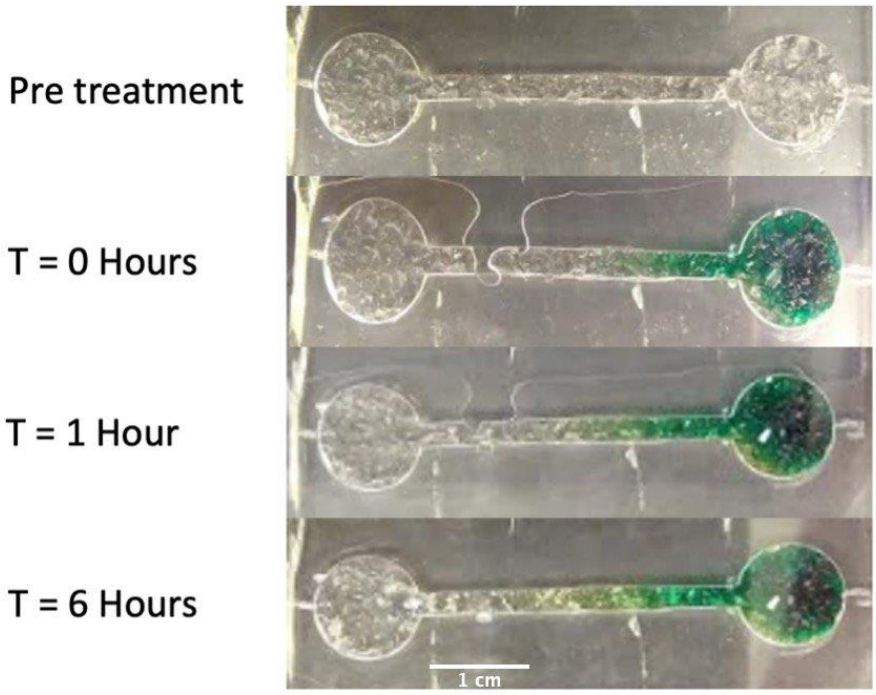

Figure 5.3. A visible gradient of food dye in chemotaxis chambers was established within minutes of dye addition. Food dye was added to chemotaxis chambers to visualise the ability of soluble organic solutions to establish a concentration gradient. A gradient was established within minutes of treatment and remained for six hours.

Profiles of fluorescence from either bacteria or dyes were extracted from images of chambers. Although overall trends in these images were visible, the heterogeneity of the substrate introduced a large amount of variability into profiles. Applying a median filter to data and normalisation based on Equation 5.1 enabled trends in the movement of fluorescent substances to be observed and compared. Profiles of fluorescent dyes were extracted from images, normalised, and converted to an expected exudate density (E, g mm^{-2}) based on Equation 5.6. Profiles of fluorescent bacteria were extracted from images, and converted to estimated bacterial density (B, g mm^{-2}) based on Equation 5.1 (Table 5.3). A decrease in fluorescent signal intensity was observed for the majority of chambers containing both bacteria and dyes. This was accounted for in modelling by including the decay parameter U (Equation 5.12).

Table 5.3. Parameter values for the normalisation of image data and conversion of pixel intensity values to g mm^{-2}.

Parameter	Value	Parameter	Value
V_{tot}	0.26 ml	V_{field}	8.925e-4 ml
α	1e-14 g	C_E	2.5e-13 g ml^{-1}
$\sum_{i,j} \hat{I}$	Initial mean value of 1825	$\sum_{i,j} \hat{I}_{\propto}$	Initial mean value of 138
$\bar{y}$	5.77e6 CFU ml^{-1}	h_E	1.62e-18 g
h_B	2.74e-14 g		

Fluorescent dye profiles

Root exudates could not be detected through imaging. Two fluorescent dyes with extreme adsorption properties were used as an indicator of potential rates of exudate diffusion within the channel. SRB was used because it is known to be adsorbed by the particles. FDA is known to remain in solution in transparent soil. Dye profiles revealed a decrease in E along the length of the channel, beginning at a mean value of 2e-11 g mm^{-2} at the edge of the chemoattractant well and reducing to a mean value of 8.5e-12 g mm^{-2} at the edge of the bacterial inoculant well. A decrease in total E was observed for both chambers over four hours (mean decrease of 6.1e-8 g mm^{-2}). Parameters for Equation 5.11 were fit to fluorescent dye data sets (Table 5.4, Figure 5.4).

Table 5.4. Mean fit parameter values for Equations 5.11 and 5.12.

Parameter	Mean fit value	SD
D_E	1.62e-1 $mm^2\ s^{-1}$	6.21e-2 $mm^2\ s^{-1}$
D_B	1.64e-3 $mm^2\ s^{-1}$	1.16e-3 $mm^2\ s^{-1}$
U_E	9.4e-3 g $mm^{-2}\ s^{-1}$	4.31e-3 g $mm^{-2}\ s^{-1}$
U_B	7.6e-3 g $mm^{-2}\ s^{-1}$	2.53e-3 g $mm^{-2}\ s^{-1}$
Q	6.7e-3 g $mm^{-2}\ s^{-1}$	3.42e-3 g $mm^{-2}\ s^{-1}$
J	6.24e-13 g mm^{-2}	NA
G	1.17e-11 g $mm^{-2}\ s^{-1}$	NA
Z	0.36	NA

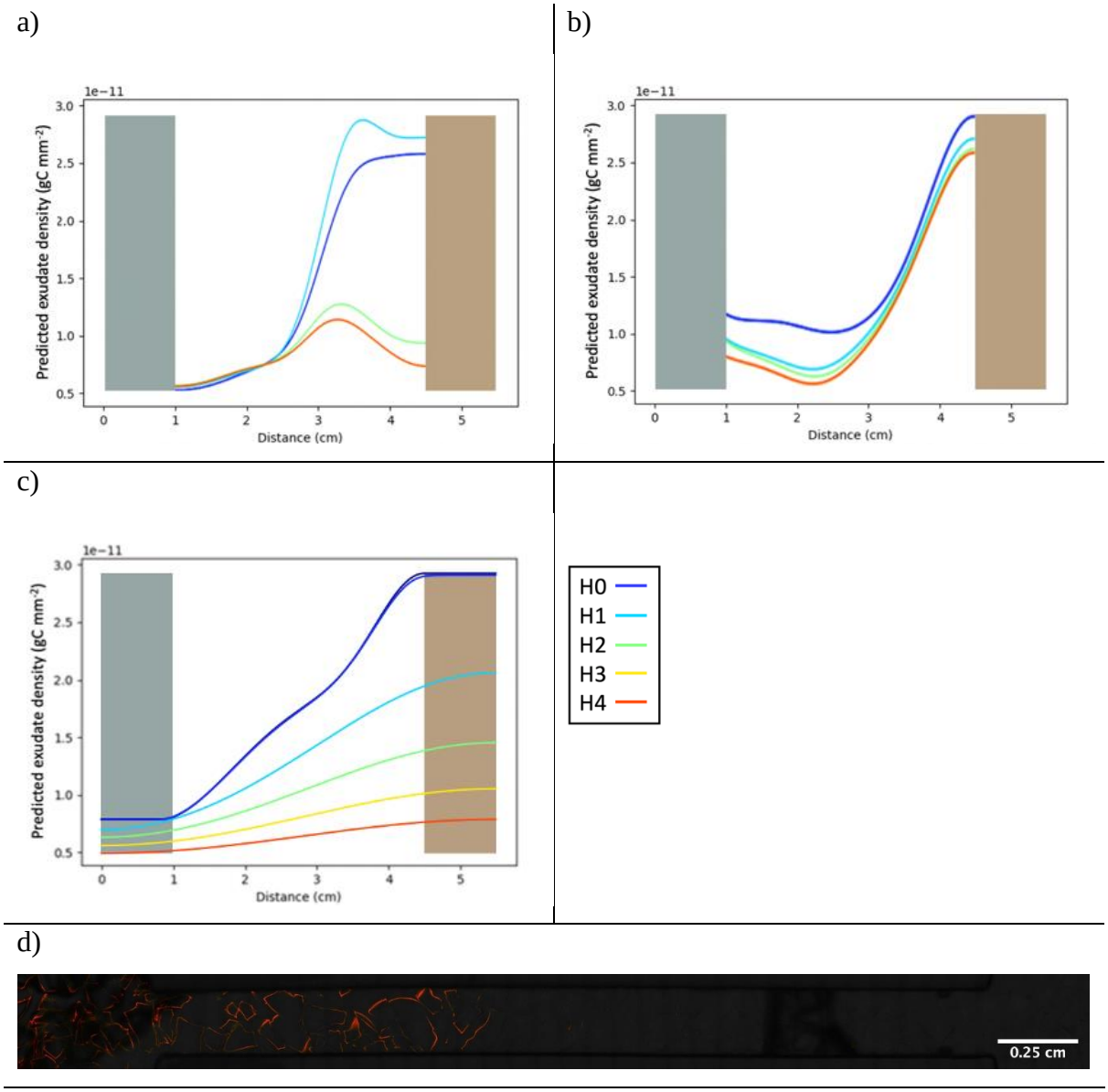

Figure 5.4. Fluorescent dyes were imaged to give an estimate of how exudates may behave in chemotaxis chambers. a) Profile of SRB in chemotaxis chambers over time extracted from images and converted to estimated values of g mm^{-2} based on Equation 5.6. b) Profile of DFA in chemotaxis chambers over time extracted from images and converted to estimated values of g mm^{-2} based on Equation 5.6. c) Parameter values for Equation 5.0 were estimated based on minimization of total model error according to Equation 5.13 (Table 5.4). Based on mean parameter values, a model of exudate/chemoattractant was developed. Initial conditions are the average of the conditions for dye images. Predictions made based on this model are shown. d) Image of the chemotaxis channel at hour 2 for a chamber

containing SRB showing fluoresce in red. Different line colours represent time points with an hourly increment running from hour 0 (H0, dark blue) to hour 4 (H4, red).

Fluorescent bacteria profiles

Bacteria were imaged in chemotaxis chambers in the absence of root exudate to quantify their movement in the absence of a chemoattractant. Exudate negative bacterial profiles were generated for four chambers. Profiles revealed a decrease in B along the length of the channel, beginning at a mean value of 2.6e-11 g mm^{-2} (SD = 5.57e-12 g mm^{-2}) at the edge of the bacterial inoculant well and reducing to a mean value of 3.25e-12 (SD = 1.08e-12) at the edge of the chemoattractant well. Parameters for Equation 5.12 were fit to exudate negative data sets (Table 5.4, Figure 5.5).

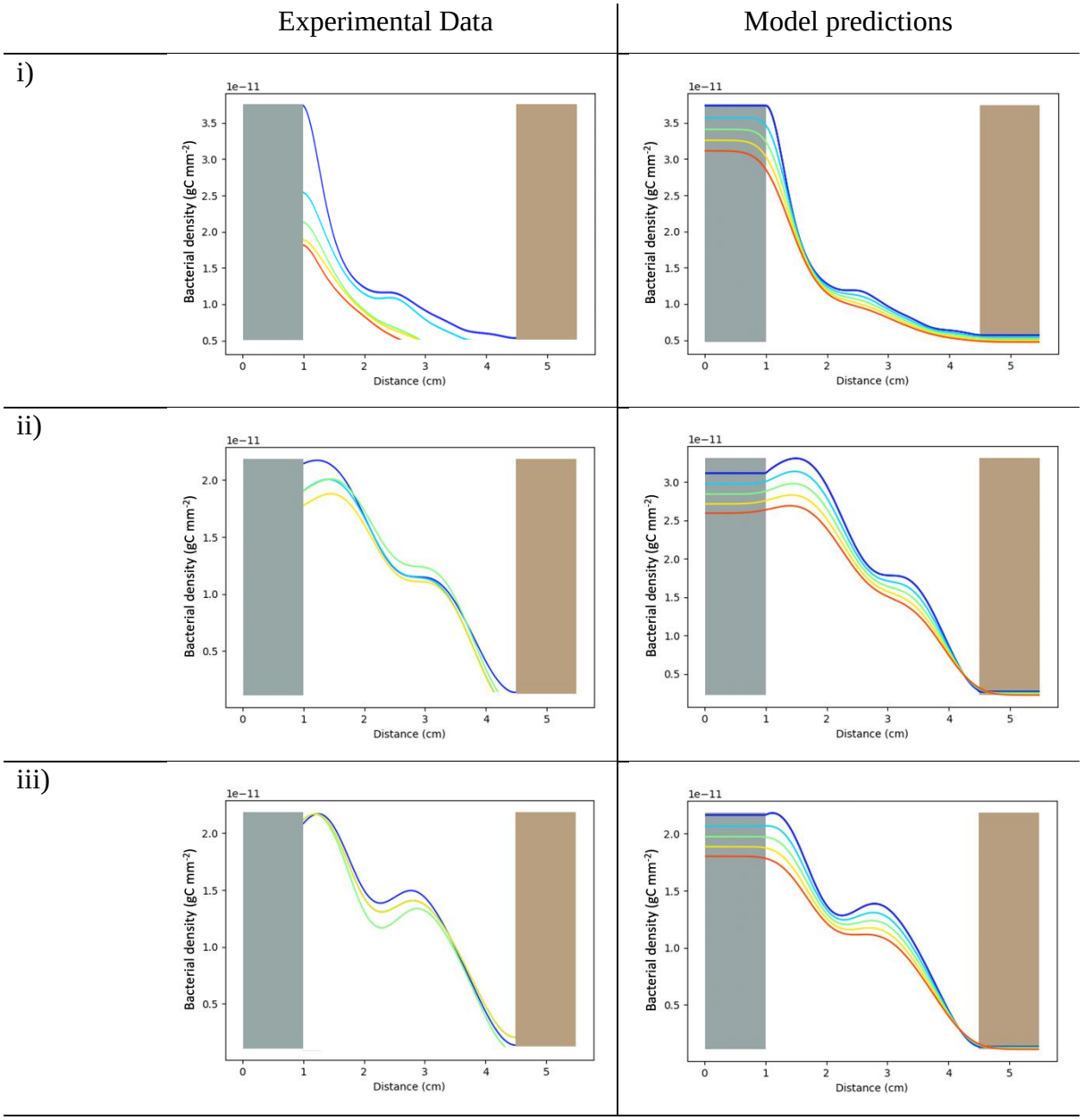

Figure 5.5. Profiles of bacterial density in the absence of exudate were extracted from images. Pixel intensity values were converted to estimated values of g mm^{-2} based on Equation 5.7. Three data sets are shown above on the left (i:iii). Model parameters for Equation 5.12 were fit to data sets by minimization of the total model error according to Equation 5.13 (Table 5.4). Model predictions are shown above on the right. Different line colours represent time points with an hourly increment running from hour 0 (H0, dark blue) to hour 4 (H4, red).

Bacterial chemotaxis was quantified by imaging fluorescent bacteria in the presence of root exudates. Exudate positive bacterial profiles were generated for five chambers. A great deal of heterogeneity was observed in the data. Generally, profiles displayed a decrease in mean B at the edge of the bacterial inoculant well (mean decrease of 9.5e-12 g mm^{-2}, SD = 5.71e-12 g mm^{-2}) and an increase in mean B at the edge of the chemoattractant well (mean increase of 2.5e-12 g mm^{-2}, SD = 1.22e-12 g mm^{-2}) over the four hours of the experiment. For most images there was also evidence of a region of depleted bacterial density, although this varied between chambers (Figure 5.6). Diffusion and decay parameters (D_E, D_B, U_E, and U_B) were taken from the mean fits of Equation 5.9 for fluorescent dye data sets and Equation 5.10 for exudate negative data sets. The convection term (Q) was then fit to exudate positive data based on the coupled Equations 5.10, taking initial values of E from the mean values of fluorescent dye profiles (Table 5.4, Figure 5.6). Despite the heterogeneity of the data, models were capable of being used to predict overall trends in bacterial movement when initial conditions were imported from data.

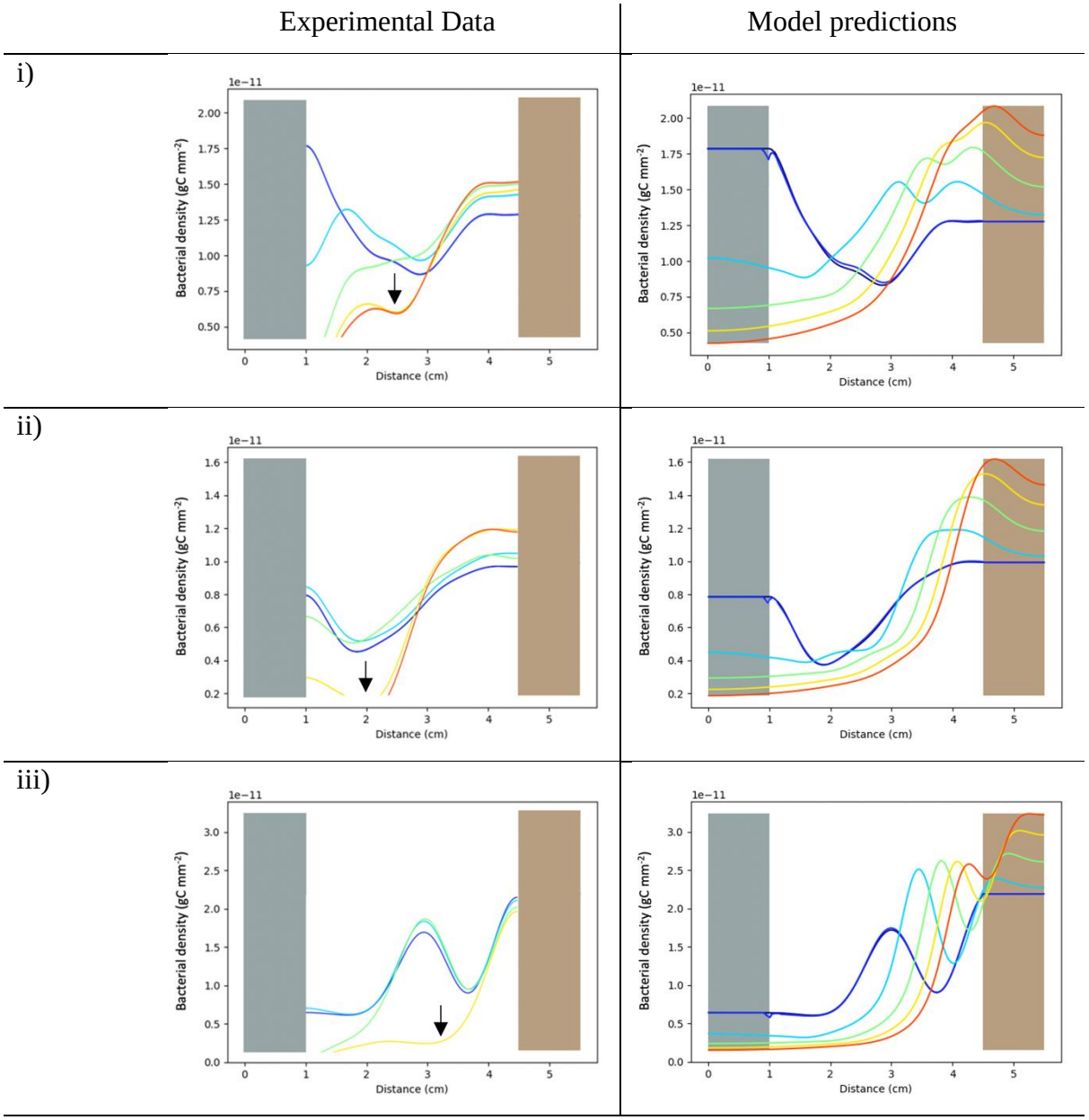

Figure 5.6. Profiles of bacterial density in the presence of exudate were extracted from images. Profile of bacterial fluorescence in chemotaxis chambers over time were extracted from images and converted to estimated values of g mm^{-2} based on Equation 5.7. Three data sets are shown above on the left (i: iii). Arrows indicate potential regions of depletion at t = 4 hours. Model parameters for Equation 5.13 were fit to data sets by minimization of the total model error according to Equation 5.13 (Table 5.3). Model predictions are shown above on the right. Different line colours represent time points with an hourly increment running from hour 0 (H0, dark blue) to hour 4 (H4, red).

Following these results, bacterial proliferation was incorporated into models of chemotaxis to link observations of bacterial proliferation in exudates, made in Chapter 3 (Figure 3.3 b), to bacterial movement. The Monod equation predicted higher rates of bacterial proliferation than were observed in the presence of root exudate in Chapter 3 (Chapter 3, Figure 3.3b). Parameter values for the Monod growth equation (Equation 5.12) were imported based on fits to proliferation in the presence of root exudate data from Chapter 3 (Table 3.4) to the logistic equation (Equation 5.14) converted to g mm^{-2} (Table 5.2) or calculated based on Equation 5.16. The coupling parameter (Z) was estimated based on comparison of bacterial density predictions from the logistic and Monod equations (Table 5.4).

To predict patterns of bacterial density in the presence of a root, models of bacterial chemotaxis and proliferation (Equation 5.12) were solved in 2-dimensions with a region of fixed exudation representing the root. From an even distribution of bacterial density (B) of 2.8e-9 g mm^{-2}, B in the root region was predicted to increase to 9.39e-9 g mm^{-2} (Figure 5.7).

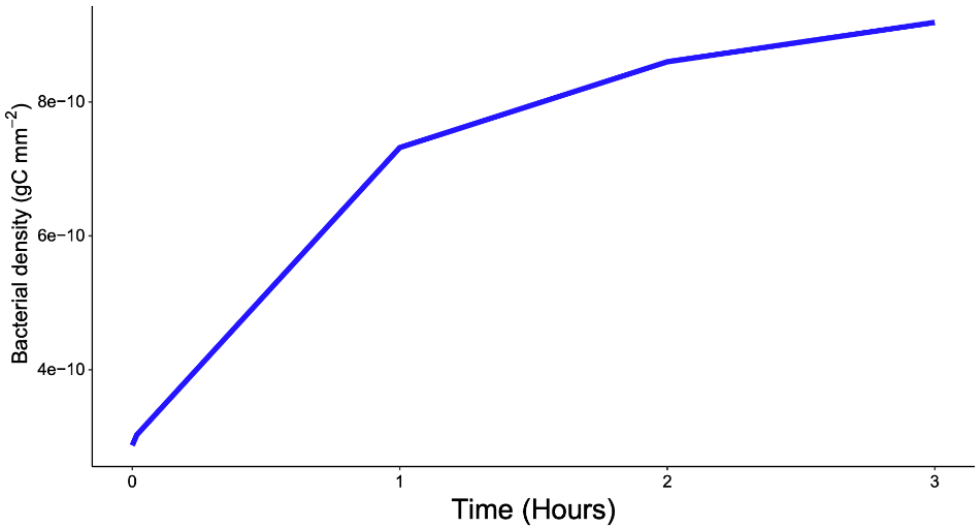

Figure 5.7. In two-dimensional simulations of chemotaxis, the sum of bacterial density in the root region increased with time. Simulations based on equation 5.12 were run in two dimensions over three hours, with a 2.8 mm x 0.2 mm root region with a fixed exudate value of 3.73e-9 g mm^{-2}. Other model parameters were based on the fit values reported in Tables 5.3 and 5.4.

In these simulations, the size of the root region was fixed, and exudation was set to be the same across the root region. As a result, the distribution of B remained largely homogenous along the length of the root region. However, an area of elevated B was present in cells at the tip of the root. An area of depleted B directly below and to either side of the root was created, measuring approximately 0.5 mm from the root region at hour 3 (Figures 5.8 and 5.12).

	Bacterial model	Exudate model
Hour 0	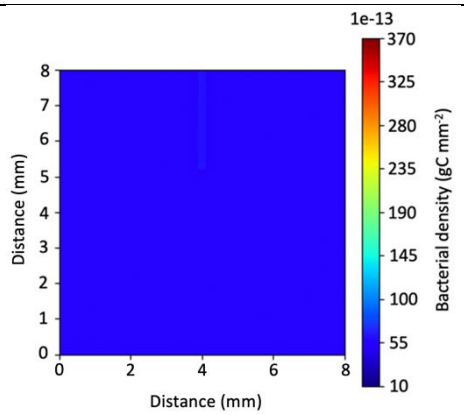	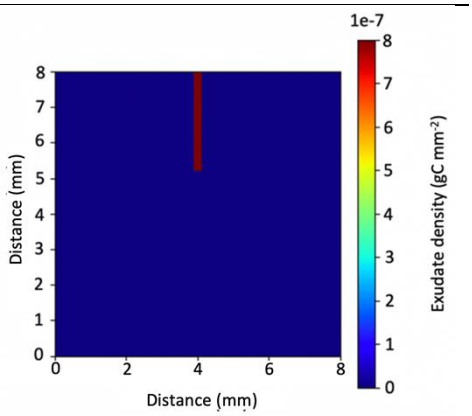
Hour 1	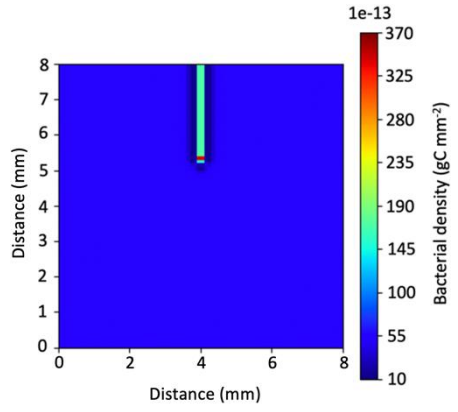	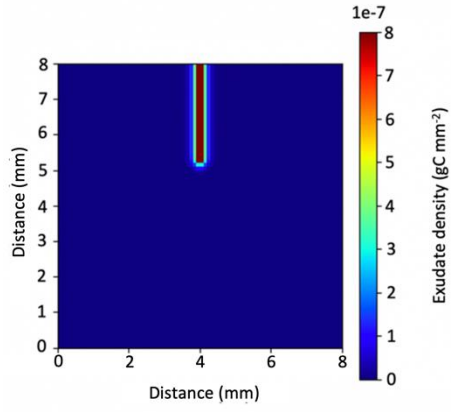
Hour 2	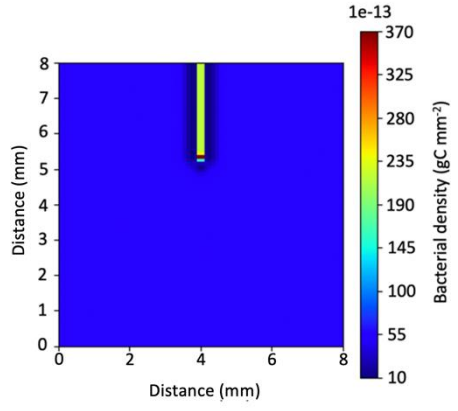	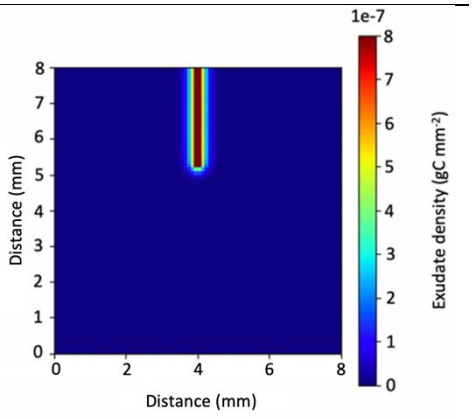

Hour 3

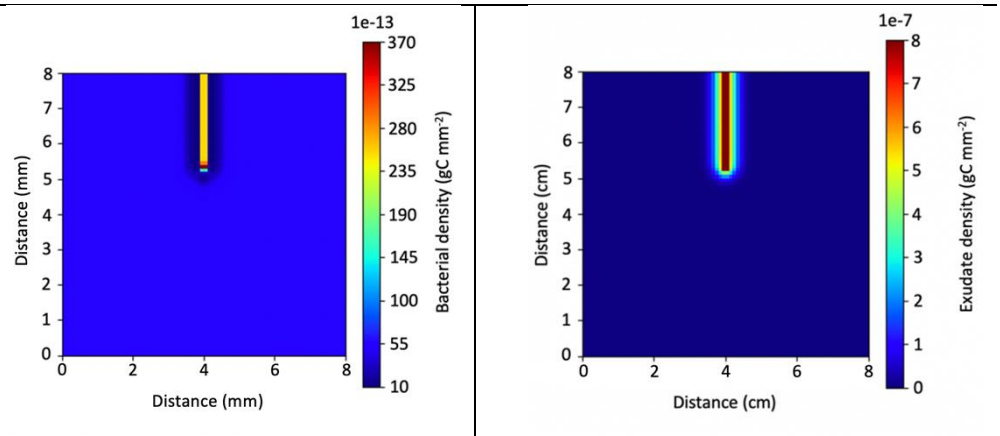

Figure 5.8. Simulations were run to predict bacterial movement in two-dimensions. Simulations based on equation 5.12 were run in two dimensions over three hours, with a 2.8 mm x 0.2 mm root region with a fixed exudate value of 3.73e-9 g mm^{-2}. Decay parameters U_E and U_B were set to 0. All other model parameters were based on the fit values reported in Tables 5.3 and 5.4.

A root growth rate (R_r) of 0.065 mm hour^{-1} was subsequently incorporated into a 72-hour simulation (Figure 5.9). For longer simulations, decay parameters U_E and U_B were set to 0. This resulted in a heterogenous distribution of B along the length of the root region, with the highest values at the shoot-end (8.2e-10 g mm^{-2}) and the lowest at the most distal end of the root (5.12e-11 g mm^{-2}) at t = 72 hours (Figure 5.10).

	Bacterial model	Exudate model
Hour 1	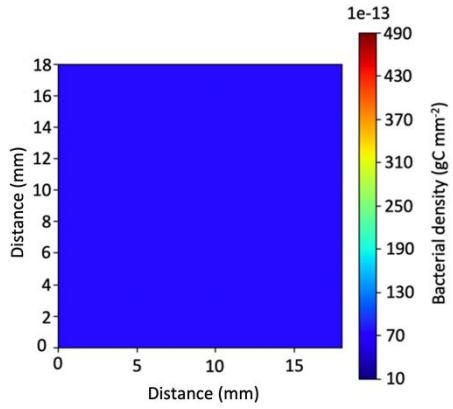	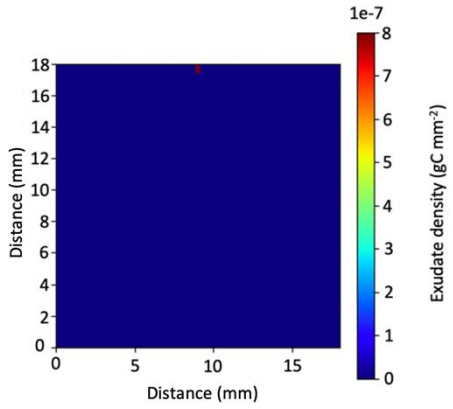
Hour 24	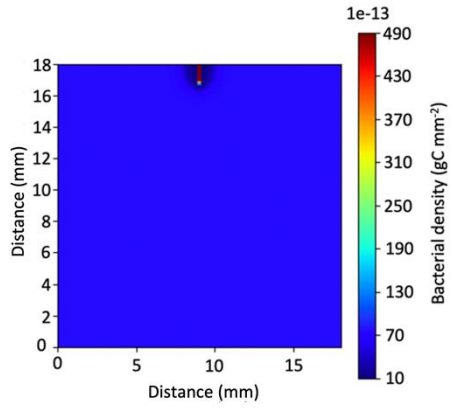	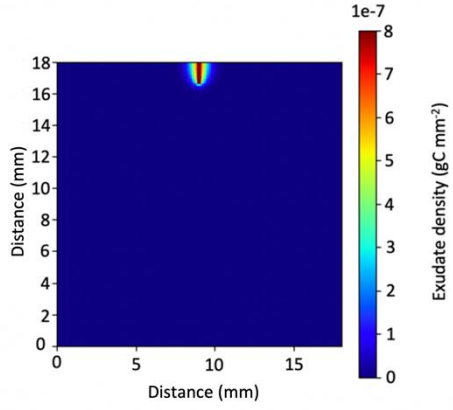
Hour 48	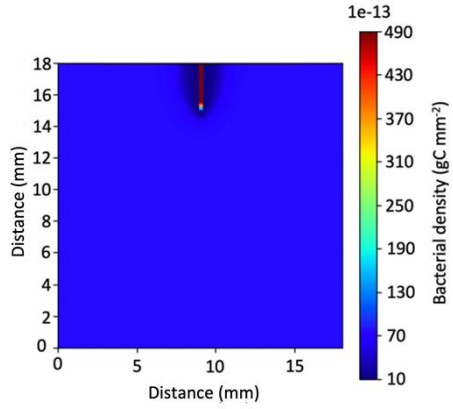	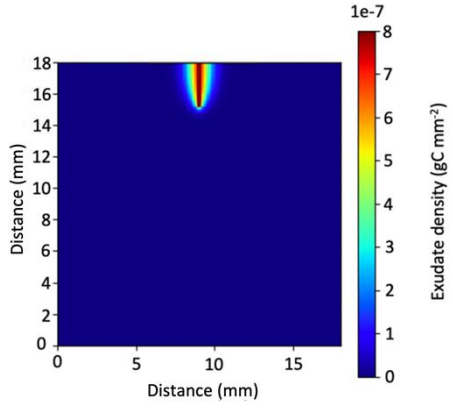

Hour 72	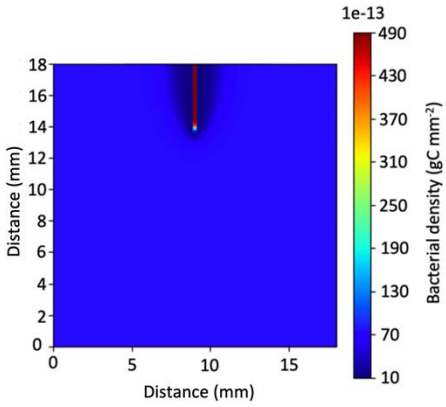	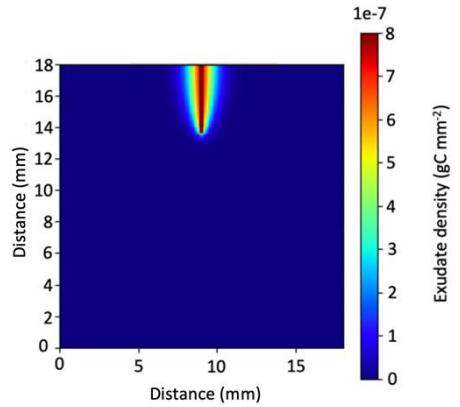

Figure 5.9. Simulations were run to predict bacterial movement in two-dimensions which incorporated a root growth rate. Simulations based on equation 5.12 were run in two dimensions over 72 hours, with a root region with a fixed exudate value of 3.73e-9 g mm^{-2}. From an initial length of 1 mm, the root region increased in length at a rate of 0.065 mm $hour^{-1}$. Decay parameters U_E and U_B were set to 0. All other model parameters were based on the fit values reported in Tables 5.3 and 5.4.

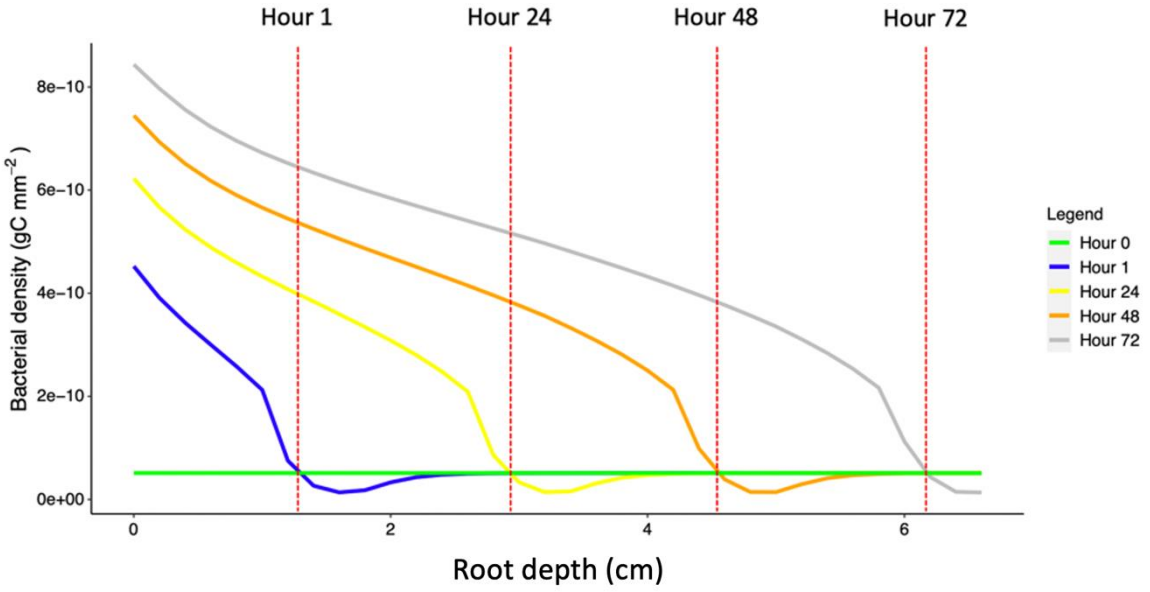

Figure 5.10. When root growth rate was incorporated into two-dimensional models of bacterial chemotaxis, a heterogenous profile of bacterial density in the root region was established. Profiles of bacterial density along the centre of the root region were generated based on the simulation of bacterial chemotaxis with an expanding root region (Figure 5.9). Dashed red lines represent the most distal, and newest point of the root region at each time point.

This simulation was then run under high and low exudate diffusivity conditions. Under high conditions (D_E = 0.318 mm s^{-1}), the region of depleted B extended approximately 1.5 mm to either side of the root region, while under low conditions, (D_E = 0.018 mm s^{-1}) the region of depleted B extended approximately 0.74 mm to either side of the root region, (Figure 5.11). Two-dimensional models of bacterial movement in soil were used to predict trends in bacterial density as the result of rhizodepositions and root growth.

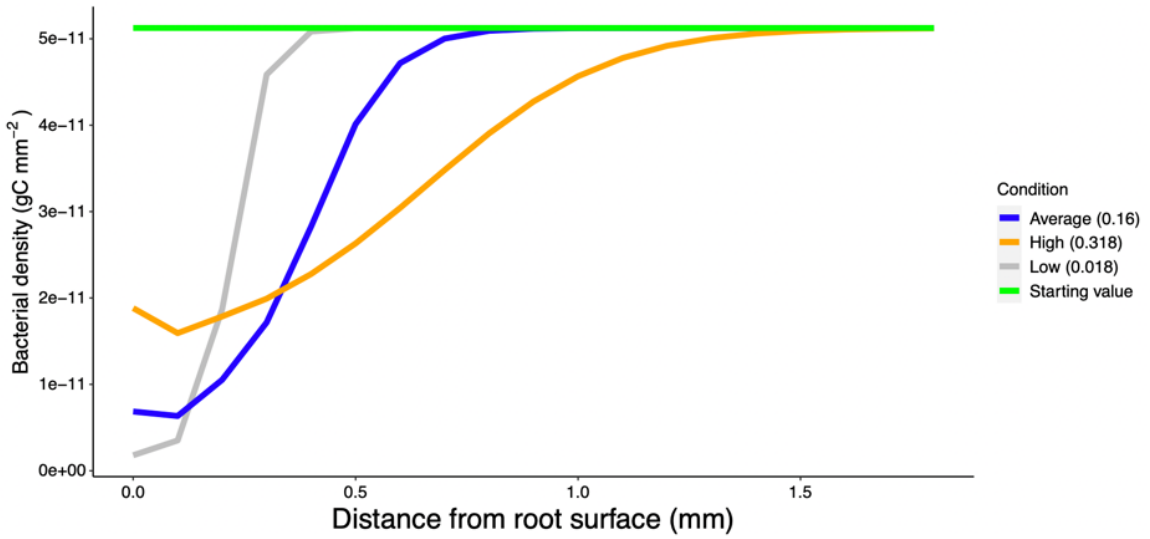

Figure 5.11. The region of depleted bacterial density around the root increased in simulations with a higher diffusion parameter (D_E) value assigned to exudate. Curves above represent predicted bacterial density at hour 72 with perpendicular distance from the root region. Simulations of bacterial chemotaxis with high, low, and average values for D_E were run, based on Equation 5.12. The root region had a fixed exudate value of 3.73e-9 g mm^{-2} and grew from an initial length of 1 mm at a rate of 0.065 mm hour^{-1}.

Discussion

To assess the role of bacterial movement in establishing patterns of rhizoplane colonisation, the aim of this chapter was to develop an experimental and mathematical framework for quantifying and modelling microbial movement in response to chemoattractants in a granular environment and to integrate it into a root colonisation model. This work builds on previous published studies, which examined chemotaxis in homogenous liquid or gel environments (Law and Aitken, 2005; Reyes-Darias *et al.*, 2016), in porous media (Bhattacharjee *et al.*, 2021), or in soil (Bashan, 1986; Yang *et al.*, 2019). The work in this chapter presents a novel method for understanding the role of chemotaxis in soil processes in conditions similar to natural soils at a high degree of spatial and temporal resolution than has previously been possible. It has numerous applications for developing a better understanding of bacterial movement in soil.

A method for quantifying chemotaxis in a granular environment

Bacterial chemotaxis assays require two key components. The first is a means by which to establish a concentration gradient of the potential chemoattractant. The second is a means by which to quantify the movement of bacteria (Yang, 2018; Law and Aitken, 2005). In this chapter, concentration gradients of root exudate in transparent soil and semisolid agar were established through diffusion. This is a common method for chemotaxis assays in homogenous conditions. While it does not allow control over the concentration gradient (Law and Aitken, 2005), for the purposes of this chapter, these conditions were sufficient to capture the movement of bacteria in response to root exudate. The diffusivity of exudate in a granular environment, and its impact on microbial chemotaxis, is a key component of determining root colonisation rates and patterns. No attempt to adjust or control the diffusivity of exudate was therefore made. In future work, a continuous flow apparatus could be used to modulate exudate density, and simulate different rhizodeposition conditions (Law and Aitken, 2005).

The framework for quantifying and modelling microbial chemotaxis in this chapter could be expanded to explore the impact of different soil structures on microbial movement. Particle size, chemistry, and water content could all be altered, to observe the impact on chemotaxis. For example, reducing the moisture content of transparent soil would be expected to reduce bacterial motility. This has a range of potential uses for developing our understanding of the rhizoplane colonisation process. There are wider implications for the study of microbial process

in bulk soil, where chemotaxis drives processes such as contaminant bioremediation (Witt *et al.*, 1999; Yang *et al.*, 2019).

Only the most basic assessment of exudate composition was made in this chapter since for the purposes of developing the chemotaxis assay, the exact makeup of exudate did not need to be known. Exudate composition is likely to have a high degree of variability between plants and based on the age of plants (Hayat, Faraz and Faizan, 2017; Sasse, Martinoia and Northen, 2018; Vranova *et al.*, 2013a). This may impact the reproducibility of results presented in this chapter and is something which should be examined in future work. Exudate composition can be determined through high-performance liquid chromatography (HPLC) (Giles *et al.*, 2017) or other forms of chromatography (Monchgesang *et al.*, 2016). The frameworks developed in this chapter could then be used to assess chemotaxis in response to different components of exudate. By examining exudate compositions under different conditions, and the resulting chemotaxis response from microbes, a better understanding of the plants ability to recruit different soil-borne microbial strains could be developed. The experimental framework presented in this chapter will therefore be extremely valuable for increasing the relevance of such studies to agricultural systems.

In this chapter, diffusion coefficients were derived based on continuous quantification of movement in a granular environment. This has rarely been achieved in the past and enables new insights to be gained into the activity of microbes and chemoattractants in the soil. Diffusivity of exudates in soil is highly variable (Darrah, 1991a) and the diffusion coefficient for exudates reported in this chapter (1.62e-1 mm^2 s^{-1}) is considerably higher than values reported in previous studies, such as Sung *et al.* (2006) who report 3.6e-5 mm^2 s^{-1}. In this chapter, movement of exudates was inferred based on the movement of fluorescent dyes in chemotaxis chambers so this may not have been an accurate model system for the movement of exudate in soil. In the past, the profile of exudates diffusing in soil has been examined through radioactive C imaging (Kuzyakov, Raskatov and Kaupenjohann, 2003; Sauer, Kuzyakov and Stahr, 2006). Transparent soil could provide another method for generating these profiles through the tagging of plant metabolites with fluorescent marker proteins and subsequent imaging of their movement once released into soil (Tanz *et al.*, 2013). The mean diffusion coefficient for bacterial density (1.64e-3 mm^2 s^{-1}) reported in this chapter was comparable to the bacterial diffusion coefficient reported for models of biofilm formation by El Moustaid *et al.* (2013) (1.2e-3 mm^2 s^{-1}). While Cremer *et al.* (2017) and Liu *et al.* (2019)

both report higher diffusion coefficients for bacteria in semi-solid agar, at 3e-3 mm^2 s^{-1} and 8.16 mm^2 s^{-1} respectively. Lower diffusion coefficients could be the result of the heterogenous medium, the bacterial strain, or bacterial affinity for soil particles, as observed in Chapter 4.

In this chapter, the heterogeneity of transparent soil introduced a high degree of variability into the data used to develop models. The study of bacterial processes in heterogenous environments is necessary for understanding soil processes, such as root colonisation. However, introducing such heterogeneity into experiments typically results in more diverse plant and bacterial activity, resulting in more diverse data. To compensate for heterogeneity in images, data was normalised. While normalisation allowed trends in bacterial populations to be assessed, it likely meant the loss of small-scale movements of bacteria as they interacted with soil particles. The fact that chemotaxis channels were imaged only in two dimensions, and at a relatively low magnification, also meant that the movement of individual bacterial cells could not be tracked. Nonetheless, models could predict overall trends of movements in bacterial populations, even in the highly heterogenous environment. Future work could explore bacterial chemotaxis over shorter time periods on a smaller scale through acquiring images of a smaller area at higher resolution and in three dimensions, similar to work carried out in other forms of transparent media (Massalha *et al.*, 2017; Bhattacharjee *et al.*, 2021). As discussed in Chapter 4, the addition of index matching fluid to chambers could have enabled higher quality imaging, although it may have influenced bacterial activity (Downie *et al.*, 2015). However, the methods used in this chapter represent a significant improvement on previous methods of quantifying chemotaxis, due to their similarity to natural soil conditions.

Modelling provides insights into the colonisation process

In this chapter, the diffusion and convection of bacterial density are modelled through a system of partial differential equations. The Keller-Segal model is commonly used to explain the behaviour of microbial populations in response to chemoattractants in liquid (Tindall *et al.*, 2008; Keller and Segel, 1971). Bhattacharjee et al. (2021) showed that it can also be applied to modelling chemotaxis in a heterogenous environment. This study quantified the movement of bacteria in a porous medium; however, this was not developed to have similar properties to soil. Elements of the Keller-Segal model have been incorporated into previous models of microbial processes in soil, such as root tip colonisation (Dupuy and Silk, 2016) and soil carbon dynamics (Hammoudi and Iosifescu, 2018). The work presented in this chapter represents a significant step forward for the quantification and modelling of chemotaxis in soil. Where

previous models have been largely based on parameters derived from the literature, the model presented above is fully calibrated based on experimental results.

The proliferation of bacteria was incorporated into models of chemotaxis through Monod-kinetics (Equation 5.11) (Monod, 1966). This enables prediction of changes in bacterial density based on the concentration of a substrate and is well suited to modelling bacterial processes in soil (Demoling, Figueroa and Baath, 2007; Haichar *et al.*, 2008). In soil, conversion of available carbon to microbial biomass is balanced by the loss of biomass through respiration and mortality (Chapman and Gray, 1986). In a natural environment, the increase in microbial biomass is often also balanced by an increase in predation, leading to 'cryptic growth' in which total increases in bacterial density does do match increases in rates of bacterial proliferation due to changes in mortality rates (Demoling, Figueroa and Baath, 2007; Rousk and Baath, 2011; Chapman and Gray, 1986). In equation 5.12, the increase in bacterial density was set to be related to a proportional decrease in substrate through the coupling parameter, Z (0.36). It is likely that Z accounted for some level of bacterial mortality, as well as the inefficiency of microbial populations at converting available carbon to biomass, and the inability of bacteria to metabolise certain compounds (Vallino, Hopkinson and Hobbie, 1996). Substrate-induced respiration can be used to quantify the efficiency of microbial populations at converting a substrate to biomass based on CO_2 production (Reischke, Rousk and Baath, 2014; Blagodatsky, Heinemeyer and Richter, 2000; Stenstrom, Stenberg and Johansson, 1998). Efficiency at converting carbon to biomass can range from 5 to 90 %, meaning an efficiency of 36 % is not unexpected (Vallino, Hopkinson and Hobbie, 1996). Including bacterial proliferation in models of chemotaxis enabled observations of bacterial activity made in Chapter 3 to be integrated with the quantification of bacterial movement made in this chapter.

For simulations of bacterial movement in the presence of exudate released from a growing root domain, a gradient of bacterial density was established along the root regions. Numerous studies which have reported low levels of colonisation at the root tip relative to more mature roots (Massalha *et al.*, 2017; Schmidt *et al.*, 2018; Humphris *et al.*, 2005). Such patterns in colonisation were not observed during live imaging in Chapter 4 of this thesis. Exclusion of microbes from attachment and the lack of available sites for colonisation may be responsible for disrupting such a pattern, leading to increased fluorescence in other areas. The framework presented in this chapter does not account for movement of bacteria along the root surface which may result from concentration gradients established by variable rhizodeposition.

Hypotaxis, the movement of microbial populations in response to a concentration gradient through directional growth on a surface, is also likely to play a role in determining colonisation patterns (Roy *et al.*, 2017). Such factors may need to be included in future models of bacterial chemotaxis to explain observed trends in colonisation.

Models of microbial movement and proliferation in this chapter predicted a zone of depleted bacterial diversity immediately surrounding the root. The establishment of a such a zone of depletion has been predicted by previous models of microbial movement in soil (Newman and Watson, 1977), and such a zone was evident during chemotaxis assays. In Chapter 4 of this thesis, no trend in fluorescence was detected in the medium immediately surrounding roots grown in transparent soil. Zones of depletion have also not been reported in studies comparing bacterial density in media or bulk soil relative to the rhizosphere (DeAngelis *et al.*, 2009; Massalha *et al.*, 2017). Massalha *et al.* (2017) report higher densities of *Bacillus subtilis* increasing with proximity to the root in a gel medium, with a proportional reduction in the density of *Escherichia coli* due to competition. In Chapter 3 of this thesis, a reduction of bacterial density in microcosms containing roots growing in liquid media was taken to indicate that a large proportion of the bacterial population had established itself in association with the root. It may be the case that this was the result of the static liquid environment. In bulk soil, aspects not considered by the model, such as water flow or microbial competition, may disrupt such patterns. More work to determine the bacterial density in transparent soil could provide evidence to support or contradict the presence of a depletion zone.

The two-dimensional model of the root developed in this chapter is relatively simple. It does not account for differences in exudation rate across either space or time, which are known to heavily impact microbial activity (Kuzyakov and Blagodatskaya 2015). Future development of the two-dimensional framework could incorporate factors such as the heterogenous distributions of bacteria within soil, zero-flux regions representing soil particles, flow rates of media within the soil, and variability in exudation rates.

Quantifying microbial movement in soil is necessary for understanding the root colonisation process

In Chapter 3, four key stages in the colonisation of roots were outlined; i) bacteria detect the presence of root exudates, begin to proliferate and move towards the root, ii) weak attachments are formed between bacteria and the root surface, establishing a large proportion of the bacterial

population in close association with the root, iii) strong attachments between bacteria and the root form, bacterial proliferation on the root surface begins, together this leads to an increase in colonisation rate, and iv) a carrying capacity is reached at which the rate of attachment and proliferation on the root surface are in equilibrium with death and disassociation of bacteria (Chapter 3, Figure 3.10). The frameworks for quantifying microbial colonisation, proliferation, and attachment presented in Chapters Three and Four of this thesis were not able to assess microbial movement in soil. The work presented in this chapter supports the stages of colonisation presented above. Importantly, the novel work presented in this chapter indicates that it is likely that a large proportion of bacterial density is established near the root within the first four hours of inoculation. In a natural environment, such a population would likely experience high levels of competition with other microorganisms and may act as an antagonist against plant pathogens.

Conclusion

The experimental framework developed in this chapter provides valuable insight into the behaviour of soil-borne microbes in the presence of a range of chemoattractants. It is the first model of chemotaxis in soil which is fully calibrated based on experimental data acquired in a granular environment. It also shows that classic models and approaches to understanding microbial movement can be applied to soil-borne microorganisms. Future work should aim to develop the modelling framework to fully predict the behaviour of microbes in heterogenous media in two and three-dimensions. The work presented in this chapter lays the groundwork for establishing a system by which microbial process in soil can be individually quantified and integrated into a more complete understanding of the process of rhizoplane colonisation. The challenge remains to establish the link between bacterial movement, quantified in this chapter, with proliferation and attachment to the rhizosphere quantified in Chapters Three and Four.

Chapter 6. Discussion: building a complete picture of root surface colonisation

The aim of this thesis was to develop a set of experimental and theoretical frameworks that can be used to isolate and quantify four microbial processes involved in root surface colonisation:

i) Bacterial growth in response to root derived nutrients.
ii) Bacterial chemotaxis in a heterogenous soil like environment in response to the presence of plant exudates.
iii) Bacterial attachment to the rhizoplane.
iv) Bacterial growth on the rhizoplane.

In Chapter 2, a model system of lettuce (*Lactuca sativa*) and *Pseudomonas fluorescens* isolate SBW25 was developed. In later chapters, frameworks were developed using this model system in order to achieve the four aims listed above. The work presented in this thesis allows unique insight into the process of root colonisation to be gained and modelled across both space and time. Taken together, the main findings (Table 6.1) can be used to propose overall trends in the dynamics of different stages of colonisation.

In Chapter 3, the growth of bacteria in plant root exudates and in the presence of plant roots were determined, achieving aim (i). Also in Chapter 3, rates of bacterial attachment and proliferation on the rhizoplane, and the relative contribution of each process to colonisation, were determined, achieving aims (ii) and (iii). Beyond the development of a framework capable of achieving these independent quantifications of attachment and proliferation, the main finding of this chapter was the determination of the timing of important stages during the early colonisation of lettuce roots by *Pseudomonas fluorescens*. Between hours 0 and 24 post inoculation, a dense bacterial population is established near the root (Figure 6.1, Panels i:iv).

Many of the main findings in Chapter 4 supported the observations of the timing of colonisation made in Chapter 3. Here, the increase in bacteria on the root surface was measured via their fluorescence in a live imaging system. This had the advantage that observations were made in a granular environment, but the disadvantage that colonisation and attachment could no longer be distinguished. In Chapter 4, it was found that little lag time was observed between inoculation and an increase in fluorescence when compared to the increase in bacterial attachment quantified in Chapter 3. This indicates that, while a certain period of priming is necessary prior to the formation of strong attachment and proliferation on the root surface, bacteria were capable of responding to the presence of the root at the time of inoculation.

The main findings in Chapter 5 were the quantification and modelling of bacterial movement in response to root exudates in a granular environment, achieving aim (iv). Here, a depletion in bacterial density in some areas of the soil as the result of bacterial movement towards rhizodepositions was observed within hours of inoculation (Figure 6.1, Panel iv). In Chapter 4, a build-up in bacteria on transparent soil particles near the root was observed. The affinity of bacteria for soil particles may impede continued bacterial movement through soil which may lead to lower levels of root colonisation in the soil relative to a liquid media environment. Proliferation, stimulated by rhizodepositions, further increases bacterial density near the root. At approximately 24 hours post inoculation, the rate of strong attachment to the root and bacterial proliferation on the root surface begin to increase, peaking at hour 38 (Figure 6.1, Panels vi:vii). From this point, the rate of colonisation begins to decline until a carrying capacity is reached at approximately hour 72 (Figure 6.1, Panel viii). Limitations of either nutrients or suitable colonisation sites are likely to lead to an equilibrium between colonisation and bacterial death on or disassociation from the root surface. As the root grows, new rhizodepositions are released and new potential colonisation sites are created (Figure 6.1, Panel ix).

Table 6.1. A summary of the main findings of this thesis broken down by chapter.

Chapter	Main findings
2. Model selection and characterisation	Development of a model plant and bacterial system suitable for imaging the colonisation process. Characterisation of bacterial growth in bacterial growth media.
3. Characterisation of colonisation and attachment rates	Independent characterisation of bacterial attachment and colonisation rates for the model system. Characterisation of bacterial growth in the presence of a root, in the absence of a root, and in the presence of root exudates. Estimation of the timing of key events in colonisation (Figure 3.10)
4. Live quantification of bacterial colonisation	Verification of the timing of colonisation proposed in Chapter 3 in a granular environment. Observation of a zone of depletion surrounding the root. Observation of an increase in colonisation density on particles surrounding the root. Determination of root growth rate in a granular environment.
5. A dynamic model of bacterial movement and root colonisation	Quantification of bacterial movement in a granular environment based on live imaging.

Development of a model for bacterial chemotaxis in response to root exudate which incorporates bacterial growth based on experimental observations.

Development of a theoretical predictive model for bacterial chemotaxis in response to root exudate produced from a growing root, based on experimentally derived parameters.

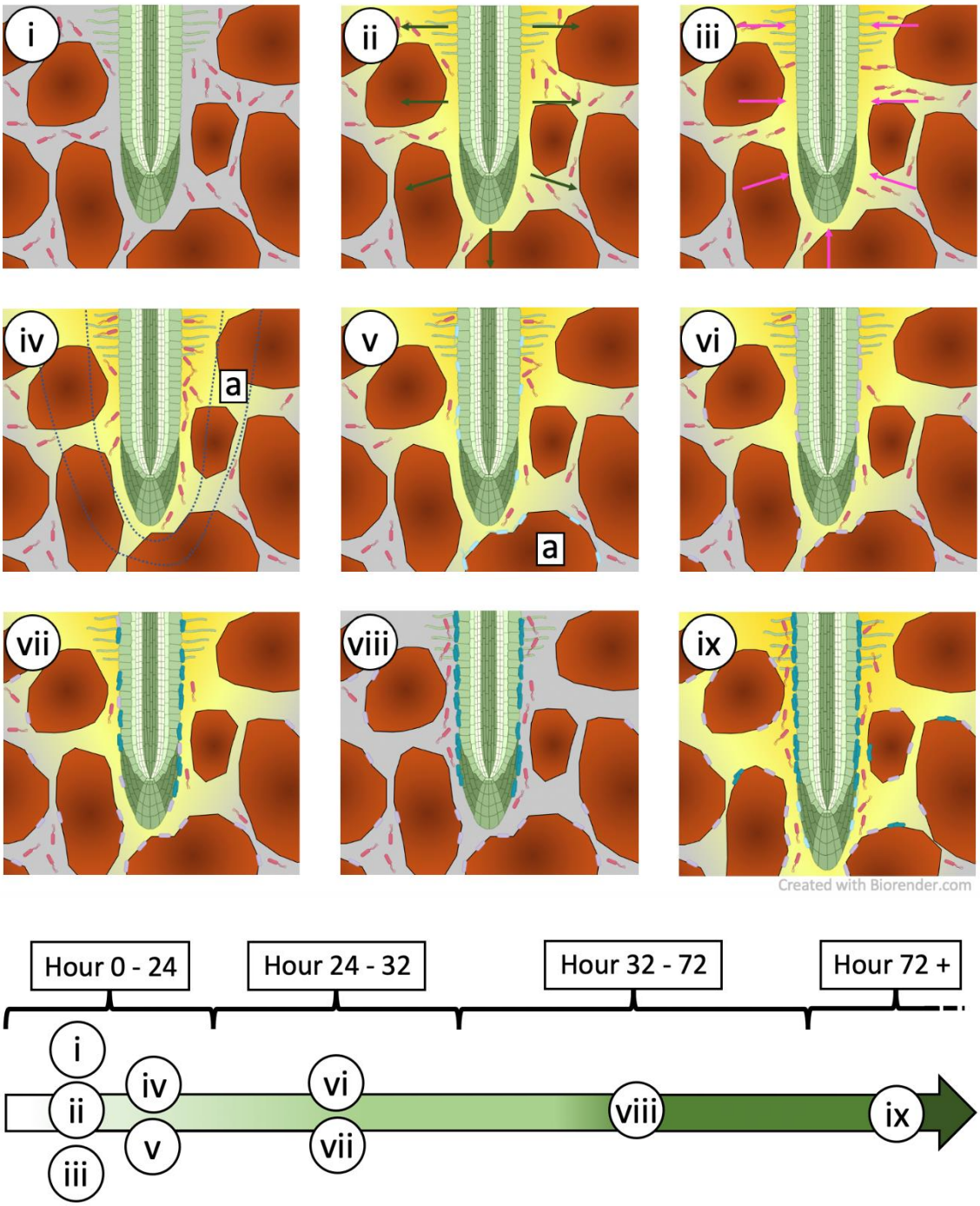

Figure 6.1. Proposed stages and timing for bacterial colonisation of the rhizoplane by *Pseudomonas fluorescens* SBW25. i) Within hours of a growing root encountering a population of bacteria, ii) rhizodeposition (black arrows) establishes a concentration gradient of chemoattractants in the soil (yellow region), or growth medium; soil conditions influence the distance that chemoattractants can travel, while the heterogeneity of the soil environment leads to an uneven spread of exudates. iii) Unattached bacteria in the media around the root (pink) respond to this concentration gradient by moving towards the root (pink arrows). iv)

Within the first 24 hours of the colonisation process, this leads to the establishment of a dense population of bacteria surrounding the root. iv.a) Bacterial movement may lead to a depletion zone around the root (marked by the blue dashed line). v) At a not yet determined time within the first 24 hours, weak attachment of bacteria to the roots surface begins (light blue bacteria). v.a) Bacterial affinity for soil particles also leads to a build-up in bacterial density on particles. vi) At approximately 24 hours, the rate of strong attachment to the root surface begins to increase (purple bacteria). vii) Bacterial proliferation on the root surface also leads to an increase in root colonisation density (dark blue bacteria). viii) From approximately hour 32 to hour 72, rates of attachment and proliferation on the rhizoplane begin to slow. Due to limited resources, either in the form of plant derived nutrients or available colonisation sites, a carrying capacity for the root surface is reached at approximately hour 72. At this point, recruitment and proliferation on the rhizoplane are in equilibrium with death and disassociation of bacteria. ix) Root growth and rhizodeposition continues. As the root moves through soil, it encounters new bacteria and new areas suitable for colonisation are generated.

Applications of the frameworks developed in this thesis

The frameworks developed in this thesis have been used to derive key parameters for plant and bacterial activity relating to colonisation, such as attachment and proliferation rates. Already, these have been used to develop a model of bacterial chemotaxis in soil based on experimental observations, which hasn't previously been achieved. Moving forward, such quantifications could also prove valuable for populating theoretical models of microbial processes, such as that described by Dupuy and Silk (2016). Certain key parameters relating to the activity of *Pseudomonas fluorescens* SBW25, such as the diffusivity in transparent soil reported in Chapter 5, or the growth parameters in different conditions reported in Chapters 3, could immediately be used in other models, as has been shown by the development of a theoretical model for the movement of bacteria towards a moving root in Chapter 5 using growth parameters from Chapter 3. The availability of such key parameter values relating to plant and bacterial activities below the soil has been limited in the past meaning the work presented in this thesis offers a valuable data source for the development of future models. Beyond the data generated in this thesis, the experimental frameworks developed are largely novel and present

researchers with reproducible methods by which these parameters can be quantified for other systems of model organisms.

While colonisation of the rhizosphere is a necessary component for the action of many plant beneficial microbial strains, the level to which attachment to the root surface is necessary is unknown (Chin-A-Woeng *et al.*, 2000; Kamilova *et al.*, 2005). In Chapter 3, a framework for the independent quantification of bacterial attachment to and proliferation on the rhizoplane was developed. Based on this work, the proportion of bacterial populations which are at varying stages of attachment or association with the root surface can now be established. The work presented in Chapter 3 has shown that both processes make a substantial contribution to the rate of colonisation, and therefore recruitment from the surrounding media remains important for the entirety of the colonisation process. This means that, during inoculation of plants with beneficial microorganisms, a key focus should be to maintain high levels of inoculant in soil to enable recruitment.

Future directions

Developing a more complete model of bacterial colonisation of the rhizoplane

Future development should build on the foundation of the frameworks developed in this thesis to isolate, quantify, and understand more rhizosphere processes, such as bacterial colonisation of soil particles. The next step should be to integrate data, generated in isolation by each framework, into a cohesive model of root colonisation. A fully integrated model of root surface colonisation, which is based on a foundation of experimental data, could be used to describe patterns of colonisation observed in soil. This would be useful for understanding the factors which influence the colonisation of plant roots by beneficial plant associated microorganisms as well as pathogens. The two-dimensional model of bacterial movement in response to root exudate, developed in Chapter 5, took a step towards this, by integrating parameters derived from separate experiments. This simple simulation could be built upon to develop a more complete spatial and temporal model of colonisation on the root surface in two or three-dimensions. By integrating a root area or volume which produces exudate at varying rates in both space and time, and which bacteria cannot enter, spatial patterns of bacterial distribution around the root could be predicted. By incorporating models of attachment and proliferation on the root surface, developed in Chapter 3, predictions of patterns in the spatial organisation and timing of root surface colonisation could be made. A heterogenous soil environment could be incorporated into models based on regions which neither microbes nor exudate can pass

through. Based on imaging of roots grown in transparent soil, initial conditions for these models could be imported which mimic the position of real roots and soil particles.

Studying colonisation at the individual level

In Chapter 4, the distribution of bacteria on the root was quantified through live imaging of roots grown in transparent soil. No significant difference between bacterial densities in different root regions was detected. Distribution of colonisation density on the root surface is unlikely to be the result of chemotaxis and bacterial movement alone. The structure of the root likely makes some areas more favourable to colonisation than others (Schmidt *et al.*, 2018; Noirot-Gros *et al.*, 2018). This thesis aimed to study bacterial distributions at a population level, rather than at this spatial scale, but the framework could certainly be expanded to do this. Higher magnification imaging of root surface colonisation for a subsection of the root could be integrated into the framework for the study of root surface colonisation developed in Chapter 4. This could provide insight into the factors which determine the localisation of attachment on the roots surface. By integrating available space for colonisation into models of attachment or bacterial movement, spatial distributions of colonisation could be more easily described and understood. At this level of magnification, tracking of individual bacterial cells on the root surface may be possible (Duvernoy *et al.*, 2018) which could help to provide information on how bacterial migration on the root surface contributes to establishing colonisation patterns.

Applying the frameworks developed in this thesis

Competition between microbes is also known to heavily influence colonisation (Haas and Keel, 2003; Lugtenberg and Kamilova, 2009). The frameworks presented in each chapter of this thesis could be expanded to include multiple strains of competing or cooperating microbes. In doing so, the influence of competition on the timing and distributions of colonisation, as well as the development of niche exclusion in microbial communities could be examined. For example, the influence of pathogen supressing strains, such as *Pseudomonas fluorescens,* on root colonisation by a pathogen such as *Fusarium culmorumi* could be investigated.

The framework for quantifying and modelling bacterial chemotaxis developed in Chapter 5 could be expanded to incorporate a variety of chemoattractants, or even a growing root. Based on the imaging settings optimised for detecting the movement of bacterial populations in chemotaxis chambers, the movement of bacteria in transparent soil mesocosms, as described in Chapter 4, could be quantified. Massalha *et al*. (2017) carried out such a quantification based on live imaging of *Bacillus subtilis* near *Arabidopsis thaliana* roots grow in a transparent gel

medium. By describing changes in bacterial density with distance from the root surface, diffusion, and chemotaxis of microbes in a two or three-dimensional soil environment could be quantified and modelled. This would provide an experimentally verifiable model for bacterial movement in soil which goes beyond any currently available.

Conclusion

Realising the full potential of beneficial microbial strains in agricultural systems will require a detailed quantitative understanding of the root colonisation process, which has not previously been available. Quantifying and modelling root surface colonisation is therefore a key step for understanding the dynamic interactions which determine the structure of the plant microbiome. Modelling microbial interactions with plants is complex, with numerous factors to be considered, and a solid foundation of experimental data is needed. The work presented in this thesis has shown that isolating and quantifying different aspects of colonisation can allow the timing and importance of factors such as microbial movement, attachment, and proliferation to be determined. Each of the frameworks developed in this thesis offers unique insight into the process of root surface colonisation and makes a substantial contribution to our knowledge of plant bacterial interactions. The work presented has led to new insights into interactions between *Pseudomonas fluorescens* isolate SBW25 and lettuce that can be applied to a vast range of plant-microbe interactions and thus beyond the study of this model system, it has highlighted the need for a holistic understanding of microbial interactions with plant roots. Ultimately, improvements to our understanding of root colonisation could allow for the targeted manipulation of the plant microbiome to maintain plant growth promoting strains or deter pathogens. Although further work will be needed, the frameworks developed in this thesis will allow the competence of rhizosphere strains at colonising the root surface to be assessed in greater detail. This will allow for the testing and selection of strains for characteristics such as high attachment rates or rapid movement in response to root exudates, which will ensure their maintenance in crop systems.

References

Addo-Danso, S., Prescott, C. and Smith, A. (2016) 'Methods for estimating root biomass and production in forest and woodland ecosystem carbon studies: A review', Forest Ecology and Management, 359, pp. 332-351.

Adler, J. (1973) 'A method for measuring chemotaxis and use of the method to determine optimum conditions for chemotaxis by Escherichia coli', Microbiology, 74(1), pp. 77-91.

Aguilar, M., Aguilar, F. and Negreiros, J. (2009) 'Off-the-shelf laser scanning and close-range digital photogrammetry for measuring agricultural soils microrelief', Biosystems Engineering, 103(4), pp. 504-517.

Albareda, M., Dardanelli, M., Sousa, C., Megias, M., Temprano, F. and Rodriguez-Navarro, D. (2006) 'Factors affecting the attachment of rhizospheric bacteria to bean and soybean roots', Fems Microbiology Letters, 259(1), pp. 67-73.

Alexander, F. and Jackson, R. (1954) 'Examination of soil micro-organisms in their natural environment', Nature, 174(4433), pp. 750-751.

Alexandre, G. (2015) 'Chemotaxis Control of Transient Cell Aggregation', Journal of Bacteriology, 197(20), pp. 3230-3237.

Allard-Massicotte, R., Tessier, L., Lecuyer, F., Lakshmanan, V., Lucier, J., Garneau, D., Caudwell, L., Vlamakis, H., Bais, H. and Beauregard, P. (2016) 'Bacillus subtilis Early Colonization of Arabidopsis thaliana Roots Involves Multiple Chemotaxis Receptors', Mbio, 7(6).

Ardre, M., Dufour, D. and Rainey, P. (2019) 'Causes and Biophysical Consequences of Cellulose Production by Pseudomonas fluorescens SBW25 at the Air-Liquid Interface', Journal of Bacteriology, 201(18).

Arnold, D. and Preston, G. (2019) 'Pseudomonas syringae: enterprising epiphyte and stealthy parasite', Microbiology-Sgm, 165(3), pp. 251-253.

Ascough, G. and Fennell, C. (2004) 'The regulation of plant growth and development in liquid culture', South African Journal of Botany, 70(2), pp. 181-190.

Atkinson, J., Pound, M., Bennett, M. and Wells, D. (2019) 'Uncovering the hidden half of plants using new advances in root phenotyping', Current Opinion in Biotechnology, 55, pp. 1-8.

Audenaert, K., Pattery, T., Cornelis, P. and Hofte, M. (2002) 'Induction of systemic resistance to Botrytis cinerea in tomato by Pseudomonas aeruginosa 7NSK2: Role of salicylic acid, pyochelin, and pyocyanin', Molecular Plant-Microbe Interactions, 15(11), pp. 1147-1156.

Bach, E., dos Santos Seger, G. D., de Carvalho Fernandes, G., Lisboa, B. B. and Passaglia, L. M. P. (2016) 'Evaluation of biological control and rhizosphere competence of plant growth promoting bacteria', Applied soil ecology, 99, pp. 141-149.

Bach, E., Williams, R., Hargreaves, S., Yang, F. and Hofmockel, K. (2018) 'Greatest soil microbial diversity found in micro-habitats', Soil Biology & Biochemistry, 118, pp. 217-226.

Badri, D., Chaparro, J., Zhang, R., Shen, Q. and Vivanco, J. (2013) 'Application of Natural Blends of Phytochemicals Derived from the Root Exudates of Arabidopsis to the Soil Reveal That Phenolic-related Compounds Predominantly Modulate the Soil Microbiome', Journal of Biological Chemistry, 288(7), pp. 4502-4512.

Badri, D. and Vivanco, J. (2009) 'Regulation and function of root exudates', Plant Cell and Environment, 32(6), pp. 666-681.

Bais, H. P., Fall, R. and Vivanco, J. M. (2004) 'Biocontrol of Bacillus subtilis against infection of Arabidopsis roots by Pseudomonas syringae is facilitated by biofilm formation and surfactin production', Plant Physiology, 134(1), pp. 307-319.

Bakken, L. R. (1997) 'Culturable and nonculturable bacteria in soil', Modern soil microbiology., pp. 47-61.

Bakker, P., Pieterse, C. and van Loon, L. (2007) 'Induced systemic resistance by fluorescent Pseudomonas spp.', Phytopathology, 97(2), pp. 239-243.

Bantinaki, E., Kassen, R., Knight, C., Robinson, Z., Spiers, A. and Rainey, P. (2007) 'Adaptive divergence in experimental populations of Pseudomonas fluorescens. III. mutational origins of wrinkly spreader diversity', Genetics, 176(1), pp. 441-453.

Barahona, E., Navazo, A., Yousef-Coronado, F., Aguirre de Cárcer, D., Martínez-Granero, F., Espinosa-Urgel, M., Martín, M. and Rivilla, R. (2010) 'Efficient rhizosphere colonization by Pseudomonas fluorescens f113 mutants unable to form biofilms on abiotic surfaces', Environmental microbiology, 12(12), pp. 3185-3195.

Baranyi, J. and Roberts, T. A. (1994) 'A dynamic approach to predicting bacterial growth in food', International journal of food microbiology, 23(3-4), pp. 277-294.

Barbier, M. and Damron, F. (2016) 'Rainbow Vectors for Broad-Range Bacterial Fluorescence Labeling', Plos One, 11(3).

Bashan, Y. (1986) 'Migration of the rhizosphere bacteria Azospirillum brusilense and Pseudomonas fluorescens towards wheat roots in the soil', Microbiology, 132(12), pp. 3407-3414.

Bashan, Y., de-Bashan, L., Prabhu, S. and Hernandez, J. (2014) 'Advances in plant growth-promoting bacterial inoculant technology: formulations and practical perspectives (1998-2013)', Plant and Soil, 378(1-2), pp. 1-33.

Baveye, P., Otten, W., Kravchenko, A., Balseiro-Romero, M., Beckers, E., Chalhoub, M., Darnault, C., Eickhorst, T., Garnier, P., Hapca, S., Kiranyaz, S., Monga, O., Mueller, C., Nunan, N., Pot, V., Schluter, S., Schmidt, H. and Vogel, H. (2018) 'Emergent Properties of Microbial Activity in Heterogeneous Soil Microenvironments: Different Research Approaches Are Slowly Converging, Yet Major Challenges Remain', Frontiers in Microbiology, 9.

Beauchamp, C. (1993) 'Mode of action of plant growth promoting rhizobacteria and their potential use as biological-control agents', Phytoprotection, 74(1), pp. 19-27.

Beck, M., Wyrsch, I., Strutt, J., Wimalasekera, R., Webb, A., Boller, T. and Robatzek, S. (2014) 'Expression patterns of FLAGELLIN SENSING 2 map to bacterial entry sites in plant shoots and roots', Journal of Experimental Botany, 65(22), pp. 6487-6498.

Bengough, A., McKenzie, B., Hallett, P. and Valentine, T. (2011) 'Root elongation, water stress, and mechanical impedance: a review of limiting stresses and beneficial root tip traits', Journal of Experimental Botany, 62(1), pp. 59-68.

Berendsen, R., Pieterse, C. and Bakker, P. (2012) 'The rhizosphere microbiome and plant health', Trends in Plant Science, 17(8), pp. 478-486.

Berg, G. and Smalla, K. (2009) 'Plant species and soil type cooperatively shape the structure and function of microbial communities in the rhizosphere', Fems Microbiology Ecology, 68(1), pp. 1-13.

Berggren, I., Alström, S., Van Vuurde, J. and Mårtensson, A. M. (2005) 'Rhizoplane colonisation of peas by Rhizobium leguminosarum bv. viceae and a deleterious Pseudomonas putida', FEMS microbiology ecology, 52(1), pp. 71-78.

Berne, C., Ducret, A., Hardy, G. and Brun, Y. (2015) 'Adhesins Involved in Attachment to Abiotic Surfaces by Gram-Negative Bacteria', Microbiology Spectrum, 3(4).

Berthet, B. and Maizel, A. (2016) 'Light sheet microscopy and live imaging of plants', Journal of Microscopy, 263(2), pp. 158-164.

Besset-Manzoni, Y., Rieusset, L., Joly, P., Comte, G. and Prigent-Combaret, C. (2018) 'Exploiting rhizosphere microbial cooperation for developing sustainable agriculture strategies', Environmental Science and Pollution Research, 25(30), pp. 29953-29970.

Bhattacharjee, T., Amchin, D. B., Ott, J. A., Kratz, F. and Datta, S. S. (2021) 'Chemotactic Migration of Bacteria in Porous Media', Biophysical Journal.

Bingham, I. and Bengough, A. (2003) 'Morphological plasticity of wheat and barley roots in response to spatial variation in soil strength', Plant and Soil, 250(2), pp. 273-282.

Blagodatsky, S., Heinemeyer, O. and Richter, J. (2000) 'Estimating the active and total soil microbial biomass by kinetic respiration analysis', Biology and Fertility of Soils, 32(1), pp. 73-81.

Blossfeld, S., Gansert, D., Thiele, B., Kuhn, A. and Losch, R. (2011) 'The dynamics of oxygen concentration, pH value, and organic acids in the rhizosphere of Juncus spp.', Soil Biology & Biochemistry, 43(6), pp. 1186-1197.

Bodner, G., Leitner, D. and Kaul, H.-P. (2014) 'Coarse and fine root plants affect pore size distributions differently', Plant and soil, 380(1), pp. 133-151.

Bogino, P., Abod, A., Nievas, F. and Giordano, W. (2013) 'Water-Limiting Conditions Alter the Structure and Biofilm-Forming Ability of Bacterial Multispecies Communities in the Alfalfa Rhizosphere', Plos One, 8(11).

Boller, T. and Felix, G. (2009) 'A Renaissance of Elicitors: Perception of Microbe-Associated Molecular Patterns and Danger Signals by Pattern-Recognition Receptors', Annual Review of Plant Biology, 60, pp. 379-406.

Box, J. and Ramseur, E. (1993) 'Minirhizotron wheat root data - comparisons to soil core root data', Agronomy Journal, 85(5), pp. 1058-1060.

Brumley, D., Carrara, F., Hein, A., Yawata, Y., Levin, S. and Stocker, R. (2019) 'Bacteria push the limits of chemotactic precision to navigate dynamic chemical gradients', Proceedings of the National Academy of Sciences of the United States of America, 116(22), pp. 10792-10797.

Brunner, I., Herzog, C., Dawes, M., Arend, M. and Sperisen, C. (2015) 'How tree roots respond to drought', Frontiers in Plant Science, 6.

Brzostek, E., Greco, A., Drake, J. and Finzi, A. (2013) 'Root carbon inputs to the rhizosphere stimulate extracellular enzyme activity and increase nitrogen availability in temperate forest soils', Biogeochemistry, 115(1-3), pp. 65-76.

Bulgarelli, D., Garrido-Oter, R., Munch, P., Weiman, A., Droge, J., Pan, Y., McHardy, A. and Schulze-Lefert, P. (2015) 'Structure and Function of the Bacterial Root Microbiota in Wild and Domesticated Barley', Cell Host & Microbe, 17(3), pp. 392-403.

Busby, P., Soman, C., Wagner, M., Friesen, M., Kremer, J., Bennett, A., Morsy, M., Eisen, J., Leach, J. and Dangl, J. (2017) 'Research priorities for harnessing plant microbiomes in sustainable agriculture', Plos Biology, 15(3).

Carbone, D., Gargano, I., Pinto, G., De Natale, A. and Pollio, A. (2017) 'Evaluating microalgae attachment to surfaces: a first approach towards a laboratory integrated assessment', Chemical Engineering Transactions, 57, pp. 73-78.

Carroll, D., Holden, N., Gifford, M. and Dupuy, L. (2020) 'Framework for Quantification of the Dynamics of Root Colonization byPseudomonas fluorescensIsolate SBW25', Frontiers in Microbiology, 11.

Carter, M. R. and Gregorich, E. G. (2007) Soil sampling and methods of analysis. CRC press.

Castaneda-Ojeda, M., Moreno-Perez, A., Ramos, C. and Lopez-Solanilla, E. (2017) 'Suppression of Plant Immune Responses by the Pseudomonas savastanoi pv. savastanoi NCPPB 3335 Type III Effector Tyrosine Phosphatases HopAO1 and HopAO2', Frontiers in Plant Science, 8.

Chapman, S. and Gray, T. (1986) 'Importance of cryptic growth, tield factors and maintinence energy in models of microbial growth in soil', Soil Biology & Biochemistry, 18(1), pp. 1-4.

Chaudhary, D., Khulan, A. and Kim, J. (2019) 'Development of a novel cultivation technique for uncultured soil bacteria', Scientific Reports, 9.

Chin-A-Woeng, T., Bloemberg, G., Mulders, I., Dekkers, L. and Lugtenberg, B. (2000) 'Root colonization by phenazine-1-carboxamide-producing bacterium Pseudomonas chlororaphis PCL1391 is essential for biocontrol of tomato foot and root rot', Molecular Plant-Microbe Interactions, 13(12), pp. 1340-1345.

Chuberre, C., Plancot, B., Driouich, A., Moore, J., Bardor, M., Gugi, B. and Vicre, M. (2018) 'Plant Immunity Is Compartmentalized and Specialized in Roots', Frontiers in Plant Science, 9.

Cipriano, M. A., Lupatini, M., Lopes-Santos, L., da Silva, M. J., Roesch, L. F., Destéfano, S. A., Freitas, S. S. and Kuramae, E. E. (2016) 'Lettuce and rhizosphere microbiome responses to growth promoting Pseudomonas species under field conditions', FEMS microbiology ecology, 92(12).

Claesson, M., Wang, Q., O'Sullivan, O., Greene-Diniz, R., Cole, J., Ross, R. and O'Toole, P. (2010) 'Comparison of two next-generation sequencing technologies for resolving highly complex microbiota composition using tandem variable 16S rRNA gene regions', Nucleic Acids Research, 38(22).

Cooper, L., Daly, K., Hallett, P., Koebernick, N., George, T. and Roose, T. (2018) 'The effect of root exudates on rhizosphere water dynamics', Proceedings of the Royal Society a-Mathematical Physical and Engineering Sciences, 474(2217).

Costa, E., Perez, J. and Kreft, J. (2006) 'Why is metabolic labour divided in nitrification?', Trends in Microbiology, 14(5), pp. 213-219.

Cremer, J., Arnoldini, M. and Hwa, T. (2017) 'Effect of water flow and chemical environment on microbiota growth and composition in the human colon', Proceedings of the National Academy of Sciences, 114(25), pp. 6438-6443.

Crespo, M. and Valverde, C. (2009) 'A Single Mutation in the oprF mRNA Leader Confers Strict Translational Control by the Gac/Rsm System in Pseudomonas fluorescens CHA0', Current Microbiology, 58(2), pp. 182-188.

Dakora, F. and Phillips, D. (2002) 'Root exudates as mediators of mineral acquisition in low-nutrient environments', Plant and Soil, 245(1), pp. 35-47.

Darrah, P. (1991a) 'Measuring the diffusion-coefficient of rhizosphere exudates in soil .1. the diffusion of non-sorbing compounds', Journal of Soil Science, 42(3), pp. 413-420.

Darrah, P. (1991b) 'Models of the rhizosphere .1. microbial-population dynamics around a root releasing soluble and insoluble carbon', Plant and Soil, 133(2), pp. 187-199.

Darrah, P. (1991c) 'Models of the rhizosphere .2. a quasi 3-dimensional simulation of the microbial-population dynamics around a growing root releasing soluble exudates', Plant and Soil, 138(2), pp. 147-158.

de Boer, W., Wagenaar, A., Gunnewiek, P. and van Veen, J. (2007) 'In vitro suppression of fungi caused by combinations of apparently non-antagonistic soil bacteria', Fems Microbiology Ecology, 59(1), pp. 177-185.

de Faria, M., Costa, L., Chiaramonte, J., Bettiol, W. and Mendes, R. (2021) 'The rhizosphere microbiome: functions, dynamics, and role in plant protection', Tropical Plant Pathology, 46(1), pp. 13-25.

de Jong, H., Casagranda, S., Giordano, N., Cinquemani, E., Ropers, D., Geiselmann, J. and Gouze, J. (2017) 'Mathematical modelling of microbes: metabolism, gene expression and growth', Journal of the Royal Society Interface, 14(136).

De Mot, R. and Vanderleyden, J. (1991) 'Purification of a root-adhesive outer membrane protein of root-colonizing Pseudomonas fluorescens', FEMS microbiology letters, 81(3), pp. 323-327.

de Weert, S., Vermeiren, H., Mulders, I. H. M., Kuiper, I., Hendrickx, N., Bloemberg, G. V., Vanderleyden, J., De Mot, R. and Lugtenberg, B. J. J. (2002) 'Flagella-driven chemotaxis towards exudate components is an important trait for tomato root colonization by Pseudomonas fluorescens', Molecular Plant-Microbe Interactions, 15(11), pp. 1173-1180.

De Wolf, E. and Isard, S. (2007) 'Disease cycle approach to plant disease prediction', Annual Review of Phytopathology, 45, pp. 203-220.

DeAngelis, K., Brodie, E., DeSantis, T., Andersen, G., Lindow, S. and Firestone, M. (2009) 'Selective progressive response of soil microbial community to wild oat roots', Isme Journal, 3(2), pp. 168-178.

Dechesne, A., Pallud, C., Debouzie, D., Flandrois, J., Vogel, T., Gaudet, J. and Grundmann, G. (2003) 'A novel method for characterizing the microscale 3D spatial distribution of bacteria in soil', Soil Biology & Biochemistry, 35(12), pp. 1537-1546.

Demoling, F., Figueroa, D. and Baath, E. (2007) 'Comparison of factors limiting bacterial growth in different soils', Soil Biology & Biochemistry, 39(10), pp. 2485-2495.

Dennis, P. G., Miller, A. J. and Hirsch, P. R. (2010) 'Are root exudates more important than other sources of rhizodeposits in structuring rhizosphere bacterial communities?', FEMS microbiology ecology, 72(3), pp. 313-327.

Dietrich, L., Okegbe, C., Price-Whelan, A., Sakhtah, H., Hunter, R. and Newman, D. (2013) 'Bacterial Community Morphogenesis Is Intimately Linked to the Intracellular Redox State', Journal of Bacteriology, 195(7), pp. 1371-1380.

Doan, T., Doan, T., Kangas, M., Ernest, A., Tran, D., Wilson, C., Holmes, A., Doyle, E. and Brooks, T. (2017) 'A Low-Cost Imaging Method for the Temporal and Spatial Colorimetric Detection of Free Amines on Maize Root Surfaces', Frontiers in Plant Science, 8.

Downie, H., Holden, N., Otten, W., Spiers, A. J., Valentine, T. A. and Dupuy, L. X. (2012) 'Transparent Soil for Imaging the Rhizosphere', Plos One, 7(9), pp. 6.

Downie, H. F., Adu, M., Schmidt, S., Otten, W., Dupuy, L. X., White, P. and Valentine, T. A. (2015) 'Challenges and opportunities for quantifying roots and rhizosphere interactions through imaging and image analysis', Plant, cell & environment, 38(7), pp. 1213-1232.

Dupuy, L., Gregory, P. and Bengough, A. (2010) 'Root growth models: towards a new generation of continuous approaches', Journal of Experimental Botany, 61(8), pp. 2131-2143.

Dupuy, L. X. and Silk, W. K. (2016) 'Mechanisms of Early Microbial Establishment on Growing Root Surfaces', Vadose Zone Journal, 15(2), pp. 13.

Duvernoy, M., Mora, T., Ardre, M., Croquette, V., Bensimon, D., Quilliet, C., Ghigo, J., Balland, M., Beloin, C., Lecuyer, S. and Desprat, N. (2018) 'Asymmetric adhesion of rod-shaped bacteria controls microcolony morphogenesis', Nature Communications, 9.

Earl, A., Losick, R. and Kolter, R. (2008) 'Ecology and genomics of Bacillus subtilis', Trends in Microbiology, 16(6), pp. 269-275.

Egamberdiyeva, D. (2007) 'The effect of plant growth promoting bacteria on growth and nutrient uptake of maize in two different soils', Applied Soil Ecology, 36(2-3), pp. 184-189.

Ehlers, K. and Oster, G. (2012) 'On the Mysterious Propulsion of Synechococcus', Plos One, 7(5).

El Moustaid, F., Eladdadi, A. and Uys, L. (2013) 'Modeling bacterial attachment to surfaces as an early stage of biofilm development', Mathematical Biosciences & Engineering, 10(3), pp. 821.

Fakih, M., Delenne, J., Radjai, F. and Fourcaud, T. (2019) 'Root growth and force chains in a granular soil', Physical Review E, 99(4).

Feng, H., Zhang, N., Du, W., Zhang, H., Liu, Y., Fu, R., Shao, J., Zhang, G., Shen, Q. and Zhang, R. (2018) 'Identification of Chemotaxis Compounds in Root Exudates and Their Sensing Chemoreceptors in Plant-Growth-Promoting Rhizobacteria Bacillus amyloliquefaciens SQR9', Molecular Plant-Microbe Interactions, 31(10), pp. 995-1005.

Feng, H., Zhang, N., Fu, R., Liu, Y., Krell, T., Du, W., Shao, J., Shen, Q. and Zhang, R. (2019) 'Recognition of dominant attractants by key chemoreceptors mediates recruitment of plant growth-promoting rhizobacteria', Environmental microbiology, 21(1), pp. 402-415.

Feyen, J., Jacques, D., Timmerman, A. and Vanderborght, J. (1998) 'Modelling water flow and solute transport in heterogeneous soils: A review of recent approaches', Journal of Agricultural Engineering Research, 70(3), pp. 231-256.

Fuchslueger, L., Bahn, M., Fritz, K., Hasibeder, R. and Richter, A. (2014) 'Experimental drought reduces the transfer of recently fixed plant carbon to soil microbes and alters the bacterial community composition in a mountain meadow', New Phytologist, 201(3), pp. 916-927.

Fukuda, R., Ogawa, H., Nagata, T. and Koike, I. (1998) 'Direct determination of carbon and nitrogen contents of natural bacterial assemblages in marine environments', Applied and Environmental Microbiology, 64(9), pp. 3352-3358.

Gage, D. (2004) 'Infection and invasion of roots by symbiotic, nitrogen-fixing rhizobia during nodulation of temperate legumes', Microbiology and Molecular Biology Reviews, 68(2), pp. 280-+.

Gamalero, E., Lingua, G., Berta, G. and Lemanceau, P. (2003) 'Methods for studying root colonization by introduced beneficial bacteria', Agronomie, 23(5-6), pp. 407-418.

Gamalero, E., Lingua, G., Capri, F. G., Fusconi, A., Berta, G. and Lemanceau, P. (2004a) 'Colonization pattern of primary tomato roots by Pseudomonas fluorescens A6RI characterized by dilution plating, flow cytometry, fluorescence, confocal and scanning electron microscopy', Fems Microbiology Ecology, 48(1), pp. 79-87.

Gamalero, E., Trotta, A., Massa, N., Copetta, A., Martinotti, M. and Berta, G. (2004b) 'Impact of two fluorescent pseudomonads and an arbuscular mycorrhizal fungus on tomato plant growth, root architecture and P acquisition', Mycorrhiza, 14(3), pp. 185-192.

Gamez, R., Cardinale, M., Montes, M., Ramirez, S., Schnell, S. and Rodriguez, F. (2019) 'Screening, plant growth promotion and root colonization pattern of two rhizobacteria (Pseudomonas fluorescens Ps006 and Bacillus amyloliquefaciens Bs006) on banana cv. Williams (Musa acuminata Colla)', Microbiological Research, 220, pp. 12-20.

Gao, F. and Han, L. (2012) 'Implementing the Nelder-Mead simplex algorithm with adaptive parameters', Computational Optimization and Applications, 51(1), pp. 259-277.

Gargallo-Garriga, A., Preece, C., Sardans, J., Oravec, M., Urban, O. and Penuelas, J. (2018) 'Root exudate metabolomes change under drought and show limited capacity for recovery', Scientific Reports, 8.

Gašparíková, O., Mistrík, I. and Čiamporová, M. 2002. Waisel, Y., Eshel, A., Kafkafi, U., eds. Plant roots–the hidden half. Oxford University Press.

George, T. S., Richardson, A. E., Hadobas, P. A. and Simpson, R. J. (2004) 'Characterization of transgenic Trifolium subterraneum L. which expresses phyA and releases extracellular phytase: growth and P nutrition in laboratory media and soil', Plant Cell and Environment, 27(11), pp. 1351-1361.

Gerwitz, A. and Page, E. (1974) 'An empirical mathematical model to describe plant root systems', Journal of Applied Ecology, pp. 773-781.

Gibson, A. M., Bratchell, N. and Roberts, T. (1988) 'Predicting microbial growth: growth responses of salmonellae in a laboratory medium as affected by pH, sodium chloride and storage temperature', International journal of food microbiology, 6(2), pp. 155-178.

Giles, C. D., George, T. S., Brown, L. K., Mezeli, M. M., Richardson, A. E., Shand, C. A., Wendler, R., Darch, T., Menezes-Blackburn, D. and Cooper, P. (2017) 'Does the combination of citrate and phytase exudation in Nicotiana tabacum promote the acquisition of endogenous soil organic phosphorus?', Plant and Soil, 412(1-2), pp. 43-59.

Gobran, G., Clegg, S. and Courchesne, F. (1998) 'Rhizospheric processes influencing the biogeochemistry of forest ecosystems', Plant-induced soil changes: Processes and feedbacks: Springer, pp. 107-120.

Gonazlez, J., Friero, E., Selfa, L., Froilan, S. and Jouve, N. (2016) 'A Comparative Study of Root System Architecture in Seedlings of Brachypodium spp. Using Three Plant Growth Supports', Cereal Research Communications, 44(1), pp. 69-78.

Gooderham, W. and Hancock, R. (2009) 'Regulation of virulence and antibiotic resistance by two-component regulatory systems in Pseudomonas aeruginosa', Fems Microbiology Reviews, 33(2), pp. 279-294.

Grundmann, G., Dechesne, A., Bartoli, F., Flandrois, J., Chasse, J. and Kizungu, R. (2001) 'Spatial modeling of nitrifier microhabitats in soil', Soil Science Society of America Journal, 65(6), pp. 1709-1716.

Gunawardena, U. and Hawes, M. (2002) 'Tissue specific localization of root infection by fungal pathogens: Role of root border cells', Molecular Plant-Microbe Interactions, 15(11), pp. 1128-1136.

Guyer, J., Wheeler, D. and Warren, J. (2009) 'FiPy: Partial Differential Equations with Python', Computing in Science & Engineering, 11(3), pp. 6-15.

Guyonnet, J. P., Cantarel, A. A., Simon, L. and Haichar, F. e. Z. (2018) 'Root exudation rate as functional trait involved in plant nutrient-use strategy classification', Ecology and evolution, 8(16), pp. 8573-8581.

Haas, D. and Keel, C. (2003) 'Regulation of antibiotic production in root-colonizing Pseudomonas spp. and relevance for biological control of plant disease', Annual Review of Phytopathology, 41, pp. 117-153.

Haichar, F., Marol, C., Berge, O., Rangel-Castro, J., Prosser, J., Balesdent, J., Heulin, T. and Achouak, W. (2008) 'Plant host habitat and root exudates shape soil bacterial community structure', Isme Journal, 2(12), pp. 1221-1230.

Haichar, F., Santaella, C., Heulin, T. and Achouak, W. (2014) 'Root exudates mediated interactions belowground', Soil Biology & Biochemistry, 77, pp. 69-80.

Hammoudi, A. and Iosifescu, O. (2018) 'Mathematical Analysis of a Chemotaxis-Type Model of Soil Carbon Dynamic', Chinese Annals of Mathematics Series B, 39(2), pp. 253-280.

Hansen, M., Kragelund, L., Nybroe, O. and Sorensen, J. (1997) 'Early colonization of barley roots by Pseudomonas fluorescens studied by immunofluorescence technique and confocal laser scanning microscopy', Fems Microbiology Ecology, 23(4), pp. 353-360.

Hassan, K., Johnson, A., Shaffer, B., Ren, Q., Kidarsa, T., Elbourne, L., Hartney, S., Duboy, R., Goebel, N., Zabriskie, T., Paulsen, I. and Loper, J. (2010) 'Inactivation of the GacA response regulator in Pseudomonas fluorescens Pf-5 has far-reaching transcriptomic consequences', Environmental Microbiology, 12(4), pp. 899-915.

Hayat, S., Faraz, A. and Faizan, M. (2017) 'Root exudates: Composition and impact on plant–microbe interaction', Biofilms in Plant and Soil Health. John Wiley & Sons Ltd, pp. 179-193.

Heeb, S. and Haas, D. (2001) 'Regulatory roles of the GacS/GacA two-component system in plant-associated and other Gram-negative bacteria', Molecular Plant-Microbe Interactions, 14(12), pp. 1351-1363.

Heeb, S., Itoh, Y., Nishijyo, T., Schnider, U., Keel, C., Wade, J., Walsh, U., O'Gara, F. and Haas, D. (2000) 'Small, stable shuttle vectors based on the minimal pVS1 replicon for use in gram-negative, plant-associated bacteria', Molecular Plant-Microbe Interactions, 13(2), pp. 232-237.

Henry, G., Thonart, P. and Ongena, M. (2012) 'PAMPs, MAMPs, DAMPs and others: an update on the diversity of plant immunity elicitors', Biotechnologie Agronomie Societe Et Environnement, 16(2), pp. 257-268.

Hiltpold, I., Jaffuel, G. and Turlings, T. (2015) 'The dual effects of root-cap exudates on nematodes: from quiescence in plant-parasitic nematodes to frenzy in entomopathogenic nematodes', Journal of Experimental Botany, 66(2), pp. 603-611.

Hinsa, S., Espinosa-Urgel, M., Ramos, J. and O'Toole, G. (2003) 'Transition from reversible to irreversible attachment during biofilm formation by Pseudomonas fluorescens WCS365 requires an ABC transporter and a large secreted protein', Molecular Microbiology, 49(4), pp. 905-918.

Hinsa, S. and O'Toole, G. (2006) 'Biofilm formation by Pseudomonas fluorescens WCS365: a role for LapD', Microbiology-Sgm, 152, pp. 1375-1383.

Hinsinger, P., Bengough, A. G., Vetterlein, D. and Young, I. M. (2009) 'Rhizosphere: biophysics, biogeochemistry and ecological relevance', Plant and soil, 321(1-2), pp. 117-152.

Holden, N., Pritchard, L. and Toth, I. (2009) 'Colonization outwith the colon: plants as an alternative environmental reservoir for human pathogenic enterobacteria', Fems Microbiology Reviews, 33(4), pp. 689-703.

Hsu, C. and Micallef, S. (2017) 'Plant-mediated restriction of Salmonella enterica on tomato and spinach leaves colonized with Pseudomonas plant growth-promoting rhizobacteria', International Journal of Food Microbiology, 259, pp. 1-6.

Hu, J., Wei, Z., Kowalchuk, G., Xu, Y., Shen, Q. and Jousset, A. (2020) 'Rhizosphere microbiome functional diversity and pathogen invasion resistance build up during plant development', Environmental Microbiology, 22(12), pp. 5005-5018.

Hubbard, C., Brock, M., van Diepen, L., Maignien, L., Ewers, B. and Weinig, C. (2018) 'The plant circadian clock influences rhizosphere community structure and function', Isme Journal, 12(2), pp. 400-410.

Humphris, S. N., Bengough, A. G., Griffiths, B. S., Kilham, K., Rodger, S., Stubbs, V., Valentine, T. A. and Young, I. M. (2005) 'Root cap influences root colonisation by Pseudomonas fluorescens SBW25 on maize', Fems Microbiology Ecology, 54(1), pp. 123-130.

Ipina, E., Otte, S., Pontier-Bres, R., Czerucka, D. and Peruani, F. (2019) 'Bacteria display optimal transport near surfaces', Nature Physics, 15(6), pp. 610-+.

Jiang, N., Floro, E., Bray, A., Laws, B., Duncan, K. and Topp, C. (2019) 'Three-Dimensional Time-Lapse Analysis Reveals Multiscale Relationships in Maize Root Systems with Contrasting Architectures', Plant Cell, 31(8), pp. 1708-1722.

Johnsen, K. and Nielsen, P. (1999) 'Diversity of Pseudomonas strains isolated with King's B and Gould's S1 agar determined by repetitive extragenic palindromic-polymerase chain reaction, 16S rDNA sequencing and Fourier transform infrared spectroscopy characterisation', FEMS microbiology letters, 173(1), pp. 155-162.

Jones, D., Kemmitt, S., Wright, D., Cuttle, S., Bol, R. and Edwards, A. (2005) 'Rapid intrinsic rates of amino acid biodegradation in soils are unaffected by agricultural management strategy', Soil Biology & Biochemistry, 37(7), pp. 1267-1275.

Jones, D., Nguyen, C. and Finlay, R. (2009) 'Carbon flow in the rhizosphere: carbon trading at the soil-root interface', Plant and Soil, 321(1-2), pp. 5-33.

Jones, J. and Dangl, J. (2006) 'The plant immune system', Nature, 444(7117), pp. 323-329.

Jovanovic, M., Lefebvre, V., Laporte, P., Gonzalez-Rizzo, S., Lelandais-Brière, C., Frugier, F., Hartmann, C. and Crespi, M. (2007) 'How the environment regulates root architecture in dicots', Advances in Botanical Research, 46, pp. 35-74.

Jungk, A. O. (2002) 'Dynamics of nutrient movement at the soil-root interface', Plant roots: CRC Press, pp. 919-1016.

Juyal, A., Otten, W., Baveye, P. and Eickhorst, T. (2021) 'Influence of soil structure on the spread of Pseudomonas fluorescens in soil at microscale', European Journal of Soil Science, 72(1), pp. 141-153.

Kalogiros, D., Adu, M., White, P., Broadley, M., Draye, X., Ptashnyk, M., Bengough, A. and Dupuy, L. (2016) 'Analysis of root growth from a phenotyping data set using a density-based model', Journal of Experimental Botany, 67(4), pp. 1045-1058.

Kamilova, F., Kravchenko, L. V., Shaposhnikov, A. I., Azarova, T., Makarova, N. and Lugtenberg, B. (2006) 'Organic acids, sugars, and L-tryptophane in exudates of vegetables growing on stonewool and their effects on activities of rhizosphere bacteria', Molecular Plant-Microbe Interactions, 19(3), pp. 250-256.

Kamilova, F., Validov, S., Azarova, T., Mulders, I. and Lugtenberg, B. (2005) 'Enrichment for enhanced competitive plant root tip colonizers selects for a new class of biocontrol bacteria', Environmental Microbiology, 7(11), pp. 1809-1817.

Kampf, J., Gerwig, J., Kruse, K., Cleverley, R., Dormeyer, M., Grünberger, A., Kohlheyer, D., Commichau, F. M., Lewis, R. J. and Stülke, J. (2018) 'Selective pressure for biofilm formation in Bacillus subtilis: differential effect of mutations in the master regulator SinR on bistability', Mbio, 9(5), pp. e01464-18.

Karapetyan, S. and Dong, X. (2018) 'Redox and the circadian clock in plant immunity: A balancing act', Free Radical Biology and Medicine, 119, pp. 56-61.

Kawasaki, A., Okada, S., Zhang, C., Delhaize, E., Mathesius, U., Richardson, A., Watt, M., Gilliham, M. and Ryan, P. (2018) 'A sterile hydroponic system for characterising root exudates from specific root types and whole-root systems of large crop plants', Plant Methods, 14.

Kearns, D. (2013) 'You get what you select for: better swarming through more flagella', Trends in Microbiology, 21(10), pp. 508-509.

Keller, E. and Segel, L. (1971) 'Model for chemotaxis', J Theor Biol, 30(2), pp. 225234Kierstead.

Kendall, K. and Roberts, A. (2015) 'van der Waals forces influencing adhesion of cells', Philosophical Transactions of the Royal Society B-Biological Sciences, 370(1661).

Kiers, E., Rousseau, R., West, S. and Denison, R. (2003) 'Host sanctions and the legume-rhizobium mutualism', Nature, 425(6953), pp. 78-81.

Kisluk, G., Hoover, D. G., Kneil, K. E. and Yaron, S. (2012) 'Quantification of low and high levels of Salmonella enterica serovar Typhimurium on leaves', LWT-Food Science and Technology, 45(1), pp. 36-42.

Knee, E., Gong, F., Gao, M., Teplitski, M., Jones, A., Foxworthy, A., Mort, A. and Bauer, W. (2001) 'Root mucilage from pea and its utilization by rhizosphere bacteria as a sole carbon source', Molecular Plant-Microbe Interactions, 14(6), pp. 775-784.

Knights, H., Jorrin, B., Haskett, T. and Poole, P. (2021) 'Deciphering bacterial mechanisms of root colonization', Environmental Microbiology Reports.

Kour, D., Rana, K. L., Sheikh, I., Kumar, V., Yadav, A. N., Dhaliwal, H. S. and Saxena, A. K. (2019) 'Alleviation of drought stress and plant growth promotion by Pseudomonas libanensis EU-LWNA-33, a drought-adaptive phosphorus-solubilizing bacterium', Proceedings of the National Academy of Sciences, India Section B: Biological Sciences, pp. 1-11.

Kragh, K. N., Alhede, M., Kvich, L. and Bjarnsholt, T. (2019) 'Into the well—A close look at the complex structures of a microtiter biofilm and the crystal violet assay', Biofilm, 1, pp. 100006.

Kumari, P., Sayas, T. and Kleiman, M. (2020) 'Biomimetic Replication of Root Surface Microstructure using Alteration of Soft Lithography', Jove-Journal of Visualized Experiments, (162).

Kumpf, R. and Nowack, M. (2015) 'The root cap: a short story of life and death', Journal of Experimental Botany, 66(19), pp. 5651-5662.

Kuzyakov, Y. and Blagodatskaya, E. (2015) 'Microbial hotspots and hot moments in soil: concept & review', Soil Biology and Biochemistry, 83, pp. 184-199.

Kuzyakov, Y., Raskatov, A. and Kaupenjohann, M. (2003) 'Turnover and distribution of root exudates of Zea mays', Plant and Soil, 254(2), pp. 317-327.

Kuzyakov, Y. and Razavi, B. (2019) 'Rhizosphere size and shape: Temporal dynamics and spatial stationarity', Soil Biology & Biochemistry, 135, pp. 343-360.

Köhl, J., Kolnaar, R. and Ravensberg, W. J. (2019) 'Mode of action of microbial biological control agents against plant diseases: relevance beyond efficacy', Frontiers in plant science, 10, pp. 845.

Lagunas, B., Walker, L., Hussain, R. M. F., Hands-Portman, I., Woolley-Allen, K. and Gifford, M. L. (2018) 'Histological Profiling Over Time to Optimize Root Cell Type-Specific Reporter Lines for Cell Sorting', Root Development: Springer, pp. 165-175.

Law, A. M. and Aitken, M. D. (2005) 'Continuous-flow capillary assay for measuring bacterial chemotaxis', Applied and environmental microbiology, 71(6), pp. 3137-3143.

Lennon, J. and Jones, S. (2011) 'Microbial seed banks: the ecological and evolutionary implications of dormancy', Nature Reviews Microbiology, 9(2), pp. 119-130.

Lewis, D. and Quirk, J. (1967) 'Phosphate diffusion in soil and uptake by plants', Plant and Soil, 26(1), pp. 99-118.

Li, P., Lu, Y., Chen, H. and Day, B. (2020) 'The Lifecycle of the Plant Immune System', Critical Reviews in Plant Sciences, 39(1), pp. 72-100.

Li, Q., Li, X., Tang, B. and Gu, M. (2018) 'Growth Responses and Root Characteristics of Lettuce Grown in Aeroponics, Hydroponics, and Substrate Culture', Horticulturae, 4(4).

Liu, W., Cremer, J., Li, D., Hwa, T. and Liu, C. (2019) 'An evolutionarily stable strategy to colonize spatially extended habitats', Nature, 575(7784), pp. 664-668.

Lloyd-Jones, G., Laurie, A. and Tizzard, A. (2005) 'Quantification of the Pseudomonas population in New Zealand soils by fluorogenic PCR assay and culturing techniques', Journal of Microbiological Methods, 60(2), pp. 217-224.

Lugtenberg, B. and Kamilova, F. (2009) 'Plant-Growth-Promoting Rhizobacteria', Annual Review of Microbiology, 63, pp. 541-556.

Malamoud, K., McBratney, A., Minasny, B. and Field, D. (2009) 'Modelling how carbon affects soil structure', Geoderma, 149(1-2), pp. 19-26.

Mao, Z., Bonis, M., Rey, H., Saint-Andre, L., Stokes, A. and Jourdan, C. (2013) 'Which processes drive fine root elongation in a natural mountain forest ecosystem?', Plant Ecology & Diversity, 6(2), pp. 231-243.

Marchesi, J., Sato, T., Weightman, A., Martin, T., Fry, J., Hiom, S. and Wade, W. (1998) 'Design and evaluation of useful bacterium-specific PCR primers that amplify genes coding for bacterial 16S rRNA', Applied and Environmental Microbiology, 64(2), pp. 795-799.

Maroniche, G., Rubio, E., Consiglio, A. and Perticari, A. (2016) 'Plant-associated fluorescent Pseudomonas from red lateritic soil: Beneficial characteristics and their impact on lettuce growth', Journal of General and Applied Microbiology, 62(5), pp. 248-257.

Martinez-Gil, M., Yousef-Coronado, F. and Espinosa-Urgel, M. (2010) 'LapF, the second largest Pseudomonas putida protein, contributes to plant root colonization and determines biofilm architecture', Molecular Microbiology, 77(3), pp. 549-561.

Martins, A., O'Callaghan, F., Bengough, A., Loades, K., Pasqual, M., Kolb, E. and Dupuy, L. (2020) 'The helical motions of roots are linked to avoidance of particle forces in soil', New Phytologist, 225(6), pp. 2356-2367.

Martins, A., O'Callaghan, F., Bengough, A. G., Loades, K. W., Pasqual, M., Kolb, E. and Dupuy, L. X. (2019) 'The helical motions of roots are linked to avoidance of particle forces in soil', The New phytologist.

Massalha, H., Korenblum, E., Malitsky, S., Shapiro, O. H. and Aharoni, A. (2017) 'Live imaging of root–bacteria interactions in a microfluidics setup', Proceedings of the National Academy of Sciences, 114(17), pp. 4549-4554.

Matthysse, A. (1983) 'Role of bacterial cellulos fibrils in Agrobacterium-Tumefaciens infection', Journal of Bacteriology, 154(2), pp. 906-915.

Mavrodi, O. V., Mavrodi, D. V., Parejko, J. A., Thomashow, L. S. and Weller, D. M. (2012) 'Irrigation differentially impacts populations of indigenous antibiotic-producing Pseudomonas

spp. in the rhizosphere of wheat', Applied and Environmental Microbiology, 78(9), pp. 3214-3220.

Mavrodi, O. V., McWilliams, J. R., Peter, J. O., Berim, A., Hassan, K. A., Elbourne, L. D. H., LeTourneau, M. K., Gang, D. R., Paulsen, I. T., Weller, D. M., Thomashow, L. S., Flynt, A. S. and Mavrodi, D. V. (2021) 'The effect of root exudates on the transcriptome of rhizosphere Pseudomonas spp', bioRxiv, pp. 2021.01.08.425997.

Mendis, H., Thomas, V., Schwientek, P., Salamzade, R., Chien, J., Waidyarathne, P., Kloepper, J. and De La Fuente, L. (2018) 'Strain-specific quantification of root colonization by plant growth promoting rhizobacteria Bacillus firmus I-1582 and Bacillus amyloliquefaciens QST713 in non-sterile soil and field conditions', Plos One, 13(2).

Mengiste, T., VanAlfen, N., Leach, J. and Lindow, S. (2012) 'Plant Immunity to Necrotrophs', Annual Review of Phytopathology, Vol 50, 50, pp. 267-294.

Merlin, C., McAteer, S. and Masters, M. (2002) 'Tools for characterization of Escherichia coli genes of unknown function', Journal of Bacteriology, 184(16), pp. 4573-4581.

Merritt, J. H., Kadouri, D. E. and O'Toole, G. A. (2006) 'Growing and analyzing static biofilms', Current protocols in microbiology, (1), pp. 1B. 1.1-1B. 1.17.

Mills, K. K. and Bauer, W. D. (1985) 'Rhizobium attachment to clover roots', Journal of Cell Science, pp. 333-345.

Mitter, E., de Freitas, J. and Germida, J. (2017) 'Bacterial Root Microbiome of Plants Growing in Oil Sands Reclamation Covers', Frontiers in Microbiology, 8.

Miyata, M., Robinson, R., Uyeda, T., Fukumori, Y., Fukushima, S., Haruta, S., Homma, M., Inaba, K., Ito, M., Kaito, C., Kato, K., Kenri, T., Kinosita, Y., Kojima, S., Minamino, T., Mori, H., Nakamura, S., Nakane, D., Nakayama, K., Nishiyama, M., Shibata, S., Shimabukuro, K., Tamakoshi, M., Taoka, A., Tashiro, Y., Tulum, I., Wada, H. and Wakabayashi, K. (2020) 'Tree of motility - A proposed history of motility systems in the tree of life', Genes To Cells, 25(1), pp. 6-21.

Mobley, H., Green, D., Trifillia, A., Johnson, D., Chippendale, G., Lockatell, C., Jones, B. and Warren, J. (1990) 'Pyelonephritogenic Escherichia-Coli and killing of cultured human renal proximal tubular epithelial-cells - role of hemolysin in some strains', Infection and Immunity, 58(5), pp. 1281-1289.

Monchgesang, S., Strehmel, N., Schmidt, S., Westphal, L., Taruttis, F., Muller, E., Herklotz, S., Neumann, S. and Scheel, D. (2016) 'Natural variation of root exudates in Arabidopsis thaliana-linking metabolomic and genomic data', Scientific Reports, 6.

Monod, J. (1966) 'From enzymatic adaptation to allosteric transitions', Science, 154(3748), pp. 475-483.

Muci, A. L., Jorquera, M. A., Avila, A. I., Rengel, Z., Crowley, D. E. and Mora, M. D. (2012) 'A combination of cellular automata and agent-based models for simulating the root surface colonization by bacteria', Ecological Modelling, 247, pp. 1-10.

Mulia, R. and Dupraz, C. (2006) 'Unusual fine root distributions of two deciduous tree species in southern france: What consequences for modelling of tree root dynamics?', Plant and Soil, 281(1-2), pp. 71-85.

Murashige, T. and Skoog, F. (1962) 'A revised medium for rapid growth and bio assays with tobacco tissue cultures', Physiologia plantarum, 15(3), pp. 473-497.

Nan, B., McBride, M., Chen, J., Zusman, D. and Oster, G. (2014) 'Bacteria that Glide with Helical Tracks', Current Biology, 24(4), pp. R169-R173.

Naveed, M., Brown, L., Raffan, A., George, T., Bengough, A., Roose, T., Sinclair, I., Koebernick, N., Cooper, L., Hackett, C. and Hallett, P. (2017) 'Plant exudates may stabilize or weaken soil depending on species, origin and time', European Journal of Soil Science, 68(6), pp. 806-816.

Naylor, D. and Coleman-Derr, D. (2018) 'Drought Stress and Root-Associated Bacterial Communities', Frontiers in Plant Science, 8.

Nazarov, P., Baleev, D., Ivanova, M., Sokolova, L. and Karakozova, M. (2020) 'Infectious Plant Diseases: Etiology, Current Status, Problems and Prospects in Plant Protection', Acta Naturae, 12(3), pp. 46-59.

Neidhardt, F. C., Bloch, P. L. and Smith, D. F. (1974) 'Culture medium for enterobacteria', Journal of bacteriology, 119(3), pp. 736-747.

Neumann, G., Bott, S., Ohler, M. A., Mock, H. P., Lippmann, R., Grosch, R. and Smalla, K. (2014) 'Root exudation and root development of lettuce (Lactuca sativa L. cv. Tizian) as affected by different soils', Frontiers in Microbiology, 5.

Newman, E. and Watson, A. (1977) 'Microbial abundance in the rhizosphere: a computer model', Plant and Soil, 48(1), pp. 17-56.

Nguyen, C. (2003) 'Rhizodeposition of organic C by plants: mechanisms and controls', Agronomie, 23(5-6), pp. 375-396.

Noirot-Gros, M., Forrester, S., Malato, G., Larsen, P. and Noirot, P. (2019) 'CRISPR interference to interrogate genes that control biofilm formation in Pseudomonas fluorescens', Scientific Reports, 9.

Noirot-Gros, M., Shinde, S., Akins, C., Johnson, J., Zerbs, S., Wilton, R., Kemner, K., Noirot, P. and Babnigg, G. (2020) 'Functional Imaging of Microbial Interactions With Tree Roots Using a Microfluidics Setup', Frontiers in Plant Science, 11.

Noirot-Gros, M. F., Shinde, S., Larsen, P. E., Zerbs, S., Korajczyk, P. J., Kemner, K. M. and Noirot, P. H. (2018) 'Dynamics of Aspen Roots Colonization by Pseudomonads Reveals Strain-Specific and Mycorrhizal-Specific Patterns of Biofilm Formation', Frontiers in Microbiology, 9, pp. 16.

Nunan, N., Wu, K., Young, I., Crawford, J. and Ritz, K. (2003) 'Spatial distribution of bacterial communities and their relationships with the micro-architecture of soil', Fems Microbiology Ecology, 44(2), pp. 203-215.

Nuruzzaman, M., Lambers, H., Bolland, M. and Veneklaas, E. (2006) 'Distribution of carboxylates and acid phosphatase and depletion of different phosphorus fractions in the rhizosphere of a cereal and three grain legumes', Plant and Soil, 281(1-2), pp. 109-120.

Oburger, E. and Jones, D. (2018) 'Sampling root exudates - Mission impossible?', Rhizosphere, 6, pp. 116-133.

Oku, S., Komatsu, A., Nakashimada, Y., Tajima, T. and Kato, J. (2014) 'Identification of Pseudomonas fluorescens Chemotaxis Sensory Proteins for Malate, Succinate, and Fumarate, and Their Involvement in Root Colonization', Microbes and Environments, 29(4), pp. 413-419.

Oku, S., Komatsu, A., Tajima, T., Nakashimada, Y. and Kato, J. (2012) 'Identification of Chemotaxis Sensory Proteins for Amino Acids in Pseudomonas fluorescens Pf0-1 and Their Involvement in Chemotaxis to Tomato Root Exudate and Root Colonization', Microbes and Environments, 27(4), pp. 462-469.

Olanrewaju, O., Glick, B. and Babalola, O. (2017) 'Mechanisms of action of plant growth promoting bacteria', World Journal of Microbiology & Biotechnology, 33(11).

Passera, A., Compant, S., Casati, P., Maturo, M. G., Battelli, G., Quaglino, F., Antonielli, L., Salerno, D., Brasca, M. and Toffolatti, S. L. (2019) 'Not just a pathogen? Description of a plant-beneficial Pseudomonas syringae strain', Frontiers in microbiology, 10, pp. 1409.

Pausch, J. and Kuzyakov, Y. (2011) 'Photoassimilate allocation and dynamics of hotspots in roots visualized by C-14 phosphor imaging', Journal of Plant Nutrition and Soil Science, 174(1), pp. 12-19.

Pavlova, A., Leontieva, M., Smirnova, T., Kolomeitseva, G., Netrusov, A. and Tsavkelova, E. (2017) 'Colonization strategy of the endophytic plant growth-promoting strains of Pseudomonas fluorescens and Klebsiella oxytoca on the seeds, seedlings and roots of the epiphytic orchid, Dendrobium nobile Lindl', Journal of Applied Microbiology, 123(1), pp. 217-232.

Peng, X., Horn, R. and Hallett, P. (2015) 'Soil structure and its functions in ecosystems: Phase matter & scale matter', Soil & Tillage Research, 146, pp. 1-3.

Pertot, I., Giovannini, O., Benanchi, M., Caffi, T., Rossi, V. and Mugnai, L. (2017) 'Combining biocontrol agents with different mechanisms of action in a strategy to control Botrytis cinerea on grapevine', Crop Protection, 97, pp. 85-93.

Petzoldt, T. (2016) 'Estimation of Growth Rates with Package growthrates'.

Pfeifer, J., Kirchgessner, N., Colombi, T. and Walter, A. (2015) 'Rapid phenotyping of crop root systems in undisturbed field soils using X-ray computed tomography', Plant Methods, 11.

Pflugfelder, D., Metzner, R., van Dusschoten, D., Reichel, R., Jahnke, S. and Koller, R. (2017) 'Non-invasive imaging of plant roots in different soils using magnetic resonance imaging (MRI)', Plant Methods, 13.

Philippot, L., Hallin, S., Borjesson, G. and Baggs, E. (2009) 'Biochemical cycling in the rhizosphere having an impact on global change', Plant and Soil, 321(1-2), pp. 61-81.

Phillips, R., Finzi, A. and Bernhardt, E. (2011) 'Enhanced root exudation induces microbial feedbacks to N cycling in a pine forest under long-term CO2 fumigation', Ecology Letters, 14(2), pp. 187-194.

Ping, L., Birkenbeil, J. and Monajembashi, S. (2013) 'Swimming behavior of the monotrichous bacterium Pseudomonas fluorescens SBW25', Fems Microbiology Ecology, 86(1), pp. 36-44.

Pires, L., Roque, W., Rosa, J. and Mooney, S. (2019) '3D analysis of the soil porous architecture under long term contrasting management systems by X-ray computed tomography', Soil & Tillage Research, 191, pp. 197-206.

Pla, M., Oltra, S., Esteban, M., Andreu, S. and Palop, A. (2015) 'Comparison of Primary Models to Predict Microbial Growth by the Plate Count and Absorbance Methods', Biomed Research International, 2015.

Porcel, R., Zamarreno, A., Garcia-Mina, J. and Aroca, R. (2014) 'Involvement of plant endogenous ABA in Bacillus megaterium PGPR activity in tomato plants', Bmc Plant Biology, 14.

Portell, X., Pot, V., Garnier, P., Otten, W. and Baveye, P. (2018) 'Microscale Heterogeneity of the Spatial Distribution of Organic Matter Can Promote Bacterial Biodiversity in Soils: Insights From Computer Simulations', Frontiers in Microbiology, 9.

Preece, C., Farre-Armengol, G., Llusia, J. and Penuelas, J. (2018) 'Thirsty tree roots exude more carbon', Tree Physiology, 38(5), pp. 690-695.

Preece, C. and Penuelas, J. (2016) 'Rhizodeposition under drought and consequences for soil communities and ecosystem resilience', Plant and Soil, 409(1-2), pp. 1-17.

Preston, G., Bertrand, N. and Rainey, P. (2001) 'Type III secretion in plant growth-promoting Pseudomonas fluorescens SBW25', Molecular Microbiology, 41(5), pp. 999-1014.

Preston, G., Spiers, A., Zhang, X., Jackson, R., Gal, M., Knight, C., Gehrig, S., Malone, J., Moon, C., Godfrey, S., Robinson, Z., Bertrand, N., Field, D., Rainey, P., Iacobellis, N., Collmer, A., Hutcheson, S., Mansfield, J., Morris, C., Murillo, J., Schaad, N., Stead, D. and Surico, G. (2003) 'Pseudomonas in the underworld: The secret life of Pseudomonas fluorescens SBW25', Pseudomonas Syringae and Related Pathogens: Biology and Genetics, pp. 347-353.

Proctor, C. and He, Y. (2021) 'Modeling Root Exudate Accumulation Gradients to Estimate Net Exudation Rates by Peatland Soil Depth', Plants-Basel, 10(1).

Quan, M. and Liang, J. (2017) 'The influences of four types of soil on the growth, physiological and biochemical characteristics of Lycoris aurea (L' Her.) Herb', Scientific Reports, 7.

R Core Team 2018. R: A language and environment for statistical computing; 2015.

Raaijmakers, J., Vlami, M. and de Souza, J. (2002) 'Antibiotic production by bacterial biocontrol agents', Antonie Van Leeuwenhoek International Journal of General and Molecular Microbiology, 81(1-4), pp. 537-547.

Rabot, E., Wiesmeier, M., Schluter, S. and Vogel, H. (2018) 'Soil structure as an indicator of soil functions: A review', Geoderma, 314, pp. 122-137.

Rainey, P. B. (1999) 'Adaptation of Pseudomonas fluorescens to the plant rhizosphere', Environmental Microbiology, 1(3), pp. 243-257.

Rainey, P. B. and Bailey, M. J. (1996) 'Physical and genetic map of the Pseudomonas fluorescens SBW25 chromosome', Molecular microbiology, 19(3), pp. 521-533.

Ramos, C., Molbak, L. and Molin, S. (2000) 'Bacterial activity in the rhizosphere analyzed at the single-cell level by monitoring ribosome contents and synthesis rates', Applied and Environmental Microbiology, 66(2), pp. 801-809.

Raynaud, X. and Nunan, N. (2014) 'Spatial Ecology of Bacteria at the Microscale in Soil', Plos One, 9(1).

Reischke, S., Rousk, J. and Baath, E. (2014) 'The effects of glucose loading rates on bacterial and fungal growth in soil', Soil Biology & Biochemistry, 70, pp. 88-95.

Reyes-Darias, J. A., García, V., Rico-Jiménez, M., Corral-Lugo, A. and Krell, T. (2016) 'Identification and characterization of bacterial chemoreceptors using quantitative capillary and gradient plate chemotaxis assays'.

Richards, F. (1959) 'A flexible growth function for empirical use', Journal of experimental Botany, 10(2), pp. 290-301.

Richter-Heitmann, T., Eickhorst, T., Knauth, S., Friedrich, M. and Schmidt, H. (2016) 'Evaluation of Strategies to Separate Root-Associated Microbial Communities: A Crucial Choice in Rhizobiome Research', Frontiers in Microbiology, 7.

Rodriguez-Navarro, D., Dardanelli, M. and Ruiz-Sainz, J. (2007) 'Attachment of bacteria to the roots of higher plants', Fems Microbiology Letters, 272(2), pp. 127-136.

Roesch, L., Fulthorpe, R., Riva, A., Casella, G., Hadwin, A., Kent, A., Daroub, S., Camargo, F., Farmerie, W. and Triplett, E. (2007) 'Pyrosequencing enumerates and contrasts soil microbial diversity', Isme Journal, 1(4), pp. 283-290.

Romano, I., Ventorino, V. and Pepe, O. (2020) 'Effectiveness of Plant Beneficial Microbes: Overview of the Methodological Approaches for the Assessment of Root Colonization and Persistence', Frontiers in Plant Science, 11.

Rossez, Y., Holmes, A., Wolfson, E. B., Gally, D. L., Mahajan, A., Pedersen, H. L., Willats, W. G. T., Toth, I. K. and Holden, N. J. (2014) 'Flagella interact with ionic plant lipids to mediate adherence of pathogenic Escherichia coli to fresh produce plants', Environmental Microbiology, 16(7), pp. 2181-2195.

Rossez, Y., Wolfson, E., Holmes, A., Gally, D. and Holden, N. (2015) 'Bacterial Flagella: Twist and Stick, or Dodge across the Kingdoms', Plos Pathogens, 11(1).

Rousk, J. and Baath, E. (2011) 'Growth of saprotrophic fungi and bacteria in soil', Fems Microbiology Ecology, 78(1), pp. 17-30.

Roy, J., Mazzaferri, J., Filep, J. and Costantino, S. (2017) 'A Haptotaxis Assay for Neutrophils using Optical Patterning and a High-content Approach', Scientific Reports, 7.

Ryan, P., Delhaize, E., Watt, M. and Richardson, A. (2016) 'Plant roots: understanding structure and function in an ocean of complexity', Annals of Botany, 118(4), pp. 555-559.

Sanguankiattichai, N., Chandrasekar, B., Buscaill, P., Van Der Hoorn, R. and Preston, G. (2019) 'Pseudomonas syringae produces an inhibitor of a plant defence-related Beta-galactosidase', Molecular Plant-Microbe Interactions, 32(10), pp. 170-171.

Sasse, J., Martinoia, E. and Northen, T. (2018) 'Feed your friends: do plant exudates shape the root microbiome?', Trends in plant science, 23(1), pp. 25-41.

Sauer, D., Kuzyakov, Y. and Stahr, K. (2006) 'Spatial distribution of root exudates of five plant species as assessed by C-14 labeling', Journal of Plant Nutrition and Soil Science, 169(3), pp. 360-362.

Savary, S., Willocquet, L., Pethybridge, S., Esker, P., McRoberts, N. and Nelson, A. (2019) 'The global burden of pathogens and pests on major food crops', Nature Ecology & Evolution, 3(3), pp. 430-+.

Schirawski, J. and Perlin, M. (2018) 'Plant-Microbe Interaction 2017The Good, the Bad and the Diverse', International Journal of Molecular Sciences, 19(5).

Schlaeppi, K., Dombrowski, N., Oter, R., van Themaat, E. and Schulze-Lefert, P. (2014) 'Quantitative divergence of the bacterial root microbiota in Arabidopsis thaliana relatives', Proceedings of the National Academy of Sciences of the United States of America, 111(2), pp. 585-592.

Schmidt, H., Nunan, N., Höck, A., Eickhorst, T., Kaiser, C., Woebken, D. and Raynaud, X. (2018) 'Recognizing patterns: spatial analysis of observed microbial colonization on root surfaces'.

Schneider, C., Rasband, W. and Eliceiri, K. (2012) 'NIH Image to ImageJ: 25 years of image analysis', Nature Methods, 9(7), pp. 671-675.

Schoch, C. and Seifert, K. and Huhndorf, S. and Robert, V. and Spouge, J. and Levesque, C. and Chen, W. and Dentinger, B. and Dieguez-Uribeondo, J. and Divakar, P. and Douglas, B. and Duenas, M. and Duong, T. and Eberhardt, U. and Edwards, J. and Elshahed, M. and Fliegerova, K. and Furtado, M. and Garcia, M. and Ge, Z. and Griffith, G. and Griffiths, K. and Groenewald, J. and Groenewald, M. and Grube, M. and Gryzenhout, M. and Guo, L. and Hagen, F. and Hambleton, S. and Hamelin, R. and Hansen, K. and Harrold, P. and Heller, G. and Herrera, G. and Hirayama, K. and Hirooka, Y. and Ho, H. and Hoffmann, K. and Hofstetter, V. and Hognabba, F. and Hollingsworth, P. and Hong, S. and Hosaka, K. and Houbraken, J. and Hughes, K. and Huhtinen, S. and Hyde, K. and James, T. and Johnson, E. and Johnson, J. and Johnston, P. and Jones, E. and Kelly, L. and Kirk, P. and Knapp, D. and Koljalg, U. and Kovacs, G. and Kurtzman, C. and Landvik, S. and Leavitt, S. and Liggenstoffer, A. and Liimatainen, K. and Lombard, L. and Luangsa-Ard, J. and Lumbsch, H. and Maganti, H. and Maharachchikumbura, S. and Martin, M. and May, T. and McTaggart, A. and Methven, A. and Meyer, W. and Moncalvo, J. and Mongkolsamrit, S. and Nagy, L. and Nilsson, R. and Niskanen, T. and Nyilasi, I. and Okada, G. and Okane, I. and Olariaga, I. and Otte, J. and Papp, T. and Park, D. and Petkovits, T. and Pino-Bodas, R. and Quaedvlieg, W. and Raja, H. and Redecker, D. and Rintoul, T. and Ruibal, C. and Sarmiento-Ramirez, J. and

Schmitt, I. and Schussler, A. and Shearer, C. and Somtome, K. and Stefani, F. and Stenroos, S. and Stielow, B. and Stockinger, H. and Suetrong, S. and Suh, S. and Sung, G. and Suzuki, M. and Tanaka, K. and Tedersoo, L. and Telleria, M. and Tretter, E. and Untereiner, W. and Urbina, H. and Vagvolgyi, C. and Vialle, A. and Vu, T. and Walther, G. and Wang, Q. and Wang, Y. and Weir, B. and Weiss, M. and White, M. and Xu, J. and Yahr, R. and Yang, Z. and Yurkov, A. and Zamora, J. and Zhasng, N. and Zhuang, W. and Schindel, D. (2012) 'Nuclear ribosomal internal transcribed spacer (ITS) region as a universal DNA barcode marker for Fungi', Proceedings of the National Academy of Sciences of the United States of America, 109(16), pp. 6241-6246.

Schreiter, S., Ding, G., Heuer, H., Neumann, G., Sandmann, M., Grosch, R., Kropf, S. and Smalla, K. (2014) 'Effect of the soil type on the microbiome in the rhizosphere of field-grown lettuce', Frontiers in Microbiology, 5.

Scott, E., Rattray, E., Prosser, J., Killham, K., Glover, L., Lynch, J. and Bazin, M. (1995) 'A mathmatical-model for dispersal of bacterial inoculants colonizing the wheat rhizosphere', Soil Biology & Biochemistry, 27(10), pp. 1307-1318.

Semmler, A., Whitchurch, C. and Mattick, J. (1999) 'A re-examination of twitching motility in Pseudomonas aeruginosa', Microbiology-Sgm, 145, pp. 2863-2873.

Shaner, N., Steinbach, P. and Tsien, R. (2005) 'A guide to choosing fluorescent proteins', Nature Methods, 2(12), pp. 905-909.

Sharpton, T. (2014) 'An introduction to the analysis of shotgun metagenomic data', Frontiers in Plant Science, 5.

Shelake, R., Pramanik, D. and Kim, J. (2019) 'Exploration of Plant-Microbe Interactions for Sustainable Agriculture in CRISPR Era', Microorganisms, 7(8).

Shi, S., Condron, L., Larsen, S., Richardson, A., Jones, E., Jiao, J., O'Callaghan, M. and Stewart, A. (2011) 'In situ sampling of low molecular weight organic anions from rhizosphere of radiata pine (Pinus radiata) grown in a rhizotron system', Environmental and Experimental Botany, 70(2-3), pp. 131-142.

Shimshick, E. J. and Hebert, R. R. (1979) 'Binding characteristics of N2-fixing bacteria to cereal roots', Applied and environmental microbiology, 38(3), pp. 447-453.

Shinde, S., Zerbs, S., Collart, F. R., Cumming, J. R., Noirot, P. and Larsen, P. E. (2019) 'Pseudomonas fluorescens increases mycorrhization and modulates expression of antifungal defense response genes in roots of aspen seedlings', BMC plant biology, 19(1), pp. 4.

Silby, M., Cerdeno-Tarraga, A., Vernikos, G., Giddens, S., Jackson, R., Preston, G., Zhang, X., Moon, C., Gehrig, S., Godfrey, S., Knight, C., Malone, J., Robinson, Z., Spiers, A., Harris, S., Challis, G., Yaxley, A., Harris, D., Seeger, K., Murphy, L., Rutter, S., Squares, R., Quail, M., Saunders, E., Mavromatis, K., Brettin, T., Bentley, S., Hothersall, J., Stephens, E., Thomas, C., Parkhill, J., Levy, S., Rainey, P. and Thomson, N. (2009) 'Genomic and genetic analyses of diversity and plant interactions of Pseudomonas fluorescens', Genome Biology, 10(5).

Silk, W. and Bogeat-Triboulot, M. (2014) 'Deposition rates in growing tissue: Implications for physiology, molecular biology, and response to environmental variation', Plant and Soil, 374(1-2), pp. 1-17.

Sood, S. (2003) 'Chemotactic response of plant-growth-promoting bacteria towards roots of vesicular-arbuscular mycorrhizal tomato plants', Fems Microbiology Ecology, 45(3), pp. 219-227.

Spiers, A. (2007) 'Wrinkly-Spreader Fitness in the Two-Dimensional Agar Plate Microcosm: Maladaptation, Compensation and Ecological Success', Plos One, 2(8).

Spiers, A., Kahn, S., Bohannon, J., Travisano, M. and Rainey, P. (2002) 'Adaptive divergence in experimental Populations of Pseudomonas fluorescens. I. Genetic and phenotypic bases of wrinkly spreader fitness', Genetics, 161(1), pp. 33-46.

Spiers, A. J., Bohannon, J., Gehrig, S. M. and Rainey, P. B. (2003) 'Biofilm formation at the air–liquid interface by the Pseudomonas fluorescens SBW25 wrinkly spreader requires an acetylated form of cellulose', Molecular microbiology, 50(1), pp. 15-27.

Stenstrom, J., Stenberg, B. and Johansson, M. (1998) 'Kinetics of substrate-induced respiration (SIR): Theory', Ambio, 27(1), pp. 35-39.

Strigul, N. and Kravchenko, L. (2006) 'Mathematical modeling of PGPR inoculation into the rhizosphere', Environmental Modelling & Software, 21(8), pp. 1158-1171.

Suarez, R., Wong, A., Ramirez, M., Barraza, A., Orozco, M., Cevallos, M., Lara, M., Hernandez, G. and Iturriaga, G. (2008) 'Improvement of drought tolerance and grain yield in common bean by overexpressing trehalose-6-phosphate synthase in rhizobia', Molecular Plant-Microbe Interactions, 21(7), pp. 958-966.

Sung, K., Kim, J., Munster, C., Corapcioglu, M., Park, S., Drew, M. and Chang, Y. (2006) 'A simple approach to modeling microbial biomass in the rhizosphere', Ecological Modelling, 190(3-4), pp. 277-286.

Sylvia, D. M., Fuhrmann, J. J., Hartel, P. G. and Zuberer, D. A. (2005) Principles and applications of soil microbiology. Pearson.

Tahrioui, A., Quesada, E. and Llamas, I. (2013) 'Genetic and phenotypic analysis of the GacS/GacA system in the moderate halophile Halomonas anticariensis', Microbiology-Sgm, 159, pp. 462-474.

Tanz, S., Castleden, I., Small, I. and Millar, A. (2013) 'Fluorescent protein tagging as a tool to define the subcellular distribution of proteins in plants', Frontiers in Plant Science, 4.

Team, R. C. 2018. R: A language and environment for statistical computing; 2015.

Tharayil, N. and Triebwasser, D. (2010) 'Elucidation of a Diurnal Pattern of Catechin Exudation by Centaurea stoebe', Journal of Chemical Ecology, 36(2), pp. 200-204.

Tindall, M. J., Maini, P. K., Porter, S. L. and Armitage, J. P. (2008) 'Overview of mathematical approaches used to model bacterial chemotaxis II: bacterial populations', Bulletin of mathematical biology, 70(6), pp. 1570.

Toal, M., Yeomans, C., Killham, K. and Meharg, A. (2000) 'A review of rhizosphere carbon flow modelling', Plant and Soil, 222(1-2), pp. 263-281.

Tognacchini, A., Salinitro, M., Puschenreiter, M. and van der Ent, A. (2020) 'Root foraging and avoidance in hyperaccumulator and excluder plants: a rhizotron experiment', Plant and Soil, 450(1-2), pp. 287-302.

Tomlinson, A. and Fuqua, C. (2009) 'Mechanisms and regulation of polar surface attachment in Agrobacterium tumefaciens', Current Opinion in Microbiology, 12(6), pp. 708-714.

Trippe, K., McPhail, K., Armstrong, D., Azevedo, M. and Banowetz, G. (2013) 'Pseudomonas fluorescens SBW25 produces furanomycin, a non-proteinogenic amino acid with selective antimicrobial properties', Bmc Microbiology, 13.

Trivedi, P. and Wang, N. (2014) 'Host immune responses accelerate pathogen evolution', Isme Journal, 8(3), pp. 727-731.

Tsoularis, A. and Wallace, J. (2002) 'Analysis of logistic growth models', Mathematical biosciences, 179(1), pp. 21-55.

Turnbull, G., Morgan, J., Whipps, J. and Saunders, J. (2001) 'The role of bacterial motility in the survival and spread of Pseudomonas fluorescens in soil and in the attachment and colonisation of wheat roots', Fems Microbiology Ecology, 36(1), pp. 21-31.

Unge, A. and Jansson, J. (2001) 'Monitoring population size, activity, and distribution of gfp-luxAB-tagged Pseudomonas fluorescens SBW25 during colonization of wheat', Microbial ecology, 41(4), pp. 290-300.

Unge, A., Tombolini, R., Molbak, L. and Jansson, J. (1999) 'Simultaneous monitoring of cell number and metabolic activity of specific bacterial populations with a dual gfp-luxAB marker system', Applied and Environmental Microbiology, 65(2), pp. 813-821.

Vacheron, J., Moenne-Loccoz, Y., Dubost, A., Goncalves-Martins, M., Muller, D. and Prigent-Combaret, C. (2016) 'Fluorescent Pseudomonas Strains with only Few Plant-Beneficial Properties Are Favored in the Maize Rhizosphere', Frontiers in Plant Science, 7.

Vallino, J., Hopkinson, C. and Hobbie, J. (1996) 'Modeling bacterial utilization of dissolved organic matter: Optimization replaces Monod growth kinetics', Limnology and Oceanography, 41(8), pp. 1591-1609.

Valverde, C., Heeb, S., Keel, C. and Haas, D. (2003) 'RsmY, a small regulatory RNA, is required in concert with RsmZ for GacA-dependent expression of biocontrol traits in Pseudomonas fluorescens CHA0', Molecular Microbiology, 50(4), pp. 1361-1379.

Vanneste, J., Leach, J. and Lindow, S. (2017) 'The Scientific, Economic, and Social Impacts of the New Zealand Outbreak of Bacterial Canker of Kiwifruit (Pseudomonas syringae pv. actinidiae)', Annual Review of Phytopathology, Vol 55, 55, pp. 377-399.

Vejan, P., Abdullah, R., Khadiran, T., Ismail, S. and Nasrulhaq Boyce, A. (2016) 'Role of plant growth promoting rhizobacteria in agricultural sustainability—a review', Molecules, 21(5), pp. 573.

Velmourougane, K., Prasanna, R. and Saxena, A. K. (2017) 'Agriculturally important microbial biofilms: Present status and future prospects', Journal of Basic Microbiology, 57(7), pp. 548-573.

Virtanen, P., Gommers, R., Oliphant, T. E., Haberland, M., Reddy, T., Cournapeau, D., Burovski, E., Peterson, P., Weckesser, W. and Bright, J. (2020) 'SciPy 1.0: fundamental algorithms for scientific computing in Python', Nature methods, 17(3), pp. 261-272.

Vishwakarma, K., Kumar, N., Shandilya, C., Mohapatra, S., Bhayana, S. and Varma, A. (2020) 'Revisiting plant–microbe interactions and microbial consortia application for enhancing sustainable agriculture: A review', Frontiers in Microbiology, 11, pp. 3195.

Vranova, V., Rejsek, K., Skene, K., Janous, D. and Formanek, P. (2013a) 'Methods of collection of plant root exudates in relation to plant metabolism and purpose: A review', Journal of Plant Nutrition and Soil Science, 176(2), pp. 175-199.

Vranova, V., Rejsek, K., Skene, K. R., Janous, D. and Formanek, P. (2013b) 'Methods of collection of plant root exudates in relation to plant metabolism and purpose: a review', Journal of Plant Nutrition and Soil Science, 176(2), pp. 175-199.

Vurukonda, S., Vardharajula, S., Shrivastava, M. and SkZ, A. (2016) 'Enhancement of drought stress tolerance in crops by plant growth promoting rhizobacteria', Microbiological Research, 184, pp. 13-24.

Walker, T. S., Bais, H. P., Deziel, E., Schweizer, H. P., Rahme, L. G., Fall, R. and Vivanco, J. M. (2004a) 'Pseudomonas aeruginosa-plant root interactions. Pathogenicity, biofilm formation, and root exudation', Plant Physiology, 134(1), pp. 320-331.

Walker, T. S., Bais, H. P., Déziel, E., Schweizer, H. P., Rahme, L. G., Fall, R. and Vivanco, J. M. (2004b) 'Pseudomonas aeruginosa-plant root interactions. Pathogenicity, biofilm formation, and root exudation', Plant physiology, 134(1), pp. 320-331.

Wasson, A., Nagel, K., Tracy, S. and Watt, M. (2020) 'Beyond Digging: Noninvasive Root and Rhizosphere Phenotyping', Trends in Plant Science, 25(1), pp. 119-120.

Watt, M., Hugenholtz, P., White, R. and Vinall, K. (2006) 'Numbers and locations of native bacteria on field-grown wheat roots quantified by fluorescence in situ hybridization (FISH)', Environmental Microbiology, 8(5), pp. 871-884.

Watt, M., McCully, M. and Kirkegaard, J. (2003) 'Soil strength and rate of root elongation alter the accumulation of Pseudomonas spp. and other bacteria in the rhizosphere of wheat', Functional Plant Biology, 30(5), pp. 483-491.

Watt, M., Silk, W. and Passioura, J. (2006) 'Rates of root and organism growth, soil conditions, and temporal and spatial development of the rhizosphere', Annals of Botany, 97(5), pp. 839-855.

Wendlandt, C., Regus, J., Gano-Cohen, K., Hollowell, A., Quides, K., Lyu, J., Adinata, E. and Sachs, J. (2019) 'Host investment into symbiosis varies among genotypes of the legume Acmispon strigosus, but host sanctions are uniform', New Phytologist, 221(1), pp. 446-458.

Westhoek, A., Clark, L., Culbert, M., Dalchau, N., Griffiths, M., Jorrin, B., Karunakaran, R., Ledermann, R., Tkacz, A., Webb, I., James, E., Poole, P. and Turnbull, L. (2021) 'Conditional sanctioning in a legume & ndash;Rhizobium mutualism', Proceedings of the National Academy of Sciences of the United States of America, 118(19).

Wheatley, R. M. and Poole, P. S. (2018) 'Mechanisms of bacterial attachment to roots', Fems Microbiology Reviews, 42(4), pp. 448-461.

Wheeler, D., Dung, J. and Johnson, D. (2019) 'From pathogen to endophyte: an endophytic population of Verticillium dahliae evolved from a sympatric pathogenic population', New Phytologist, 222(1), pp. 497-510.

Wieland, G., Neumann, R. and Backhaus, H. (2001) 'Variation of microbial communities in soil, rhizosphere, and rhizoplane in response to crop species, soil type, and crop development', Applied and Environmental Microbiology, 67(12), pp. 5849-5854.

Williams, A., Langridge, H., Straathof, A., Muhamadali, H., Hollywood, K., Goodacre, R. and de Vries, F. (2021) 'Root functional traits explain root exudation rate and composition across a range of grassland species', Journal of Ecology.

Wilton, R., Ahrendt, A., Shinde, S., Sholto-Douglas, D., Johnson, J., Brennan, M. and Kemner, K. (2018) 'A New Suite of Plasmid Vectors for Fluorescence-Based Imaging of Root Colonizing Pseudomonads', Frontiers in Plant Science, 8.

Witt, M., Dybas, M., Worden, R. and Criddle, C. (1999) 'Motility-enhanced bioremediation of carbon tetrachloride-contaminated aquifer sediments', Environmental Science & Technology, 33(17), pp. 2958-2964.

Wojciechowski, T., Gooding, M., Ramsay, L. and Gregory, P. (2009) 'The effects of dwarfing genes on seedling root growth of wheat', Journal of Experimental Botany, 60(9), pp. 2565-2573.

Wolfe, A. and Berg, H. (1989) 'Migration of bacteria in semisolid agar', Proceedings of the National Academy of Sciences of the United States of America, 86(18), pp. 6973-6977.

Wright, K. M., Crozier, L., Marshall, J., Merget, B., Holmes, A. and Holden, N. J. (2017) 'Differences in internalization and growth of E scherichia coli O157: H7 within the apoplast of edible plants, spinach and lettuce, compared with the model species N icotiana benthamiana', Microbial biotechnology, 10(3), pp. 555-569.

Xue, P., Carrillo, Y., Pino, V., Minasny, B. and McBratney, A. (2018) 'Soil Properties Drive Microbial Community Structure in a Large Scale Transect in South Eastern Australia', Scientific Reports, 8.

Yang, C.-Y. (2018) Application of Microfluidic Device for the Study of Bacteria. eScholarship, University of California.

Yang, L., Chen, X., Zang, X., Radosevich, M., Ripp, S., Zhuang, J. and Sayler, G. (2019) 'Surface-Adsorbed Contaminants Mediate the Importance of Chemotaxis and Haptotaxis for Bacterial Transport Through Soils', Frontiers in Microbiology, 10.

Yin, C., Vargas, J., Schlatter, D., Hagerty, C., Hulbert, S. and Paulitz, T. (2021) 'Rhizosphere community selection reveals bacteria associated with reduced root disease', Microbiome, 9(1).

Young, I., Crawford, J., Nunan, N., Otten, W., Spiers, A. and Sparks, D. (2008) 'Microbial distribution in soils: physics and scaling', Advances in Agronomy, Vol 100, 100, pp. 81-121.

Yu, K., Liu, Y., Tichelaar, R., Savant, N., Lagendijk, E., van Kuijk, S. J., Stringlis, I. A., van Dijken, A. J., Pieterse, C. M. and Bakker, P. A. (2019) 'Rhizosphere-associated Pseudomonas suppress local root immune responses by Gluconic Acid-mediated lowering of environmental pH', Current Biology, 29(22), pp. 3913-3920. e4.

Zhalnina, K., Louie, K. B., Hao, Z., Mansoori, N., da Rocha, U. N., Shi, S., Cho, H., Karaoz, U., Loqué, D. and Bowen, B. P. (2018) 'Dynamic root exudate chemistry and microbial substrate preferences drive patterns in rhizosphere microbial community assembly', Nature microbiology, 3(4), pp. 470.

Zhao, J., Bodner, G., Rewald, B., Leitner, D., Nagel, K. and Nakhforoosh, A. (2017) 'Root architecture simulation improves the inference from seedling root phenotyping towards mature root systems', Journal of Experimental Botany, 68(5), pp. 965-982.

Zhou, Q., Shimada, J. and Sato, A. (2001) 'Three-dimensional spatial and temporal monitoring of soil water content using electrical resistivity tomography', Water Resources Research, 37(2), pp. 273-285.

Zhu, B., Gutknecht, J., Herman, D., Keck, D., Firestone, M. and Cheng, W. (2014) 'Rhizosphere priming effects on soil carbon and nitrogen mineralization', Soil Biology & Biochemistry, 76, pp. 183-192.

Supplementary materials

Scripts

R script: Fitting growth models to colonisation data (NLS):

```
library(dplyr)
library(growthrates)
library(tidyverse)
#=======

my.data = read.csv("file_name.csv", sep = ",", header = TRUE) #rename to relevant file name and loaction
attach(my.data)
head(my.data)

time = my.data$ #modify to relevant time

y_data = my.data$ #modify to relevant y data values

my.data = data.frame(time,y_data)

#=======
#Baranyi

p     = c(y0 = , mumax = , K = , h0 = ) #best guess for the model parameters
lower = c(y0 = , mumax = , K = , h0 = ) #reasonable lower limits
upper = c(y0 = , mumax = , K = , h0 = ) #reasonable upper limits

mod1 = fit_growthmodel(FUN = grow_baranyi, p = p, my.data$time, my.data$y_data,
                       lower = lower, upper = upper)
```

```
baranyi = function(time, y0, mumax, K, h0){
 A = time + 1/mumax * log(exp(-mumax * time) + exp(-h0) -
        exp(-mumax * time - h0))
      log_y = log(y0) + mumax * A - log(1 + (exp(mumax * A) -
        1)/exp(log(K) - log(y0)))
}

baranyi.analysis = nls (y_data~
        baranyi(time, y0, mumax, K, h0),
                                    data = my.data,
                                          start = list(y0 = as.vector(coef(mod1))[1],
mumax = as.vector(coef(mod1))[2], K = as.vector(coef(mod1))[3], h0 =
as.vector(coef(mod1))[4]),
                                                trace = T
)

summary(baranyi.analysis)

AIC(baranyi.analysis)

#=========================================
#richards

p     = c(y0 = , mumax = ,K = , beta = )#best guess for the model parameters
lower = c(y0 = , mumax = , K = , beta = )#reasonable lower limits
upper = c(y0 = , mumax = , K = , beta = )#reasonable upper limits

mod2 = fit_growthmodel(FUN = grow_richards, p = p, my.data$time, my.data$y_data,
        lower = lower, upper = upper)

richards = function(time, y0, mumax, K, beta){
```

```
        K * (1 - exp(-beta * mumax * time) * (1 - (y0/K)^-beta))^(-1/beta)
}

richards.analysis = nls (y_data~
        richards(time, y0, mumax, K, beta),
        data = my.data,
        start = list(y0 = as.vector(coef(mod2))[1], mumax = as.vector(coef(mod2))[2], K =
        as.vector(coef(mod2))[3], beta = as.vector(coef(mod2))[4]),
        trace = T
)

summary(richards.analysis)

AIC(richards.analysis)

#=========================================
#gomperts
p     = c(y0 = , mumax = , K = )#best guess for the model parameters
lower = c(y0 = , mumax = , K = )#reasonable lower limits
upper = c(y0 = , mumax = , K = )#reasonable upper limits

mod3 = fit_growthmodel(FUN = grow_gompertz, p = p, my.data$time, my.data$y_data,
        lower = lower, upper = upper)

gompertz = function(tmie, y0, mumax, K){
        K * exp(log(y0/K) * exp(-mumax * time))
}

gompertz.analysis = nls (y_data~
        gompertz(time, y0, mumax, K),
```

```
	start = list(y0 = as.vector(coef(mod3))[1], mumax = as.vector(coef(mod3))[2], K = as.vector(coef(mod3))[3]),
	trace = T
)

summary(gompertz.analysis)

AIC(gompertz.analysis)

#=========================================
#logistic

p     = c(y0 = , mumax = , K = )#best guess for the model parameters
lower = c(y0 = , mumax = , K = )#reasonable lower limits
upper = c(y0 = , mumax = , K = )#reasonable upper limits

mod4 = fit_growthmodel(FUN = grow_logistic, p = p, my.data$time, my.data$y_data,
	lower = lower, upper = upper)

logistic = function(time, y0,mumax, K){
	(K * y0) / (y0 + (K - y0) * exp(-mumax * time))
}

logistic.analysis = nls (y_data~
	logistic(time, y0,mumax, K),
	start = list(y0 = as.vector(coef(mod4))[1], mumax = as.vector(coef(mod4))[2], K = as.vector(coef(mod4))[3]),
	trace = T
)

summary(logistic.analysis)
```

```
AIC(logistic.analysis)

#=========================================
#logistic decline model

curve_decline = function(time, parms){
        with(as.list(parms), {
        y = a+b*(1-exp(-c/time))
return(as.matrix(data.frame(time=my.data$time, y=my.data$y_data)))
})
}

mygrowthmodel = growthmodel(decline, c("a", "b", "c"))

p     = c(a =, b = ,c =)#best guess for the model parameters
lower = c(a = , b = , c = )#reasonable lower limits
upper = c(a = , b =, c =)#reasonable upper limits

mod5 = fit_growthmodel(FUN = curve_decline, p = p, my.data$times, my.data$y_data, #
replace function with relevant model, logistic or decline1
        lower = lower, upper = upper)

curve_decline1=function(time,a,b,c){
        a+b*(1-exp(-c/time))
}

curve.analysis = nls (y_data~
        curve_decline1(time, a, b, c),
        start = list(a = as.vector(coef(mod5))[1], b = as.vector(coef(mod5))[2], c =
        as.vector(coef(mod5))[3]),
```

```
        trace = T
)

summary(curve.analysis)

AIC(curve.analysis)

#=========================================
```

R script: Bootstrap confidence interval estimation

```
library(tidyverse)
library(growthrates)

my.data = read.csv("", sep = ",", header = TRUE) #rename to relevant file name and loaction
attach(my.data)
head(my.data)

times =  #modify to relevant time

y_data = #modify to relevant y data values

my.data = data.frame(times,y_data)

my.data = my.data %>% drop_na(y_data)

#reasonable guesses and limits

y01 =
y0h =
y0l =

mumax1 =
mumaxh =
mumaxl =

K1 =
Kh =
Kl =
```

```
h01 =
h0h =
h0l =

beta1 =
betah =
betal =

a1 =
ah =
al =

b1 =
bh =
bl =

c1 =
ch =
cl =

#====================
#models

baranyi = function(time, y0, mumax, K, h0){
 A = time + 1/mumax * log(exp(-mumax * time) + exp(-h0) -
          exp(-mumax * time - h0))
       log_y <- log(y0) + mumax * A - log(1 + (exp(mumax * A) -
          1)/exp(log(K) - log(y0)))
}
```

```
richards = function(time, y0, mumax, K, beta){
        K * (1 - exp(-beta * mumax * time) * (1 - (y0/K)^-beta))^(-1/beta)
}

gompertz = function(tmie, y0, mumax, K){
        K * exp(log(y0/K) * exp(-mumax * time))
}

logistic = function(time, y0,mumax, K){
        (K * y0) / (y0 + (K - y0) * exp(-mumax * time))
}

curve_decline = function(time, parms){
        with(as.list(parms), {
        y = a+b*(1-exp(-c/time))
return(as.matrix(data.frame(time=my.data$time, y=my.data$y_data)))
})
}

#====================
fun = #select function

nls_start = nls (my.data$y_data~
         fun(my.data$times, y0,mumax, K), #choose your function
                        start = list(y0= y01, mumax= mumax1, K= K1), #reasonable guess
                                trace = T, data = my.data,control = list(maxiter = (10^9),
minFactor = 0)
)
```

```
Model_parms = (as.numeric(as.vector(coef(nls_start))))

Model_data = fun(my.data$times,Model_parms[1],Model_parms[2],Model_parms[3]) #add
in ,Model_parms[4] if baranyi or richards

#======================

BT = 1000 # number of bootstraps

z = matrix(ncol = length(coef(nls_start)), nrow  = (0))

for(j in 1:BT){

        choice = floor(runif(length(my.data$y_data), min = 1, max =
length(my.data$y_data)))

        y = matrix(ncol = ncol(my.data), nrow  = (0))

        for( i in choice){
                x = as.numeric(as.vector(my.data[i,]))
                y = rbind.data.frame(y, (x))

        }

        colnames(y)<-colnames(my.data)
        attach(y)

        p     = c(y0 =Model_parms[1], mumax = Model_parms[2],K = Model_parms[3])
        lower = c(y0 =y0l, mumax =mumaxl,   K = Kl) #reasonible limit
        upper = c(y0 =y0h , mumax =mumaxh ,   K = Kh) #reasonible limit
```

```
        nls1 = fit_growthmodel(FUN = fun, p = p, y$times, y$y_data, #choose function,
logistic or decline1
                lower = lower, upper = upper)


        z = rbind.data.frame(z, (as.numeric(as.vector(coef(nls1)))))


        print(z)


}


new_fits = matrix(ncol = length(my.data$times), nrow  = 0)
for(k in 0:BT){
        fits = fun(my.data$times, z[k,1],z[k,2],z[k,3]) # add z[k,4] if needed (Baranyi,
Richards)
        new_fits = rbind.data.frame(new_fits, (fits))
}


new_fits$ave.y = row.Means(new_fits[1:])


x_vals = matrix(ncol = 0, nrow  = BT)
for(m in 1:nrow(new_fits)){
        x = ave.y - as.numeric(as.vector(new_fits[m,]))
        x = (x)^2
        x = sum(x)
        x = x/length(new_fits[1,])
        x = sqrt(x)
        x_vals = rbind.data.frame(x_vals, (x))
        print(x_vals)
}


x_vals = x_vals %>% drop_na(x_vals)
```

```
final_error = sum(x_vals)/(BT-1)
print(final_error)

#============================
```

R script: calculation bacterial attachment rate

```
#script for calculating rate of attachment

library(dplyr)
library(tidyverse)
library(growthrates)
library(deSolve)
library(lattice)
library(ggplot2)
library(gridExtra)
library(cowplot)        #load packages

rm(list=ls())
graphics.off()
detach(my.data)         #clear previous work

#================

Kc = 8.855974
y0c = 0.007333
muc = 0.184677
Kp = 9.04029218
y0p = 0.02508862
mup = 0.09949397      #prameters fit using growthrates

Kp = Kc #constrain carrying capacity to that calculated for total attachment

time = c(1:96)
#=================
```

```
Yc = function(time){
        Kc/(1+(Kc/y0c-1)*exp(-muc*time))
}                                       #logistic equation for total colonisation

Yc1 = expression(
        Kc/(1+(Kc/y0c-1)*exp(-muc*time))
)

D(Yc1,'time') #differentiate it

Gc = function(time){
        Kc * ((Kc/y0c - 1) * (exp(-muc * time) * muc))/(1 + (Kc/y0c -
        1) * exp(-muc * time))^2
}                                       #growth rate for total colonisation

points = Gc(time)

plot(time,points)

#======================

Yp = function(time){
        Kp/(1+(Kp/y0p-1)*exp(-mup*time))
}                                       #logistic equation for proliferation

Yp1 = expression(
        Kp/(1+(Kp/y0p-1)*exp(-mup*time))
)
```

```
D(Yp1,'time') #differentiate it

Gp = function(time){
        Kp * ((Kp/y0p - 1) * (exp(-mup * time) * mup))/(1 + (Kp/y0p -
        1) * exp(-mup * time))^2
}                                               #growth rate for proliferation

pointsp = Gp(time)

plot(time,pointsp)

summary(pointsp)
summary(points)

#======================

Gcont = function(time){
        mup*(Yc(time)*(Kp-Yc(time))/Kp)
}                       #substitute y0 for Yc

pointscont = Gcont(time)

summary(pointscont)

Ga = function(time){
        Gc(time) - Gcont(time)
}                                               #rate of attacment is difference between two
rates

pointsattached = Ga(time)
```

```
plot(time,pointsattached)

#======================

rates = data.frame(time, points, pointsp, pointsattached)

#============================================================

#intergrate that Ga equation to get reasonable values for attachment

intval <- integrate(Ga,lower=0,upper=10)
str(intval)
intval$value

attachment.values <- vector("numeric",96)

for(i in 0:96){
        intval = integrate(Ga,lower=0,upper=i)
        str(intval)
        attachment.values[i] = (intval$value)
}

attachment.values

#============================================================

total.values = Yc(time)

proliferation.values = Yp(time)
```

```
model.values = data.frame(time,total.values,proliferation.values,attachment.values)

#================================
#plot rates

my_colors = c("Total"="blue1","Proliferation"="darkorange","Attachment"="brown2")

cleanup_grid = theme(panel.border = element_blank(),
        panel.grid.major = element_blank(),
        panel.grid.minor = element_blank(),
        panel.background = element_blank(),
        axis.line = element_line(color = "black"),
)

cleanup_text = theme(axis.text.x = element_text(color = "black", size = 12, angle = 0, hjust =
.5, vjust = .5, face = "plain"),
        axis.text.y = element_text(color = "black", size = 12, angle = 0, hjust = 0.8, vjust =
0.4, face = "plain"),
        axis.title.x = element_text(color = "black", size = 20, angle = 0, hjust = .5, vjust = 0,
face = "plain"),
        axis.title.y = element_text(color = "black", size = 20, angle = 90, hjust = .5, vjust = .5,
face = "plain"))


p <- ggplot(rates, aes(time)) +
        scale_color_manual(name = "Legend", values = my_colors) +

        geom_line(aes(y=points, col = "Total"), size = 1.3) +

        geom_line(aes(y=pointsp, col = "Proliferation"), size = 1.3) +
```

```
        labs(x="Time (Hour)", y=expression("Rate "~(CFU[normalised]~Hour^1))) +

        cleanup_grid +
        cleanup_text +


        theme(legend.text=element_text(size=12)) +

        theme(legend.title=element_text(size=12))

#=====================================
#plot CFUnormalised

my_colors = c("Total"="blue1","Proliferation"="darkorange","Attachment"="brown2")

cleanup_grid = theme(panel.border = element_blank(),
        panel.grid.major = element_blank(),
        panel.grid.minor = element_blank(),
        panel.background = element_blank(),
        axis.line = element_line(color = "black"),
)

cleanup_text = theme(axis.text.x = element_text(color = "black", size = 12, angle = 0, hjust =
.5, vjust = .5, face = "plain"),
        axis.text.y = element_text(color = "black", size = 12, angle = 0, hjust = 0.8, vjust =
0.4, face = "plain"),
        axis.title.x = element_text(color = "black", size = 20, angle = 0, hjust = .5, vjust = 0,
face = "plain"),
        axis.title.y = element_text(color = "black", size = 20, angle = 90, hjust = .5, vjust = .5,
face = "plain"))
```

```
p <- ggplot(model.values, aes(time)) +
        scale_color_manual(name = "Legend", values = my_colors) +

        geom_line(aes(y=total.values, col = "Total"), size = 1.3) +

        geom_line(aes(y=proliferation.values, col = "Proliferation"), size = 1.3)     +


        geom_line(aes(y=attachment.values, col = "Attachment"), size = 1.3)        +


        labs(x="Time (Hours)", y=expression(CFU[normalised])) +

        cleanup_grid +
        cleanup_text +


        theme(legend.text=element_text(size=12)) +

        theme(legend.title=element_text(size=12))

#====================================

Gcont = function(time){
        mup*(Yc(time)*(Kp-Yc(time))/Kp)
}                               #substitute y0 for Yc

plot(time,Gcont(time))

boc <- vector("numeric",96)
```

```
for(i in 0:96){
        intval = integrate(Gcont,lower=0,upper=i)
        str(intval)
        boc[i] = (intval$value)
}

plot(time,boc)

Gcont(time)

#=====================================
```

R script: calculation of the contribution of attachment at time t to total colonisation density at t = 96 hours

```
#script for calculating rate of attachment

library(dplyr)
library(tidyverse)
library(growthrates)
library(deSolve)
library(lattice)
library(ggplot2)
library(gridExtra)
library(cowplot)        #load packages

rm(list=ls())
graphics.off()
detach(my.data) #remove previous work

#========================


Kc = 8.855974
y0c = 0.007333
muc = 0.184677
Kp = Kc
y0p = 0.02508862
mup = 0.09949397      #prameters from growthrates

time = c(1:96)
```

```
Yc = function(time){
        Kc/(1+(Kc/y0c-1)*exp(-muc*time))
}                                          #logistic equation for total colonisation

Yc1 = expression(
        Kc/(1+(Kc/y0c-1)*exp(-muc*time))
)

D(Yc1,'time') #differentiate it

Rc = function(time){
        Kc * ((Kc/y0c - 1) * (exp(-muc * time) * muc))/(1 + (Kc/y0c -
        1) * exp(-muc * time))^2
}                                          #growth rate for total colonisation

points = Rc(time)

plot(time,points)

#======================

Yp = function(time){
        Kp/(1+(Kp/y0p-1)*exp(-mup*time))
}                                          #logistic equation for proliferation

Yp1 = expression(
        Kp/(1+(Kp/y0p-1)*exp(-mup*time))
)

D(Yp1,'time') #differentiate it
```

```
Rp = function(time){
        Kp * ((Kp/y0p - 1) * (exp(-mup * time) * mup))/(1 + (Kp/y0p -
        1) * exp(-mup * time))^2
}                                                   #growth rate for proliferation

pointsp = Rp(time)

plot(time,pointsp)

summary(pointsp)
summary(points)

#======================

Rcont = function(time){
        mup*(Yc(time)*(Kp-Yc(time))/Kp)
}                           #substitute y0 for Yc

pointscont = Rcont(time)

summary(pointscont)

Ra = function(time){
        Rc(time) - Rcont(time)
}

#======================

pt = function(time){
```

```
        Ra(time)/Kc*(
        mup*Yc(time)*(
        Kp-Yc(time)
        )/Kp
        )
}

points  = pt(time)

plot(time,points)


a = function(time){
        Ra(time)/Kc
}

first_part = a(time)

#========

Rpc = function(time){
        mup*(Yc(time)*(Kp-Yc(time))/Kp)
}

integrate(Rpc,lower=0,upper=96)
integrate(Rpc,lower=1,upper=96)

int.values <- vector("numeric",96)

for(i in 0:96){
```

```
        intval = integrate(Rpc,lower=i,upper=96)
        str(intval)
        int.values [i] = (intval$value)
}

int.values

vals = first_part*int.values

plot(time,first_part*int.values)

#=========================

frame = data.frame(vals,time)

#=========================

cleanup_grid = theme(panel.border = element_blank(),
        panel.grid.major = element_blank(),
        panel.grid.minor = element_blank(),
        panel.background = element_blank(),
        axis.line = element_line(color = "black"),
                                        )

cleanup_text = theme(axis.text.x = element_text(color = "black", size = 12, angle = 0, hjust =
.5, vjust = .5, face = "plain"),
        axis.text.y = element_text(color = "black", size = 12, angle = 0, hjust = 0.8, vjust =
0.4, face = "plain"),
        axis.title.x = element_text(color = "black", size = 20, angle = 0, hjust = .5, vjust = 0,
face = "plain"),
```

```
        axis.title.y = element_text(color = "black", size = 20, angle = 90, hjust = .5, vjust = .5,
face = "plain"))


#==================


p <- ggplot(frame, aes(time)) +
        geom_line(aes(y= vals), size = 1.3, col = "Black") +
        labs(x="Time (Hours)", y=expression("Proportion of"~italic(K[c]))) +

        cleanup_grid +
        cleanup_text +
        scale_x_continuous(breaks = round(seq(0, 100, by = 10),1)) +

        theme(legend.text=element_text(size=12)) +
        theme(legend.title=element_text(size=12))
```

Python script: applying filter to root profile data and exporting initial conditions as a pickle

```
import matplotlib.pyplot as plt
from scipy.ndimage import gaussian_filter
import numpy as np
from scipy.signal import medfilt
from scipy.ndimage.filters import minimum_filter
import os
from matplotlib import cm



folder = ""       #relevant folder
files = os.listdir(folder)
DATA = []
for file in files:
        if 'csv' in file:
                f = open(folder + file,'r')
                X = []
                Y = []
                for line in f:
                        row = line.split(',')
                        X.append(row[0])
                        Y.append(row[1])
                DATA.append([np.array(X[1:]).astype('float'), np.array(Y[1:]).astype('float')])
TOT = []
plt.figure(1)
i = 0
for D in DATA:
        i+=1              #incriment a variable in a loop
        X = D[0][::5]
```

```
        Y = D[1][::5]

##################################################
#select and filter just the first data set, then subtract mean value from -ve control

X = DATA[0][0][::5]
Y = DATA[0][1][::5]
Z =  # relevant mean value for -ve control

sig = 301
Y = medfilt(Y, kernel_size=sig)
Y = gaussian_filter(Y, sigma = sig*1.8)

sig = 301
Z = medfilt(Z, kernel_size=sig)
Z = gaussian_filter(Z, sigma = sig*1.8)

Y = Y - Z # to normailze
##################################################
#prepare T = 0 filtered conditions to be dumped and loaded later to use as starting conditions for model

T0_conditions = [[X],[Y]]

import pickle

pickle.dump( T0_conditions, open( "save7.p", "wb" ) )

T0_conditions = pickle.load( open( "save7.p", "rb" ))
```

Python script: fitting parameters to chemotaxis models

```
import matplotlib.pyplot as plt
from scipy.ndimage import gaussian_filter
import numpy as np
from scipy.signal import medfilt
from scipy.ndimage.filters import minimum_filter
import os
from matplotlib import cm
from fipy import Grid1D, VanLeerConvectionTerm, CellVariable, TransientTerm, DiffusionTerm, Viewer, ExponentialConvectionTerm, ImplicitSourceTerm, ConvectionTerm, ImplicitSourceTerm, FaceVariable
import time
import numpy as np
import pylab as plt
import matplotlib.colors as colors
from matplotlib import cm
import copy
import scipy
from scipy.optimize import minimize
import pickle
import math as maths

folder = "" #folder containing data

#####################################################
#setting up the data

files = os.listdir(folder)
DATA = []
for file in files:
```

```
    if 'csv' in file:
        f = open(folder + file,'r')
        X = []
        Y = []
        for line in f:
            row = line.split(',')
            X.append(row[0])
            Y.append(row[1])
        DATA.append([np.array(X[1:]).astype('float'), np.array(Y[1:]).astype('float')])

#####################################################

#####################################################

# Model / simulation parameters

D  = 0.00164   # Diffusion coefficient
L1 = 3.5       # Length of the channel
L2 = 1         # Lenngth of reservoir
L3 = 1         # length of second resevoir (sink)
NX = 550       # Number of cells in the simulation
nt = 5.        # Data shown every nt time point
dt0 = 0.1      # time steps
U = 0.007620  # decay term
rm = int(n/nt)
mu =    #monod max growth rate
Q =     #convection term
K =     #monod growth term
Z =     #coupling coefficient
```

```
D_C  =          # Diffusion coefficient
U_C = # decay term
K_C = K

#####################################################

MiMin = []
for i in range(len(DATA)):
        Y = DATA[i][1][::5]
        sig = 301

        Y = medfilt(Y, kernel_size=sig)
        Y = gaussian_filter(Y, sigma = sig*1.8)
        MiMin.append(min(Y))

min_Y = min(MiMin)

plt.figure("Data")
TOT_DATA = []
for i in range(len(DATA)):
        X = DATA[i][0][::5]
        Y = DATA[i][1][::5]
        sig = 301
        Y = medfilt(Y, kernel_size=sig)
        Y = gaussian_filter(Y, sigma = sig*1.8)
        Y = [element - min_Y for element in Y]
        Y = Y[::(int(len(Y)/((L1)/(L1+L2+L3)*NX)))]
#       Y = Y[0:int(NX*L1/(L1+L2+L3))]
        X = X[::(int(len(X)/((L1)/(L1+L2+L3)*NX)))]
```

```
#       X = X[0:int(NX*L1/(L1+L2+L3))] #have to clip the data slightly as rouding based on int() commandmakes it slightly longer than 150
        XY = [X,Y]
        TOT_DATA.append(XY)
        c = cm.viridis(int(float(i+1)/float(len(DATA))*256.))
        plt.plot(X,Y, color = c)
        plt.xlabel("Distance (cm)")
        plt.ylabel("Filtered Signal Intensity")

Cstart = TOT_DATA[0][1][0]
Cend = TOT_DATA[0][1][-1]
Cmiddle = TOT_DATA[0][1]

Y_DATA = []
for i in range(len(TOT_DATA)):
        Y = TOT_DATA[i][1]
        Y_DATA.append(Y) #makes it easier to subtract later on to just remove the x values now

##################################################

print("Should be 5...",len(TOT_DATA))
print("Should be 0...",min(TOT_DATA[-1][-1]))

#load in original data
folder = "C:\\Users\\delil\\Desktop\\Clean_Scripts\\Exudate_Negative_Data\\"

T0_conditions = pickle.load( open( "save_pos.p", "rb" ))

C0T = T0_conditions[0][1]
C0 = C0T[0]
```

```
T0_conditions_C_1 = pickle.load( open( "", "rb" ))
T0_conditions_C_2 = pickle.load( open( "", "rb" )) #pickles for normalised dyes

x = T0_conditions_C_2[1][::int(len(T0_conditions_C_2[1][0])/3000)]
x = np.array(x[:3000])

y = T0_conditions_C_1[1][::int(len(T0_conditions_C_1[1])/3000)]
y = np.array(y[:3000])

len(x)-len(y)

z = (x+y)

C0T_C = [element/2 for element in z]

C0_C = C0T_C[0]
C1_C = C0T_C[-1]

##############################################################################
##########################

# Setting data and equations, then solve the problem
# Initiate the Grid

m = Grid1D(nx=NX, Lx=L1+L2+L3)
m_C = Grid1D(nx=NX, Lx=L1+L2+L3)

# Initial conditions can be overwritten with data
INI0 = np.arange(NX)*0.
```

```
INI0[0:int(NX*L2/(L1+L2+L3))] = 10

INI0[int(NX*L2/(L1+L2+L3)):]=1 #fill firts L2 (resevoir) with C0 value


################################################################################
##########################


INI0_D = np.arange(NX)*0.


INI0_D[0:int(NX*L2/(L1+L2+L3))] = C0 #fill firts L2 (resevoir) with C0 value


T2 = C0T[::

        int(len(C0T)/(NX - len(INI0[0:int(NX*L2/(L1+L2+L3))]) -
len(INI0[int(NX*(L1+L2)/(L1+L2+L3)):])))

] # fill middle L1 (chanel) with T0 values


INI0_D[int(NX*L2/(L1+L2+L3)):int(NX*(L1+L2)/(L1+L2+L3))] =
T2[:(int(NX*(L1+L2)/(L1+L2+L3))-int(NX*L2/(L1+L2+L3)))]


INI0_D[int(NX*(L1+L2)/(L1+L2+L3)):] = C1 #fill final l3 (resevoir) with the laste value in
T0 conditions


INI0  = INI0_D #hashtag this to turn on and off data


################################################################################
##########################

#carbon conditions


INI0_C = np.arange(NX)*0.


INI0_C[0:int(NX*L2/(L1+L2+L3))] = C0_C #fill final l3 (resevoir)


T2 = C0T_C[::
```

```
        int(len(C0T_C)/(NX - len(INI0_C[0:int(NX*L2/(L1+L2+L3))]) -
len(INI0_C[int(NX*(L1+L2)/(L1+L2+L3)):])))
]

INI0_C[int(NX*L2/(L1+L2+L3)):int(NX*(L1+L2)/(L1+L2+L3))] =
T2[:int((NX*(L1+L2)/(L1+L2+L3))-(NX*L2/(L1+L2+L3)))]

INI0_C[int(NX*(L1+L2)/(L1+L2+L3)):] = C1_C #fill firts L2 (resevoir)

INI0_C = INI0_C[::-1]

#############################################################################
#########################

############################################################

def error(parms):

        D,U = parms #replace with whatever you're fitting for, eg: "D,U,Q = parms"

        n = 240 # this needs to be reset

        v0 = CellVariable(mesh=m, value=INI0)

        v0_C = CellVariable(mesh=m, value=INI0_C)

        eqn_C = TransientTerm(var=v0_C) ==      (
                DiffusionTerm(coeff =D_C,var=v0_C) #diffusion
                - ImplicitSourceTerm(coeff = U_C,var=v0_C) #decay
                - ImplicitSourceTerm(coeff = Z*(mu*(v0_C/(v0_C+K))),var=v0) #monod
growth
```

```
            )

        eqn_B = TransientTerm(var=v0) ==  (
                DiffusionTerm(coeff =D,var=v0) #diffusion
                - ConvectionTerm(coeff = Q*v0_C.grad, var=v0) #convection
                - ImplicitSourceTerm(coeff = U,var=v0) #decay #decay
                + ImplicitSourceTerm(coeff = (mu*(v0_C/(v0_C+K))),var=v0)      #monod
growth
                )

        eqn = eqn_C & eqn_B



        DATA0 = []
        DATA0.append(np.array(copy.copy(v0)))

        for t in range(int(n)):
                eqn.solve(dt=dt0)
                if t%rm == 0:   # data shown every time t is a multiple of rm
                        DATA0.append(np.array(v0))

        TOT_SIM = []

        for i in range(len(DATA0)-1):
                Y = DATA0[i][(int(NX*L2/(L1+L2+L3))):(int(NX*(L1+L2)/(L1+L2+L3)))]
                TOT_SIM.append(Y)

        SUM = []
        SUM = np.subtract(Y_DATA,TOT_SIM)
        SUM = np.square(SUM)
```

```
        SUM = np.sqrt(SUM/len(Y_DATA))
        TOT_ERROR = maths.sqrt(np.sum(SUM)/len(Y_DATA))
        print(TOT_ERROR)
        return(TOT_ERROR)

##############################################

test_parameters = [0.01,0.01] # reasonable guess

print(error(test_parameters))

##############################################

res = minimize(error, test_parameters, args=(), method = 'nelder-Mead',
jac=None, hess=None, hessp=None, bounds=None, constraints=(),
tol=None, callback=None, options=None)

print("Fit parameters...",res.x)

print("Fit error...",error(res.x))
##############################################
plt.show()
##############################################
```

Python script: one-dimensional chemotaxis

```
from fipy import Grid1D, VanLeerConvectionTerm, CellVariable, TransientTerm,
DiffusionTerm, Viewer, ExponentialConvectionTerm, ImplicitSourceTerm,
ConvectionTerm, ImplicitSourceTerm, FaceVariable
import time
import numpy as np
import pylab as plt
import matplotlib.colors as colors
from matplotlib import cm
import copy
import math as maths
import pickle

#####################################################

#####################################################

# Model / simulation parameters

D  =    # Diffusion coefficient
L1 =    # Length of the channel
L2 =    # Lenngth of reservoir
L3 =    # length of second resevoir (sink)
NX = 550        # Number of cells in the simulation(higher means more accurate solutions)
n= 240.         # Number of time steps
nt = 5.  # Data shown every nt time point, change based on length of DATA
dt0 = 0.1       # time steps
U = 0.007620  # decay term
rm = int(n/nt)
mu =            #max growth rate
```

```
Q =             #chemotaxis coefficient
K =             #monod corefficient
Z =             #coupling coefficient

D_C  =# Diffusion coefficient
U_C = # decay term
K_C = K

##########################################################################################################
#load in original data
folder = "" #data file location

T0_conditions = pickle.load( open( "", "rb" )) #pickle name

C0T = T0_conditions[0][1]
C0 = C0T[0]
C1 = C0T[-1]  # Initial conditions reversed

T0_conditions_C_1 = pickle.load( open( "", "rb" ))  #dye pickle data
T0_conditions_C_2 = pickle.load( open( "", "rb" ))  #dye pickle data

x = T0_conditions_C_2[1][::int(len(T0_conditions_C_2[1][0])/3000)]
x = np.array(x[:3000])

y = T0_conditions_C_1[1][::int(len(T0_conditions_C_1[1])/3000)]
y = np.array(y[:3000])

len(x)-len(y)
```

```
z = (x+y)

C0T_C = [element/2 for element in z]

C0_C = C0T_C[0]
C1_C = C0T_C[-1]

##############################################################################
##########################
# Setting data and equations, then solve the problem
# Initiate the Grid
m = Grid1D(nx=NX, Lx=L1+L2+L3)
m_C = Grid1D(nx=NX, Lx=L1+L2+L3)

# Initial conditions
INI0 = np.arange(NX)*0.
INI0[0:int(NX*L2/(L1+L2+L3))] = 10
INI0[int(NX*L2/(L1+L2+L3)):]=1 #fill firts L2 (resevoir) with C0 value
##############################################################################
##########################

INI0_D = np.arange(NX)*0.

INI0_D[0:int(NX*L2/(L1+L2+L3))] = C0 #fill firts L2 (resevoir) with C0 value

T2 = C0T[::
        int(len(C0T)/(NX - len(INI0[0:int(NX*L2/(L1+L2+L3))]) -
len(INI0[int(NX*(L1+L2)/(L1+L2+L3)):])))
] # fill middle L1 (chanel) with T0 values
```

```
INI0_D[int(NX*L2/(L1+L2+L3)):int(NX*(L1+L2)/(L1+L2+L3))] =
T2[:(int(NX*(L1+L2)/(L1+L2+L3))-int(NX*L2/(L1+L2+L3)))]


INI0_D[int(NX*(L1+L2)/(L1+L2+L3)):] = C1 #fill final l3 (resevoir) with the laste value in
T0 conditions


INI0  = INI0_D #hashtag this to turn on and off data


##############################################################################
##########################

#carbon conditions


INI0_C = np.arange(NX)*0.


INI0_C[0:int(NX*L2/(L1+L2+L3))] = C0_C #fill final l3 (resevoir)


T2 = C0T_C[::

        int(len(C0T_C)/(NX - len(INI0_C[0:int(NX*L2/(L1+L2+L3))]) -
len(INI0_C[int(NX*(L1+L2)/(L1+L2+L3)):])))

]


INI0_C[int(NX*L2/(L1+L2+L3)):int(NX*(L1+L2)/(L1+L2+L3))] =
T2[:int((NX*(L1+L2)/(L1+L2+L3))-(NX*L2/(L1+L2+L3)))]


INI0_C[int(NX*(L1+L2)/(L1+L2+L3)):] = C1_C #fill firts L2 (resevoir)


INI0_C = INI0_C[::-1]


##############################################################################
##########################


# Grid
```

```
v0 = CellVariable(mesh=m, value=INI0)

v0_C = CellVariable(mesh=m, value=INI0_C)

##################################################

############################################################

DATA0_C = []
DATA0_C.append(np.array(copy.copy(v0_C)))
DATA0 = []
DATA0.append(np.array(copy.copy(v0)))

############################################################
viewer = Viewer(vars=v0)

for t in range(int(n)):

        eqn_C = TransientTerm(var=v0_C) ==         (
                DiffusionTerm(coeff =D_C,var=v0_C) #diffusion
                - ImplicitSourceTerm(coeff = U_C,var=v0_C) #decay
                - ImplicitSourceTerm(coeff = Z*(mu*(v0_C/(v0_C+K))),var=v0) #monod
growth
                )

        eqn = TransientTerm(var=v0) ==       (
                DiffusionTerm(coeff =D,var=v0) #diffusion
                - ConvectionTerm(coeff = Q*v0_C.grad, var=v0) #convection
                - ImplicitSourceTerm(coeff = U,var=v0) #decay
                + ImplicitSourceTerm(coeff = (mu*(v0_C/(v0_C+K))),var=v0)      #monod
growth
```

```
            )

        coupled_eqn = eqn_C & eqn

        viewer.plot()

        coupled_eqn.solve(dt=dt0) # choose model
        if t%rm == 0:
            DATA0.append(np.array(v0))
            DATA0_C.append(np.array(v0_C))

############################################################

plt.figure("Output")
n = len(DATA0)
for i in range(n):
        c = cm.jet(int(float(i)/float(n)*256.))
        plt.plot(np.array(m.cellCenters[0]), DATA0[i],color = c)

        plt.fill_between([L2,0], [55,55], y2=0, alpha=0.2)
        plt.fill_between([L2+L1+L3,L1+L2], [55,55], y2=0, alpha=0.2)
        plt.xlabel("Distance (cm)")
        plt.ylabel("Filtered Signal Intensity")


plt.figure("Carbon")
n = len(DATA0)
for i in range(n):
        c = cm.jet(int(float(i)/float(n)*256.))
        plt.plot(np.array(m.cellCenters[0]), DATA0_C[i],color = c)
```

```
plt.fill_between([L2,0], [85,85], y2=0, alpha=0.2)
plt.fill_between([L2+L1+L3,L1+L2], [85,85], y2=0, alpha=0.2)
plt.xlabel("Distance (cm)")
plt.ylabel("Filtered Signal Intensity")
```

Python script: two-dimensional chemotaxis

```
from fipy import Grid2D, VanLeerConvectionTerm, CellVariable, TransientTerm,
DiffusionTerm, Viewer, ExponentialConvectionTerm, ImplicitSourceTerm,
ConvectionTerm, ImplicitSourceTerm, FaceVariable
import time
import numpy as np
import pylab as plt
import matplotlib.colors as colors
from matplotlib import cm
import copy
import math as maths
import pickle

# Model / simulation parameters

D  =    # Diffusion coefficient
U = 0   # Decay term
Q =     # Gradient coefficient
K =     # Monod half velocity
Z =     # Coupling coefficient
mu =    # Monod maximum growth

D_C  =          # Carbon Diffusion coefficient
U_C = 0         # Carbon Decay term

NX = 160                    #chamber size
NY = NX                         #chamber length = width
DX = 1.                         #cell size
DY = DX                         #chamber length = width
L = NX*DX                   #number of cells
```

```
dt0 = 0.1                # time steps
nt = 5.                  # Data shown every nt time point
n= 240.`                 # Number of time steps
rm = int(n/nt)

RW = 2 #root width
RL = 28 #root length
RWC = RW*DX # root width in cells
RLC = RL*DY # root length in cells

Ca =    #initial value of carbon in fluourescence units
B =     # initial bacterial value

#############################################################################
#########################

# Initiate the Grid
m = Grid2D(dx=DX, dy=DY, nx=NX, ny=NY)

#############################################################################
#########################

# initial conditions with equal B in all cells
INI = np.zeros((int(L),int(L)))
INI[:] = B
INI = INI.reshape(int(L*L))

v0 = CellVariable(mesh=m,value=INI)

#########################################################
```

```
in0 = np.arange(int(L*L))*0.

for i in range(int(RLC)): #set values of in0 to have Ca at root based on RW & RL
        centre = int(i*L + L/2 + 1)
        centre1 = int(i*L + L/2)
        centre2 = int(i*L + L/2 + 1)
        for j in range(int(RWC/2 +1)):
                if(RWC == 1):
                        x = centre
                        in0[x-1] = Ca
                elif(RWC == 2):
                        x = centre1
                        in0[x-1] = Ca #issue here
                        x = centre2
                        in0[x-1] = Ca
                else:
                        x = centre
                        in0[x-1] = Ca
                        x = centre - j
                        in0[x-1] = Ca
                        x = centre + j
                        in0[x-1] = Ca

in0 = in0[::-1]

v0_C = CellVariable(name = "Carbon",mesh = m,value = in0)

############################################################
```

```
DATA0 = []
DATA0.append(np.array(copy.copy(v0)))
EXUDATE = []
EXUDATE.append(np.array(copy.copy(v0_C)))

viewer = Viewer(vars=v0, datamin=0., datamax=30)

for t in range(int(n)):

        eqn_C = TransientTerm(var=v0_C) ==         (
                DiffusionTerm(coeff =D_C,var=v0_C) #diffusion
                - ImplicitSourceTerm(coeff = U_C,var=v0_C) #decay
                - ImplicitSourceTerm(coeff = Z*(mu*(v0_C/(v0_C+K))),var=v0) #monod
growth
                )

        eqn = TransientTerm(var=v0) ==       (
                DiffusionTerm(coeff =D,var=v0) #diffusion
                - ConvectionTerm(coeff = Q*v0_C.grad, var=v0) #convection
                - ImplicitSourceTerm(coeff = U,var=v0) #decay
                + ImplicitSourceTerm(coeff = (mu*(v0_C/(v0_C+K))),var=v0)      #monod
growth
                )

        coupled_eqn = eqn_C & eqn

        coupled_eqn.solve(dt = dt0)

        eqn.solve(dt=dt0)

        y = list(v0_C)
```

```
y = y[::-1]

for i in range(int(RLC)):
        centre = int(i*L + L/2 + 1)
        centre1 = int(i*L + L/2)
        centre2 = int(i*L + L/2 + 1)
        for j in range(int(RWC/2 +1)):
                if(RW == 1):
                        c = centre
                        y[c-1] = Ca
                elif(RWC == 2):
                        c = centre1
                        y[c-1] = Ca
                        c = centre2
                        y[c-1] = Ca
                else:
                        c = centre
                        y[c-1] = Ca
                        c = centre - j
                        y[c-1] = Ca
                        c = centre + j
                        y[c-1] = Ca

y = y[::-1]

v0_C = CellVariable(name = "Carbon",
        mesh = m,
        value = y)
```

```
        viewer.plot()
        if t%rm == 0:
                DATA0.append(np.array(v0))
                EXUDATE.append(np.array(v0_C))

############################################################
```

Python script: two-dimensional chemotaxis with root growth

```
from fipy import Grid2D, VanLeerConvectionTerm, CellVariable, TransientTerm,
DiffusionTerm, Viewer, ExponentialConvectionTerm, ImplicitSourceTerm,
ConvectionTerm, ImplicitSourceTerm, FaceVariable
import time
import numpy as np
import pylab as plt
import matplotlib.colors as colors
from matplotlib import cm
import copy
import math as maths
import pickle

# Model / simulation parameters

D  =            # Diffusion coefficient
U = 0           # Decay term
Q =             # Gradient coefficient
K =             # Monod half velocity
Z =             # Coupling coefficient
mu =            # Monod maximum growth

D_C  =          #low diffusion senario
U_C = 0         # Carbon Decay term

NX = 180        #chamber size
NY = NX         #chamber length = width
DX = 1.                 #cell size
DY = DX         #chamber length = width
L = NX*DX       #number of cells
```

```
dt0 = 0.1               # time steps
nt = 5.                 # Data shown every nt time point, change based on length of DATA
n= 4320.                # Number of time steps
rm = int(n/nt)

RW =                    #root width
RL =                    #starting root length
RWC = RW*DX             #root width in cells
RLC = RL*DY             #root length in cells
RGR =                   #root growth rate calibrated based on rgr of 0.065 mm/hour

Ca =    #initial value of carbon g/ml
B =     # initial bacterial value g/ml

#############################################################################
##########################

# Initiate the Grid
m = Grid2D(dx=DX, dy=DY, nx=NX, ny=NY)

#############################################################################
##########################

# initial conditions with equal B in all cells
INI = np.zeros((int(L),int(L)))
INI[:] = B
INI = INI.reshape(int(L*L))

v0 = CellVariable(
        mesh=m,
```

```
        value=INI)

############################################################

in0 = np.arange(int(L*L))*0.

for i in range(int(RLC)): #set values of in0 to have Ca at root based on RW & RL
        centre = int(i*L + L/2 + 1)
        centre1 = int(i*L + L/2)
        centre2 = int(i*L + L/2 + 1)
        for j in range(int(RWC/2 +1)):
                if(RWC == 1):
                        x = centre
                        in0[x-1] = Ca
                elif(RWC == 2):
                        x = centre1
                        in0[x-1] = Ca #issue here
                        x = centre2
                        in0[x-1] = Ca
                else:
                        x = centre
                        in0[x-1] = Ca
                        x = centre - j
                        in0[x-1] = Ca
                        x = centre + j
                        in0[x-1] = Ca

in0 = in0[::-1]

v0_C = CellVariable(name = "Carbon",
```

```
        mesh = m,
        value = in0)

############################################################

DATA0 = []
DATA0.append(np.array(copy.copy(v0)))
EXUDATE = []
EXUDATE.append(np.array(copy.copy(v0_C)))

viewer = Viewer(vars=v0, datamin=0., datamax=30)

for t in range(int(n)):

        eqn_C = TransientTerm(var=v0_C) ==         (
                DiffusionTerm(coeff =D_C,var=v0_C) #diffusion
                - ImplicitSourceTerm(coeff = U_C,var=v0_C) #decay
                - ImplicitSourceTerm(coeff = Z*(mu*(v0_C/(v0_C+K))),var=v0) #monod
growth
                )

        eqn = TransientTerm(var=v0) ==       (
                DiffusionTerm(coeff =D,var=v0) #diffusion
                - ConvectionTerm(coeff = Q*v0_C.grad, var=v0) #convection
                - ImplicitSourceTerm(coeff = U,var=v0) #decay
                + ImplicitSourceTerm(coeff = (mu*(v0_C/(v0_C+K))),var=v0)      #monod
growth
                )

        coupled_eqn = eqn_C & eqn
```

```
coupled_eqn.solve(dt = dt0)

eqn.solve(dt=dt0)

y = list(v0_C)

y = y[::-1]

for i in range(int(RLC+RGR*t)):
        centre = int(i*L + L/2 + 1)
        centre1 = int(i*L + L/2)
        centre2 = int(i*L + L/2 + 1)
        for j in range(int(RWC/2 +1)):
                if(RW == 1):
                        c = centre
                        y[c-1] = Ca
                elif(RWC == 2):
                        c = centre1
                        y[c-1] = Ca
                        c = centre2
                        y[c-1] = Ca
                else:
                        c = centre
                        y[c-1] = Ca
                        c = centre - j
                        y[c-1] = Ca
                        c = centre + j
                        y[c-1] = Ca

y = y[::-1]
```

```
        v0_C = CellVariable(name = "Carbon",
                    mesh = m,
                    value = y)

        viewer.plot()
        if t%rm == 0:
                    DATA0.append(np.array(v0))
                    EXUDATE.append(np.array(v0_C))

############################################################
```